Transcriptional and Post-transcriptional Regulation of Organophosphate Degradation (*opd*) Gene in *Sphingobium fuliginis* ATCC 27551

Thesis submitted for the degree of
Doctor of Philosophy
in
Animal Biology
By

N. APARNA
(15LAPH01)

Supervisor
Prof. S. Dayananda

Department of Animal Biology
School of Life Sciences
University of Hyderabad
Hyderabad –500046
INDIA

2020

University of Hyderabad
(A Central University established in 1974 by an act of parliament) HYDERABAD – 500 046, INDIA

CERTIFICATE

This is to certify that this thesis entitled **"Transcriptional and Post-transcriptional Regulation of Organophosphate Degradation (*opd*) Gene in *Sphingobium fuliginis* ATCC 27551"** submitted by **Ms. N. Aparna,** bearing registration number **15LAPH01** in partial fulfilment of the requirements for award of Doctor of Philosophy in the **Department of Animal Biology, School of Life Sciences** is a bonafide work carried out by her, under my supervision and guidance.

This thesis is free from plagiarism and has not been submitted previously in part or in full to this or any other University or Institution for award of any degree or diploma.

Publications

1. *J. Biol. Chem.* **291**, 7774–85 (2016); DOI 10.1074/jbc.M116.715110
2. Rev Environ Health. **31**, 57-61 (2016); DOI 10.1515/reveh-2015-0042
3. *J. Biol. Chem.* **290**, 29920–30 (2015); DOI 10.1074/jbc.M115.661249

International conference

Poster presentation in 59th annual conference of Association of Microbiologists of India (9th-12th December, 2018)

Further, the student has passed the following courses towards fulfillment of coursework requirement for Ph.D.

S. No.	Course Code	Name	Credits	Pass/Fail
1	AS 801	Seminar	1	Pass
2	AS 802	Research Ethics & Management	2	Pass
3	AS 803	Biostatistics	2	Pass
4	AS 804	Analytical Techniques	3	Pass
5	AS 805	Lab Work	4	Pass

Research Supervisor
Prof. S. DAYANANDA
Dept. of Animal Biology.
School of Life Sciences
University of Hyderabad
Hyderabad-500 046. T.S.

Anita Jagola 24/12/2020
Head of the Department
अध्यक्ष / HEAD
जंतु जैविकी विभाग
Department of Animal Biology

Dean of the school
DEAN
School of Life Sciences
University of Hyderabad
Hyderabad - 500 046.

University of Hyderabad
(A Central University established in 1974 by an act of parliament) HYDERABAD – 500 046, INDIA

DECLARATION

This is to declare that the work embodied in this thesis entitled **"Transcriptional and Post-transcriptional Regulation of Organophosphate Degradation (*opd*) Gene in *Sphingobium fuliginis* ATCC 27551"** has been carried out by me under the supervision of Prof. S. Dayananda, Department of Animal Biology, School of Life Sciences. The work presented in this thesis is a bonafide research work and has not been submitted for any degree or diploma in any other University or Institute. A report on plagiarism statistics from the University Librarian is enclosed.

Aparna N.
N. Aparna
(15LAPH01)

S. Dayananda
Prof. S. Dayananda
(Research supervisor)
Prof. S. DAYANANDA
Dept. of Animal Biology.
School of Life Sciences
University of Hyderabad
Hyderabad-500 046. T.S.

Date: 24.12.2020

Acknowledgements

*I would like to express my deep gratitude to my supervisor, **Prof. Dayananda Siddavattam**, for suggesting me this area of research, his close guidance, timely suggestions, constant help and support.*

I thank my doctoral committee members Prof. Aparna Dutta Gupta (late), Prof. Appa Rao Podile and Prof. Manjula Sritharan for their constant guidance and encouragement.

I thank the current and former Deans, School of Life Sciences, Prof. S. Dayananda, Prof. K.V.A Ramaiah, Prof. Reddanna, and Prof. A.S Raghavendra, for providing all the facilities in the school.

I thank Prof. Anita Jagota, Head, Dept. of Animal Biology, and former Head's Prof. Jagan Pongubala, and Prof. B. Senthil kumaran for allowing me to use the Department facilities.

This work would have not been possible without the help of Dr. Arati Ramesh, Reader-F, NCBS for allowing me to work in her lab and for her valuable suggestions.

I thank Anaganjali for helping me in all my RNA related experiments.

I am thankful to Prof. Kota Arun Kumar and Ms. Dipti Singh for guiding and helping me in the qRT-PCR experiments.

I specially thank Dr. Manjula Reddy, Principal Scientist, CCMB for providing Keio collection strains.

I thank the help and suggestions of all the faculty members in the School of Life Science, and for allowing me to use their laboratory facilities at different stages of my work.

I am thankful to my labmates Dr. Emmanuel Paul, Dr. Devi prasanna, Dr. Swetha, Dr. Sunil, Dr. Ashok and Dr. Venkateshwar Reddy, Dr. Devyani, Dr. Ramurthy. Dr. Harshitha, Dr. Hari, Ms. Annapoorni Laxman Sagar, Ms. Ganeshwari Dhurve, Mr. Akbar Pasha, Mr. Jay Prakash, Ms. Sandhya, for the help and enjoyable company.

I thank Dr. Bindu Madhav Reddy and Ms. Navya for assisting in preparing the plagiarism report.

The financial support provided by BBL Fellowship, DST-SERB-CII (Prime Minister's Fellowship), and is greatly acknowledged.

I thank DBT, ICMR, UGC, UPE-II, UGC-SAP and DBT-CREBB, Aurobindo pharma, for providing financial support to lab and for the infrastructural facility of the school.

Thanks to the non-teaching staff Mr. Rajendra, Mr. Upendra, Mr. Mallesh and Mr. Krishna, Mr. Jagan, Mr. Srinu, Mr. Nikhil, Mr. Sravan and Mr. Praveen for their technical help.

I am extremely grateful to my parents Sri. Devanand, Smt. Gowri Sankari, my husband Mr. Shankar and to all my family members for their love, and constant support during my endeavours.

I thank Almighty for filling my life with such wonderful people around and also for giving me the patience needed to endure every difficulty encountered.

Table of contents

List of Tables

List of Figures

Abbreviations

OPH	:	Organophosphorous Hydrolase
Opd	:	*organophosphate degrading gene*
IRE	:	Iron Response Element
IRP	:	Iron Regulatory Protein
ATCC	:	American Type Culture Collection
IME	:	Integrative Mobilizable Element
Fur	:	Ferric uptake regulator
Acn	:	Aconitase
S.f	:	*Sphingobium fuliginis*
^{0}C	:	degree Celsius
h	:	hour
ml	:	millilitre
gm	:	gram
dNTP	:	deoxynucleoside triphosphate
Fe-Ent	:	Ferric-enterobactin
IPTG	:	Isopropyl β-D-1-thiogalactopyranoside
Kb	:	Kilobase
kDa	:	kilo Dalton
µM	:	Micro molar
M	:	Molar
PCR	:	Polymerase Chain Reaction
PMF	:	Proton Motive Force
PTE	:	Phosphotriesterase
RT	:	Room temperature
*Sf*TonBDT	:	*Sphingobium fuliginis* TonB dependent Transport System
TonBDT	:	TonB dependent transport system
Tat	:	Twin Arginine Translocase
TBDT	:	TonB dependent transporter

Introduction

1.1. Bacterial phosphotriesterases (PTE):

Phosphotriesterases (PTEs) are metallo-enzymes that hydrolyze the third ester bond of Organophosphate (OP) insecticides and nerve agents. They exist in all forms of life including bacteria, insects and mammals (Zhang et al., 2019). The PTEs found in bacteria are classified into three distinct structural groups viz Organophosphorus acid anhydrolase (OPAA), Methyl parathion hydrolase (MPH) and Organophosphorus hydrolase (OPH), (Singh, 2009; Parthasarathy, 2017).

1.2. Organophosphorus Acid Anhydrolase (OPAA):

Organophosphorous Acid Anhydrolase (OPAA) is an OP-degrading enzyme. Originally, OPAAs were isolated from *Alteromonas* (Cheng et al., 1993; Cheng et al., 1999). Although, the OPAAs hydrolyze OP compounds with high catalytic efficiency, the physiological substrates for OPAAs are not OP compounds. The OPAAs are dipeptidases and hydrolyze peptide linkage of dipeptides having proline at their C-terminal position (Cheng et al., 1993). OPAAs are therefore renamed as prolidases and their ability to degrade OPs is due to structural similarity between OPs and dipeptides (Stepankova et al., 2013; Weaver et al., 2014). After identification of physiological substrates, the OPAAs are no more treated as part of PTEs. However, the physiological substrates for other two PTEs (MPH and OPH) are unknown. They are assumed to have evolved in response to the detrimental effects of organophosphorous residues accumulated in agricultural soils due to repeated and indiscriminate use as insecticides (Singh et al., 2014).

1.3. Methyl parathion hydrolase (MPH):

Methyl Parathion Hydrolase is found in various phylogenetically distinct bacteria, and is found to be active against several organophosphates, but it has a narrow substrate range when compared to OPH. MPH was isolated from *Plesiomonas* sp. M6 (Zhongli et al., 2001), *Pseudomonas* sp. WBC-3 (Dong et al.,

2005), *Pseudomonas* sp. A3 (Zhongli et al., 2001), the soil bacteria collected from different regions of China. Among these isolates, MPH purified from *Pseudomonas* strain is well characterized (Zhongli et al., 2001). MPH exists as a dimer in which each subunit has a mixed-hybrid, binuclear zinc center (Fig.1). It hydrolyzes a wide range of organophosphorous compounds like methyl parathion, DDVP, chlorpyrifos, malathion, fenitrothion (Yang et al., 2008). MPH has significant arylesterase and lactonase activities (Baier & Tokuriki, 2014). MPH possesses promiscuous esterase/lipase, lactonase, and phosphodiesterase activity in addition to its native phosphotriesterase activity (Baier & Tokuriki, 2014). Methyl parathion is an ideal substrate for MPH purified from *Pseudomonas* sp. WBC-3 (Dong et al., 2005). It can degrade chlorpyrifos, ethyl parathion, and sumithion (Chu et al., 2003). The MPH coding methyl parathion degrading (*mpd*) genes have been isolated only from the bacterial strains isolated from agricultural soils of China. Their homologues are not found outside Chinese soils suggesting influence of local environmental factors behind the *mpd* evolution (Singh, 2009).

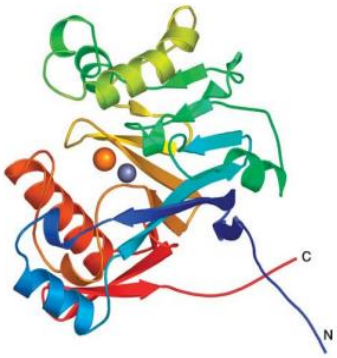

Fig.1: The crystal structure of MPH depicting the binuclear zinc center (Dong et al., 2005)

1.4. Organophosphorus Hydrolase (OPH):

Organophosphate hydrolase (OPH) hydrolyzes the compounds that are structurally related to parathion. They have a broad substrate specificity, temperature range, pH optima and high stability (Brown, 1980; Donarski et al., 1989; Dumas et al., 1989). OPH exhibits activity against organophosphates like parathion, methyl parathion and fenusulfothion and organophosphate chemical warfare agents like sarin, soman with high catalytic efficiency (Singh, 2009). It

can catalyze the cleavage of P-O bonds, P-F and P-S bonds with distinct efficiencies (Singh & Walker, 2006). OPH is encoded by organophosphate degradation (*opd*) gene frequently associated with mobile genetic elements like transposons and self-transmissible plasmids (Pandeeti et al., 2011). Initially OPH was characterized and purified from *Flavobacterium* sp. ATCC 27551, a soil microorganism isolated from the paddy fields of Philippines (Sethunathan & Yoshida, 1973). This soil isolate has recently been reclassified using polyphasic taxonomic tools as *Sphingobium fuliginis* ATCC27551 (Kawahara et al., 2010). Subsequently, their presence was noticed in most of the soil bacteria isolated from agricultural soils collected from different continents.

OPH is a 39kDa metalloprotein and contains a homodimeric $(\beta/\alpha)_8$ barrel fold (Fig.2). The active site of the native OPH contains two zinc ions per monomer, with direct interactions with four histidine residues and one aspartate (Omburo et al., 1992; Benning et al., 1994). Additionally, these metal ions are linked by a water molecule and a carbamoylated lysine residue (Vanhooke et al., 1996). Though Zn^{2+} ions serve as natural cofactors, they can be replaced with Co^{2+}, Cd^{2+}, Ni^{2+}, or Mn^{2+} without compromising on catalytic properties of the enzyme (Omburo et al., 1992). The OPH producing bacteria that share either weak or no taxonomic relationship have been isolated from soil samples collected from diverse geographical regions (Sethunathan & Yoshida, 1973; Serdar et al., 1982; Somara & Siddavattam, 1995; Horne et al., 2002). Many of them use these OP compounds as source of carbon and phosphate (Singh & Walker, 2006). Out of all OP degrading bacterial strains *Flavobacterium* sp. (ATCC 27551) (Sethunathan & Yoshida, 1973; Brown, 1980), isolated from the rice fields of IRRI and *Pseudomonas diminuta* (Serdar et al., 1982), isolated from sewage samples collected from USA were used as model systems to study genetics and biochemistry of OP degradation. Genome sequences are available for both of them and the genome based classification has re-designated both of them as *Sphingobium fuliginis* ATCC27551 and *Sphingopyxis wildii* (Kawahara et al., 2010; Parthasarathy et al., 2016; Azam et al., 2019).

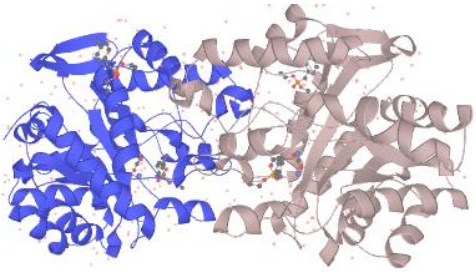

Fig.2: Three dimensional structure of organophosphate hydrolase isolated from *Brevundimonas diminuta* (Benning et al., 2001).

1.5. Structural comparison of MPH with OPH:

Both MPH and OPH hydrolyze identical substrates despite having no structural similarity between these two enzymes. Supporting their unique catalytic properties, these two structurally dissimilar enzymes share similar structure of active site (Dong et al., 2005). Both contain a similar bi-nuclear zinc center. The two metal ions found at active site are separated by a distance of 3.4 A° and are coordinated through the side chains of four histidine residues (His55, His57, His201 and His230) and Asp301. The metal ions are bridged via a carbamylate group form Lys169 and a nucleophile hydroxide ion (Benning et al., 2001) (Fig.3). This type of functional convergence from structurally independent enzymes is considered as symbol of convergent molecular evolution (Tawfik, 2006).

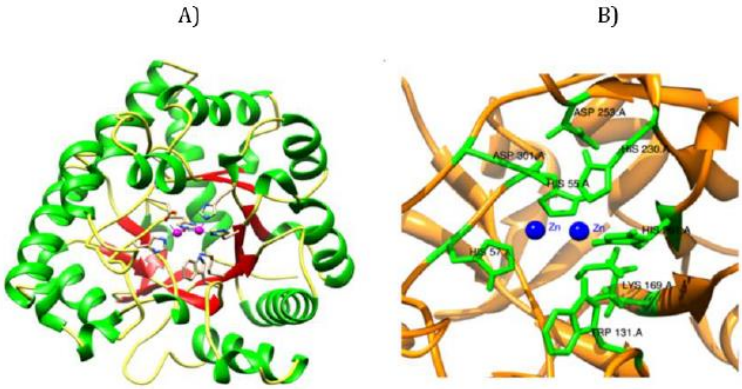

Fig.3: Structural comparison between MPH and OPH. Panel A shows the crystal structure of OPH. Panel B shows the co-ordination environment provided by four histidine residues (His55, His57, His201, and His230), Asp301 and two zinc ions at the active site of OPH (Benning et al., 1994, 2001).

1.6. OPH is a lipoprotein:

OPH is a membrane associated protein. It contains a signal peptide which is 29 amino acids in length (Mulbry & Karns, 1989a, 1989b; Gorla et al., 2009). It also contains a **T**win **A**rginine **T**ransport (Tat) motif with a consensus sequence of MQT**RR**VVLK (Gorla et al., 2009). The Tat pathway translocates fully folded and active proteins across the bacterial inner membrane (Sargent, 1998; Weiner et al., 1998). Generally the TAT motif is found in extracellular or membrane associated proteins with large cofactors or membrane proteins that are found to be part of multi-protein complexes (Berks, 1996; Berks et al., 2005). In contrast to the established notion, our laboratory discovered existence of fully conserved Tat motif (T**RR**VVLK) in the signal sequence of OPH. The twin arginines are required for the membrane targeting of OPH (Gorla et al., 2009). Interestingly, the signal peptide of the OPH also contains a well conserved lipo-box motif along with an invariant cysteine (Fig.4). This amino acid residue is linked to a diacyl glycerol moiety, through which OPH anchors to the inner membrane facing periplasmic space (Parthasarathy et al., 2016; Parthasarathy et al., 2017).

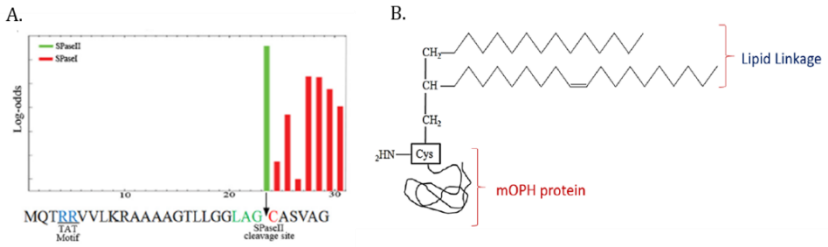

Fig.4: Prediction of Lipo-box in the signal peptide of OPH. Panel A shows bioinformatic analysis of the OPH signal peptide. The predicted SPase (Signal Peptidase) II cleavage site (green bar), lipo-box (green font), and the invariant cysteine residue (red font) found at the junction of the SPaseII cleavage site are shown. Potential SPaseI cleavage sites are indicated with red bars. The twin arginine motif of the Tat signal peptide is underlined. Panel B shows mature form of OPH is linked to diacylglycerol (Parthasarathy et al., 2016).

1.7. OPH is part of membrane associated multi-protein complex:

Existence of Tat motif in the signal peptide of metallo-enzyme like OPH is rather an unusual phenomenon. While investigating further, our laboratory has purified membrane associated OPH and determined its native molecular mass (Fig.5) Both BN-PAGE and gel filtration chromatography have shown that molecular mass of affinity purified membrane associated OPH is 294 kDa.

However, the SDS-PAGE profile revealed existence of several proteins in affinity purified OPH revealing that it is a part of multi-protein complex (Parthasarathy et al., 2016). Further studies have revealed that the co-purified proteins along with OPH were components of outer membrane transport system, otherwise known as TonB Dependent Transport (TonBDT) system. The outer membrane localized TonB dependent transporter (TBDT), the inner membrane associated Proton Motive Force (PMF) components, ExbB/ExbD and energy transducer, TonB were found to be associated with OPH (Gudla et al., 2019).

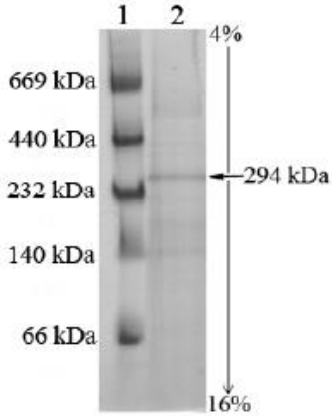

Fig.5: Purification of OPH complex. Analysis performed by a BN-PAGE (4%-16% acrylamide). Lane 1 shows molecular size markers. IMAC purified OPH complex is shown in Lane 2.

1.8. TonB dependent transport system-iron acquisition:

Iron acts as a cofactor for innumerable proteins involved in many intricate cellular processes (Miethke & Marahiel, 2007). The expression of bacterial iron acquisition systems is stringently regulated in response to iron, being increased under iron limitation (Litwin & Calderwood, 1993). So as to adapt to iron deprivation, many bacteria have evolved several sophisticated strategies to scavenge iron from the environment. The most common strategy is the synthesis and secretion of siderophores which are low-molecular weight molecules that bind iron with high affinity in the extracellular milieu and re-enter cells using specific membrane transporters (Schaible & Kaufmann, 2004; Tanabe et al., 2005; Hider & Kong, 2010; Kurth et al., 2016; Lin et al., 2017). Siderophores are classified into different classes, such as catecholate, phenolate, carboxylate, hydroxamate, and mixed-ligand type (Hider & Kong, 2010). Certain bacteria do not have genetic makeup to synthesize siderophores but can uptake

heterologous ferric siderophores which are produced by other microbial species (Venturi et al., 1995).

Gram negative bacteria rely on multiple mechanisms to scavenge iron, which is needed for their growth (Posey, 2000). One intricate mechanism is by the synthesis of TBDTs. In addition to ferric-siderophores a number of other nutrients like vitamin B12, nickel chelates, and carbohydrates are transported by TBDTs (Schauer et al., 2008). TBDTs show high affinity and specificity towards siderophores. The energy required for their transport is provided by ExbB/ExbD and TonB (Wiener, 2005; Ferguson & Deisenhofer, 2004; Postle, 2007). As iron uptake is vital for most bacteria, expression of TBDTs is tightly regulated in a variety of ways that include metal dependent regulators, σ/anti-σ factors, small RNAs and riboswitches (Noinaj et al., 2010).

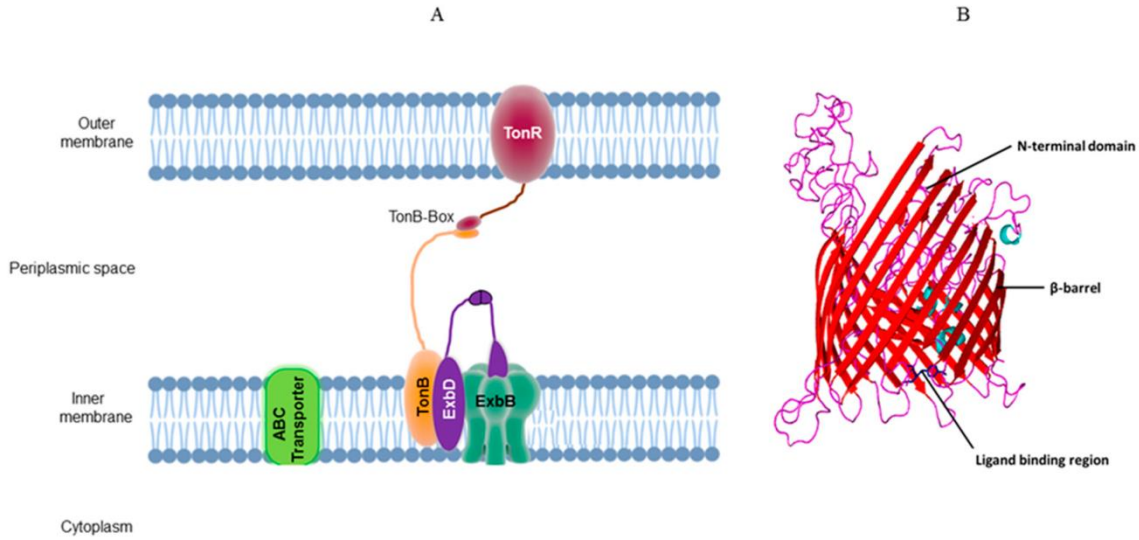

Fig.6: TonB dependent transport system. Panel A shows a schematic diagram of TonB dependent transport system. Panel B shows typical structural features of a TonB dependent outer membrane Transporter (TBDT) (Gudla et al., 2019). The 22β barrel structure, N-terminal plug domain and ligand binding domain are indicated with arrows (Samantarrai et al., 2020).

1.9. Regulation of iron uptake:

Although, iron is an essential micro-nutrient its limitation affects the cellular metabolism and its excess induces toxic effects in the cells (Winterbourn, 1995; Kehrer, 2000). Therefore, the concentration of intracellular iron needs to be strictly regulated. Bacteria follow exceptionally fine regulatory mechanisms to maintain iron homeostasis. They include both transcriptional and post

transcriptional regulation mechanisms.

1.10. Transcriptional regulation:

The regulation of iron metabolism in bacteria is typically responsive to iron availability. In many bacteria this regulation is mediated by ferric-uptake regulator (Fur). In *E. coli*, Fur protein controls the iron-dependent expression of more than 90 genes (Hantke K, 2000; Hantke, 2001). It represses transcription of iron uptake genes, upon interaction with Fe^{2+} ions and causes de-repression in its absence (Andrews et al., 2003). The binding of metal ions to Fur increases its affinity for its DNA binding site by atleast ~100-fold (Helmann, 2014). Approximately 1μM free iron is sufficient to activate DNA binding *in vitro* (Ma et al., 2012). The Fur protein is made up of a C-terminal domain (which binds to the $Fe^{2+}$to mediate the dimerization of Fur protein) and an N-terminal (DNA-binding) domain (Coy & Neilands, 1991; Stojiljkovic & Hantke, 1995). The Fe^{2+}-Fur complex binds at the promoter regions of Fur-repressed genes (Bagg & Neilands, 1985; Escolar et al., 1998).

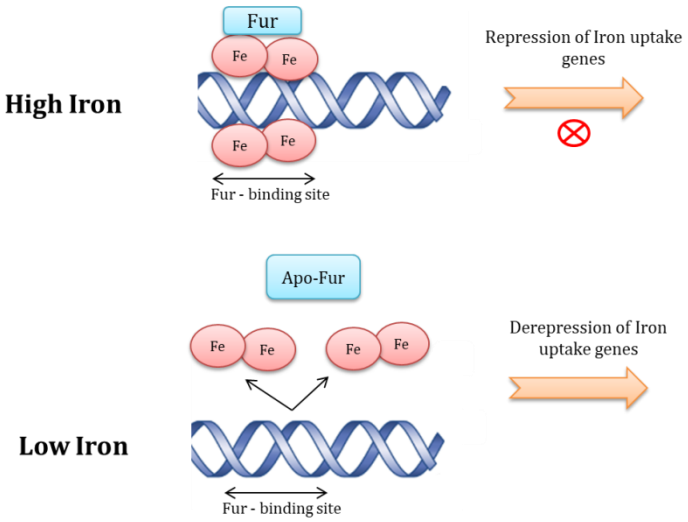

Fig.7: Schematic diagram showing gene repression mediated by Ferric uptake regulator (Coy & Neilands, 1991; Andrews et al., 2003)

1.11. Iron starvation sigma factors (σ^{19}):

In addition to the Fur dependent repression and activation, the transcription of iron responsive genes is driven by a RNA polymerase (ββ'α2ω) containing a special sigma factor, σ^{19} also known as ECF sigma factor (extra cytoplasmic

sigma factor) (Helmann, 2002; Paget & Helmann, 2003). The σ^{19} is sequestered from cytoplasm by an anti-sigma factor associated with inner membrane (Visca et al., 2002). The membrane associated anti-σ factor interacts with outer membrane located TBDT only when it binds to siderophore-iron complex (Fig.8). Such interactions stimulate phosphorylation of anti-σ factor and the phosphorylated anti-σ factor does not bind to σ^{19} thus facilitating its release into cytoplasm**.** Once available in the cytoplasm the σ^{19} associates with core polymerase and directs transcription from iron responsive genes (Koebnik, 2005; Llamas et al., 2014).

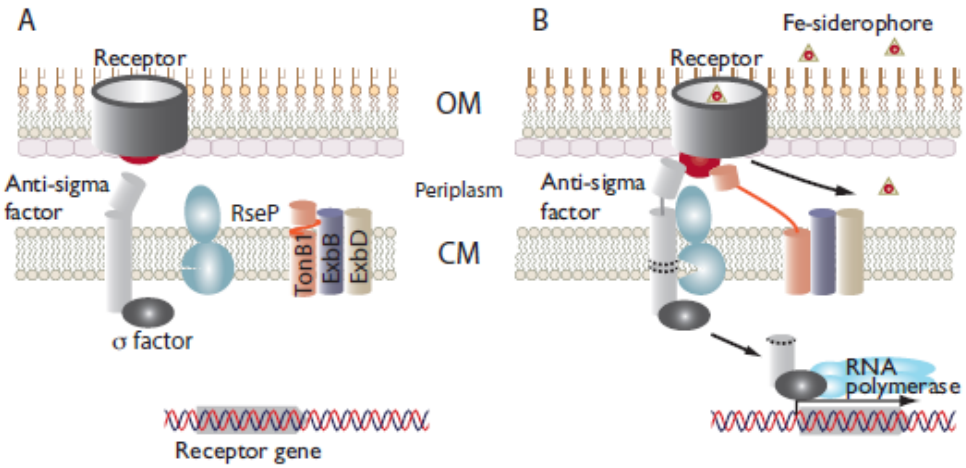

Fig.8: Mechanism of signal transduction followed by sigma factors in response to iron. Panel A shows inactive state the anti-sigma factor and the sequestered membrane associated ECF sigma factor. Panel B shows release of ECF sigma factor from membrane in the presence of ferric-siderophore. The TonB interacts with the outer membrane transporter, TBDT-ferric-siderophore and transduces signal to the anti-sigma factor. The transduced signal activates protease system which cleavages the trans-membrane domain of the anti-sigma factor. The ECF sigma factor bound to anti-sigma factor is released into the cytoplasm to activate iron responsive genes. OM, outer membrane; CM, cytoplasmic membrane (Llamas et al., 2014)

1.12. Post transcriptional regulation:

A quintessential way adapted by the bacteria to survive in various environmental conditions is by primary alteration of their gene expression, which is usually achieved by a complex interplay of molecular mechanisms (Fröhlich et al., 2018). Certain bacteria employ sRNAs to fine-tune their gene expression at the post-transcriptional level. They usually act by direct base-pairing interactions with their cognate mRNAs, which occasionally requires Hfq binding. Upon base-pairing between sRNA and target mRNAs, the translation and/or stability of

these target transcripts are affected. This leads to either repression or de-repression of gene expression (Waters & Storz, 2009). The post-transcriptional regulation of certain iron responsive genes occurs by the sRNA RyhB. The RyhB is a 90nt RNA molecule which down-regulates a set of iron- responsive genes. Under iron limiting condition, this sRNA is negatively regulated by Fur (Masse & Gottesman, 2002). The RyhB represses the mRNA of genes that are positively regulated by Fur (Escolar et al., 1999; Hantke, 2001).

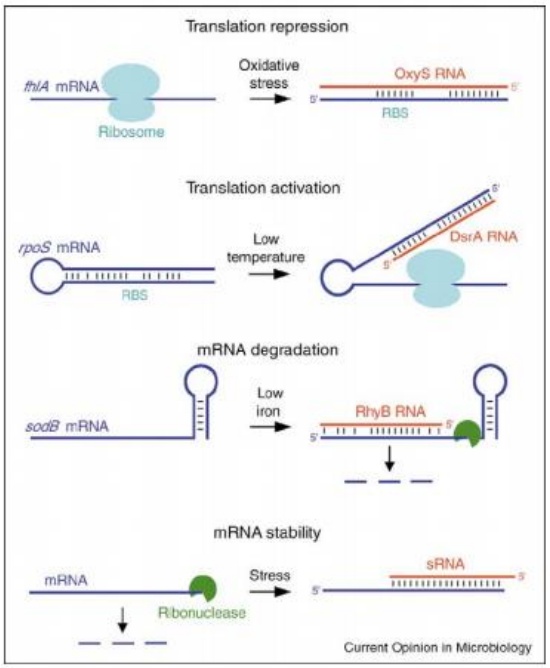

Fig.9: Different known and potential regulatory outcomes brought about by sRNA base pairing with mRNAs. sRNAs (red) can repress or activate translation by blocking or promoting ribosome binding to mRNAs (blue). sRNAs also can destabilize or possibly stabilize mRNAs by increasing or decreasing accessibility to ribonucleases (Storz et al., 2004).

1.13. Iron Responsive Elements and Iron Regulatory Proteins:

Iron-responsive elements (IREs) are conserved cis-regulatory mRNA motifs which are usually of 25-30nt in length (Theil & Eisenstein, 2000). They are located in the UTRs of mRNAs that code for proteins involved in iron metabolism. The canonical hairpin loop of an Iron response element is typically composed of a 6nt apical loop (5'-CAGWGH-3'; where W stands for Adenine or Uracil and H stands for Adenine, Cytosine or Uracil). It also consists of a stem region with five paired nucleotides and a small asymmetrical bulge (in the 5' strand) with an unpaired 'C' residue on the the stem. The stem region of an iron

response element forms base pairs of medium stability, and folds into a α-helix distorted by the presence an unpaired C8 nt (in the 5' bulge region). The base pairs found in IRE can follow either Watson-Crick or wobble pairing (U.G or G.U). The apical loop and the pseudo-triloop are separated by a conserved base pair (C14:G18) followed by an unpaired nt (N19, Fig.10). The C14:G18 base pair and the unpaired nt do not make contact with IRP, suggesting that the bridge C14:G18 serves only a structural function for IRP recognition. The pseudo-triloop and the C8 nucleotide make multiple contacts with IRP (Walden et al., 2006).

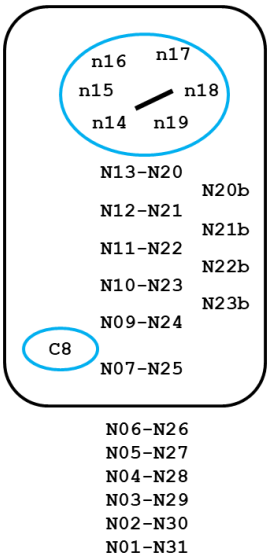

Fig. 10: Schematic diagram showing the structure of an IRE motif. The rectangular region indicates the IRE core region. The C-bulge (C8) and 6 nucleotide apical loop are shown within a blue circle. The presence of possible 3' bulge nucleotides are represented as N20b, N21b, N22b and N23b (Ricky S. Joshi, 2012) .

IRPs (Iron regulatory proteins) recognize and interact with IREs exclusively found in mRNAs coded by certain iron response genes (Khan et al., 2017; Zhou & Tan, 2017) . Aconitases are a classic example of IRPs. They are moon-lighting proteins which contain 4Fe-4S cluster for the enzymatic activity and they catalyze the inter-conversion of citrate to isocitrate in TCA cycle (Volz, 2008; Castro et al., 2019). They are bi-functional proteins that function as IRE-Binding Proteins (IRE-BP) and regulate iron metabolism and function as isoform of and enzyme catalyzing an important reaction in TCA cycle (Volz, 2008; Mande, 2011). IRPs bind to IRE located in the un-translated region (UTR) and relieve translational inhibition from the target mRNA. However, when intracellular iron

is sufficient for various cellular activities, the IRP aconitase regains its enzyme activity and functions as TCA cycle enzyme (Fig.11). The IRE and IRP mediate post-transcriptional regulation control the expression of a number of iron responsive genes. IRPs recognize iron concentration and regulate the expression of iron responsive genes, in order to optimize cellular iron availability.

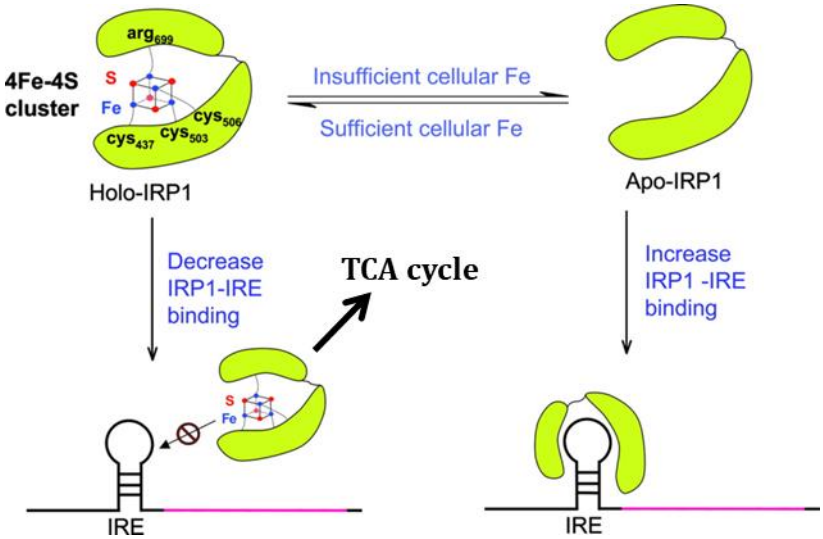

Fig.11: Moonlighting function of aconitase-IRP. The mRNA binding activity of aconitase is regulated by the presence of an [4Fe-4S] cluster, the cofactor required for aconitase activity when cellular iron levels are high; the [4Fe-4S] cluster is present in aconitase and abrogates IRP binding. Under iron-depleted conditions the [4Fe-4S] cluster is absent, and the apo-aconitase functions as IRP (E. S. Hanson. & E. A. Leibold, 1999).

1.14. Iron and catabolism of aromatic compounds:

Iron availability is an essential criterion in the oxidative breakdown of aromatic hydrocarbon compounds. This kind of degradation by microorganisms occurs through several steps of oxidation, that are catalyzed by oxygenases (Haddock, 2010; Fuchs et al., 2011). Oxygenases are grouped into monooxygenases and dioxygenases. The monooxygenases aid in the incorporation of an O2 atom from oxygen molecule into the product while reducing the second atom into H2O using e- from an external donor. While the dioxygenases incorporate both O2 atoms into the substrate (Wang et al., 2017). Degradation of aromatic compounds by dioxygenases involves ring-opening step. Most of these oxygenases (shown in Table.1) contain iron as a cofactor for the activation of oxygen (Coulter & Ballou, 1999; Dinkla et al., 2001). Iron-dependent dioxygenases can use either heme or non heme cofactors in their active site

(Ohlendorf et al., 1988). These enzymatic reactions activate certain pathways that facilitate the bacteria to use organic molecules as carbon and energy sources for their survival (Wang et al., 2017). As the availability of iron is of paramount importance in the oxidative degradation of hydrocarbons, the kinetics of this degradation might possibly be affected by iron limitation. Growth of *P. putida* on toluene is compromised under iron limiting conditions as degradation pathway involving toluene monoxygenase is affected (Dinkla et al., 2001). In support of the iron dependent activities of enzymes involved in carbon metabolism, a strong connection exists between carbon metabolism and iron uptake. Crp is a global transcriptional regulator which is involved in the metabolism of carbon. It regulates the transcription of *fur* gene which codes for the Fur protein (Lorenzo et al., 1988). Different metabolic pathways in the cells are coordinated by the functional interactions existing between these regulons (Gutierrez-Rios, 2003). Many iron responsive genes are subjected to dual control by Catabolite repressor protein (Crp) and Ferric uptake regulator (Fur). Crp regulation of Fur-controlled genes and Fur regulation of Crp-controlled genes allows the integration of signals for iron and carbon sufficiency (Zhang et al., 2005). However, the signals coordinating iron and carbon metabolism are assumed to be intricate and most of them remain to be identified.

1.15. Linkage between *opd* genes and genes coding aromatic compound metabolism:

Our lab has determined complete genome sequence of *S. wildii* and *S. fuliginis* ATCC 27551 (Parthasarathy et al., 2016; Azam et al., 2019). The ~ 5Mb genome sequence of *S. fuliginis* ATCC 27551 with a GC content of 64.4% is distributed between two chromosomes and four indigenous plasmids (Azam et al., 2019). Out of the four plasmids, designated as pSF1, pSF2, pSF3, and pSF4, only two (pSF1 and pSF2) are self-transmissible and contain the complete genetic repertoire for a T4SS. The other two plasmids (pSF3 and pSF4) are mobilizable and both showed the presence of an *oriT* and relaxase-encoding sequences. The sequence of plasmid pSF3 coincided with the previously determined sequence of pPDL2 and included an *opd* gene encoding

organophosphate hydrolase as a part of the mobile element (Azam et al., 2019; Pandeeti et al., 2012). Both of the sequences of pPDL2 and pSF3 showed exact synteny, except in the region spanning 12,680–18,619bp. This region showed the existence of 5,939bp duplication in the sequence of pSF3. This duplication was seen near the *opd* element. In this region, the *opd* and *mfhA* genes are flanked by IS21 and a duplicated Tn3. Plasmid pSF3 also contains a functional integration module that can integrate at an attachment (*attB*) site such as those typically found in integrative mobilizable elements. These two unique structural features of plasmid pSF3 strongly suggest it's involvement in the lateral transfer of the *opd* gene among soil bacteria (Pandeeti et al., 2012; Azam et al., 2019). The sequence of pSF3 contains other structural genes that code for dioxygenases involved in degradation of aromatic compounds like protocatechuate (Pandeeti et al., 2012). A ring cleavage dioxygenase (protocatechuate 4, 5- dioxygenase) encoded by *ligBA* and other genes involved in aromatic compound degradation exists as part of mobile element along with a transporter involved in transport of aromatic compounds (Fig.12).

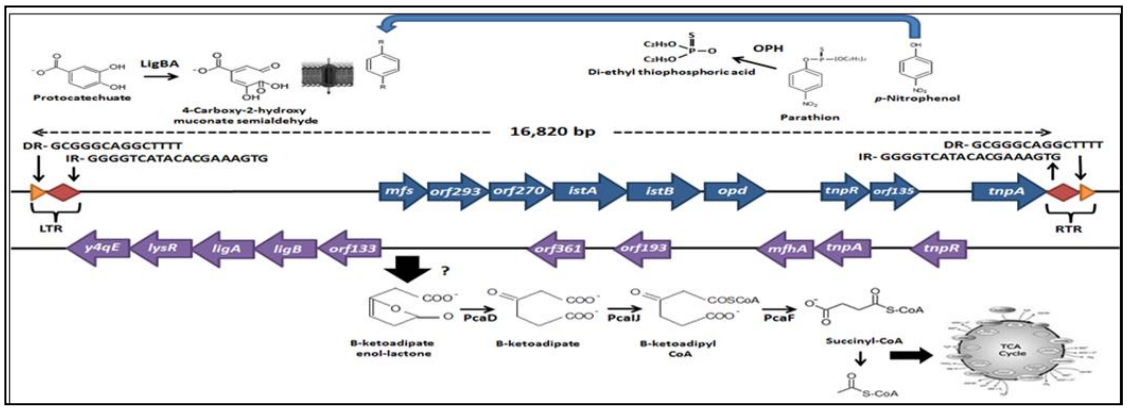

Fig.12. Linkage between integrative mobilizable element (IME) borne *opd* gene and genes coding enzymes involved in aromatic compound metabolism in *Sphinogobium fuliginis* ATCC 27551. The map indicates existence of genes involved in aromatic compound degradation as part of *opd* element. The Tn3-specific terminal repeats found upstream and downstream of transposable element Tn3 and y4qE are shown with arrows (Pandeeti et al., 2012).

Similarly, the complete genome sequence of *Sphingopyxis wildii* has indicated the presence of a single chromosome with a size of~ 4.15 Mb and two indigenous plasmids represented, pCMS1 (65,908bp) and pCMS2 (30,654bp). The self-transmissible plasmid pCMS1 contains aromatic oxygenases and ring

cleavage dioxygenases adjacent to the *opd* gene coding OPH (Fig.13). In addition to oxygenases the mobile elements contain genes coding β-ketoadipate pathway involved in complete mineralization of aromatic compounds (Parthasarathy et al., 2016).

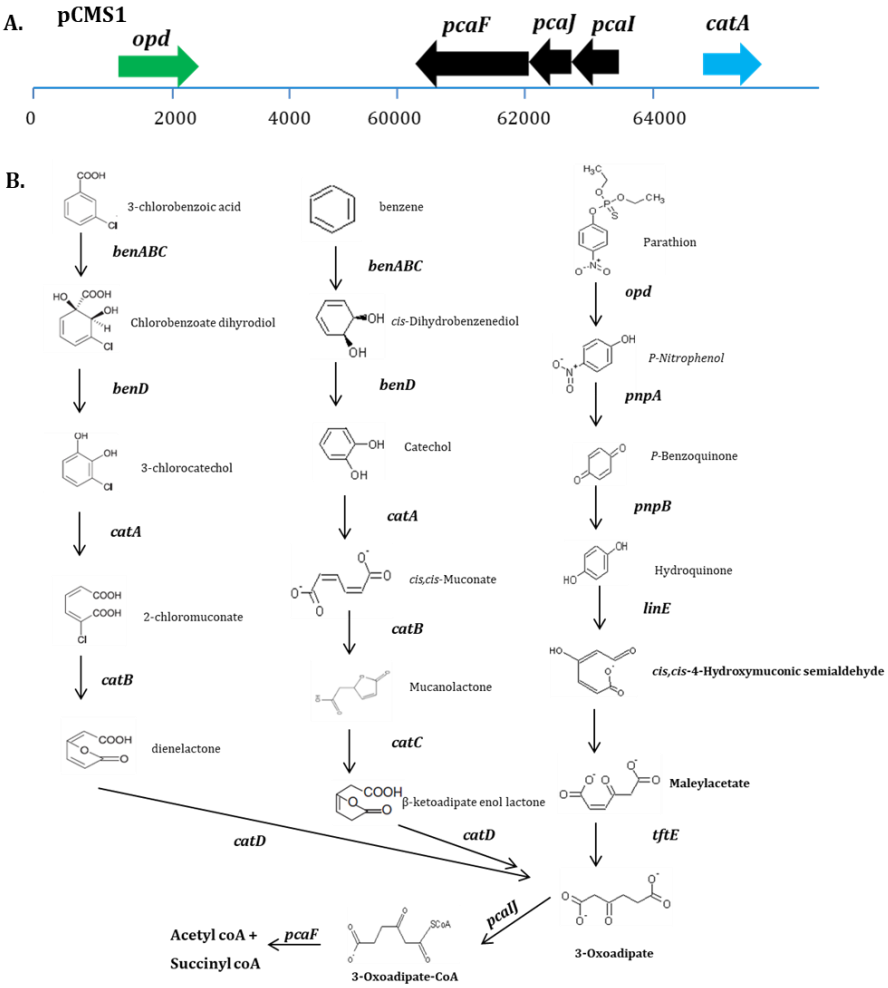

Fig.13. The link between plasmid (pCMS1) borne *opd* gene and genes coding enzymes involved in aromatic compound metabolism in *Sphingopyxis wildii.* Panel A shows the location of *opd* and genes involved in aromatic compound degradation in pCMS1. Panel B shows the degradation pathways.

1.16a. Hypothesis:

The OPH is a constitutively expressed enzyme. Available literature shows no regulation on expression of *opd* gene. However, our lab has accidentally noticed a sudden increase in expression of OPH when truncated *opd* gene coding mature form of OPH was cloned in *E. coli* expression vector (Siddavattam et al., 2006). This observation has just indicated existence of some regulatory switch at the 5' region of *opd* mRNA. We could not explain the reasons as there was no physiological reason behind the increased expression of OPH. This increase in expression was noticed only when the gene's promoter and signal peptide coding region was removed.

Our recent studies started unraveling the physiological role of OPH. As described in earlier sections of the introduction our lab has shown existence of OPH as part of Ton-complex, a primary component in TonBDT system, involved in transport of nutrients across outer membrane (Gudla et al., 2019). Since TonBDT is known to transport of Fe-Ent (ferric-enterobactin) our lab has tested to know if Fe-Ent serves as substrate for OPH. Our recent work showed interactions between OPH and Fe-Ent and suggested a role for OPH in transport of Fe-Ent (Parapatla et al., 2020). In the light of these results, we have revisited the 5' region of *opd* mRNA and tried to find a link between removal of signal peptide coding region of *opd* gene and its increased expression. Interestingly a sequence that showed very significant similarity to the well characterized IRE was identified in the region of *opd* mRNA that specifies signal peptide of OPH (Fig.14, panel A). Further examination of *opd* promoter region indicated presence of a *fur*-box motif suggesting that *opd* gene is part of iron-responsive gene (Fig.14, panel B). The proposed hypothesis is critically examined by following the below mentioned well-defined objectives, and our experimental results described in this thesis suggest, *opd* as an iron responsive gene.

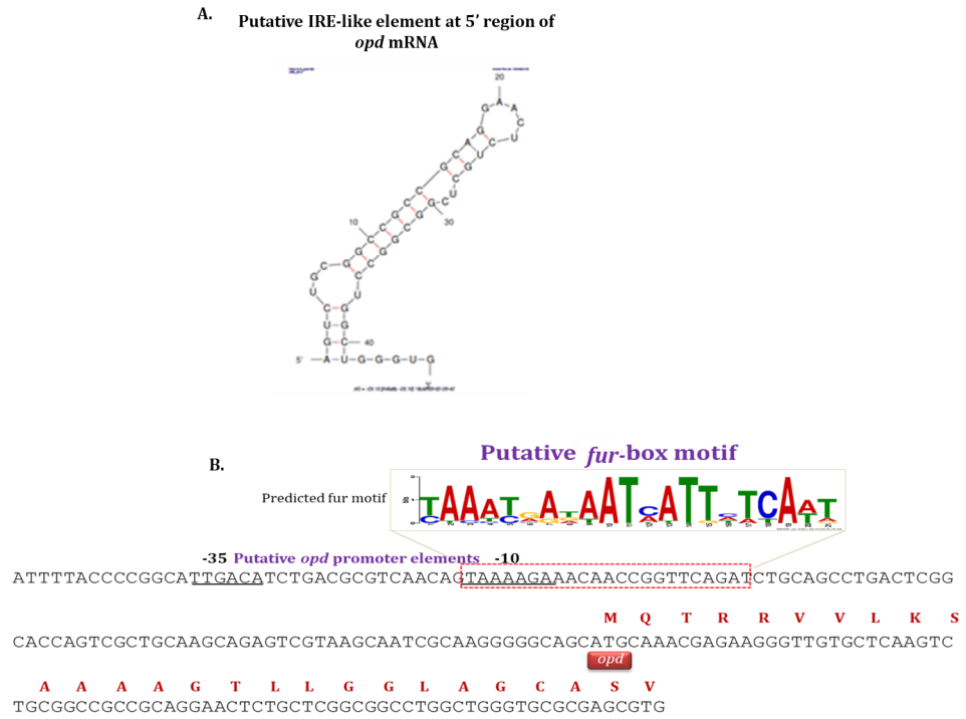

Fig. 14: Panel A shows the structure of IRE-like element identified at the 5' region of *opd* mRNA. The *fur*-box motif found overlapping *opd* gene promoter is shown in panel B.

1.16b. Objectives:

- Influence of iron on expression of *opd* gene in *Sphingobium fuliginis* ATCC 27551.
- Role of predicted *fur*-box motif in regulation of *opd* gene expression.
- Characterization of IRE-like element identified at the 5' region of *opd* mRNA and elucidation of its role in translational inhibition of *opd* mRNA.
- Elucidation of *opd* element encoded small RNA-IRE interactions and their influence on *opd* gene expression.

General Materials & Methods

Table 1 A. Antibiotics

Name of the Antibiotic	Name of the supplier
Ampicillin sodium salt	HIMEDIA
Chloramphenicol	HIMEDIA
Gentamycin	HIMEDIA
Kanamycin Sulfate	HIMEDIA
PolymyxinB	HIMEDIA
Streptomycin	HIMEDIA
Tetracycline hydrochloride	HIMEDIA

Table 1 B. Chemicals

Name of the Chemical	Name of the Supplier
Absolute alcohol	SRL
Acetic Acid (Glacial)	SRL
Acetone	SRL
Acetonitrile	SRL
Acrylamide	Sigma-Aldrich
Agar agar	HIMEDIA
Agarose	SeaKem
Ammonium chloride	SRL
Ammonium persulphate	GE Healthcare Lifesciences
Ammonium nitrate	SRL

Bovine serum albumin	HIMEDIA
β-mercaptoethanol	Sigma-Aldrich
Bromophenol blue	SRL
Butanol	SRL
Calcium chloride	SRL
Calcium nitrate	SRL
Chloroform	SRL
Ches (N-cyclohexyl-2-aminoethanesulfonic acid)	SRL
Coomassie Brilliant Blue G-250	HIMEDIA
Coomassie Brilliant Blue R-250	HIMEDIA
Cobalt chloride	SRL
Dipotassium hydrogen phosphate	Sigma-Aldrich
2, 2'-Dipyridyl	Sigma-Aldrich
Diammonium hydrogen phosphate	Sigma-Aldrich
Dimethyl sulfoxide (DMSO)	Sigma-Aldrich
Ethylenediaminetetraacetic acid (EDTA)	SRL
Ethidium bromide	HIMEDIA
Ferrous sulphate	Sigma-Aldrich
Ficoll	SRL
Glucose	HIMEDIA
Glycerol	SRL
Glycine	SRL
Glycogen	Sigma-Aldrich
Hydrochloric acid	SRL
L-Arginine	SRL

Iso-amyl alcohol	Fischer Scientific
Iso-propyl alcohol	Fischer Scientific
Isopropyl thiogalactopyranoside (IPTG)	G-biosciences
Lithium Chloride	SRL
Methyl parathion	Sigma-Aldrich
Magnesium sulphate	SRL
Magnesium chloride	SRL
Manganese sulphate	SRL
Methanol	SRL
NADP (Nicotinamide Adenine Dinucleotide Phosphate)	Sigma-Aldrich
Nickle Chloride	SRL
N,N'-Methylene bis acrylamide	GE Healthcare Lifesciences
N,N'-Dimethyl formamide	Sigma-Aldrich
Peptone	HIMEDIA
Phenol (water saturated)	SRL
Phosphoric acid	Merck
Ponceau	Sigma-Aldrich
ONPG (O-nitrophenyl-β-D-galactopyranoside)	Sigma-Aldrich
Phenol Saturated	SRL
PIPES (piperazine-N,N′-bis(2-ethanesulfonic acid)	HIMEDIA
Potassium chloride	Qualigens

Potassium hydroxide	SRL
Potassium dihydrogen ortho phosphate	Merck
PMSF	GE Healthcare Life sciences
Protease inhibitor cocktail	Sigma-Aldrich
Skimmed milk powder	HIMEDIA
Sodium acetate	HIMEDIA
Sodium carbonate	HIMEDIA
Sodium citrate	SRL
Sodium chloride	SRL
Sodium dodecyl sulfate	SRL
Sodium hydrogen orthophosphate	SRL
Sodium hydroxide	SRL
Sucrose	SRL
RNase A	Thermo Fisher Scientific
Tetra ethyl methylene diamine (TEMED)	Sigma-Aldrich
Tris-base	SRL
Triton X-100	Sigma-Aldrich
Trizol	Sigma-Aldrich
Tryptone	HIMEDIA
Tween 20	AMRESCO
X-gal	SRL
Xylene cyanol	SRL
Yeast extract	HIMEDIA

Table 1 C. Restriction enzymes and DNA modifying enzymes

Name of the Enzyme	**Name of the Supplier**
BamHI	Thermo Fisher Scientific
BglII	Thermo Fisher Scientific
EcoRI	Thermo Fisher Scientific
HindIII	Thermo Fisher Scientific
KpnI	Thermo Fisher Scientific
NdeI	Thermo Fisher Scientific
NotI	Thermo Fisher Scientific
PstI	Thermo Fisher Scientific
SacI	Thermo Fisher Scientific
SalI	Thermo Fisher Scientific
SmaI	Thermo Fisher Scientific
XhoI	Thermo Fisher Scientific
Alkaline Phosphatase	Thermo Fisher Scientific
T4 DNA Ligase	Thermo Fisher Scientific
Pfu DNA polymerase	Thermo Fisher Scientific
Phusion® High-Fidelity DNA polymerase	New England Biolabs
Polynucleotide kinase	Thermo Fisher Scientific
T1 RNase	Thermo Fisher Scientific
Taq DNA polymerase	Thermo Fisher Scientific

T4 RNA polymerase	Thermo Fisher Scientific
Calf Intestinal Phophatase	Thermo Fisher Scientific
Emerald Amp Max PCR master mix	Takara Bio
DNase-I	Thermo Fisher Scientific
RNase A	Thermo Fisher Scientific
1kb DNA Ladder	Thermo Fisher Scientific
20bp DNA ladder	Takara Bio
Unstained Protein Ladder, 10-200kDa	Thermo Fisher Scientific

2.1. Growth Media

The following growth media were prepared and used for the propagation of bacteria. The media were stringently autoclaved at 15 psi for 20min. For preparation of solid media, 2g of agar was added to 100ml of broth and sterilized. Whenever required appropriate concentrations of antibiotic and chemical stocks were added after cooling the medium to 50^0-60^0C.

2.1.1. Luria-Bertani (LB) medium

To prepare Luria-Bertani (LB) medium, peptone (10g), yeast extract (5g) and NaCl (10g) were dissolved in 1000ml of deionised H_2O. The contents of media were thoroughly mixed before adjusting the pH to 7.0 with 5 N NaOH and sterilized as described above.

2.1.2. Minimal Salts medium for *E. coli*

Minimal media for the growth of *E. coli* was prepared by dissolving 1.2g of KH_2PO_4, 4.8g of K_2HPO_4 in 1000ml of deionised H_2O. This medium was autoclaved at 15psi for 20 min. After sterilization, filter sterilized stock solutions of 10% $MgSO_4.7H_2O$, 20% $CaNO_3.4H_2O$, 1% $FeSO_4$ and 50% glucose were added to the above solution to obtain concentration of 0.2g $MgSO_4.7H_2O$ (2ml from stock), 0.04g $CaNO_3.4H_2O$ (200µl from stock) 0.001g $FeSO_4$ (1ml from stock 1% $FeSO_4$) and 2ml of 50% glucose to 1000ml of above solution to get complete minimal salts medium.

2.1.3. Minimal Salts medium for *Sphingobium fuliginis* ATCC27551

Minimal Salts medium for *Sphingobium fuliginis* was prepared by dissolving 0.5g of $(NH_4)_2HPO_4$ and 0.1g of K_2HPO_4 in 1000ml of deionised H_2O. This medium was autoclaved at 15psi for 20 min. After sterilization the solution was cooled to room temperature and stock solutions of 50% glucose, 1% $FeSO_4.7H_2O$, 1% $Ca(NO_3)_2$, 20% $MgSO_4.7H_2O$ were added in such way, so as to obtain a final concentration of 0.1% glucose, 0.001% $FeSO_4.7H_2O$, 0.001% $Ca(NO_3)_2$, 0.01% $MgSO_4.7H_2O$ to 1000ml of above solution to get complete minimal salts medium.

2.2. Preparation of iron free media and solutions

Minimal salts media and component solutions were made iron free by passing through chelex 100 resin (Bio-Rad).

2.2.1. Preparation of high iron solution

Ferrous sulphate (1%) was made by dissolving of 1g of $FeSO_4.7H_2O$ in 100ml of deionised, iron free H_2O. The stock solution was sterilized and 100µl of the above stock solution was added to 100ml of culture medium to give a final concentration of 10µg Fe/ml.

2.2.2. Preparation of low iron solution

A stock solution of 2µg Fe/ml was prepared by adding 20µl of 1% $FeSO_4$ stock solution in 20ml of deionised iron free H_2O. The stock solution was sterilized and 1ml of the stock solution was added to 100ml of culture medium to give a final concentration of 0.02µg Fe/ml.

2.2.3. Preparation of iron free glassware

The glassware was initially soaked in 2% methanolic KOH for 24hr and rinsed for 3 to 4 times with deionised H_2O and then subsequently soaked in 6N HCl for 24hr and washed with deionised H_2O. Then the iron free glassware was sterilized by autoclaving at 15psi for 20 min.

2.3. Preparation of Antibiotic & Chemical stock solutions

Ampicillin: The stock solution of ampicillin was prepared by dissolving 1g of ampicillin in 10ml of sterile deionised H_2O and filtered through 0.2µM syringe filter. This stock solution was stored at -20^{0}C. Whenever required, 10µl of stock solution was added to 10ml of medium to get a final concentration of 100µg/ml

of ampicillin in the medium.

Chloramphenicol: The stock solution of chloramphenicol was prepared by dissolving 300mg of chloramphenicol in 10ml of 70% ethanol (v/v) and filtered through 0.2µM syringe filter. This stock solution was stored at -20^{0}C. Whenever required, 10µl of stock solution was added to 10ml of medium to get a final concentration of 30µg/ml of chloramphenicol in the medium.

Gentamycin: The stock solution of gentamycin was prepared by dissolving 200mg of gentamycin sulfate in 10ml of sterile deionised H_2O and filtered through 0.2µM syringe filter. The stock solution was stored at -20^{0}C. Whenever required, 10µl of gentamycin stock solution was added to 10ml of medium to get a final concentration of 20µg/ml of gentamycin in the medium.

Kanamycin: The stock solution of kanamycin was prepared by dissolving 300mg of kanamycin sulfate in 10ml of sterile deionised H_2O and filtered through 0.2µM syringe filter. The stock solution was stored at -20^{0}C. Whenever required, 10µl of kanamycin stock solution was added to 10ml of medium to get a final concentration of 30µg/ml of kanamycin in the medium.

Polymyxin B: The stock solution of polymyxin B was prepared by dissolving 100mg of polymyxin B in 10ml of sterile deionised H_2O and filtered through 0.2µM syringe filter. The stock solution was stored at -20^{0}C. Whenever required, 10µl of polymyxin B stock solution was added to 10ml of medium to get a final concentration of 10µg/ml of polymyxin B in the medium.

Streptomycin: The stock solution of streptomycin was prepared by dissolving 200mg of streptomycin in 10ml of sterile deionised H_2O and filtered through 0.2µM syringe filter. The stock solution was stored at -20^{0}C. Whenever required, 10µl of streptomycin stock solution was added to 10ml of medium to get a final concentration of 20µg/ml of streptomycin in the medium.

Tetracycline: The stock solution of tetracycline was prepared by dissolving 200mg of tetracycline in 10ml of 70% ethanol (v/v) and filtered through 0.2µM syringe filter. This stock solution was stored at -20^{0}C. Whenever required, 10µl of stock solution was added to 10ml of medium to get a final concentration of 20µg/ml of tetracycline in the medium.

IPTG: The stock solution (1M) was prepared by dissolving 238mg of IPTG in 1ml of sterile deionised H_2O and stored at -20^{0}C. Whenever required, 10µl of the stock solution was added to 10ml of medium to get a final concentration of 1mM.

X-Gal: The stock solution of X-gal (4%) was prepared by dissolving 40mg of X-gal in 1ml of N, N'-dimethylformamide. Whenever required, 10µl of stock solution was added to 10ml of medium.

2.4. DNA manipulation:

2.4.1 Preparation of solutions and buffers

2.4.1a. TAE buffer

A stock solution of 50x TAE (Tris-Acetate- EDTA) buffer was prepared by mixing 242gm of Tris base, 100ml of 0.5M EDTA (pH 8.0) and 57.1 ml of glacial acetic acid to 900ml of deionised H_2O, after complete dissolution of the contents the solution was made up to 1000ml with deionised H_2O. Whenever required, appropriate volume of 50x TAE was diluted to obtain 1x TAE.

2.4.1.b. 6x Gel loading buffer

Bromophenol blue (12.5mg), 12.5mg of xylene cyanol FF and 7.5gm of Ficoll (Type 400; Pharmacia) were dissolved in 75ml of deionised H_2O and finally made up to 100ml and stored at RT.

2.4.1.c. Ethidium bromide

The stock solution of ethidium bromide (100mg) was mixed with 10ml of deionised H_2O, in an amber glass bottle. This solution was further diluted to get a stock concentration of 1mg/ml. While preparing agarose gel 5µl of stock solution was added to 100ml of gel solution to get a final concentration of 0.05µg/ml.

2.4.2. Solutions for plasmid isolation

2.4.2.a. Solution I: To prepare solution I comprised of 250mM glucose (10ml), 0.2M Tris pH 8.0 (6.25ml), 1 ml 0.5M EDTA (1ml) were dissolved in 25ml sterile deionised H_2O and finally the volume was made upto 50ml with sterile deionised H_2O. This solution was autoclaved for 20 min at 15psi on liquid cycle and stored at 4^{0}C. Whenever required stock solution of DNase free RNase A was added at a final concentration of 100µg/ml.

2.4.2.b. Solution II: Equal volumes of 0.4N NaOH and 2% SDS solutions were

freshly mixed and used as Solution II.

2.4.2.c. Solution III (3M sodium acetate pH 4.8): To prepare Solution III, 24.61g of CH_3COONa was dissolved in 80ml of sterile deionised H_2O and its pH was adjusted to 4.8 with glacial acetic acid. Then the volume was made upto 100ml and stored at 4^0C.

2.4.2.d. Phenol chloroform solution: Phenol chloroform was made by mixing equal volumes of water saturated phenol and chloroform.

2.4.2.e. Chloroform: Isoamyl alcohol solution: Chloroform (96ml) and Isoamyl alcohol (4ml) were mixed and stored in amber colour bottle at 4^0C.

2.4.2.f. TE buffer: Working solution of TE buffer was prepared by adding 5ml of 0.2M Tris-Cl, 0.2 ml of 0.5M EDTA to 80ml of deionised H_2O and finally upto 100ml. This solution was autoclaved and stored at 4^0C.

2.4.3. Isolation of plasmid DNA

Plasmid isolation was done by alkaline lysis method following standard procedures (Birnboim & Doly, 1979). A single colony containing desired plasmid was inoculated into 3ml LB medium substituted with required antibiotic and was incubated for 12h at 37^0C with shaking. Bacterial cells were harvested from a 1ml of overnight culture by centrifuging the culture at 13,000 rpm for 1 minute. The pellet was then resuspended in 100µl of TEGL by vortexing it vigorously. This was mixed with 200µl of solution-II (freshly prepared) (equal volume of 1% SDS, 0.2N NaOH) and incubated on ice for 4 to 5 min before adding 150µl of ice-cold solution-III (3M CH_3COONa, pH 4.8). The contents were then thoroughly mixed by inverting the tube. Then tube was kept on ice for 3-5 min. The contents were centrifuged at 13,000 rpm for 10 min. The supernatant was then transferred into a fresh eppendorf tube and extracted with equal volumes of phenol chloroform and later with chloroform: isoamyl alcohol (24:1). The clear aqueous phase was again transferred to a fresh eppendorf tube and the plasmid DNA was precipitated by adding $1/10^{th}$ volumes of 3M CH_3COONa, pH 4.8 and 2 volumes of ethanol and tubes were incubated at -80^0C for 20 min. The plasmid was collected by centrifugation at 13000rpm for 20 min. The traces of salts in the plasmid were removed by washing with cold 70% ethanol. The plasmid was

further dried and redissolved in 30µl of TE.

2.4.4. Purification of plasmids using QIAgen Mini preparation kit method

Plasmid DNA was purified using QIAgen mini preparation kit. The overnight culture obtained from growing a single bacterial colony carrying plasmid, was centrifuged at 13000 rpm for 1min and the supernatant was discarded. The pellet was resuspended in 250µl of buffer P1 and was lysed by adding 250µl of buffer P2 prior to mixing the tubes by inverting them 4-6 times. After lysis of the cells the contents were neutralized by adding 350µl of buffer N3 prior to mixing of the contents by inverting immediately. Then tubes were centrifuged for 10 min to pellet down the debris. After centrifugation the supernatant was transferred into a QiAprep column placed in a collecting tube. The supernatant was allowed to pass through the column for 1 min by centrifuging at 13000 rpm. The column was washed with 750µl of wash buffer (PE). Finally, the DNA was eluted from column by adding 50µl buffer EB, followed by brief centrifugation at 13000 rpm. The plasmid DNA was stored at -20^{0}C until further use.

2.4.5. DNA Quantification

The quantification of nucleic acids was done spectrophotometrically by using a Nano Drop ND-1000 system. About 1µl of sample were pipetted on the sample pedestal and the absorbance peak of nucleic acid in the sample was measured at 260nm. Protein contamination in the sample was estimated by measuring the 260/280 ratio of approximately 1.8 considered as pure for DNA. In addition, the nucleic acid purity can be further determined by measuring the ratio of absorbance at 260nm/230nm, which typically results in values between 1.8 to 2.2 for nucleic acid samples without contaminants.

2.4.6. Agarose gel electrophoresis

A slab of 0.8% agarose was prepared by adding 0.8 g of agarose in 100ml of 1XTAE and boiling for 3 min. This molten agarose was allowed to cool to approximately 45^{0}C, and 0.5ug/ml of etbr was added. This whole mixture was poured into the casting unit along with 1mm thickness comb, and allowed to solidify. The solidified gel is then then kept in electrophoresis tank and filled with 1X tank-buffer (~ 300ml) keeping the wells towards anode side. DNA

samples were carefully loaded into the wells and were separated by performing electrophoresis applying constant voltage (100V). The molecular size markers were mixed with loading dye (1Kb ladder) and loaded adjacent to the wells used to load DNA samples and the size of unknown DNA was measured based on electrophoretic mobility.

2.4.7. Polymerase Chain Reaction (PCR)

PCR amplification reactions were carried out in a 25µl reaction volume contained 2.5mM $MgCl_2$, dNTP mix containing 200µM each of dATP, dCTP, dGTP and dTTP mix , 10 picomoles of each forward primer (FP) and reverse primer (RP), 1.0U of *pfu* DNA polymerase, 10-20ng of plasmid or 40-80ng of genomic or plasmid DNA was used as template. Amplifications were carried out in the thermal cycler (Bio-Rad) by adjusting the PCR programme as per the amplicon size and annealing temperature of the primers. Amplicons were analyzed on an 0.8-1.0% agarose gel.

2.4.8. Molecular Cloning

2.4.8.a. Restriction Digestion

Restriction digestion was carried out with the required restriction endonuclease (1.0U) in a volume of 20µl along with 2µl of 1X reaction buffer and 1.0µg DNA. In general, the reaction mixture was incubated for 2-3h at 37^0C according to the manufacturer's instructions.

2.4.8.b. Gel extraction

After separation of DNA fragments generated either by restriction digestion, or by PCR amplification; agarose gel piece containing desired DNA fragment was carefully excised and placed in a clean sterile eppendorf tube. The DNA from the gel piece was carefully extracted by using GeneJET gel extraction kit (Thermo scientific) following manufacturer's protocols. Briefly, gel piece containing DNA fragment was excised using a sterile scalpel and weight of the gel piece was measured by placing it in a clean Eppendorf tube. The gel slice was then mixed with one volume (v/w) of volume of binding buffer and the mixture was incubated at 50-60^0C for 10 min with intermittent mixing of the microfuge tube by inversion. After dissolution of the gel piece the tube was vortexed briefly

before loading loading the contents onto the column. The solubilized gel mixture (800µl) was transferred on to GeneJET purification column and centrifuged at 13000 rpm for 1 min. To the same column, 700µl of wash buffer was added and centrifuged at 13000 rpm for 1 min. The column was then placed in a clean microfuge tube and 50µl of elution buffer was added to the column and centrifuged at 13000 rpm for 1 min. The eluted DNA was stored at -20^{0}C until further use.

2.4.8.c. Dephosphorylation of vector

The digested vector DNA used in ligation was dephosphorylated with FastAP Thermosensitive Alkaline Phosphatase (Thermo scientific) to prevent self-ligation. Dephosphorylation reaction was performed in a 20µl reaction mix containing 1µg of vector and 1X buffer supplied by the manufacturer. The reaction was initiated by adding 1.0U of alkaline phosphatase. The contents were incubated at 37^{0}C for 10 min before inactivating the alkaline phosphatase by heating the reaction mixture at 80^{0}C for 20 min. The dephosphorylated vector was then stored at -20^{0}C until further use.

2.4.8.d. DNA Ligation

The gel extracted vector and insert DNA were subjected to ligation by using T4 DNA ligase (Thermo scientific) and incubated at 22^{0}C for at least 12hr according to the manufacturer's instructions. About 100ng of total DNA with a molar ratio (vector**:** insert) of 1:3 was used in ligation reaction. The following equation was used to calculate the appropriate amounts of DNA.

$$mass_{insert}[ng] = \frac{mass_{vector}[ng] \times size_{insert}[bp]}{size_{vector}[bp]} \times 3$$

2.5. Gene transfer methods

2.5.1. Transformation

The competent cells were initially thawed by placing them on ice. The ligation mixture/plasmid of interest was added and incubated on ice for 30 min. After 30 min, the cells were subjected to heat shock at 42^{0}C for exactly 1 min 30 sec and immediately chilled on ice for 2 min. Further, 750µl of LB broth was added and

incubated at 37^0C for 45 min. The cells were collected by centrifugation and resuspended in 70µl of LB broth and plated on required selective LB media. When needed 2% X-gal and 1mM IPTG was added along with required antibiotic. The plates were then incubated at 37^0C for more than 12h for colonies to appear.

2.5.2. Electroporation

Cells were harvested from mid log phase cultures and made electro-competent by washing and incubating them on 10% ice cold glycerol. About 1 to 2µg of DNA was added to 100µl of electro-competent cells. The suspension was mixed by flicking the tube. The cells/DNA mixture was placed in a pre-chilled cuvette, between the electrodes and a pulse of 2.5 kV was applied for 4-5 sec using Genepulser (Bio-Rad, USA). Following the pulse, immediately 1 ml of autoclaved SOC medium [tryptone (2%), yeast extract (0.5%), NaCl (1mM), KCl (2.5mM), $MgCl_2$ (1mM), $MgSO_4$ (10mM), glucose (20mM)] was added to the cells. The cells mixed in the broth were taken in a 1.5ml tube and incubated at 37^0C for 1 hour with constant shaking. After the incubation period, the cells were diluted appropriately in SOC medium and plated on LB agar plates containing appropriate antibiotics.

2.6. Protein Methods:

2.6.1. Solutions for SDS-PAGE

2.6.1.a. Acrylamide mix Solution: Acrylamide stock solution (30%) was prepared by mixing 30g of acrylamide and 0.8g of N, N'- methylene-bis-acrylamide in 70ml of deionised H_2O. After the contents were dissolved completely the volume of the solution was made up to 100ml and stored at 4^0C.

2.6.1.b. Resolving gel buffer: Tris base (181.71gm) was dissolved in 800ml of deionised H_2O and pH was adjusted to 8.8 by adding 30ml of conc. HCl. Then the volume was made up to 1000ml with deionised H_2O. The contents were autoclaved and allowed to cool to room temperature. SDS was added to the buffer to a final concentration of 0.3% by mixing adequate amounts of SDS stock solution. The prepared resolving buffer was then stored at room temperature until further use. When required the stock was used to get a final concentration of 390mM Tris-HCl, pH 8.8.

2.6.1.c. Stacking gel buffer: Tris base (121.14g) was dissolved in 800ml of deionised H_2O and the pH was adjusted to 6.8 by adding 42ml of conc. HCl and finally the volume of the buffer was made up to 1000ml with deionised H_2O. This solution was autoclaved and allowed to cool to room temperature. SDS (0.4%) was used in preparation of stacking buffer. The prepared resolving buffer was then stored at room temperature until further use. When required the stock was used to get a final concentration of 130mM Tris-HCl, pH 6.8.

2.6.1.d. 2x SDS gel loading buffer: Stock solution of 2x SDS loading buffer was prepared by mixing 1ml of 1M Tris-Cl pH 6.8, 2g SDS, 10mg of bromophenol blue and 10ml of glycerol in 25ml of deionised H_2O and kept at 45^0C for 10 min for complete solubilization of SDS. To this reagent 0.699ml of β-mercaptoethanol was added and finally made up to 50ml with deionised H_2O. The loading dye was then distributed in 10ml aliquots and stored at -20^0C. While running protein samples on SDS-PAGE, equal volume of this buffer was added to the protein sample, the contents were then boiled for 5 min before loading on to the gel.

2.6.1.c. Staining solution: 0.25g of coomassie brilliant blue (R-250) was dissolved in 50ml of methanol. To this solution 15ml of acetic acid was added and finally made up to 100ml using deionised H_2O.

2.6.1.e. Destaining solution: Methanol (30ml) is mixed with 10ml of glacial acetic acid before making up the volume to 100ml using deionised H_2O. The destained gels were stored in 7% acetic acid solution.

2.6.2. Solutions for Protein Estimation:

2.6.2.a. Standard BSA: Stock solution (10mg/ml) of BSA (Bovine serum albumin) was prepared by dissolving 10mg of BSA in 0.17M NaCl. This solution was stored at -20^0C.

2.6.2.b. Bradford's reagent: Bradford's reagent was prepared by dissolving 10mg of coomassie brilliant blue G-250 in 50ml of 95% ethanol and adding 10ml of 85% (w/v) *ortho*phosphoric acid was added. After complete solubilization of the dye the solution was made up to 100ml with deionised H_2O. Finally, the reagent was filtered and stored in an amber bottle at 4^0C until further use. While preparing standard graph appropriate amounts of BSA stock solution was added

to various tubes containing 1 ml of Bradford's reagent to get a final concentration of BSA in the range of 2, 4, 6, 8, 10µg. The contents were then adjusted to 1.1ml by adding adequate amounts of deionised H_2O before storing the tubes in dark for 10 min. After completion of incubation period the OD of the reaction mix was measured at 595nm and the readings were used to prepare a standard graph was prepared by taking concentration of BSA on X-axis and OD values on Y-axis. The protein concentration in the unknown sample was measured by treating the sample in a similar manner and comparing its OD values with that the values obtained for BSA standards.

2.6.3. Solutions for Western Blotting:

2.6.3.a. Towbin buffer (protein transfer buffer): Tris-base (3.03g) and glycine (14.4g) was dissolved in 500ml of deionised H_2O. After dissolution of the contents 200ml of CH_3OH was added and volume was made up to 1000ml with deionised H_2O.

2.6.3.b. TBS-T Buffer: Tris-HCl: 1M, pH 7.6 (20ml), sodium chloride (8g) and Tween-20 (1ml) were added and volume was made up to 1000ml with deionised H_2O.

2.6.3.c. Blocking Reagent: The solution of skimmed milk powder (10%) was prepared in TBS-T buffer and was used for blocking the PVDF membrane.

2.6.3.d. Membrane stripping solution: Membrane stripping solution was prepared by dissolving 1.5g of glycine, 0.1g of SDS and 1ml of tween 20 in 100ml of deionised H_2O. The pH of this solution was adjusted to 2.2 with 6N HCl.

2.6.3.e. Primary antibody solution:

Primary antibody solution (2µl) of either anti-His mouse antibody (Amersham Biosciences) or Anti-OPH antibody was added to 10 ml of blocking reagent to get a titre of 1:5000 and used for probing the proteins transferred onto PVDF membranes.

2.6.3.f. Secondary antibody solution:

The secondary antibody solution of anti-mouse goat antibody (2µl) conjugated with HRP was added to 10 ml of blocking reagent to get a titre of 1:5000 and used as secondary antibody solution.

2.6.3.g. Ponceau S reagent: Ponceau salt (100mg) was dissolved in 100ml of 5% acetic acid.

2.6.3.h. Semi-Dry Western Blotting

After protein samples were separated by SDS-PAGE, the gel was soaked in Towbin buffer for 5 min. Meanwhile, PVDF membrane (Amersham Hybond-ECL, GE healthcare) was soaked in methanol for 10 min. Two layers of pre-soaked filter paper (in towbin) were placed on the positive electrode of the transfer apparatus and the transfer membrane and the gel were sandwiched between two additional layers of filter paper on top. The transfer membrane was facing the negative electrode at the bottom of the transfer apparatus, while the gel was placed on top. The apparatus was assembled according to the instructions by the manufacturer and the transfer was performed at 18V for 40 min in the transfer apparatus. After transfer of the proteins, the membrane was blocked in 10% skimmed milk suspension in TBST at room temperature for an hour, or at 4^0C overnight, with shaking at 60 rpm. After blocking, the membrane was incubated with primary antibody solution using an appropriate dilution for 1h at room temperature with gentle shaking. The membrane was washed with TBST for 10 min and, if appropriate, incubated with the secondary antibody at the correct dilution for 1h with shaking. The membrane was finally washed three to five times with TBST.

2.6.4. Protein Precipitation:

The protein sample was mixed with two times the sample volume of methanol, one sample volume of chloroform and three times the sample volume of deionised H_2O. The precipitated sample was centrifuged at 13000 rpm for 5 min and the upper layer was discarded. It was washed with three sample volumes of methanol and centrifuged at 13000 rpm for 5 min. The supernatant was carefully removed and the pellet was air dried. The pellet obtained was finally resuspended in 2x Laemmli buffer or any other buffer of choice.

2.7. Enzyme assays and preparation of reagents:

2.7.1. Reagents for β-galactosidase assay

Z buffer: The Z-buffer **(**pH 7.0) was prepared by dissolving 40mM Na_2HPO_4,

60mM NaH_2PO_4, 10mM KCl, 1mM $MgSO_4$ and 50mM β-mercaptoethanol. This solution was stored at 4^0C until further use.

ONPG (*ortho*-Nitrophenyl β-galactoside) substrate solution: About 400mg of ONPG was dissolved in 100ml of phosphate buffer prepared by dissolving $Na_2HPO_4.7H_2O$ (1.61g) and $NaH_2PO_4.H_2O$ (0.55g) in 90ml deionised H_2O (pH 7.0). This solution was then transferred to an amber bottle and stored at 4^0C until further use.

Stop solution: Sodium carbonate (1M) was prepared by dissolving 12.4g of sodium carbonate in 100ml of deionised H_2O.

2.7.2. β-galactosidase activity assay:

This assay was performed by the protocol described by (Miller, 1972). About 500µl of culture was taken from a 10ml culture and cells were harvested by centrifuging at 6000rpm for 10min. Then supernatant was discarded and the pellet was resuspended in same volume of chilled Z-buffer. The harvested cells were then permeabilized by adding 100µl of choloroform, 50µl of 0.1% SDS and mix the cells by vortex and kept at 28^0C for 5 min. After incubating at 28^0C, the volume of the reaction mixture was made up to 1ml using Z-buffer. In order to initiate the reaction 0.2ml of ONPG (4mg/ml) was added to the cell suspension. The samples were incubated at 28^0C until the faint yellow color is developed. The reaction was stopped by adding 0.5ml of 1M sodium carbonate solution. The time length of incubation was recorded. The reaction mixture was then centrifuged at 13000rpm for 1min and 1ml of clear supernatant was taken to check the absorbance at 420nm and 550nm. The β-galactosidase activity was measured by monitoring the yellow color (due to the release of *ortho*-nitrophenol) from substrate ONPG. The β-galactosidase activity was calculated by using the below given formula and the specific activity was represented as Miller units.

$$\text{Miller Units} = \frac{1000\text{x}\ [(\text{OD420}-1.75\text{xOD550})]}{\text{TxVxOD600}}$$

Where,

T = time gap between addition of ONPG and addition of sodium carbonate

solution in min

V = volume of the culture added to the reaction mixture

A600 = OD_{600} (of the culture)

A420 = OD_{420} (of the reaction mixture)

2.7.3. Reagents for Methyl parathion activity assay

CHES buffer: CHES buffer (200mM) was prepared by adding 4.15g of CHES to 80ml deionised H_2O at pH 9.0. The solution was made up to 100ml with deionised H_2O.

Substrate solution: Methyl parathion stock (0.1M) was prepared by dissolving 26.3mg methyl parathion in 1ml of methanol. This solution was stored at 4^0C until further use. Whenever required, 200µM of the solution was used from the substrate stock.

Assay Buffer: The activity assay buffer contains 20mM CHES, pH 9.0 and 50µM $CoCl_2$.

2.7.4. Parathion Hydrolase Activity Assay:

The Reaction mixture contained methyl parathion (200µM) in 20mM CHES buffer (pH 9.0) (1ml). The reaction mix was incubated at 37^0C for 30 min. An increase in the absorbance at 410nm was determined, due to formation of *p*-nitrophenol (Chaudhry et al., 1988). The concentration of *p*-nitrophenol formed was determined using the extinction coefficient of PNP (17500/M/cm).

$$\text{Activity} = \frac{\text{Absorbance at 410nm}}{\text{17500 (Extinction coeff. of PNP at 410nm)}}$$

Specific activity = µM/mg of protein/min

Chapter-I

Background:

As stated in introduction, OPH exists as a membrane associated multi-protein complex in *Sphingobium fuliginis* ATCC 27551. It's associated proteins are the components of outer membrane transport system, also known as TonB dependent transport (TonBDT) system. TonBDT system comprises of an outer membrane transporter (TonR), and inner membrane localized energy transducer TonB, and proton motif pump components (ExbB/ExbD). The OPH physically interacts with ExbB/ExbD and TonB (Gudla et al., 2019). The outer membrane transport system plays a key role in acquisition of various nutrients, including ferric enterobactin (Fe-Ent). The OPH interacts with ferric enterobactin by binding to an unique site located distinctly away from the active site (Parapatla et al., 2020). Work done in our lab has recently demonstrated involvement of OPH in accelerating iron uptake. The *S. fuliginis* TonBDT system ($_{Sf}$TonBDT) reconstituted in *E. coli* has shown OPH dependent increase in iron uptake (Parapatla et al., 2020). Based on these observations the sequence of the *opd* gene, coding OPH, is carefully examined to identify *cis*-elements that respond to intracellular iron concentration. Experiments described in the first chapter are performed to identify regulatory elements such as *fur*-box and Iron Response Element (IRE) in the sequence of *opd* gene and *opd* mRNA.

3.1. Objective specific methodology:

Table 3.1: Primers used in this study

Primer Name	Sequence (5'-3')	Explanation
5' RACE Outer FP	GCTGATGGCGATGAATGAACACTG	Adapter specific outer forward primer used while performing 5' RACE.
NS1 RP	ATAGGACCGCGCACGGTATTGATCC	*opd* specific outer reverse primer used while performing 5'RACE.
5' RACE Inner FP	CGCGGATCCGAACACTGCGTTTGCTGGC TTTGATG	Adapter specific inner forward primer used while performing 5' RACE.
NS2 RP	TTTGCATGCTGCCCCCTT	*opd* specific inner reverse

		nested primer used while performing 5'RACE.
NS3 FP	AATTCGCATTGACATCTGACGCGTCAACAGTAAAAGACTGCA	Forward (FP)/ Reverse primers (RP) to generate core *opd* promoter.
NS3 RP	GTCTTTTACTGTTGACGCGTCAGATGTCAATGCG	
NS4 FP	AATTCTAAAAGAAACAACCGGTTCACTGCA	Forward (FP)/ Reverse primers (RP) used to generate partial *opd* promoter.
NS4 RP	GTGAACCGGTTGTTTCTTTTAG	
NS5 RP	CCGTAATGGGATAGGTCACGTTGG	*lacZ* specific Reverse primer used for sequencing of promoter fusions
NS6 FP	AACGAGAAGGGTTGTGCTCAAGTC	Forward primer used to perform real time PCR to quantify the transcripts of *opd*
NS6 RP	TGTGCTCGTGAGTCAGTGTGAAA	Reverse primer used to perform real time PCR to quantify the transcripts of *opd*
NS 7 FP	ACGGACGCTAATACCGGATGA	Forward primer used to perform real time PCR to quantify the transcripts of *16s* rRNA
NS 7 RP	GTACTGTCATTATCATCCCGGG	Reverse primer used to perform real time PCR to quantify the transcripts of *16s* rRNA

Table 3.2: Strains used in this study

Strain Name	Genotype or Phenotype	Reference
E. coli DH5α	*λsupE*44, Δ*lacU*169 (*Δ80 lacZΔM*15) *hsdR*17 *recA*1 *endA*1 *gyrA*96 *thi*1 *relA*1	(Hanahan, 1983)
Sphingobium fuliginis ATCC 27551	Wild type strain, Sm^r, PmB^r, *opd+*	(Kawahara et al., 2010; Sethunathan & Yoshida, 1973)

Table 3.3: Plasmids used in this study

Plasmid Name	Construct description	Reference
pTZ57R/T	Amp^r, TA vector used for cloning of PCR products	Thermo Scientific
pMP220	Tet^r, promoter probe vector	(Spaink et al., 1987)

pNS1	Amp^r, generated by cloning 5' RACE product	This study
pNS2	Tet^r, generated by cloning full length promoter region of *opd* as *EcoR*I-*Pst*I fragment in pMP220	This study
pNS3	Tet^r, generated by cloning partial promoter region of *opd* as *EcoR*I-*Pst*I fragment in pMP220	This study

3.4.1. *In silico* studies:

The potential promoter and regulatory motifs present upstream of *opd* were predicted by using Bprom (Solovyev Victor and Salamov Asaf, 2010) and MEME Suite (http://meme-suite.org/tools/meme) respectively. While predicting *opd* promoter, 500 bps upstream sequence of *opd* gene starting from the translation start site was submitted to the webserver. The tool predicts promoter elements based on the conserved promoter motifs. To identify the presence of sequence motifs that serve as binding sites to any iron regulatory transcriptional factors, the entire *opd* gene along with its predicted promoter was given as input to MEME Suite. Further analysis was done to identify regulatory sequences/structures found in mRNA by using Mfold (http://www.mfold.org/) (Zuker, 2003) and SIREs (http://ccbg.imppc.org/sires/) (Campillos et al., 2010).

3.4.2. Growth and expression analysis of OPH under differential iron concentration:

The expression of OPH was analyzed under varying iron concentrations. Prior to performing the expression studies all the glassware and the minimal media used for growth was made iron free by following procedures described in general methods section. The culture of *S. fuliginis* was inoculated in LB broth with polymixin B (10µg/ml) and incubated in a shaker at 30^{0}C. The cells at OD_{600} of 0.5-0.6 were harvested and sub-cultured in minimal media containing sufficient iron (10µg Fe/ml) to facilitate acclimatization. The cells were harvested and re-inoculated in iron sufficient and limiting (0.02µg Fe/ml) media at an Optical density of 0.05. The cell growth was analyzed for 72h (Fig 3.5.2). Equal number

of cells was taken from both conditions and OPH protein expression was analyzed by carrying out western blot using anti-OPH antibodies.

3.4.3. Absolute quantification of *opd* transcripts

The quantification of *opd* specific transcripts was done by performing qPCR. The cultures of *S. fuliginis* were grown as described above under iron sufficient and limiting conditions. The total RNA was isolated from equal number of cells and the isolated RNA was used to synthesize cDNA. Eppendorf qPCR machine operating with Realplex 2.2 software was used to perform qPCR using 30 ng cDNA template, 0.25 μM primers, and Brilliant SYBR Green reagents (Biorad). To quantify the expression levels of *opd* gene the amplicon (~150bp) was cloned into pTZ57R/T vector. In a similar way *16S* rRNA gene was also cloned, which served as an internal control. Using the constructs as template, a 10 fold dilution series was made resulting in a set of standards containing 10^2-10^7copies of the target gene. The standards and test samples were assayed in the same run. A standard curve was constructed, with the logarithm of the initial copy number of the standards plotted along the X-axis and their respective CT values plotted along the Y-axis. Data were normalized to *16s* rRNA and analysed by absolute quantification by comparing the CT value of the test sample to a standard curve. Finally, the copy number of *opd* in test sample was obtained by interpolating its CT value against the standard curve.

3.4.4. Rapid Amplification of cDNA Ends (RACE):

The RACE experiments were performed using the FirstChoice® RLM-RACE Kit (Ambion Life technologies) to validate a predicted promoter and to determine transcription start site of *opd* gene. The RNA was extracted from *S. fuliginis* cells grown to an OD of 1 in LB following the trizol method of RNA isolation described elsewhere in the thesis. The total RNA was isolated and its integrity was checked by analyzing it on agarose gel. Then it was treated with DNase I to obtain RNA free from DNA. The purity of RNA was confirmed by performing PCR reaction using *opd* specific primers. After confirming that the isolated RNA is free from

DNA contamination, it was used to perform 5' RACE experiment. Initially, 10µg of DNase treated RNA was dephosphorylated by with 1.0U of Calf Intestinal Phosphatase (CIP) for 1 h at 37^{0}C. The reaction was terminated and the RNA was extracted using acid phenol: chloroform (3:1) and then with chloroform. Later it was precipitated using cold isopropanol and 70% ethanol. The pure RNA obtained was resuspended in nuclease-free water. Subsequently, it was treated with Tobacco Acid Pyrophosphatase (TAP) and incubated at 37^{0}C for 1h. Then a 45-mer RNA adapter was ligated to the 5' end by adding T4 RNA ligase to the TAP treated RNA and incubated for 1 h at 37^{0}C. The adapter-ligated RNA was then reverse transcribed before incubating at 42^{0}C for 1 h. The cDNA thus synthesized was subsequently used to amplify the 5' end of *opd* transcript by performing an outer 5' RLM-RACE PCR (which uses adapter-specific outer forward primer and gene-specific outer reverse primer). Then a Nested PCR was performed by using inner 5' RLM-RACE PCR (which uses adapter-specific inner forward primer and gene-specific inner reverse primer). The amplicon obtained was cloned in pTZ57R/T vector and the recombinant plasmid was designated as pNS1. This plasmid was subjected to sequencing using adapter-specific primer to establish the transcription start point of *opd.*

	Stage	Reps	Temp	Time
Initial denaturation	1	1	94^{0}C	3 min
Amplification	2	35	94^{0}C 60^{0}C 72^{0}C	30 sec 30 sec 30 sec
Final Extension	3	1	72^{0}C	7 min

3.4.5. Construction of transcriptional fusions:

The transcriptional fusions of *opd* with a *lacZ* reporter, were constructed by cloning promoter elements of *opd* in pMP220 (promoter test vector). The complementary oligos containing full length (NS3FP/NS3RP) and partial (NS4FP/NS4RP) promoter regions were annealed independently. These set of self-complementary oligos appended with *Eco*RI and *Pst*I were annealed, then ligated with pMP220 digested with the similar enzymes. Post-ligation, the transformants obtained after transformation of the ligation mixture into *E. coli*

DH5α were selected on LB plates supplemented with required amounts of the tetracycline and X-gal. The recombinant colonies were screened for the presence of insert by performing sequencing reaction using NS5RP. The resulting *opd-lacZ* fusions containing full length promoter and partial promoter were designated as pNS2 and pNS3 respectively.

3.5 Results:

3.5.1. Transcriptional regulation of *opd* gene:

The *in silico* studies performed using Bprom tool have predicted the presence of promoter hexameric sequences at -10 (TAAAAG) and -35 (TTGACA) regions. These promoter hexamers have shown resemblance with the consensus *E. coli* promoter sequences. Interestingly the MEME Suite has detected the existence of a putative *fur*-box motif, overlapping the predicted -10 hexameric sequence of *opd* promoter (Fig. 3.5.1, panel A).

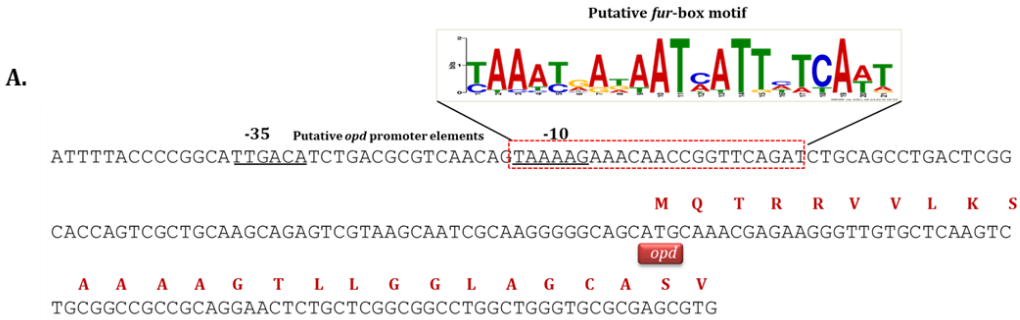

Fig.3.5.1. Prediction of the *fur*-box motif and promoter elements of *opd* gene. The putative promoter elements are underlined. The putative *fur*-box motif overlapping the -10 promoter hexamer is highlighted in a dotted red box.

3.5.2. The *opd* gene exists as a part of iron regulon:

After gaining insights through *in silico* studies further experiments were conducted to assess if *opd* existed as a part of iron regulon. Initially *S. fuliginis* cells were grown under iron limiting and iron sufficient conditions. As shown in Fig.3.5.2 the cells have grown slowly under iron limiting condition. This is rather expected growth phenotype and this type of growth pattern is commonly seen in all most all bacteria when grown under iron limiting conditions.

The culture grown under these two physiological conditions were then

harvested and the levels of OPH expression determined by performing western blot. The protein profile found in cells grown under iron limiting and iron sufficient conditions are shown in Fig.3.5.3 panel A. There exists no visual difference in protein profile of the cells grown under these two physiological conditions. However, the western performed using anti-OPH antibodies has shown at least two-fold increase in expression of OPH under iron limiting condition, suggesting that expression of OPH is induced under iron limiting condition (Fig.3.5.3, panel B). Further experiments were conducted to assess whether the enhanced OPH production is due to increased transcription of *opd* gene. An absolute quantitative real-time PCR was performed to quantify *opd* specific transcripts in cells grown under iron sufficient and iron limiting conditions. Interestingly a three-fold increase in *opd* specific transcript was found in cells grown under iron limiting conditions when compared to the cells grown under iron sufficient conditions suggesting that there is an increased transcription of *opd* gene in cells grown under iron limiting condition (Fig.3.5.3, panel C).

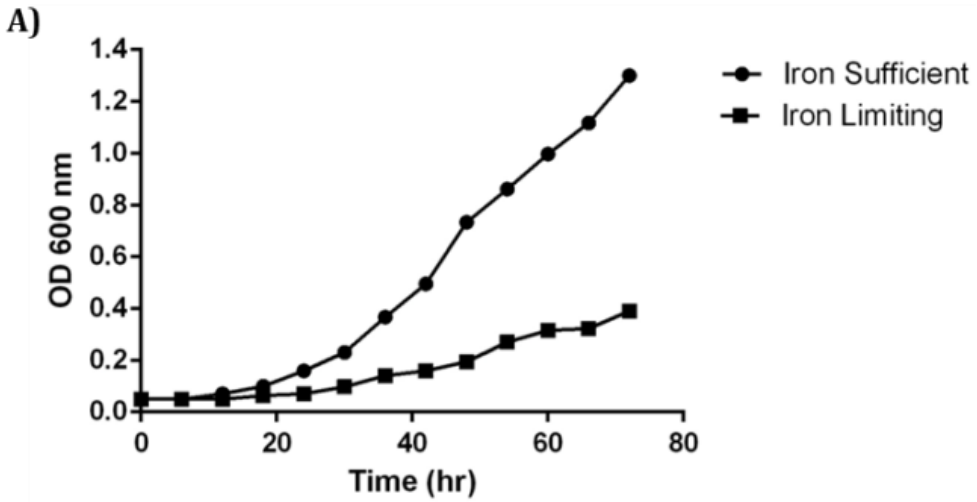

Fig.3.5.2. *S. fuliginis* growth under iron sufficient and limiting conditions

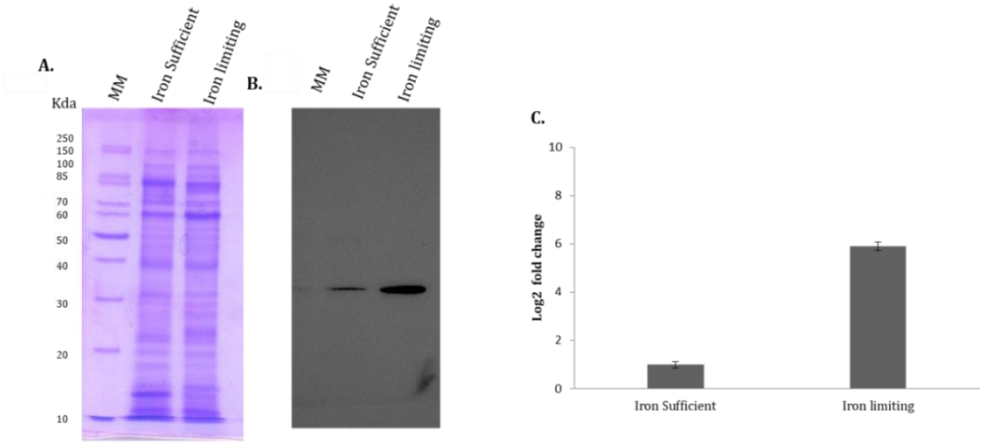

Fig.3.5.3. Influence of iron on the expression of OPH. Panel A indicates 12.5% SDS-PAGE profile of soluble proteins extracted from the cell grown in iron sufficient (lane 2) and limiting conditions (lane 3). The molecular size markers are loaded in lane 1. The corresponding western blot probed with anti-OPH antibodies is shown in panel B. Increase in expression of OPH in cells grown under iron limiting condition (lane 2) is seen as an increase in the intensity of OPH specific signal. The quantitative real-time PCR profile is shown in panel C. Increase (three-fold) in *opd* specific transcript is seen in cells grown under iron limiting conditions.

3.5.3. Determination of transcription start site (TSS) of *opd*:

The *in silico* studies have indicated existence of a promoter motif upstream of *opd*. The functional status of this predicted promoter was validated by performing both *in vitro* and *in vivo* studies. Initially, the 5' RACE was performed to determine exact TSS of *opd* gene. The transcriptional start site analysis was carried out as described in methods section described in this chapter. A~100 bp amplicon was obtained from a PCR with the adapter-specific forward and *opd* specific inner reverse primer (Fig.3.5.4, panel B). This amplicon was then cloned and the resulting recombinant plasmid, pNS1 was subjected to sequencing using adapter specific primer. The sequence of RACE specific amplicon is shown in Fig.3.5.4, panel D. The sequence when read from 5' to 3' direction clearly shows sequence of the adapter primer ligated to the *opd* mRNA. The adapter specific sequence was then followed by *opd* gene sequence and it started with 'T' suggesting that the transcription from *opd* gene is initiated from the T residue. Interestingly, the promoter hexamers predicted using *in silico* tools were exactly -10 and -35 base pairs upstream of the TSS suggesting that both *in silico* and *in vitro* studies are in total agreement in identifying the promoter motif of *opd* gene.

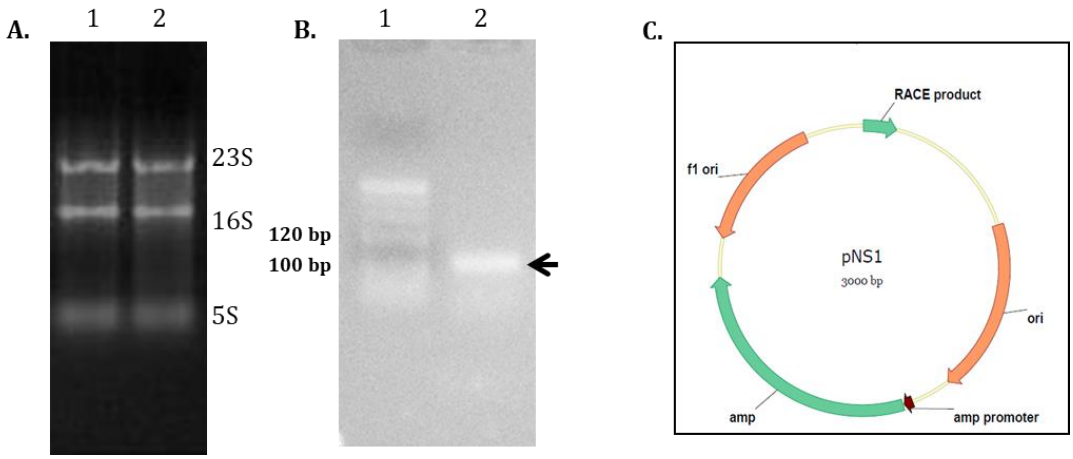

Fig.3.5.4. Detection of 5' RACE product. Panel A indicates 1% formaldehyde showing the integrity of the isolated RNA from *S. fuliginis* cells. Panel B. Agarose gel (2.5%) showing the amplicon obtained after performing nested PCR reaction. The 113bp amplicon is shown with a black arrow. Panel C shows the plasmid pNS1 map indicating the cloning of RACE product in vector pTZ57R/T.

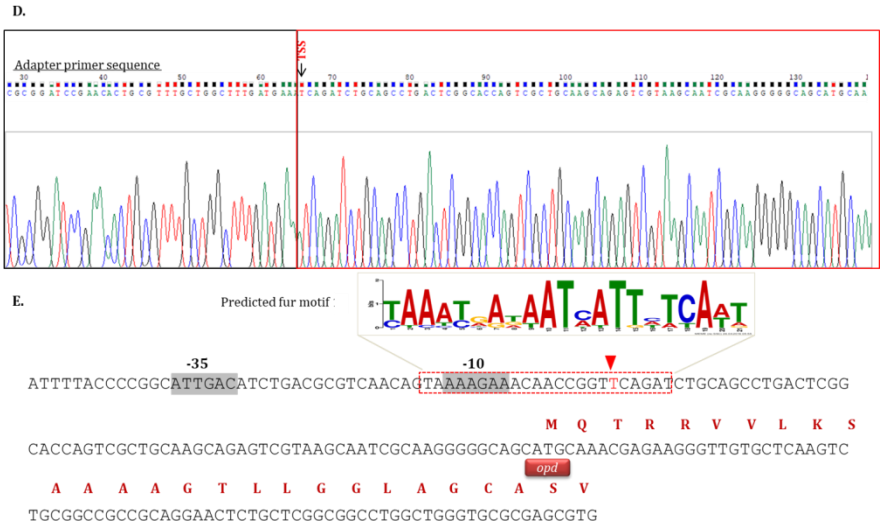

The sequence of RACE product. Panel D indicates the sequence chromatogram of the RACE product. The adapter specific sequence and sequence corresponding to *opd* gene are indicated with black and red colored boxes. The TSS of *opd* gene is indicated by an inverted black arrow. Panel E shows the *opd* gene sequence showing TSS (shown with an inverted red triangle) and promoter and putative *fur*-box motif. The sequence shown with grey shade indicates -10, -35 hexamers of the promoter. The predicted *fur*-box motif is shown in red dotted box.

3.5.5. Functional validation of *opd* promoter:

The promoter motif mapped following the determination of transcription start site was validated by performing *in vivo* studies. The *opd-lacZ* fusions were constructed by including both -35 and -10 promoter hexamers. The resulting plasmid pNS2 contains the core promoter of *opd* gene fused to promoter-less

lacZ gene of pMP220 (promoter test vector). Another *opd-lacZ* fusion, pSN3 was generated by fusing partial promoter (only -10 hexamer) of *opd* gene to *lacZ*. The construction strategies followed while generating *opd-lacZ* fusions are shown in Fig.3.5.5. The sequence of the *opd-lacZ* fusions were determined to assess proper cloning of *opd* promoters in promoter test vector. After ascertaining proper construction of promoter fusions, the plasmids pSN2 and pSN3, were transformed independently into the *E. coli* DH5α cells along with vector pMP220. These cells were then used to assay promoter activity by measuring the β-galactosidase. Initially the cells containing promoter fusions were plated on X-gal containing LB plates along with control culture having empty vector. As shown in Fig.3.5.5.a, panel A only cultures having full length promoter-*lacZ* fusion (pNS2) turned into blue color. The cells containing empty vector or containing *opd-lacZ* fusion generated by cloning only -10 hexamer remained pale in color suggesting lack of *lacZ* activation in these cells. Further quantification of β-galactosidase activity in these cells reconfirmed the results obtained through qualitative assays. As shown in Fig.3.5.5.a, panel B, 157 units of β-galactosidase activity were found in cells containing pNS2 as against to 36 units obtained in cells harbouring pNS3. These results indicate that the promoter element determined through 5' RACE is functional.

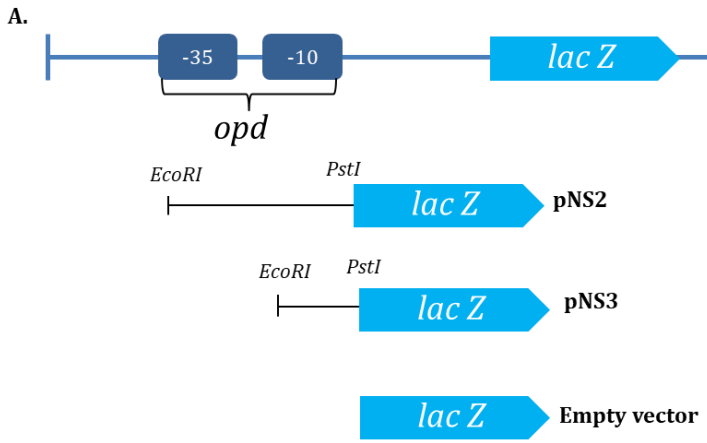

Fig.3.5.5. Construction strategy of *opd-lacZ* fusions

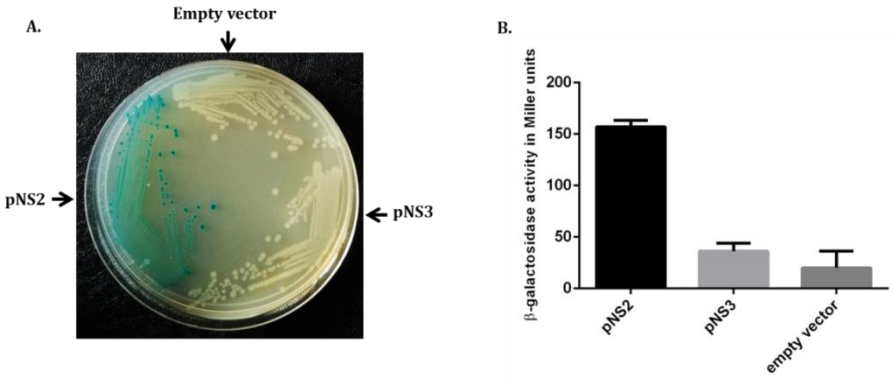

Fig.3.5.5.a. Activity of the *opd* gene promoter. Panel A indicates qualitative β-galactosidase activity assay. Panel B shows the histograms indicating β-galactosidase activity as Miller units in *E. coli* DH5α cells transformed with pNS2, pNS3 and empty vector, pMP220.

3.5.6. Post-transcriptional regulation of *opd* gene:

Further investigation was carried out using Mfold and SIREs web server to identify the presence of regulatory elements that contributes for the post-transcriptional regulation of *opd* gene. Interestingly, a structural element that matches with the structure of Iron Response Element was identified in the 5' coding region of *opd* mRNA (Fig.3.5.6). An IRE molecule comprises of a single stem-loop and a bulge region (Walden et al., 2006). IREs have been identified in a variety of prokaryotes and eukaryotes, but their validations have been limited to eukaryotic (ferritin and transferrin receptor) mRNA (Walden et al., 2012). As a similar structure was identified in *opd* gene, attempts were made to elucidate base-pairing interaction among the predicted IREs by using dot-bracket notation (Mattei et al., 2014). This was performed with the aid of RNA secondary structure prediction web server (https://rna.urmc.rochester.edu/RNAstructureWeb/). Fig.3.5.1B, shows base pairing interaction of the stem-loop region of *opd* IRE, in which symbol '.' codes for an unpaired base and symbol '( )' for an open base pair. This clearly shows the conservation of stem-loop structured IREs, in various mRNAs coding for proteins involved in iron metabolism.

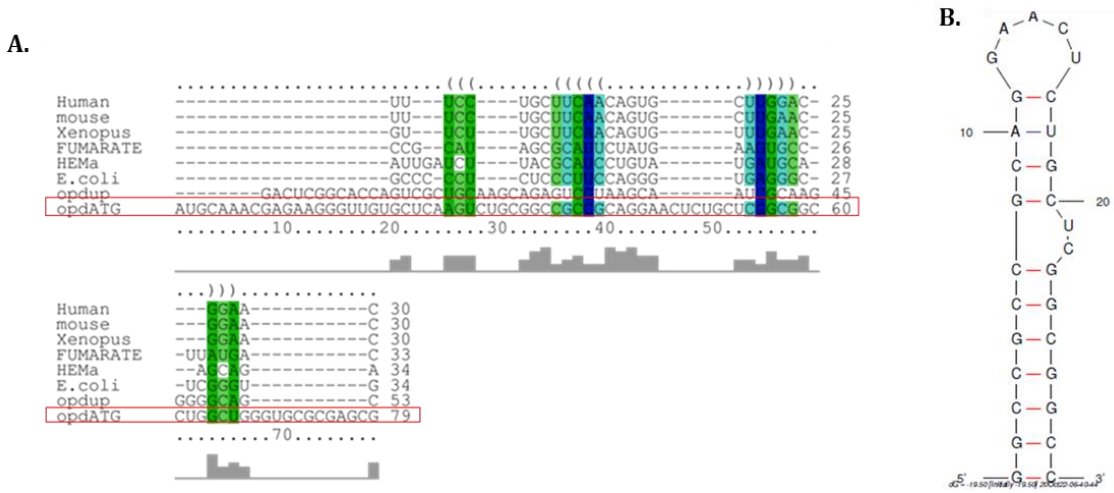

Fig.3.5.6. Structure of IRE-like element identified in *opd* mRNA. Panel A indicates structural comparison of IRE elements identified in prokaryotic and eukaryotic m RNAs. The *opd* mRNA which forms similar IRE-like secondary structure is highlighted in red box. The IRE-like structure formed at the 5' coding region of *opd* mRNA is shown in panel B.

3.6. Discussion:

Iron is indispensable for cell growth and survival for most bacteria. Organisms respond to environmental cues such as iron availability, by regulating the expression of many gene clusters as an iron stimulon, with the help of various transcriptional regulators (Baichoo & Helmann, 2002). Ferric uptake regulator (Fur), is one of the best characterized master regulator of iron-dependent gene expression (Hantke, 2001; Quatrini et al., 2005). Fur is a DNA binding protein that interacts with consensus motif known as a *fur*-box. It utilizes Fe^{2+} as a corepressor and blocks the target gene transcription (Bagg & Neilands, 1987).

In addition to Fe^{2+}, DNA binding by Fur can be activated by other divalent metal ions *in vitro* (Bagg & Neilands, 1987; de Lorenzo et al., 1987; Ochsner et al., 1995; Mills & Marletta, 2005; Gao et al., 2008). The *fur*-box motifs are typically located in proximity of the −10 and/or −35 σ_{70} promoter elements of target genes (Escolar et al., 1999). It consists of a 19-bp inverted repeat consensus sequence (5' GATAATGATAATCATTATC 3') in *E. coli* (de Lorenzo et al., 1987). Fur protein typically binds to the target DNA that has recognizable sequence similarity to the consensus of *E. coli fur*-box motif. The Fur interacts with consensus of three hexameric repeats 5'-NAT(A/T)AT-3' regardless of

orientation and number (de Lorenzo et al., 1987; Escolar et al., 1999; Cornelis et al., 2009). Usually, *fur*-boxes have a high content of adenine and thymine bases (Berg et al., 2020).

Various bacteria show a varying range of 50 to 80% sequence identity with the consensus sequence (Baichoo & Helmann, 2002; Sebastian et al., 2002; Thompson et al., 2002; Ahmad et al., 2009; Pedersen et al., 2010). Canonical *fur*-box motifs have been identified in various genera such as *Legionella pneumoniae* (Hickey & Cianciotto, 1994), *Campylobacter jejuni* (Chan et al., 1995), *Pseudomonas aeruginosa* (Ochsner & Vasil, 1996), *N. gonorrhoeae* (Desai et al., 1996), *V. anguillarum* (Chai et al., 1998), *V. cholerae* (Watnick et al., 1998) and *Y. pestis* (Fetherston et al., 1999). Incomplete target *fur*-box consensus has also been identified in certain microbes (Friedman & O'Brian, 2003; Wexler et al., 2003).

A *fur*-box motif was identified, overlapping the -10 hexameric sequence and TSS of *opd* gene. The putative *fur*-box was rich in A/T bases (~ 65%). The sequence similarity between *fur*-box motif of *opd* gene was compared with the consensus *fur*-box motif found in other bacterial genes involved in regulation of iron uptake. There exists 50% identity and 82 % similarity between consensus *fur*-box motif and the predicted *fur*-box motif identified in *opd* gene (Fig. 3.6.1).

```
S.f_fur          TAAAAGAAACAACCGGTTCAGAT
E.coli_fur       GATAATGATAATCATTATC----
                  *:** .*:.*:*.  :**
```

Fig.3.6.1. Comparison of *fur*-box motif of *opd* gene with the consensus *fur*-box motif.

In most Gram-negative bacteria, including *E. coli*, Fur acts as transcriptional regulator and modulates the transcription of iron uptake genes to control cytoplasmic levels of iron (Seo et al., 2014). Fur in coordination with a novel sigma factor, otherwise known as Extra-cytoplasmic factor (ECF) modulates the transcriptional regulation of genes required for uptake of iron. Genes encoding iron starvation sigma factor are expressed constitutively along with its cognate anti sigma factor (Cornelis et al., 2009). Under iron sufficient condition they exist in inactive state. The membrane associated anti-sigma

factor sequesters the ECF sigma factor and takes it to the membrane, preventing binding of ECF sigma factor to the promoters of Fur regulated genes. When the anti-sigma factor receives an activation signal, the proteolysis mediated by RseP/MucP cleaves the trans-membrane domain of the anti-sigma factor and facilitates its release into cytoplasm. Thus activated form of ECF sigma factor interacts with core RNA polymerase and binds to the genes responsible for theuptake of iron, as Fur protein is no longer capable of binding to the Fur box in the absence of iron (Llamas et al., 2014). Under iron-sufficient conditions, the Fe^{2+}-Fur (holo-Fur) protein is active and hence can bind to *fur*-box motif, blocking access to ECF-RNA polymerase (RNAP) complex to DNA causing repression of its cognate genes but under iron deplete conditions, Fur (Apo-Fur) protein is inactive and loses the ability to bind the *fur*-box motif, exposing the promoters of gene involved in iron uptake causing de-repression of iron responsive genes (Calderwood & Mekalanos, 1988).

The experimental results described in this chapter show the presence of a *fur*-box motif overlapping the promoter region of *opd* gene. Further, the enhanced expression of OPH is apparent in *S. fuliginis* cells grown under iron limiting condition (Fig.3.5.3). Supporting this observation, the qPCR data has clearly shown existence of three fold increase in *opd* specific transcripts in cells grown under iron limiting condition. The de-repression of *opd* gene expression is very clear from the data generated through western blot and qPCR experiments. Existence of *fur*-box motif overlapping -10 promoter region if seen together with elevated transcription *opd* gene and expression of OPH clearly suggests existence of Fur mediated regulation in *opd* gene expression. Further experiments are therefore planned to elucidate the role of Fur protein in regulation of *opd* gene expression.

In eukaryotes and certain prokaryotes, iron homeostasis is mostly mediated by post-transcriptional gene control mechanisms (Martínez-Pastor et al., 2013).This kind of regulation is caused by certain stem-loop RNA structures which are approximately ~30 nucleotides long known as Iron-Response Elements (IREs) (Rouault, 2006; Muckenthaler et al., 2008). They are located either in the

5’ or 3’ untranslated regions of the mRNA. In an iron dependent manner, IREs interact with Iron Regulatory Proteins (IRPs). They regulate iron responsive genes by either activation or repression of the IRE containing mRNAs. The classical examples of eukaryotic mRNA containing IREs are ferritin and transferrin receptors (Walden et al., 2006). The cellular iron status determines the recognition and binding of IRPs to IREs. Under low iron levels, IRPs bind to IREs, but under iron excess conditions, no interaction is observed. The binding position of IRE on the transcript determines the fate of IRP-bound mRNA (Martínez-Pastor et al., 2013). The bacterial IREs have been less characterized till date yet there are few examples of IREs identified in bacteria, which have the conserved structural motif. The interactions between IRE and IRP are in the picomolar range and are strong and selective (Walden et al., 2006). The identified eukaryotic IREs contain a conserved sequence of 5’- CAGUGX -3’ in their loop region, where X can be either an Adenine, Cytosine or Uracil but never a Guanine residue (Addess et al., 1997). In eukaryotic IREs sequence of loop region and the bulge ‘C’ are critical for the interaction of IRE/IRP. Deletion or substitution of any base in the loop region, significantly reduces its interaction with the IRP (Jaffrey et al., 1993; Walden et al., 2012).

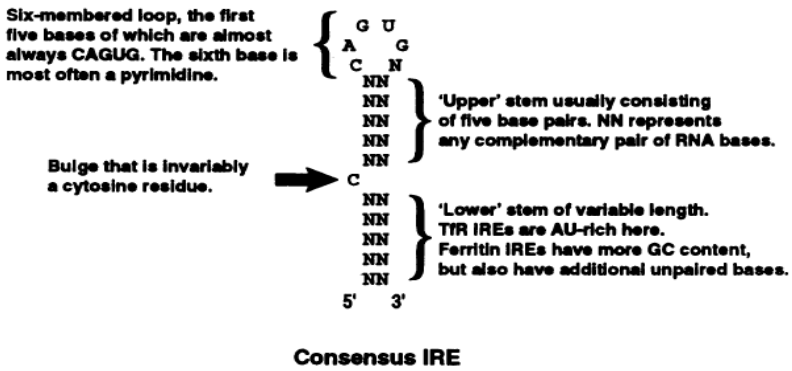

Fig.3.6.2. Consensus structure of IRE based on the IREs of known ferritin and transferrin receptor mRNAs (Jaffrey et al., 1993)

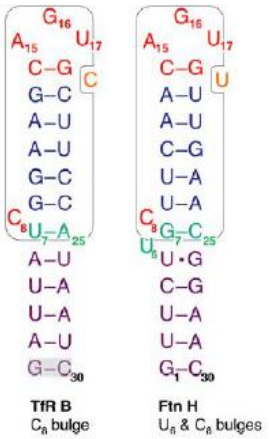

Fig.3.6.3. Secondary structures of transferrin receptor and ferritin IREs (Walden et al., 2012)

As stated earlier the bacterial IREs are not so well characterized. Therefore, an attempt was made to gain an in-depth view on bacterial IREs. The sequences and structures of 14 bacterial IREs found in Rfam database (http://rfam.xfam.org/family/RF02253#tabview=tab4) were procured and compared with the predicted IRE found in *opd* mRNA. Mapping of different bacterial IRE with *opd* mRNA, gave an idea of the sequence conservation in the critical loop region. Nearly in 12 out of 14 bacterial IREs have a 5' bulge and 6 out of 14 IREs have a 3' bulge, although nucleotide in the bulge was not necessarily a 'C'. The secondary structure of *opd* mRNA showed that the stem-loop remained unaltered even in the presence of its 5'UTR. The literature suggests that the 'C', which is present in the bulge region of IREs, is in-dispensable for the binding of IRP.

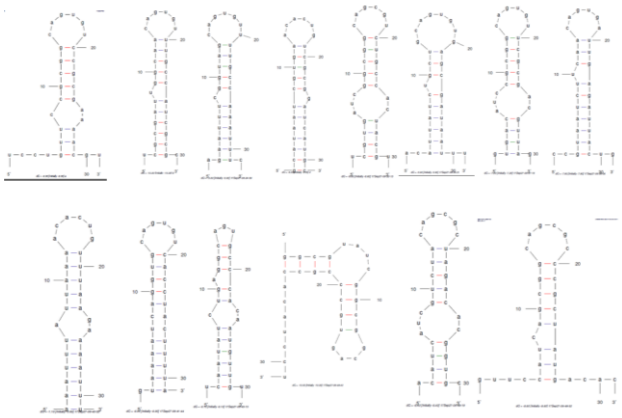

Fig.3.6.4. Predicted secondary structures of 14 bacterial IREs from Rfam

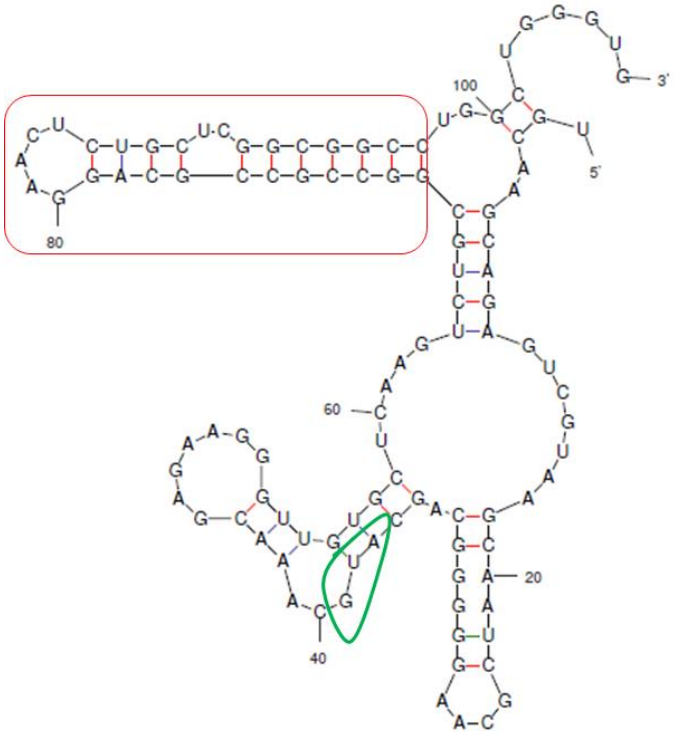

Fig.3.6.5. Predicted secondary structure of IRE-like element (*IRE*^{opd}) along with the 5'UTR region of *opd* mRNA. The *opd* start codon and IRE-like element are indicated in green and red colored boxes respectively.

Table.3.6. List of bacterial IREs retrieved from Rfam database.

S.No.	Sequence of the loop region (5'- 3')	Organism	Name of the gene controlled
1	ACACUG	*Shewanella violacea* DSS12	glutaryl-CoA dehydrogenase
		Aphanizomenon flos-aquae LD13	poly(A) polymerase
2	CAGUGU	*Arthrobacter aurescens* TC1	putative ABC transporter, ATP-binding protein
		Haematospirillum jordaniae	DNA helicase II
		Legionella sp. LegA	Transposase IS66 family protein
		Bacillus sp. FJAT-27986	lipid hydroperoxide peroxidase
		Saccharothrix sp. NRRL B-16348	Hypothetical protein

3	GCAGUGUG	Marinobacterium sp. ST58-10	Hypothetical protein
4	AGU	Rufibacter sp.DG15C	peptidase S66
5	GCAG	*Faecalibacterium prausnitzii* SL3/3	Holliday junction DNA helicase subunit RuvA
6	CAGCGC	*Natronomonas pharaonis* DSM 2160 Desulfovibrio sp. 6_1_46AFAA	Sec-independent protein translocase protein (TatC) hypothetical protein
7	CAGCGU	Lysobacter sp. Root96	hemolysin III
8	CAGUGA	*Candidatus Izimaplasma* sp. HR1	Peptidyl-prolyl cis-trans isomerase B
9	GAACU	*Sphingobium fuliginis* ATCC27551	Organophosphate hydrolase

After performing initial analysis on the structure of bacterial IREs, the sequence of loop region of *opd* IRE (5' GAACU 3') was manually compared with the IREs found in 14 different bacteria. Interestingly, four bases out of five bases found in the loop region of *opd* IRE are conserved. The first base in the loop region of bacterial IREs is majorly a purine (R). It is **'G' in *opd* IRE.** The second base had an equal propensity of being 'A' or 'C'; the ***opd IRE* has 'A'**. The third base of bacterial IREs is always a purine (R); the ***opd* IRE has 'A'**. The fourth base was pyrimidine majority of bacterial IREs (Y); the *opd* **IRE has 'C'**. Finally the fifth base in majority of bacterial IREs is a Pyrimidine (Y); interestingly, the *opd* has **'U' at this position** (Fig. 3.6.6). Further the bulge region of *opd* IRE was mapped against seven IREs having a 3'bulge. This comparison suggested that the first base in bulge region is usually a purine in all bacterial IREs, however, in *opd* IRE it is 'U'. There exists an equal propensity of 'C' or 'A' conservation in the second position of bulge region. The *opd* IRE has 'C' residue at similar position (Fig.3.6.7).

```
Loop region
1) A C A C U G - -
2) C A G U G U - -
3) G C A G U G U G
4) - - A G U - - -
5) G C A G - - - -
6) C A G C G C - -
7) C A G C G U - -
8) C A G C G A - -
9) G A A C U - - - opd
```

Fig. 3.6.6. The mapping of sequences of loop region as mentioned in table 3.6

```
Bulge region
1) G A A A
2) G G A G
3) C A C U
4) G A C G
5) A G A A
6) A C A A
7) C A C G
8) C U C G - opd
```

Fig.3.6.7. Comparison of the 3' Bulge region of IREs. The two nucleotides in 3' bulge are indicated by bold characters

The data generated in the first chapter has clearly shown i) existence of *fur*-box motif overlapping the -10 region of the *opd* promoter motif, ii) shows iron dependent transcriptional regulation and finally iii) an IRE-like element that shares structural similarity to both prokaryotic and eukaryotic IREs. Further experiments were designed to elucidate the role of *fur*-box motif and IRE-like element in regulating the expression of *opd* gene. Details of experimental design and the inferences drawn from the results are described in subsequent chapters.

Chapter-II

Background:

The objective of work described in the current chapter is to understand the functional status of predicted iron-responsive cis-regulatory elements identified in *opd* gene. In bacteria, gene regulation occurs in various levels. The initiation of gene transcription is regulated by transcriptional factors, usually transcriptional regulator proteins which modulate promoter activities. These proteins affect the expression of their cognate genes by binding to the promoter region of the genes and affecting transcription either positively or negatively. This subsequently alters abundance of their mRNAs and proteins. Besides transcriptional regulation, post-transcriptional regulation occurs through mechanisms, such as mRNA processing, regulation using riboswitches, or by antisense and small regulatory RNA (DebRoy, 2014). This kind of regulation (either transcriptional or post-transcriptional) occurs in an iron dependent manner in some bacteria and many eukaryotes.

Iron is essential as well as detrimental to cells, majorly due to production of ROS. Thus, the influx of iron into the cell and its intracellular processing is compactly regulated. This kind of regulation is carried out by the iron-dependent transcriptional regulator Fur (Ferric Uptake Regulator), in many bacteria. Fur coordinates with the concentration of intracellular Fe^{2+} and with the expression of genes involved in its metabolism (Mey et al., 2005). This effect is brought about by the cue of cytoplasmic ferrous ion concentration. The Fur protein binds to the DNA motif, otherwise known as *fur*-box identified overlapping promoter elements of iron responsive genes in an iron-dependent manner and regulates expression of iron responsive genes. The results described in previous chapter gave a *prima facie* evidence of the existence of *opd* as a part of iron regulon (Fig. 3.5.3). Further, a putative *fur*-box motif was identified in the promoter region of *opd* gene. These two observations, if seen together with the induction of *opd* gene expression under iron limiting conditions, indicate involvement of Ferric Uptake Regulator (Fur) in regulation of *opd* gene expression. The experiments described in this chapter unravel the role Fur protein in regulation of *opd* gene expression.

4.1. Objective specific methodology:

Table 4.1: Primers used in this study

Primer Name	Sequence (5'-3')	Explanation
NS8FP	AAAGAATTCCCAACTGGTACACTCTTAC	Forward and reverse primers used to amplify *fur*-box motif from *Sphingobium fuliginis.* The *EcoRI* and *XbaI* sites, appended to the primers facilitate cloning of *opd* promoter region in promoter test vector, pMP220.
NS8RP	AAATCTAGACTCTGCTTGCAGCGACTGGT	
NS9FP	AAACATATGAACCGCAAGATCGACGTCG	Forward primer used to amplify *fur* gene from *Sphingobium fuliginis*. The *Nde*I site appended to facilitate cloning of *fur* gene in pET23b vector is underlined.
NS9RP	AAACTCGAGGCTCTTGCGGTCGAGCGCGA	Reverse primer used to amplify *fur* gene from *Sphingobium fuliginis*. The *XhoI* site appended to facilitate cloning of *fur* gene in pET23b vector is underlined.
NS10 FP	TACCTGTACAATGTCCCG	Primers used to amplify *fur* region in *E. coli* MG1655 AM001
NS10RP	AGTGTACGCGTACTGGATTA	

Table 4.2: Strains used in this study

Strain Name	Genotype or Phenotype	Reference
E. coli DH5α	*λsupE*44, Δ*lacU*169 (*Δ80 lacZΔM*15) *hsdR*17 *recA*1 *endA*1 *gyrA*96 *thi*1 *relA*1	(Hanahan, 1983)
Sphingobium fuliginis ATCC 27551	Wild type strain, Sm^r, PmB^r, *opd+*	(Kawahara et al., 2010; Sethunathan & Yoshida, 1973)
E. coli Bl21-DE3	*F– ompT gal dcm lon hsdS*$_B$*(r*$_B$*–m*$_B$*–) λ(DE3 [lacI lacUV5-T7p07 ind1 sam7 nin5]) [malB+]*$_{K-12}$*(λ*$_S$*)*	(Studier & Moffatt, 1986)

E.coli NiCo (DE3)	BL21(DE3) *glmS$_{6Ala}$ slyD-CBD can-CBD arnA-CBD*	(Robichon et al., 2011)
E. coli BW25113 Δ*fur*::kan	*Δ(araD-araB)*567, ΔlacZ4787(::rrnB-3), F- *λ*-, *rph-1, Δ(rhaD-rhaB)568, hsdR514*	(Baba et al., 2006; Datsenko & Wanner, 2000)
E. coli K-12MG1655 AM001	MG1655 with *lacZ* deletion	(Madikonda et al., 2020)
E. coli NS001	Km^r. *E. coli* MG1655Δ *lac* derivative. Generated by deleting *fur* gene.	This study

Table 4.3: Plasmids used in this study

Plasmid Name	Construct description	Reference
pET23b	Amp^r. The T7 promoter driven expression vector. Facilitates expression of cloned genes with C-terminal 6xHis-tag.	Novagen
pMP220	Tet^r, promoter probe vector	(Spaink et al., 1987)
pNS4	Amp^r, plasmid generated by cloning *fur* gene of *Shingobium fuliginis* in vector pTZ57R/T.	This study
pNS5	Amp^r, Expression plasmid generated by cloning *fur* gene of *Shingobium fuliginis* in pET23b as *Nde*I and *Xho*I fragment. Codes Fur$^{C6xHis.}$	This study
pNS6	Tet^r, generated by cloning full length promoter region of *opd* along with the putative *fur*-box motif as *EcoR*I-*XbaI* fragment in pMP220	This study

4.4.1. Amplification of *fur*-box motif containing DNA:

The amplification of *opd* gene with *fur*-box motif *opd* was performed by PCR using primer set NS8FP/ NS8RP. The obtained PCR amplicon was gel excised and purified by method described elsewhere in thesis.

4.4.2. Cloning of *fur* gene:

The *fur* gene of *S. fuliginis* was amplified from the genomic DNA with NS9FP/ NS9RP having *Nde*I and *Xho*I restriction sites. The obtained amplicon was gel extracted and ligated to the easy cloning vector pTZ57R/T. Post-ligation, the

transformants obtained after transformation of the ligation mixture into DH5α were selected on LB plates supplemented with appropriate amounts of ampicillin, IPTG, X-gal. The recombinant plasmids isolated from transformants were sub-cultured and screened for the existence of insert by digesting the recombinant plasmid with *Nde*I and *Xho*I. Thus the plasmid obtained was designated as pNS4.

The *fur* gene from pNS4 was excised by digesting the plasmid with *Nde*I - *Xho*I and the excised *fur* fragment was then ligated to pET23b digested with similar enzymes. Post-ligation, the transformants obtained after transformation of the ligation mixture into DH5α were selected on LB plates having appropriate amounts of ampicillin. The plasmids isolated from transformants were sub-cultured and screened for the existence of insert and thus obtained recombinant plasmid was named as pNS5, which codes for Fur protein with a C-terminal His-tag (Fur^{C6xHis}).

4.4.3. Expression of Fur^{C6xHis}:

Following successful generation of the recombinant expression plasmid coding for Fur^{C6xHis}, the plasmid pNS5, was transformed into BL21-DE3 cells to check for the expression of Fur protein. The *E. coli* Bl21-DE3 (pNS5) was cultured till mid-logarithmic phase at 37^0C and the Fur^{C6xHis} expression was induced by supplementing 1.0mM IPTG. Cultures were subsequently incubated for 3h before analyzing the cultures to detect the expression of Fur^{C6xHis} as soluble cytoplasmic protein. Following incubation, 1ml cells were lysed by sonication with amplitude 30%, temperature 4^0C, 30 sec on and off sonic cycles. The lysate was subjected to centrifugation for 5 minutes at 13,000 rpm to get rid of debris. Clear lysate obtained was suspended in appropriate volumes of 2X loading dye and the samples were boiled and analyzed on SDS-PAGE (15%) to detect Fur^{C6xHis} by performing western blot using antibodies against His-epitope.

4.4.4. Affinity Purification of Fur^{C6xHis}:

The cell pellet obtained from 1000ml culture, after 3h induction using

1.0mM IPTG was resuspended in 10ml of 20mM Tris-HCl (pH7.8) and 300mM NaCl. After thorough resuspension of the pellet, 1mM PMSF along with 50µg lysozyme were added and this mixture was kept for lysis and vortexed at room temperature for 1h. The partially lysed cells were subjected to sonication and the cell lysate was centrifugation at 4^0C as described above. The cell-free lysate obtained was applied to the activated Ni-NTA column, pre-equilibrated with Tris-HCl (20mM, pH7.8), NaCl (300mM) and imidazole (20mM). After passing the soluble cell lysate fraction through the column matrix, column was washed with 10 CVs of 20mM Tris-HCl (pH7.8), 300mM NaCl and 50mM imidazole and eluted with different concentrations (50mM, 100mM, 200mM, 300mM, 400mM) of imidazole. The elutions were analyzed on SDS-PAGE (15%) to check the purity of the Fur^{C6xHis} protein.

4.4.5. Electrophoretic Mobility Shift Assay (EMSA): South-western blotting

The *fur*-box motif and Fur interactions were tested by performing a DNA-protein EMSA. The promoter region of *opd* including the *fur*-box motif was amplified and purified as discussed in 4.4.1. This served as the DNA component of EMSA. The typical EMSA reaction contained 0.5pmol of DNA with increasing concentration (12-32pmol) of purified Fur^{C6xHis} protein, with or without 1mM $MnSo_4$ and 2,2'-dipyridyl in binding buffer (20mM Tris (pH 7.5), 5mM DTT, 50mM $MgCl_2$, 200mM KCl, 0.5% tween20) (Fujita et al., 2020). The reaction mix was then incubated for 30min at 20^0C along with a control reaction prepared by omitting Fur protein. Following incubation, the reaction mixtures were separated on 8% non-denaturing PAGE. The resolved DNA-Fur^{C6xHis} complexes were transferred onto PVDF membrane and incubated with anti-His antibody (HRP conjugated) at RT for 1 hour. After incubation blot was developed to detect the His-tagged Fur protein in the DNA-Fur^{C6xHis} complexes.

4.4.6. Generation *fur* null mutant of *E. coli* MG1655 AM001:

Initially the *E. coli* BW25113 Δ*fur*::kan was obtained (generous gift from Dr.

Manjula Reddy, CCMB, Hyderabad) and used to generate *fur* null mutant of *E. coli* MG1655AM001 strain by following P1 Transduction method (Thomason et al., 2007).

Transduction

a) Phage P1 lysate preparation: In order to create *fur* null mutant of *E. coli*, 2.0 ml of overnight culture of donor Δ*fur*::kan from *E. coli* BW25113 strain having a mutation in *fur* gene was mixed with 0.2ml of P1 phage and incubated at 37^0C without shaking to facilitate phage adsorption. About 10ml of LB broth and sterile $CaCl_2$ (5mM) was added to this infection mixture prior to its incubation with shaking at 37^0C for 4 to 6 h or till the complete lysis of cells. After observing the cell lysis, 0.2ml of chloroform was added to the phage lysate to stop further growth of cells. This preparation was subjected to centrifugation for 10 minutes at 6000 rpm to separate cellular debris. The obtained supernatant containing transducing particles was stored at 4^0C until further use.

b) Phage infection: To the 2ml of overnight culture of *E. coli* MG1655 AM001 cells, 5mM $CaCl_2$ and 0.2ml of phage preparation was added. After addition of phage lysate, the cells were incubated at 37^0C for about 15 min to allow phage adsorption. Unadsorbed phage particles were removed by centrifugation for 10 minutes at 6000 rpm. Further 5ml of LB broth containing 10mM sodium citrate was added to the infected *E. coli* cells and allowed to incubate for 45min at 37^0C. Finally, they were harvested and resuspended in 0.2ml of LB broth and plated on LB agar plates containing 10mM sodium citrate and 50µg/ml of kanamycin. The mutation in *fur* gene was verified by PCR amplification with NS10FP/NS10RP which were designed 100bp upstream and downstream of the *fur* gene of *E. coli.* Thus obtained strain named as *E. coli* NS001, is resistant to kanamycin.

4.4.7. Construction of transcriptional fusions:

The transcriptional fusion of *opd* were generated using *lac*Z as a reporter gene The fusion, containing *fur*-box motif along with the core promoter elements of *opd* was generated by cloning it in pMP220 (promoter test vector). This region was initially PCR amplified using primer set NS8FP and NS8RP appended with

*EcoR*I and *XbaI*. The amplicon obtained was digested with respective restriction enzymes and ligated to pMP220 digested with the similar enzymes. Post-ligation the transformants obtained after transformation of the ligation mixture into *E. coli* DH5α were selected on LB plates supplemented with appropriate amounts of tetracycline and X-gal. The colonies obtained were screened using restriction digestion. The resulting *opd-lacZ* fusion including *fur*-box motif was designated as pNS5.

4.4.8. Expression of *opd* gene under *fur* negative background:

The transcriptional fusions, pNS2 and pNS5 were independently transformed into *fur* positive *E. coli* MG1655 AM001 and *fur* negative E*. coli* NS001 cells. The transformants were subjected to β-galactosidase activity assay to assess the expression of *lacZ* gene of the transcriptional fusions.

4.5.1. Results:

Gene regulatory mechanisms involve certain DNA motifs that serve as targets for transcription factors (Hutchins et al., 2013). Transcription factors interact with distinctive response elements at the promoter elements of certain genes, and affect their expression (Lee & Young, 2013). This kind of interactions can be detected by using EMSA (Garner & Revzin, 1986; Carey, 1991; Fried & Garner, 1998;). Therefore this mobility shift was exploited to elucidate the interactions between *fur*-box motif and $_{Sf}$Fur^{C6XHis}.

4.5.2. Cloning of $_{Sf}$Fur in a high copy vector:

The interactions between *fur*-box containing *opd* promoter region and $_{Sf}$Fur ^{C6XHis} were demonstrated by performing south-western blots. Initially *fur* gene from *S. fuliginis* was amplified using primer set NS9FP/NS9RP. The 423bp amplicon was checked on a 0.8% agarose gel and the excised fragment was purified before ligating it to pTZ57R/T vector. The resulting recombinant plasmid was named as pNS4 (Fig.4.5.2A panel A).

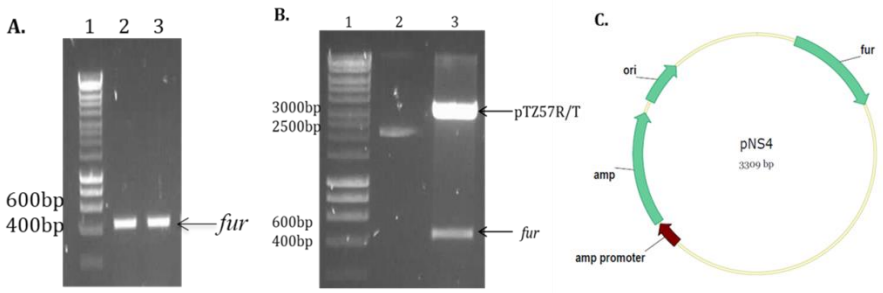

Fig.4.5.2A. Construction of pNS4. Panel A shows 0.8% agarose gel used to separate *fur* gene. Molecular size markers are loaded in lane 1. The amplified *fur* gene is loaded in lanes 2 and 3. Panel B shows image of agarose gel (0.8%) indicating the molecular marker (lane 1) undigested pNS4 (Lane 2) and pNS4 digested with *NdeI* and *XhoI*. The band corresponding to the vector and insert containing *fur* gene are shown with arrows (lane 3). Panel B shows map of pNS4.

Before proceeding to the further experiments, the *fur* gene of *S. fuliginis* was sequenced to ascertain that no mutations were inserted while amplifying the gene from the chromosomal DNA. The mutation free *fur* gene was then released from pNS4 as *NdeI*/*XhoI* fragment and ligated to the expression vector pET23b. The resulting recombinant plasmid was named as pNS5 (Fig.4.5.2B).

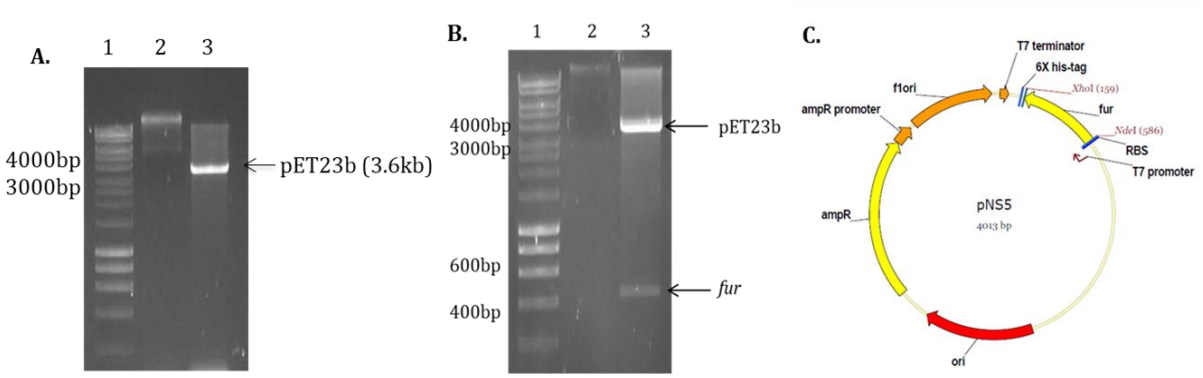

4.5.2B. Construction of pNS5. Panel A shows image of 0.8% agarose gel indicating molecular marker in lane 1, undigested pET23b vector in lane 2 and pET23b digested with *NdeI*/*XhoI* in lane 3.Panel B shows image of 0.8% agarose gel indicating molecular marker (lane 1), undigested pNS5 (lane 2) and pNS5 digested with *NdeI*/*XhoI.* The band corresponding to the vector and insert containing *fur* gene are shown with arrows (lane 3). Panel B shows map of pNS5.

4.5.3. Expression of *Sf*Fur^{C6XHis}:

The *E. coli* BL21 (pNS5) culture was grown to mid-logarithmic phase to induce expression of *Sf*Fur^{C6XHis} following procedures explained in methodology section. Proteins obtained from the harvested cells of 1 ml culture were analyzed on 12.5 % SDS-PAGE to identify expression of *Sf*Fur^{C6XHis}. As seen in Fig.4.5.3, a thick protein band (approximately 16kDa) was found only in proteins extracted from induced cultures (lane 3, Fig.4.5.3). Such band was weak in uninduced

cultures indicating over expression of $_{Sf}$Fur^{C6XHis} in BL21 cells. The western blots performed by using anti-His antibodies confirmed that the thick protein band found in induced cultures is $_{Sf}$Fur^{C6XHis} (Fig.4.5.3, panel B, lane 3).

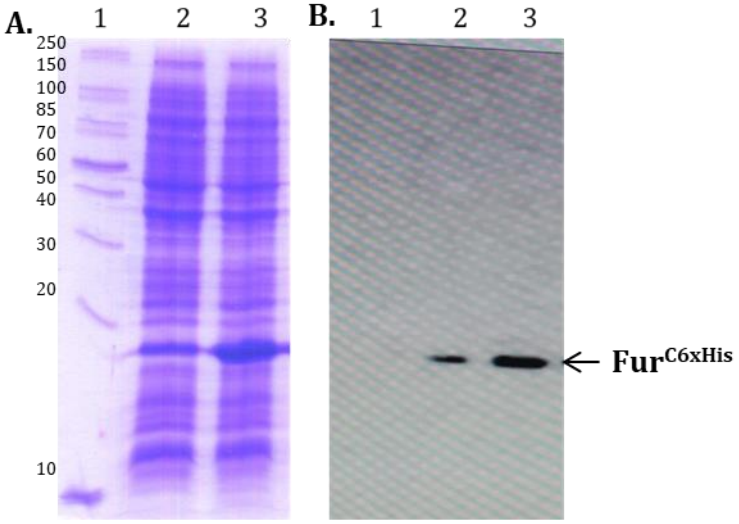

4.5.3. Expression of Fur^{C6xHis}. Panel A shows coomassie stained 12.5% SDS-PAGE to analyze the expression of Fur^{C6xHis}. Lane 1 shows the molecular marker, lane 2 shows protein uninduced whole cell lysate, lane 3 shows 3h induced protein. Panel B shows a corresponding western blot probed with anti-His antibodies to detect the expression of Fur^{C6xHis}.

4.5.4. Affinity purification of Fur^{C6xHis}:

Once the expression of $_{Sf}$Fur^{C6xHis} was standardized, the protein purification was performed using Ni-NTA matrix as described in the methodology section. The clear lysate containing $_{Sf}$Fur^{C6XHis} was obtained by inducing the expression of $_{Sf}$Fur^{C6XHis} in 1000 ml of BL21 (pNS5) cells. The clear lysate was passed through a 1.5cmx14cm Ni-NTA column at a flow rate of 1ml/minute. After passing the clear lysate through column it was washed extensively and the $_{Sf}$Fur^{C6XHis} adsorbed to the column was eluted by passing elution buffer (20mMTris and 300mM NaCl) containing various concentrations of imidazole. Each fraction was then analyzed on 12.5 % SDS-PAGE and the purity of $_{Sf}$Fur^{C6XHis} was ascertained. As shown in Fig.4.5.4, elution of $_{Sf}$Fur^{C6XHis} started with 100 mM imidazole and elution was continued till the imidazole concentration increased to 400 mM. The pure $_{Sf}$Fur^{C6XHis} was obtained when eluted using 300mM imidazole (Fig.4.5.4 Lane 8). The fractions obtained with 300 mM imidazole were pooled and the concentration of pure $_{Sf}$Fur^{C6XHis} was

determined and stored at -30^{0}C until further use.

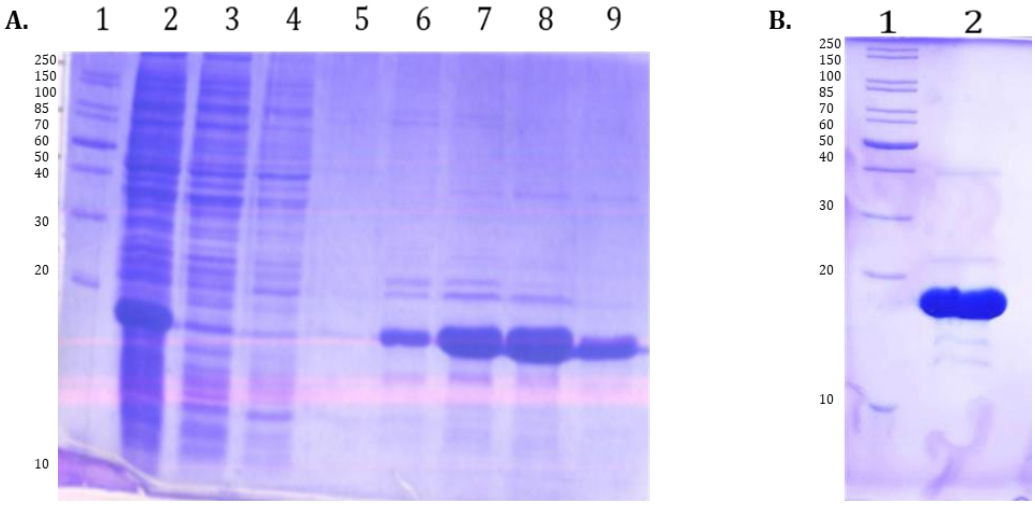

Fig.4.5.4. Affinity purification of $_{Sf}$Fur^{C6XHis}: The coomassie stained 15% SDS-PAGE (15%) showing the various stages of $_{Sf}$Fur^{C6XHis} purification. Lane 1 shows the molecular marker, lane 2 shows soluble protein fraction containing $_{Sf}$Fur^{C6XHis} , lane 3 indicates flow-through fraction, lane 4 shows wash fraction, lanes 5 to 9 corresponds to fractions obtained when eluted using 50mM, 100mM, 200mM, 300mM, 400mM. Panel B indicates the pure $_{Sf}$Fur^{C6XHis}.

4.5.5. Interactions between *opd* promoter and $_{Sf}$Fur^{C6XHis}:

There exists significant similarity between *opd fur*-box (*opd*$^{fur\text{-box}}$) and consensus *fur*-box motif identified overlapping the promoter motifs of various iron responsive genes. Therefore, initial attempts were made to perform *in vitro* assays to assess the interactions between *opd*$^{fur\text{-box}}$ and $_{Sf}$Fur^{C6XHis}. As described previously, the *opd*$^{fur\text{-box}}$ was amplified and $_{Sf}$Fur^{C6XHis} was overexpressed and purified. These two components were used to assess interactions in a metal dependent manner. South-western blots, developed by antibodies against His epitope were used to monitor the mobility shift of $_{Sf}$Fur^{C6XHis} when bound to *opd*$^{fur\text{-box}}$. The *opd*$^{fur\text{-box}}$ concentration was kept constant (0.5pm), and incubated with increasing concentrations of $_{Sf}$Fur^{C6XHis} in the presence of metal ion. A clear shift was observed when the incubation mixture was analyzed on an 8% non-denaturing PAGE indicating the formation of *opd*$^{fur\text{-box}}$-$_{Sf}$Fur^{C6XHis}. The concentration of *opd*$^{fur\text{-box}}$ -$_{Sf}$Fur^{C6XHis} complex increased with an increase of $_{Sf}$Fur^{C6XHis} indicating the formation of concentration dependent *opd*$^{fur\text{-box}}$-$_{Sf}$Fur^{C6XHis} complexes in the reaction mixture. Formation of such complexes got abrogated in the absence of metal ions. This experiment gave clear *in vitro*

evidence on the existence of specific interactions between *opd*$^{fur\text{-box}}$ and $_{Sf}$Fur^{C6XHis}. Inclusion of metal chelators in reaction mix caused dissociation of the *opd*$^{fur\text{-box}}$-$_{Sf}$Fur^{C6XHis} complex (Fig 4.5.5, Lane 9) suggesting the interactions between *opd*$^{fur\text{-box}}$ and $_{Sf}$Fur^{C6XHis} are dependent on metal ions.

8% non-denaturing PAGE

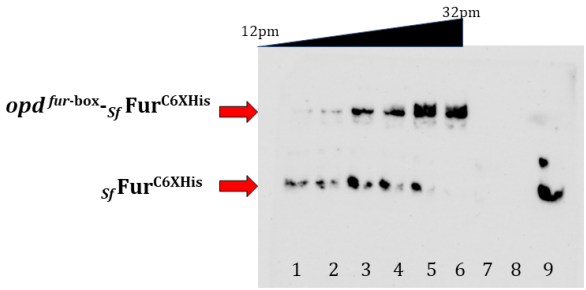

Lane	1	2	3	4	5	6	7	8	9
opd $^{fur\text{-box}}$ (0.5 pm)	+	+	+	+	+	+	Empty	+	+
$_{Sf}$Fur^{C6XHis} (pm)	12	16	20	24	28	32		-	32
Mnso4 (1mM)	+	+	+	+	+	+		+	-
DIP (100µM)	-	-	-	-	-	-		-	+

Fig.4.5.5. EMSA. South-western blotting in which 8% native PAGE was used to analyze the mobility shift, observed due to formation of *opd*$^{fur\text{-box}}$-$_{Sf}$Fur^{C6XHis} complex. The free $_{Sf}$Fur^{C6XHis} and *opd*$^{fur\text{-box}}$-$_{Sf}$Fur^{C6XHis} complex formed in a metal ion dependent manner are shown with red arrows.

4.5.6A. Influence of Fur on the regulation of *opd* gene:

The EMSA experiments helped in gaining clear *in vitro* evidence on *opd*$^{fur\text{-box}}$ and $_{Sf}$Fur^{C6XHis} interactions. In order to gain supporting evidence, *in vivo* experiments were performed using *E. coli* as model system. The amino acid sequence of $_{Ec}$Fur shows 70% similarity with the $_{Sf}$Fur (Fig.4.5.6A). Since there is such a high degree of conservation, *E. coli* was used as a model system to evaluate the role of Fur protein on regulation of *opd* gene.

```
CLUSTAL O(1.2.4) multiple sequence alignment


E.coli      ---MTDNNTALKKAGLKVTLPRLKILEVLQEPDNHHVSAEDLYKRLIDMGEEIGLATVYR      57
S.f         MNRKIDVEALCHEKGLRITEQRRVIAQVLSDA-TDHPDVEELHRRSAAIDPGISIATVYR      59
                 * ::  :: **::*  *  * :**.:  ..* ..*:*::*   :.  *.:*****

E.coli      VLNQFDDAGIVTRHNFEGGKSVFELTQQHHHDHLICLDCGKVIEFSDDSIEARQREIAAK      117
S.f         TVRLFEEAGILDRHDFGDGRARYEAAPESHHDHLIDVETGNVIEFVDPELEQLQKQIAEK      119
            .:. *::***: **:* .*:: :* : : ****** :: *:**** * .:*  *::** *

E.coli      HGIRLTNHSLYLYGHCAEGDCREDEHAHEGK     148
S.f         LGFRLVDHRMELYGVALDRKS----------     140
             *:**.:* : *** . : ..
```

Fig.4.5.6A. Similarities between *E. coli* and *S. fuliginis* Fur sequences.

4.5.6B. Generation of *fur* negative *E. coli* strain:

Since considerable homology exists between Fur proteins of *E. coli* and *S. fuliginis* we have exploited available genetic tools to delete *fur* gene from *E. coli* and to perform *opd* expression studies in *fur* positive and negative background. A *fur* null mutant was generated in *E. coli* MG1655 AM001strain by transducing it with phage P1 particle propagated using *E. coli* BW25113 Δ*fur*::kan strain in which *fur* gene is replaced with kanamycin cassette (Methodology 4.4.6). The kanamycin resistant colonies were taken and colony PCR was performed using primer set NS10FP/NS10RP to detect replacement of *fur* with kanamycin cassette. As seen in Fig.4.5.6B, panel B in all kanamycin resistant colonies an amplicon with a size of 1.5 Kb got amplified rather 500 bp amplicon seen in *fur* positive *E. coli* MG1655 AM001strain. The resulting strain is designated as *E. coli* NS001 and stored at -80^{0}C as a glycerol stock. When necessary *E. coli* NS001 was sub-cultured and used for *opd* expression studies.

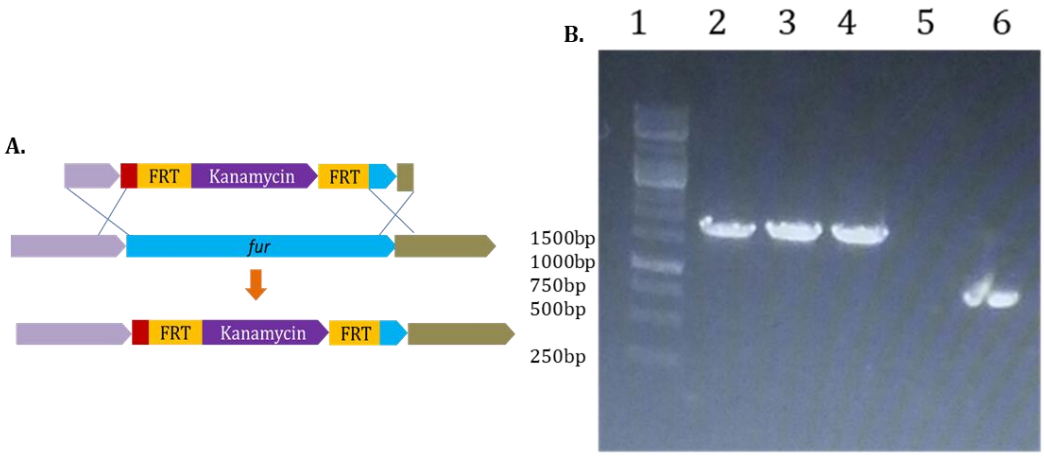

Fig.4.5.6B. Generation of *E. coli* NS001. The schematic representation of strategy used to delete *fur* gene from *E. coli* MG1655 AM001 strain is shown in panel A. Panel B shows replacement of *fur* gene with kanamycin cassette. Lane 1 of 0.8% agarose gel represents molecular weight marker. Lane 2 represents amplicon generated when PCR was performed using primer set NS10FP/NS10 RP and *fur* negative *E. coli* BW25113 Δ*fur*::kan. Lanes 3 and 4 show amplicon size generated in a similar PCR reaction using kanamycin resistant colonies of *E. coli* NS001. No template (negative) control is shown in lane 5. The lane 6 represents amplicon obtained in a PCR reaction having wild type *E. coli* MG1655 AM001 (positive control) colony.

4.5.6C. Expression of *opd* gene in *fur* negative background:

The *fur* negative *E. coli* NS001 cells were used to assess Fur dependency on *opd* gene expression. While elucidating Fur role on *opd* gene expression two transcriptional fusions were generated as explained in methodology section. One of them pNS2 contains only core promoter and the other one pNS6 contains core promoter along with the *fur*-box motif ($opd^{fur\text{-box}}$). The *E. coli*, *fur* positive cells as well as *E. coli* NS001 cells, having *fur* negative background were transformed independently with pNS2 and pNS6 and the LacZ activity was measured. In *E. coli* MG1655 AM001 (pNS2), the Fur independent de-repression was clearly seen (Fig. 4.5.6C-panel B, sector IV) as $_{Ec}$Fur cannot interact with *opd-lacZ* fusion as pNS2 is constructed by omitting $opd^{fur\text{-box}}$. However, the Fur dependent repression was evident in *E. coli* MG1655 AM001 (pNS6), due to interaction of $_{Ec}$Fur with the $opd^{fur\text{-box}}$ found in pNS6 (Fig. 4.5.6C, Panel B sector II and III). However, this repression was not seen in *E. coli* NS001 (pNS6) cells as there exists no indigenous Fur ($_{Ec}$Fur) protein in NS001 strain (Figure 4.5.6C, Panel C, sector-II and III). There was no Fur influence on LacZ activity in *E. coli* cells having pNS2 indicating lack of Fur interaction with *opd* promoter in the absence

of *opd*$^{fur\text{-box}}$ motif (Fig. 4. 5. 6C, panel C, sector 4).

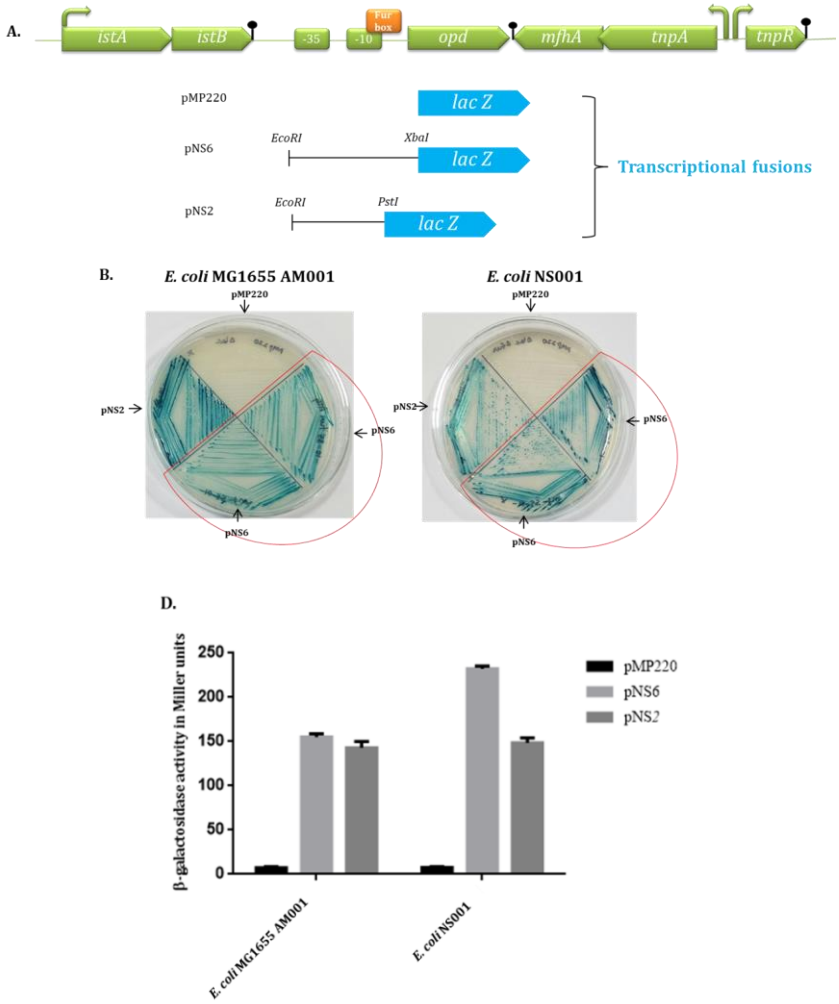

Fig.4.5.6C. Construction of transcriptional fusions with and without *opd*$^{fur\text{-box}}$. Panel A indicates extent of *opd* promoter taken while constructing *opd-lacZ* fusion. Inclusion of *opd*$^{fur\text{-box}}$ is clearly seen only in pNS6. Panel B indicate quantitative assays showing influence of Fur protein on LacZ activity. Sector-I shows *E. coli* MG1655 AM001 (pMP220). Sector II & III corresponds to *E. coli* MG1655 AM001 (pNS6). Sector-IV shows *E. coli* MG1655 AM001 (pNS2). Panel C. *E. coli* NS001 (pMP220), Sector II & III show *E. coli* NS001 (pNS6). Sector IV shows *E. coli* NS001 (pNS2). Panel D shows the quantitative *lacZ* activity measured in miller units.

4.6 Discussion:

Bacteria are always prone to dynamic environments in which nutrient attainability may increase or decrease substantially. They respond to these variations by altering their gene expression thus, express various enzymes on the basis of the source of carbon and other nutrients available to them (Jacob & Monod, 1961; Lawrence, 2002). In bacteria, both transcription and translation are integrated in space and time and are tightly regulated. This kind of regulation is critical for the survival of bacteria (McGary & Nudler, 2013).

The modulation of iron uptake and its usage are crucial for the bacterial growth and to avoid iron toxicity. In certain bacteria, this regulation relies on the master regulator, Fur (Ferric uptake regulator) (Mey et al., 2005). Fur stringently modulates the expression of genes involved in iron homeostasis (Tanui et al., 2017). Fur, was initally identified in *E. coli*. It is a global transcriptional regulator involved in iron metabolism (Hantke, 2001). Bacteria having high genomic Guanine and Cytosine content, utilise the diphtheria toxin repressor (DtxR) to regulate homeostasis of iron (Andrews et al., 2003; Giedroc & Arunkumar, 2007).

The *E. coli* Fur exists as a paradigm for the expanding family of metalloregulatory proteins. Homologs of Fur are identified in certain bacteria such as Zur (regulator for uptake of zinc) and PerR (peroxide repressor), Manganese uptake regulator Mur (regulator for uptake of manganese) (Hantke, 1981, 1984; Bsat et al., 1998; Gaballa & Helmann, 1998; Escolar et al., 1999; Menscher et al., 2012). These proteins inclusive of Fur need a bound divalent metal ion for DNA binding, *in vivo* and all these proteins exist in mutually exclusive regulons (Helmann, 1998) . The *E. coli* Fur protein is encoded by the chromosomally located *fur* gene (approx. 500bp long). It is a homo-dimeric protein made up of 17kDa monomers (Bagg & Neilands, 1987; Saito et al., 1991).

The Fur mediated repression is caused when the Fur protein recognizes a 19-bp inverted repeat known as *fur*-box or iron-box (GATAATGATAATCATTATC). It was previously proposed that 19-bp (9-1-9) inverted repeat depicts the binding site of a one Fur dimer (de Lorenzo et al., 1987). In *E. coli*, two Fur dimers recognize the 19-bp Fur box and interact with major grooves of the DNA, on the opposite faces through a helix-turn-helix-HTH binding motif. An alignment of *fur*-motif of *E. coli* and *B. subtilis* revealed existence of a distinctly conserved, 15-bp (7-1-7) repeat existing twice within this 19-bp consensus. This 19-bp box can be interpreted as head-to-head-to-tail repeat of the GATAAT (hexamer) (Baichoo & Helmann, 2002). These simple hexameric repeats demonstrate a strong binding to Fur. The symmetric AT-AT core within the hexamer could possibly bind with Fur dimer (Escolar et al., 1998,

1999).

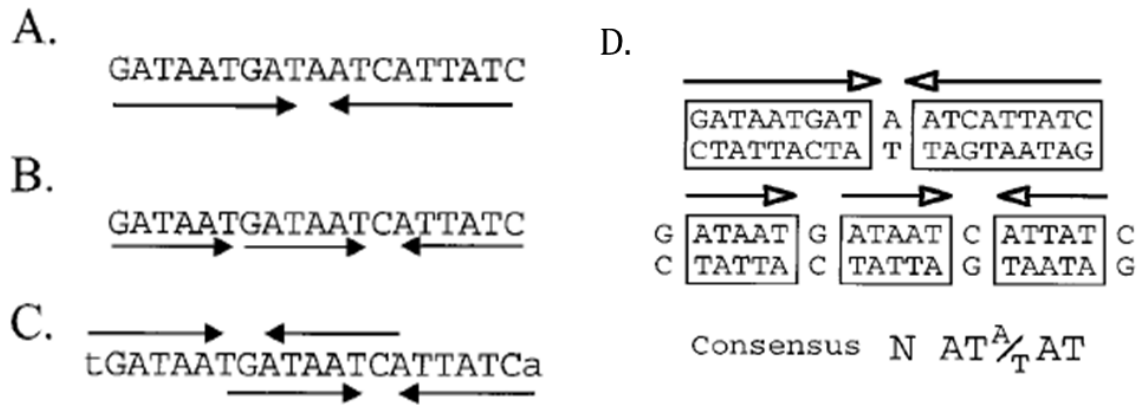

Fig. 4.6.1. Models depicting *fur*-box consensus sequence. (A) The Classical *fur*-box motif with 19-bp inverted repeat sequence, originally envisioned to bind a single Fur dimer is shown in panel A. An alternative view proposing repeated arrays of three or more copies of the hexamer GATAAT (Lucía Escolar et al., 1998, 1999) in *fur*-box motif is shown in panel B. The *fur*-box with three GATAAT motifs in a head-to-head-to- tail (6-6-1-6) array is shown in panel C. The 19-bp *fur*-box with two overlapping heptamer inverted repeats [$(7\text{-}1\text{-}7)_2$] that together define a 21-bp sequence (Baichoo & Helmann, 2002) is shown in D.

The standard interpretation shown in Fig. 4.6.1 panel D is a palindrome composed of two 9-base pair inverted repeats. It can also be conceived the as an array of three repeats of 6-base pairs (one inverted and two direct) of the sequence "NATA/TAT". The binding sites of Fur, can be assembled by merging several repeats in distinctive orientations (Escolar et al., 1999).

The consensus of *fur*-box motif of *E. coli* when compared with that of *S. fuliginis* revealed quite interesting observations (Fig.4.6.2). The order of Adenine and Thymine base pairs in the *fur*-box seems to permit many variations. Sequences recognized by Fur appear to be thoroughly degenerate. In the absence of precise sequence specificity, the base pair substitutions are allowed without loss of functionality (Deng et al., 2015). In agreement of this proposition the $opd^{fur\text{-box}}$ failed to share similarity throughout the typical consensus *fur*-box. The $opd^{fur\text{-box}}$ did not have the typical 5'-GATAAT-3' conserved hexamer in 7-1-7 consensus *fur*-box-motif. Instead it contained 5'-TAAAAGA-3' in the first 7 bases of the conserved fur-box. Likewise, in the second seven bases of conserved *fur*-box the $opd^{fur\text{-box}}$ contained 5' ACAACCG 3' (Fig. 4.6.3).

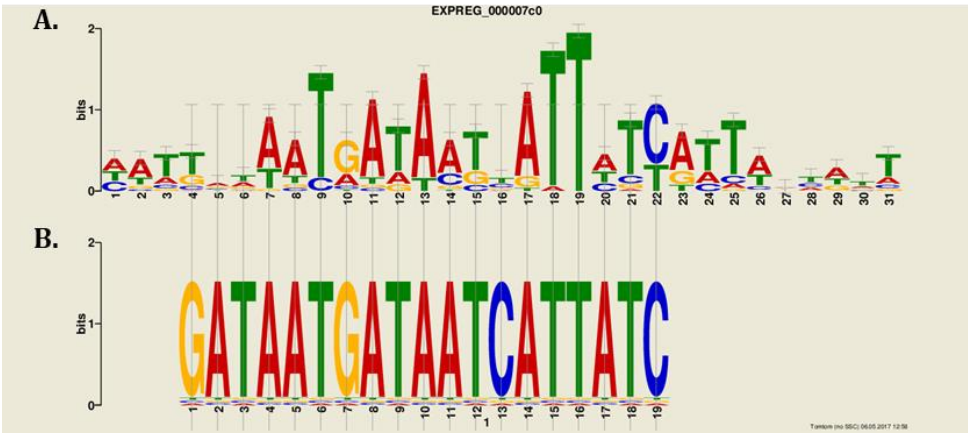

Fig.4.6.2. Comparison of *opd*$^{fur\text{-box}}$ with the $_{Ec}$*fur*-box: The consensus sequence logo, prepared by using MEME Suite in shown. The height of individual letters within a stack of letters represents the relative frequency of that letter at a given position. The overall height of the stack represents the degree of conservation at that position.

There exist considerable deviations in the *opd*$^{fur\text{-box}}$ motif. A comparative analysis was done by comparing *fur*-box motifs identified among various well defined iron responsive genes. The aligned sequences (Fig.4.6.3), disclosed the conservation of a 15-bp core region (7-1-7 repeat) instead of the classic 19-bp repeat. Escolar et al., 1998 showed the 19-bp inverted repeat, which can be viewed as three GATAAT hexamers in a head-to-head-to tail (6-6-1-6) orientation as shown in Fig.4.6.1 panel A. The 7-1-7 heptamer motif is closely linked to the proposed hexameric motif (Baichoo & Helmann, 2002).

```
                                   7-1-7 consensus sites
                                   TGATAAT-ATTATCA
                          TGATAAT-ATTATCA (L)
                                            TGATAAT-ATTATCA(R)
dhbABCKF ATTGAT A A T G A T A A T C A T T A T C A A T AGATTG
ydbN     ATTGAT A A T G A T T A T C A A T A T C G T T TGATTG
ykuN1    GTTGAC A A T G A A A A T C A T T A T C A T T TAAAGT
ykuN2    TATGAT A T T G A A A A T C A T T A T C A A C TAATGG
yuiI     GTTGAT A G T G A A A A T C A T T A T C A T A CATTGC
fhuB/D   GATGAA A A A G A G A A T C A T T A T C A T C TGTGAT
yoaJ     TCTTAT A A T G A T A A T G A T T C T C A T T TGAAGT
yclN     TATGTA A A T G A T A A T G A T A A T C A A T TACTAT
yxeB     TTATTA A T T G A T A A T G A T A A T C A T T ACTAAT
yfmC     GTTACA T G T G A T A A T G A T T C T C A T T ACTAAA
yfiY     GATCT A A A T G A T A A T G A A T T T C A A T ATTGGG
ywbL     TTATAC  A A T G A T A A T C A T T T T C A A T TATAGG
ybbB     ATTTTT  A T T G A A A A T G A T T A T C A A T TGAAAG
yfhC     TTATGA  A A T G A T A A T C A T T T T C A A T TGCATA
yusV1    AAACTA  A T T G A A A A T G A T T T T C A A A GTCAGT
yfiZ     TTTGTT  T T T G A G A A T A A T C C T C A A T TAGGGA
feuABC ybbA ATTCCA A T T G A T A A T A G T T A T C A A T TGAACA
yhfQ     AAAATT G G T G A T A A T G A T T C T C A T T CCGTGT
ywjA     AGTATA A T T G A G A A A T A T T A T C A G T TATTTA
opd      GTCAAC A G T A A A A G A A A C A A C C G G T TCAGAT
```

Fig.4.6.3. Alignment of *opd*$^{fur\text{-box}}$ with *fur*-box motifs identified in the well-defined iron response genes.

When many operator sequences were aligned to inspect the structure of *fur*-box motifs, they showed at least one overlapping 7-1-7 motif with a six-base offset (either to the left or to the right of the sequence (Fig.4.6.3). As seen in Fig.4.6.3, only in the first six operators five out of seven residues of the conserved heptamer residues are matched in the left overlapping motif, and as a corollary, the central base of the 7-1-7 motif shown in the alignment is a C, corresponding to the conserved C in the left overlapping 7-1-7 motif. Similarly, the *yxeB* and *yfmC* operators appear to have right overlapping motifs and have

the expected central G residue in the aligned 7-1-7 motif. However, one-half of the aligned operator sites do not have obvious overlapping heptamer repeats (less than four of six matches with the additional flanking bases) and may represent sites that have only one 7-1-7 motif. For these sites there is little apparent conservation of the central base in the 7-1-7 motif. Although they are less conserved, all the operator regions interact with as little as nano Molar concentrations of Fur (Baichoo & Helmann, 2002).

When *opd*$^{fur\text{-box}}$ was inspected for the presence of 7-1-7 symmetric dyad conservation (dark green dotted box in Fig. 4.6.3) interestingly, we found a match of 11 bases out of 15 base core region. The left overlap showed 5 matches (second base was 'A' instead of conserved 'G'; sixth base was 'G' instead of conserved 'A'). The right overlap showed 5 matches (second and fifth bases were 'C' instead of conserved 'T', and the seventh base was 'G' instead of conserved 'A'. The purine mismatches are highlighted in dark red while pyrimidine mismatches are highlighted in dark blue. The perfect matches are presented in bold font and rest of the mismatched bases are represented in normal font and rarely present in aligned sequences. Despite of these differences he *Sf*Fur interacted with the *opd*$^{fur\text{-box}}$ and *Sf*Fur. The formation of *opd*$^{fur\text{box}}$-*Sf*Fur complex is dependent on metal ions (Fig. 4.5.5), indicating clearly that the *opd*$^{fur\text{-box}}$ serves as target to the *Sf*Fur repressor.

After analyzing *opd*$^{fur\text{-box}}$ further analysis has also been done to analyze the structural features of the *Sf*Fur proteins. The *Ec*Fur is a dimeric protein and contains two metal-binding sites per subunit. It can bind to chemically related metal ions *in vitro* (Co^{2+} and Mn^{2+} etc.,) (Bagg & Neilands, 1987). The binding of metal ions enhances the affinity of Fur protein for its DNA-binding, several fold (Smith et al., 1996). The Fur protein is activated in the following order $Zn^{2+} \gg Co^{2+} > Fe^{2+} > Mn^{2+}$ (Mills & Marletta, 2005). Each Fur subunit has, C-terminal dimerization domain and an N-terminal DNA binding domain (Coy & Neilands, 1991; Deng et al., 2015).

Fig. 4.6.4. Domain organization of Fur. Representation of the N-terminal DBD (cyan), hinge (green) and C-terminal DD (magenta) (Deng et al., 2015)

Dimerization Domain is rich in Histidine residues, and is implicated to bind the Fe^{2+} ions to cause dimerization, whereas the DNA Binding Domain ineracts with *fur*-box (Holm et al., 1994; Coy & Neilands, 1991; Stojiljkovic & Hantke, 1995). The physiological function of Fur is to repress the iron acquisition genes under iron sufficiency but the genes with 'non-iron' functions (Table 4.6.1.) such as flagella chemotaxis, methionine biosynthesis etc., are also repressed by Fur.

Gene	Function	Reference
acnA	Aconitase, [Fe-S] protein	(M. J. Gruer & Guest, 1994)
Bfd	Release of iron from Bfr	(Quail et al., 1996)
Bfr	Iron storage	(Masse & Gottesman, 2002)
Cir	Ferric dihydroxybenzoate uptake	(Litwin & Calderwood, 1993)
cyoA	Terminal respiratory oxidase subunit	(Stojiljkovic et al., 1994)
entABC DEF	Enterobactin biosynthesis	(Litwin & Calderwood, 1993)
entS	Export of enterobactin	(Furrer et al., 2002)
fecABC DE	Ferric dicitrate transport	(Litwin & Calderwood, 1993)
fepA	Ferri-enterobactin transport	(Litwin & Calderwood, 1993)
flbB	Motility	(Stojiljkovic et al., 1994)
purr	Purine regulon regulation	(Stojiljkovic et al., 1994)
ryhB	Small regulatory RNA	(Masse & Gottesman, 2002)
sdhCDA B	TCA cycle	(Park & Gunsalus, 1995)
tonB	Siderophore and vitamin B12 transport	(Litwin & Calderwood, 1993)
fumA	Aerobic fumarase, [Fe-S] protein	(Park & Gunsalus, 1995)
fumB	Anaerobic fumarase, [Fe-S] protein	(Tseng, 2006)
nrdHIEF	Deoxyribonucleotide reductase 2	(Vassinova & Kozyrev, 2000)
nohB	Phage function	(Vassinova & Kozyrev, 2000)
gpmA	Glycolysis	(Vassinova & Kozyrev, 2000)

Table.4.6.1. List of few Fur and iron-regulated genes in *E.coli* K-12 (Stojiljkovic et al., 1994; Park & Gunsalus, 1995; Touati, 1988; Vassinova & Kozyrev, 2000; Tanui et al., 2017).

According to (Deng et al., 2015), in *P. aeruginosa*, binding of the metal ion to Fur induces conformational changes in the DNA Binding Domain. Each holo-Fur monomer consists of two metal binding sites. The site 1 links DNA Binding Domain and Dimerzation Domain. It contains a Mn^{2+} ion that is hexacoordinated by H33 and H81 from the DNA Binding Domain and H88, H90 and E1010 from the Dimerzation Domain. Mn^{2+} is also hexacoordinated by H87, D89, E108, H125 and Q111 in site 2. The site 1 is adequate for *in vitro* binding of Fur-DNA, site 2 is unessential for binding of DNA but binding activity substantially reduced upon its disruption.

Further structural studies of Fur from *P. aeruginosa* demonstrated DNA recognition with either base read out or shape read out mechanisms (Deng et al., 2015). In DNA-protein interactions, when a protein recognizes distinctive chemical structures of DNA bases it is termed as 'base readout'. 'Shape readout' is when the protein recognizes a sequence dependent DNA shape (Rohs et al., 2010). The amino acids of Fur from *P. aeruginosa* (Lysine15, Tyrosine56, and Arginine57) recognize DNA using various unique modes of interaction. The first mode being base readout, in which the phenyl ring of Tyrosine56 forms vander waals interactions with one or two consecutive Thymine bases in the major groove, such as the $-CH_3$ groups of Thymine15 and Thymine16 of *feoAB1* operator or Thymine12 of *fur*-box. The loss of Thymine nts impaired the interactions between DNA and Fur, indicating that 'Thymine' is crucial for direct contact with Fur. The base readout mode is another mechanism followed in which, Arginine57 gets inserted into the major groove, forming bidentate hydrogen bonds between its guanidium group and O6 and N7 atoms of conserved 'Guanine' (G7) of the *feoAB1* operator or G10 of *fur*-box. Arginine57 also forms a hydrogen bond with Thymine15 of *P. aeruginosa fur*-box. The DNA binding ability was severly disrupted when Arginine57 was mutated and in the next recognition mode i.e., in shape readout, Lysine15 of the L1 loop gets inserted into the minor groove with certain interactions with DNA. These interactions are not base specific (Slattery et al., 2014; Deng et al., 2015). Further structural analysis proved that Lysine15 recognizes DNA using minor-groove

shape read out (Deng et al., 2015).

Under iron sufficient conditions, Fur acts as Holo-Fur, binds ferrous iron (Fe^{2+}) and dimerizes. The resulting dimeric complex interacts with the *fur* motif, located within the promoter regions of Fur-regulated genes. This enhances extreme conformational changes and confers DNA-binding capacity which occludes the interaction with RNA polymerase thus represses transcription. This interaction results in transcriptional repression of genes involved in iron acquisition and storage (Crosa, 1997). Under iron limiting conditions, Fur acts as Apo-Fur and remains as a monomer. This form has low propensity to bind DNA, thus leading to de-repression of its cognate genes *in vivo* (Coy & Neilands, 1991; Escolar et al., 1998; Lee & Helmann, 2007).

The *Sf*Fur is a 16kDa protein, which showed 70% similarity in amino acid sequence with *Ec*Fur. The amino acids lys15, Tyr56, Arg57 are conserved in *Sf*Fur, similar to *E. coli* and *P. aeruginosa* (Fig.4.6.5). As described by (Deng et al., 2015), the recognition of *fur* motif DNA by lys15, could probably occur through a shape read out mechanism. The residues Tyr56 and Arg57 follow a base read out mechanism and have the propensity to interact with T15, T16 and G7 residues, which are the supposed recognition elements essential for direct contact with Fur (Fig.4.6.6). The shape read out mechansim, rather than sequence specific recognition, serves as an important feature of the Fur proteins. This property of shape recognition rather than sequence recognition, confers a global regulatory function to Fur.

```
CLUSTAL O(1.2.4) multiple sequence alignment


S.f         MNRKIDVEALCHEKGLRITEQRRVIAQVLSDAT-DHPDVEELHRRSAAIDPGISIATVYR      59
E.coli      ---MTDNNTALKKAGLKVTLPRLKILEVLQEPDNHHVSAEDLYKRLIDMGEEIGLATVYR      57
P.a         ----MVENSELRKAGLKVTLPRVKILQMLDSAEQRHMSAEDVYKALMEAGEDVGLATVYR      56
                  ::  :: ** :*  *  * ::*..    * ..*::::     .  :.:***** 

S.f         TVRLFEEAGILDRHDFGDGRARYEAAPESHHDHLIDVETGNVIEFVDPELEQLQKQIAEK      119
E.coli      VLNQFDDAGIVTRHNFEGGKSVFELTQQHHHDHLICLDCGKVIEFSDDSIEARQREIAAK      117
P.a         VLTQFEAAGLVVRHNFDGGHAVFELADSGHHDHMVCVDTGEVIEFMDAEIEKRQKEIVRE      116
            .:  *: **:: **:* .*:: :* : . ****:: :: *:**** * .:*  *::*. :

S.f         LGFRLVDHRMELYGVALDRKS----------     140
E.coli      HGIRLTNHSLYLYGHCAEGDCREDEHAHEGK     148
P.a         RGFELVDHNLVLYVRKKK-------------     134
             *:.*.:* : **    .
```

Fig.4.6.5.The Fur amino acid sequence alignment between *S. fuliginis*, *E. coli* and *P. aeruginosa*. The black boxes indicate the conserved amino acid residues of Lys15, Tyr56 and Arg57 which interact with *fur*-box motif.

```
        7      12  15 16
        ▼      ▼   ▼▼
TTAATCGCAACTCATTCGCAATTGC  :  feoAB1 operator of P. aeruginosa
GATAATGATAATCATTATC        :  fur-box of P. aeruginosa
GAACCGGTTGTTTCTTTTA        :  fur-box of S. fuliginis
```

Fig.4.6.6. Alignment of *fur*-box motifs. The red arrows indicate conserved residues of G7, T12, T15, T16 of *fur*-box motif that directly interact with Fur protein.

In addition to these structural similarities between *opd*$^{fur\text{-box}}$ and $_{Sf}$Fur protein with the well characterized *fur*-boxes and Fur proteins, the *in vitro* evidence generated through EMSA (Fig.4.5.5) and *in vivo* evidence gathered by using *opd-lacZ* fusions (Fig. 4.5.6C) provide undisputable evidence to show that *opd* gene is part of Fur regulon and provides experimental evidence for induction of *opd* gene expression under iron limiting conditions (see first chapter results).

Chapter-999

Background:

The preceding chapters are dedicated to describe transcriptional regulation of organophosphate degradation gene. As described in the first chapter an IRE element is identified at the 5' end of *opd* mRNA (*IRE*^{opd}). The *in silico* studies described in the first chapter have indicated structural similarities between *IRE*^{opd} and IREs identified in mRNAs coding proteins involved in iron metabolism. The current chapter is devoted to elucidate structure and function of *IRE*^{opd}. The regulation of cellular iron metabolism by IREs is a type of well-studied translational control system in eukaryotic organisms. IRE along with riboswitches exist as a part of structural RNA molecules in the UTRs. They play an important role in translational control (Hubert et al., 1996; Nudler, 2004; Winkler, 2005). IREs are approximately 30nt long, single stem-loop forming sequences. They are involved in regulation at the level of translational initiation or at the mRNA stabilization. They are found in several mRNAs of divalent metal transporter, ferroportin, mitochondrial aconitase, erythroid aminolevulinic acid synthase, transferrin receptor, ferritin (Piccinelli & Samuelsson, 2007). The IREs are extensively studied and characterized in eukaryotes but only a few prokaryotic IREs are known till date (Harrell et al., 1991; Alen & Sonenshein, 1999; Erlitzki et al., 2002; Banerjee et al., 2007; Fitzgerald & Semler, 2009). They exist either at 5'UTR or at 3'UTR. Depending on the location of their existence and also on the iron status of the cell, they interact with certain proteins termed as Iron Regulatory Proteins (IRPs) or Iron Response Element Binding Proteins (IRE-BP) and either enhance or inhibit the translation of their cognate mRNAs *in vivo*. Usually aconitases act as IRPs. Interestingly, the IRE-like element was neither found in the 5' or 3'UTR of *opd* mRNA, rather it was predicted in the 5' coding region. This unusual location has led us to investigate the structure of this IRE-like element and its interactions with aconitase from *S. fuliginis* as the IRP.

5.1. Objective specific methodology:

Table 5.1: Primers used in this study

NS11 FP	TAATACGACTCACTATAGGG	Forward primer appended with T7 promoter sequence, used to amplify *IRE*^{opd} coding DNA and non-IRE coding DNA to be used as templates to generate RNA molecules with and without IRE through *in vitro* transcription
NS11 RP	GCAATCGCAAGGGGGCAG	Reverse primer used to amplify non-IRE coding DNA.
NS12 RP	GCTCGGCGGCCTGGCTGGGTG	Reverse primer used to amplify *IRE*^{opd} coding DNA.
NS13 FP	GCAAGGGGGCCATATGCAAACGAGAAGGG	Forward primer used to amplify ORF of *opd* gene with IRE. The *Nde*I site appended to facilitate cloning in pET23b is underlined.
NS14 FP	GGGTGCGCGAGCGTGCATATGTCGATCGGCACAGGC	Forward primer used to amplify *opd* gene without IRE (*opd*$^{\Delta IRE}$). The *Nde*I site appended to facilitate cloning in pET23b is underlined.
NS13 RP	GGATCCAGATGCTCGAGTGACGCCCGC	Reverse primer used to amplify both *opd* and *opd*$^{\Delta IRE}$ genes. The *XhoI* site appended to facilitate cloning is underlined.
NS15 FP	AAACATATGACCGCCATCGGACAGGACACT	Forward primer used to amplify *aconitase* from *S. fuliginis.* The *Nde*I site appended to facilitate cloning in pET23b is underlined.
NS15 RP	AAACTCGAGGGCGGCGAGCTTGCGCAGCACAT	Reverse primer used to amplify *aconitase* from *S. fuliginis.* The *XhoI* site appended to facilitate cloning in pET23b is underlined.

Table 5.2: Strains used in this study

E. coli DH5α	*λsupE*44, Δ*lacU*169 (*Δ80 lacZΔM*15) *hsdR*17 *recA*1 *endA*1 *gyrA*96 *thi*1 *relA*1	(Hanahan, 1983)
Sphingobium fuliginis ATCC 27551	Wild type strain, Sm^r, PmB^r, *opd+*	(Kawahara et al., 2010; Sethunathan & Yoshida, 1973)
E.coli NiCo (DE3)	BL21(DE3) $glmS_{6Ala}$ *slyD-CBD can-CBD arnA-CBD*	(Robichon et al., 2011)

Table 5.3: Plasmids used in this study

pET23b	Amp^r. The T7 promoter driven expression vector. Facilitates expression of cloned genes with C-terminal 6xHis-tag.	Novagen
pMP220	Tet^r, promoter probe vector	(Spaink et al., 1987)
pPHYS	Amp^r, Expression plasmid generated by cloning full length ORF of *opd* gene including IRE in pET23b as *NdeI* and *XhoI* fragment. Codes OPH^{C6xHis}.	(Siddavattam et al., 2006)
pPHNS	Amp^r, Expression plasmid generated by cloning truncated *opd* without IRE ($opd^{\Delta IRE}$ - deletion of 86bp from translational start site) in pET23b as *NdeI* and *XhoI* fragment. Codes $_{N29\Delta}OPH^{C6xHis}$ (OPH lacking first 29 amino acids representing signal peptide).	(Pandey et al., 2009)
pPHIR	Amp^r, Expression plasmid generated by cloning *opd* variant, *opd'* having non-complementary mutations at the third base of the codon at the IRE region of *opd* in pET23b as *NdeI* and *XhoI* fragment. Codes OPH^{C6xHis}.	(Pandey et al., 2009)
pNS10	Amp^r, Expression plasmid generated by cloning *aconitase* gene of *S. fuliginis* in pET23b as *Nde*I and *Xho*I fragment. Codes $Aconitase^{C6xHis}$.	This study

5.4.1. *In vitro* transcription (IVT):

The T7 polymerase based IVT requires a pure linear DNA template having a T7 promoter, rNTPs, T7 RNA polymerase. *In vitro* transcription (IVT) assays have been developed and widely used for to study the molecular mechanisms involved in transcription (Yang & Ma, 2016). The IVT was performed using a 46bp IRE^{opd} coding DNA, designated as *ire-1* and a 35bp non-IRE forming control-DNA,

designated as *ire-2*, through-out the study.

The amplification of *ire-1* and *ire-2* was performed by PCR using primer set NS11 FP/NS12RP and NS11FP/NS11RP respectively. The obtained PCR amplicon was gel excised and purified by following method described elsewhere in thesis. The IVT reaction was performed using the purified *ire-1* and *ire-2* to generate *ire-1* and *ire-2* to RNAs, *in vitro*. The Keift and Batey (KB) buffer was used to perform IVT (Furukawa et al., 2015).

KB Buffer component	**Final concentration**
HEPES (pH 7.5)	80mM
DTT	40mM
$Mgcl_2$	24mM
Spermidine	2mM

Table.5.4.1.A. Composition of KB buffer

The procedure used to perform IVT is shown in the table 5.4.1.B. Briefly, The *in vitro* transcription of RNA was facilitated by the usage of T7 RNA polymerase, for 2.5 hours at 37^0C. Quenching of the reactions were done by using equal volume 8 M urea containing dye. RNA was subjected to an 8% urea-PAGE and visualized by UV-shadowing using F_{254} from Merck Millipore. The RNA was extracted from the gel via passive elution, precipitated using 3M CH_3COONa (pH 5.2) and then with ice cold C_2H_5OH (70%). Quantification of the purified RNA was done by measuring absorbance at 260 nm.

Component	**Volume**
DNA template	1-1.5 µg
10X KB	2.5 µl
25mM NTP	2.5 µl
T7 polymerase (1.0 U)	1 µl
Nuclease Free Water (NFW)	upto 25 µl

Table.5.4.1.B Standard IVT reaction

The pure RNA obtained after IVT was subjected to dephosphorylation using 1U of calf Intestinal Phosphatase (CIP), to facilitate subsequent end-labeling of the RNA. The Table. 5.4.1.C. shows the standard reaction condition of RNA dephosphorylation. The RNA was incubated with CIP for 15 minutes at 50^0C and heat inactivated at 95^0C for 2.5 minutes. The CIP treated RNA was subjected to treatment with phenol: chloroform: isoamyl alcohol (1µl of 20mg/ml glycogen-RNA grade procured from Invitrogen) and subsequently precipitated with 3M CH_3COONa (pH 5.2) and then with ice cold C_2H_5OH (70%). The purified RNA was quantified using nanodrop by measuring the absorbance at 260nm.

Component	Volume
RNA template	5-10 pmol
10X CIP buffer	2 µl
CIP (1.0 U)	2 µl
Nuclease Free Water (NFW)	upto 20 µl

Table.5.4.1.C Dephosphorylation reaction of RNA

The dephosphorylated RNA was then subjected to T4 Polynucleotide Kinase (PNK) treatment with radiolabeled γP^{32} isotope and incubated for 30 minutes at 37^0C. Standard labeling reaction is shown in Table 5.4.1.D. The labeling reaction was quenched by adding equal volume of 8M urea dye and the RNA was subjected to a 8% urea PAGE. The labeled RNA on gel was visualized using autoradiography. The RNA of interest was excised and extracted using passive elution, precipitated using 3M sodium actetate pH 5.2 and then with 70% ice cold ethanol. The purified RNA was resuspended in NFW and 1µl of resuspended oligo was subjected to scintillation counter and the counts were measured.

Component	Volume
RNA	20 pmol
5X PNK buffer	4 µl
PNK (1.0 U)	2 µl
$*\gamma P^{32}$	5 µl
Nuclease Free Water (NFW)	upto 20 µl

Table.5.4.1.D. 5'end labeling reaction of dephosphorylated RNA

5.4.2. In-line Probing Assay:

In-line probing assay relies on the cleavage of RNA based on its structure (Regulski & Breaker, 2008). The In-line probing reaction has four lanes viz. a No reaction lane, RNaseT1 lane, OH lane, In-line lane and the buffer compositions and reaction conditions are as shown in Table.5.4.2A.

	No Reaction	RNaseT1 ladder	OH ladder	In-line
Buffer Composition	-	T1 buffer	0.5 M Na_2CO_3 (pH 9.0 at 23°C) and 10 mM EDTA	100 mM Tris–HCl (pH 8.3 at 20°C), 40 mM $MgCl_2$, and 200 mM KCl
Reaction conditions	-	Incubated for 20min at 50^0C	Incubated for 5min at 95^0C	Incubated for 48hr at RT

Table.5.4.2.A. Standard reaction conditions of In-line probing assay

The non-IRE forming RNA as well as *IRE^{opd}* containing RNA, which was previously end-labeled was taken at 25kcpm/µl. This was subjected to reaction conditions, independently as mentioned in Table.5.4.2.A. The reactions were quenched by adding equal volume of loading 8M urea dye and the RNA was subjected to a 10% urea PAGE.

5.4.3. Expression of *opd* gene and its variants:

Following successful generation of the recombinant expression plasmids coding for OPH^{C6xHis}, $_{N29\Delta}OPH^{C6xHis}$ and OPH^{C6xHis}; the plasmids pPHYS, pPHNS and pPHIR were independently transformed into *E. coli* NiCo (DE3) cells and the expression of OPH was assessed by following procedures elaborated in methodology section. *E. coli* NiCo (DE3) cells having plasmids pPHYS, pPHNS and pPHIR were cultured till mid logarithmic phase at 37^0C and the OPH expression was induced by supplemeting 1.0mM IPTG. Cultures were subsequently incubated for 3h before analyzing the cultures to detect the expression of OPH as soluble cytoplasmic protein. Following incubation, 1ml cells were lysed by sonication with amplitude 30%, temperature 4^0C, 30 sec on and off sonic cycles. The lysate was centrifuged for 5 minutes at 13,000 rpm to get rid of debris. Clear lysate obtained was suspended in appropriate volumes of 2X loading dye and the samples were boiled and analyzed on SDS-PAGE (12.5%) to detect OPH^{C6xHis} by performing western blot using antibodies against His-epitope.

5.4.4. Cloning of aconitase (*acn*) coding gene:

The *aconitase* (*acn*) gene of *S. fuliginis* was amplified from the genomic DNA usingNS15FP/NS15RP having with *Nde*I and *Xho*I restriction sites. The PCR based amplicon was gel extracted and ligated to the expression vector pET23b. The transformants obtained after transformation of the ligation mixture into DH5α were selected on LB plates supplemented with appropriate amounts of ampicillin. The recombinant plasmid isolated from transformants were sub-cultured and screened for the existence of insert by digesting the recombinant plasmid with the same enzymes. Thus obtained plasmid was designated, pNS10 which codes for Aconitase protein with a C-terminal His-tag (Acn^{C6xHis}).

5.4.5. Expression of Acn^{C6xHis}:

Following successful generation of the recombinant expression plasmid coding for Acn^{C6xHis}, the plasmid pNS10, was transformed into *E. coli* NiCo (DE3) cells to check for the expression of Aconitase protein. The *E. coli* NiCo (pNS10) was

cultured till mid-logartmic phase at 37^0C and the Acn^{C6xHis} was induced by supplanting with 1.0mM IPTG. Cultures were subsequently incubated for 3h before analyzing the cultures to detect the expression of Acn^{C6xHis} as soluble cytoplasmic protein. Following incubation, 1ml cells were lysed by sonication with amplitude 30%, temperature 4^0C, 30 sec on and off sonic cycles. The lysate was subjected to centrifugation for 5 minutes at 13,000 rpm to get rid of debris. The clear lysate obtained was suspended in appropriate volumes of 2X loading dye and the samples were boiled and analyzed on SDS-PAGE (10%) to detect Acn^{C6xHis} by performing western blot using antibodies against His-epitope.

5.4.6. Affinity Purification of Acn^{C6xHis}:

The cell pellet obtained from 2000ml culture, after 1.5h induction using 1.0mM IPTG was resuspended in 10ml of 20mM Tris-HCl (pH7.8). Once after thorough re-suspension of the pellet, 1mM PMSF along with 50µg lysozyme were added and this mixture was kept for lysis and vortexed at room temperature for 1h. The partially lysed cells were subjected to sonication and centrifugation at 4^0C as described above. The clear cell lysate obtained was applied to the activated Ni-NTA column, pre-equilibrated with Tris-HCl (20mM, pH7.8), NaCl (500mM) and imidazole (20mM). After passing the soluble cell lysate fraction through the column matrix, column was washed with 10 CVs of Tris-HCl (20mM, pH7.8), NaCl (500mM) and imidazole (50mM) and eluted with different concentrations of imidazole. The elutions were examined on 10% SDS-PAGE, to monitor the purity of the $Aconitase^{C6xHis}$ protein.

5.4.7. Aconitase Activity:

Aconitase activity was assayed with isocitrate as substrate (Murari et al., 2015). The enzyme was reconstituted with ferrous ions to fill in the iron-sulfur clusters, so as to ensure the enzyme activity. The Fe-S cluster reconstitution of *Sf*Aconitase was performed chemically by incubating the protein in buffer containing 50mM Tris/HCl pH8.0 with ferrous ammonium sulphate hexahydrate (0.5mM), sodium sulfide (0.5mM) in the presence of dithiothreitol (5mM), for

60min at RT (Selezneva et al., 2013). The apoenzyme was prepared by incubating with the protein with 0.5mM EDTA for 15min at 20^0C to chelate iron present in the form of iron-sulphur clusters. The activity was monitored by incubating 50µg of pure protein with 1mM isocitrate in a buffer containing 50mM Tris/HCl, pH7.5, and 5mM $MnCl_2$. The conversion of isocitrate into *cis*-aconitate was measured as an increase in absorbance at 240nm.

5.4.8. EMSA:

The interactions between IRE^{opd} and IRP were determined by performing Electrophoretic Mobility Shift Assay (EMSA). While performing EMSA, *in vitro* transcribed RNA containing IRE^{opd} was incubated with purified aconitase protein. A typical EMSA reaction contained 20cps RNA with increasing concentrations (0.3-30µM) of purified $Aconitase^{C6xHis}$ protein, with or without 0.5mM EDTA and $FeSo_4$ in binding [Tris/HCl (10mM, pH 7.8), DTT (2mM), KCl (50mM), glycerol (10%)] buffer. The reaction mix was then incubated for 30min at 20^0C along with a control reaction prepared by omitting IRP. Following incubation, the reaction mixtures were separated via electrophoresis on 5% non-denaturing PAGE. The resolved RNA-protein complexes were visualized using autoradiography.

5.5. Results:

The pure RNA molecule is an essential requirement while performing molecular characterization experiments, especially while analyzing the *in vivo* structure of RNAs (Artsimovitch & Henkin, 2009). The pure RNA molecules required for structural determination are obtained by performing IVT experiments. The IVT requires a linear fragment of PCR amplified DNA with a T7 promoter. In this study two such PCR products were generated. One of them is *ire-1* and it contains T7 promoter region followed by *opd* gene coding IRE region (vide methods section). The second fragment (*ire-2*) generated is a control DNA with T7 promoter. The DNA region that followed T7 promoter is the DNA region not specifying the IRE. The sequence details of *ire-1* and *ire-2* DNA molecules are given in Fig.5.5.a.

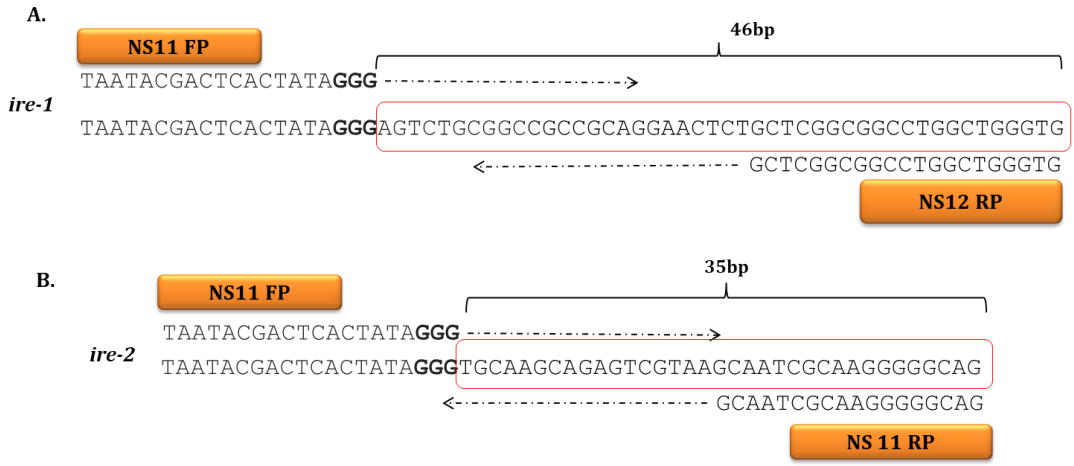

Fig.5.5.a. Diagrammatic representation of template and primers used to amplify *ire-1* and *ire-2.* Panel A corresponds to the 46bp, *IRE*^{opd} coding *ire-1* DNA. Panel B corresponds to the 35bp, non-IRE coding *ire-2* DNA. In both panels, three 'G' residues are indicated in bold and the DNA to be *in vitro* transcribed is highlighted in a red box.

In an attempt to validate existence of *IRE*^{opd} IVT was performed by using *ire-1* and *ire-2* as DNA template. After terminating the IVT reaction, the transcribed RNAs were analyzed on an 8% Urea-PAGE. The gel was placed on a serene wrap and the transcribed RNA was visualized by using UV-shadowing. Indicating successful transcription a 46nt *IRE*^{opd} and 35nt long control RNAs were noticed in IVT reactions performed using *ire-1* and *ire-2* as templates (Fig.5.5.b panel C). These RNA molecules were end radiolabelled using *γP^{32} ATP. After this 5' end labeling of RNA, they were analyzed on a 8% urea PAGE. Labeled RNA was visualized using autoradiography (Fig.5.5.b panel D). The gel pieces containing radiolabelled RNA were excised and subjected to passive elution. After elution, the gel was subjected to autoradiography to confirm the precise excision of radiolabelled RNA (Fig.5.5.b panel E).

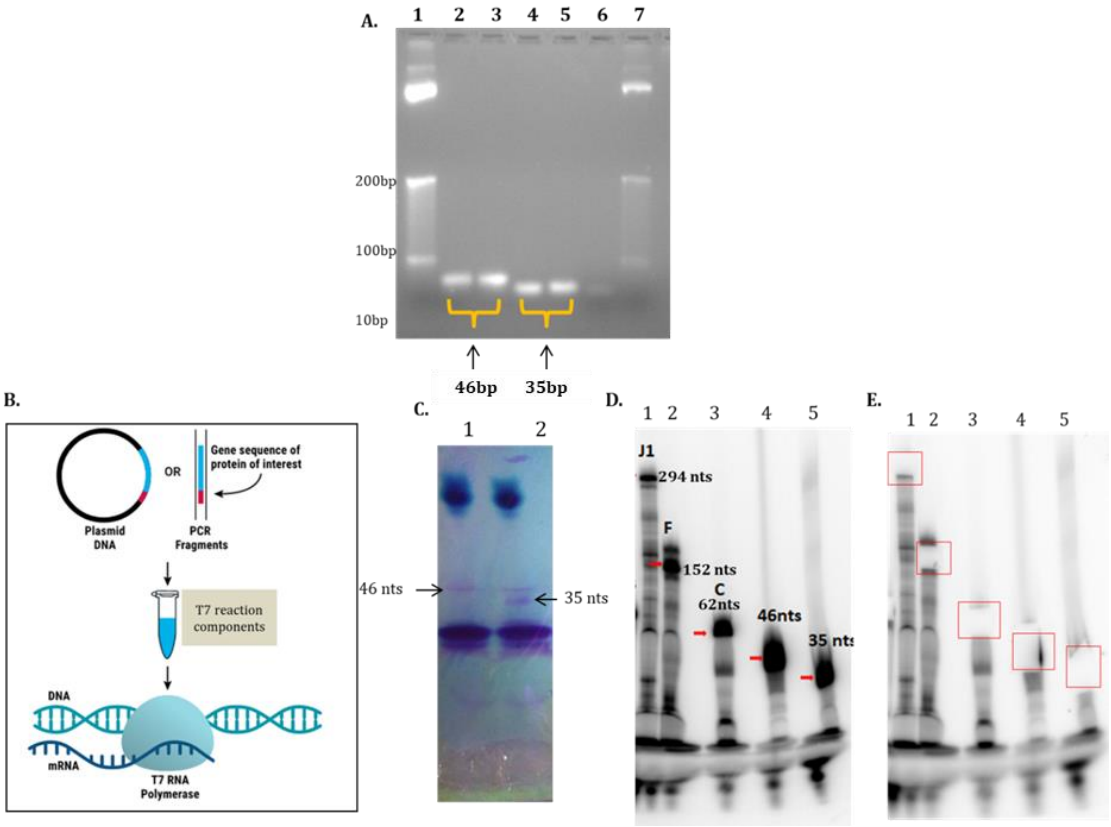

Fig.5.5.b. Steps followed during *In vitro* transcription and 5'end labeling reactions of *ire-1* and *ire-2*. Panel A shows 3% agarose gel used to separate *ire-1* and *ire-2* DNA. Molecular size markers are loaded in lane 1 and 7. The amplified *ire-1* and *ire-2* are loaded in lanes 2, 3 and lanes 4, 5, 6 respectively. Panel B shows steps involved in T7 dependent *in vitro* transcription. Panel C corresponds to 8% denaturing PAGE used to separate the transcripts formed after IVT reaction by using UV-shadowing. The arrow marks indicate *ire-1* RNA in lane 1 and *ire-2* RNA in lane 2. Panel D shows 8% denaturing PAGE used to separate the 5' end labeled RNA. Size controls are shown in lanes 1-3. Lanes 4 and 5 show radiolabelled RNA. Panel E shows the post-excision gel image corresponding to panel D. The red boxed regions are highlighted to indicate proper excision of radiolabelled RNA

5.5.1. Characterization of *IRE^{opd}*:

In-line probing assay was done to elucidate the structure of *IRE^{opd}* found at the 5' end of *opd* mRNA. The *in vitro* transcribed and radiolabelled RNA was subjected to in-line assay. This assay has four reaction lanes, among which NR corresponds to no reaction lane and it contains only radiolabelled RNA along with loading dye. Treatment of RNA with T1 RNase, generates a ladder as it cleaves the phosphodiester bond succeeding each 'G' residue and this reaction is shown in lane indicated as T1 ladder. In control reaction where *ire-2* is included there are thirteen G residues. Corresponding to that number of G residues we found 13 bands, suggesting that T1 RNase treatment worked as expected (Fig. 5.5.1, Panel A, lane T1). Similarly, in 46 nt long *IRE^{opd}* there are nineteen G residues and

hence 19 bands were identified (Fig. 5.5.1, Panel B, lane T1). In OH reaction, the RNA is subjected to partial hydrolysis and hence a ladder is generated in both control and *IRE*^{opd} mRNAs. In the In-line assay hydrolysis of RNA is based on structure. The base paired regions found in RNA are protected from hydrolysis while looped regions are susceptible. As shown in Fig.5.5.1, Panel A there exists no difference between OH and in-line lanes in the reaction mix containing *ire-2* suggesting that there exists no secondary structure in the *ire-2* (Fig.5.5.1, Panel A, lanes OH and in-line). However, in the in-line reaction performed including *IRE*^{opd} there are no bands in the ladder corresponding to C11 to G17 and C20 to C23. However, intense bands were seen from U24 to G28; C18 and U19 suggesting existence of a loop in this region. Based on in-line probing analysis the secondary structure found in *ire-1* is validated (Fig.5.5.1, Panel C) and is compared with the structure of *IRE*^{opd} predicted using *in silico* tools.

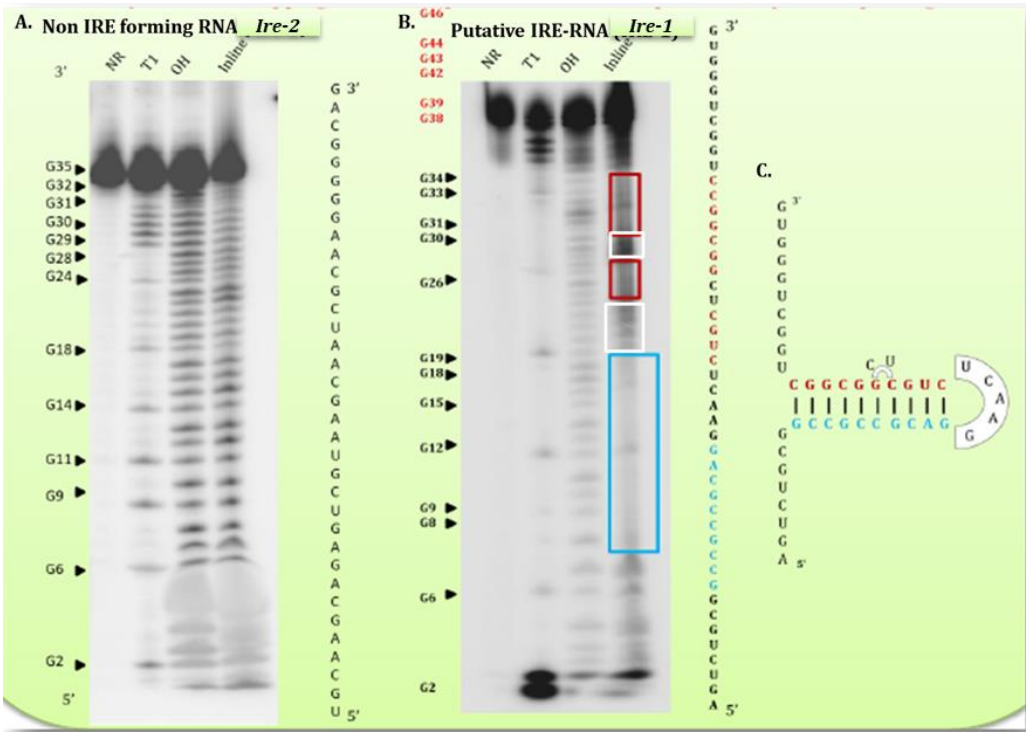

Fig.5.5.1. Validation of IRE-like element found in the 5' coding region of *opd* mRNA. Panel A and B show a 10% Urea-PAGE gel to perform the structural analysis of *ire-2* (control RNA) and *IRE*^{opd} (*ire-1*) respectively. NR lane indicates the RNA loaded without any reaction condition. The T1 reaction lane indicates RNA, which was loaded after incubation with T1 RNase for 20min at 50^{0}C to analyse the 'G' residues. The alkaline hydrolysis (OH) lane indicates the ladder formed when the RNA was incubated with buffer for 5min at 95^{0}C. The in-line lane indicates reaction mixture of RNA loaded after incubation at room temperature for 48hr. The structured regions of the In-line reaction lane of *IRE*^{opd} are indicated in red and blue boxes and the un-structured region is indicated by white box. Panel C shows the validated structure of *IRE*^{opd}

5.5.2. Cloning of *opd* gene variants in high copy vector:

This structural analysis validated the predicted IRE-like element and determined its structure as a simple stem-loop with a pseudo loop in its left arm (Fig.5.5.2.A). After establishing the structure its influence on translation of *opd* mRNA was elucidated by constructing expression plasmids pPHYS and pPHNS. In pPHYS the ORF of *opd* gene was fused to transcriptional signals of an expression vector. The second expression plasmid pPHNS contains truncated *opd* gene, $opd^{\Delta IRE}$ in which the sequence specifying IRE-like structure in *opd* mRNA is eliminated and fused to the transcriptional signals of the vector. These two constructs code *opd* mRNAs with (pPHYS) and without (pPHNS) IRE^{opd}. Since transcriptional signals are identical in these two constructs if there exists any difference in the levels of OPH expression it should to be due to influence of IRE^{opd} on translation of *opd* mRNA.

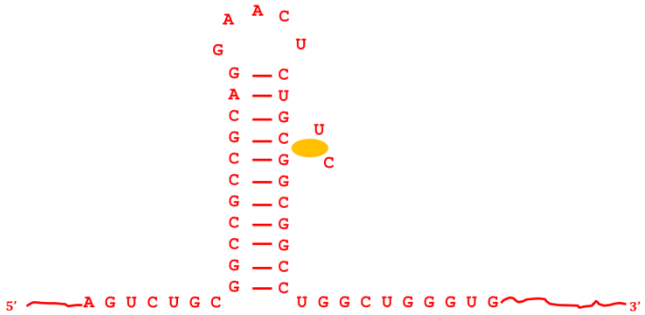

Fig5.5.2.A. *In vitro* validated structure of IRE^{opd}. The IRE-like element consists of a single stem-loop region with a pseudo loop present on its left arm.

Thirdly, full length *opd* ORF with mutations in IRE region, designated as *opd'* was constructed by introducing non-complimentary mutations. Since the predicted IRE is in coding region, the non-complementary mutations are introduced at every third base of each codon. Primary aim of generating *opd'* is to have *opd* ORF coding wild type OPH without IRE structure in *opd* mRNA. This *opd'* bearing such non-complementary mutations did not alter the primary protein sequence but remarkably disrupted the secondary structure of *opd* mRNA. *opd'* was PCR amplified with NS13FP/ NS13RP having *Nde*I and *Xho*I restriction sites.

5.5.3. Analysis of the functional role of *IRE*^{opd} on *opd* gene expression:

The expression plasmids pPHYS and pPHNS were independently transformed in *E. coli* NiCo (DE3) cells and the quantity of OPH coded by these two expression plasmids was estimated by assessing the signal intensity of OPH^{C6XHis} and $_{N29\Delta}$OPH^{C6XHis}. A significant increase in OPH expression was seen in cells having expression plasmid pPHNS constructed using *opd*$^{\Delta IRE}$ (Fig.5.5.3, panel B, lane 3) when compared to OPH encoded pPHYS, constructed using full length ORF of *opd* gene (Fig.5.5.3, Panel B, lane 2). This clearly indicated a repressive role of IRE on the expression of OPH. OPH expression in *E. coli* NiCo (pPHIR) was also assessed to know if the reduced expression of OPH is due to existence of IRE in *opd* mRNA. As stated before, the pPHIR was generated by cloning *opd'* in pET23b vector. In *opd'* the IRE-like structure is totally lost (Fig.5.5.3.a, Panel B) due to introduction of non-complementary bases at the third codon. Interestingly, the levels of OPH encoded by pPHIR significantly increased, suggesting existence of IRE dependent translational repression on expression of OPH (Fig.5.5.3.a, Panel C).

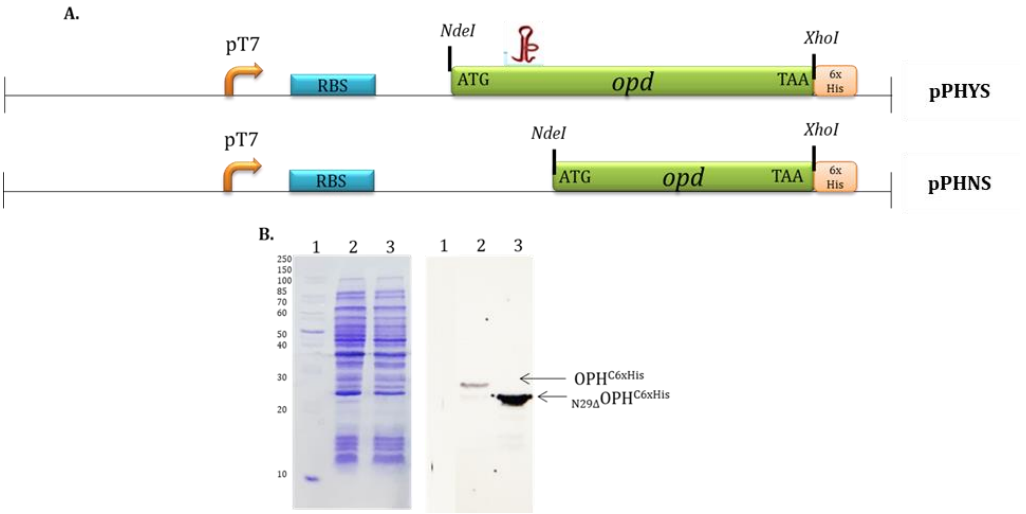

Fig.5.5.3. Functional role of IRE on *opd* expression. Panel A shows diagrammatic representation of the extent of *opd* region used to construct pPHYS and pPHNS. Panel B shows the coomassie stained, 12.5% SDS-PAGE and its corresponding western blot probed with anti-His antibodies. Lane 1 shows the molecular marker, lanes 2 and 3 show expression of OPH^{C6XHis} and $_{N29\Delta}$OPH^{C6XHis} respectively.

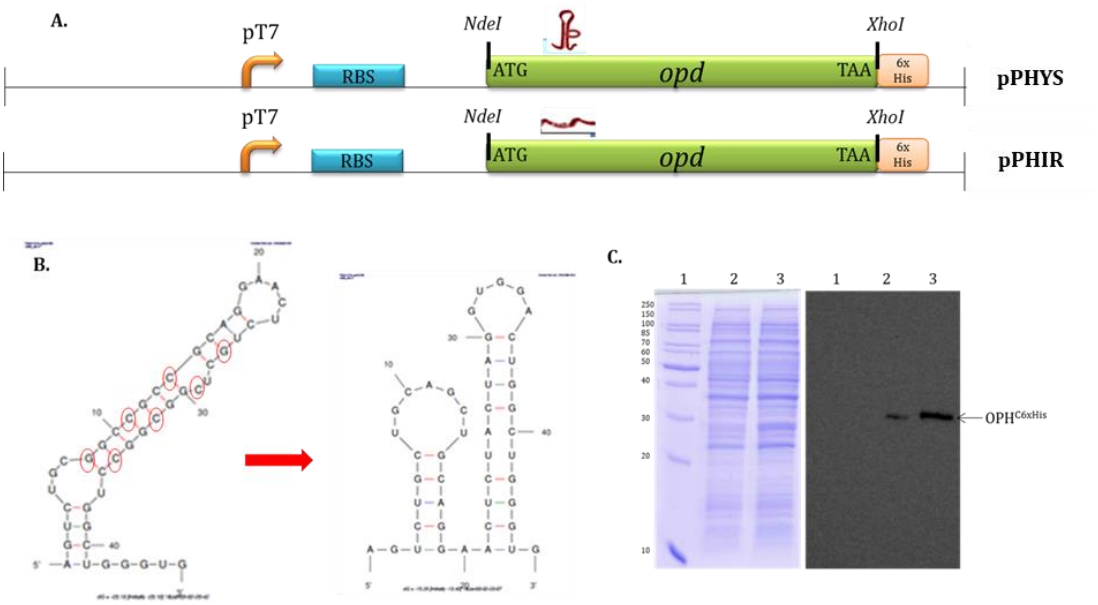

Fig.5.5.3.a. IRE dependent translational repression of OPH. Panel A shows diagrammatic representation of the extent of *opd* region used to construct pPHYS and pPHIR. The loss of *IRE*^{opd} caused by introduction of non-complementary mutations at every third base of the codon is shown in a circle is shown in panel B. Panel C shows the coomassie stained, 12.5% SDS-PAGE and corresponding western blot probed with anti-His antibodies. Lane 1 shows the molecular marker, lane 2 and 3 show levels of *opd* and *opd'* coded OPH^{C6XHis}

5.5.4. Expression and purification of *Sf*Aconitase:

IRE dependent translational regulation is mediated through IRE and IRP interactions. The IRP is apo-aconitase. Under iron limiting conditions the apo-aconitase interacts with IRE and influences the mRNA stability and translation efficiency (Cairo & Recalcati, 2007). Since *IRE*^{opd} has considerable structural similarity with the well characterized IREs, an attempt is made to see if *IRE*^{opd} interacts with apo-aconitase by performing RNA-protein EMSA.

Initially expression studies of *Sf*Aconitase (*Sf*Acn) were carried out in *E. coli* and affinity purification of *Sf*Acn was done by following strategies shown in Fig.5.5.4.b. The *Sf acn* gene was cloned in expression vector pET23b as an *NdeI* and *XhoI* fragment and expression of *Sf*Acn was induced as described in materials and methods section (Fig.5.5.4).

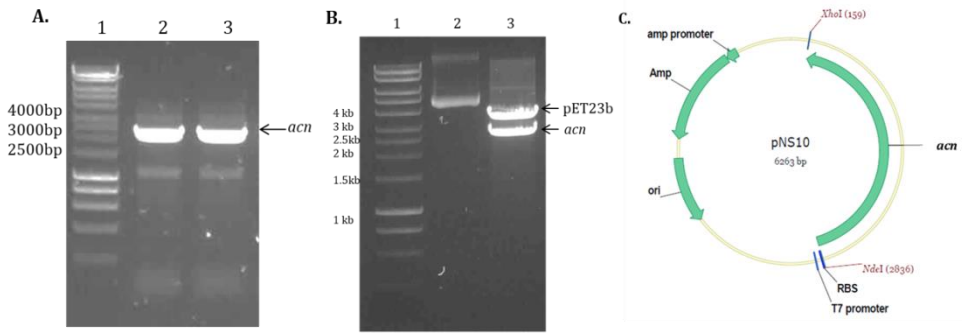

Fig.5.5.4. Construction of pNS10. Panel A shows 0.8% agarose gel used to analyze *Sf acn*. Molecular size markers are loaded in lane 1. The amplified *Sf acn* is loaded in lanes 2 and 3. Panel B shows image of agarose gel (0.8%) indicating the molecular marker (lane 1) undigested pNS10 (Lane 2) and pNS10 digested with *NdeI* and *XhoI*. The band corresponding to the vector and insert containing *Sf acn* gene are shown with arrows (lane 3). Panel C shows map of pNS10

As seen in Fig.5.5.4.a, a thick protein band (approximately 98kda) was observed and was found only in proteins extracted from induced cultures (lane 3, Fig.5.5.4.a). Such band was absent in uninduced cultures indicating over expression of *Sf*Acn^{C6XHis} in *E. coli* NiCo (DE3) cells. The western blots performed by using anti-His antibodies confirmed that the thick protein band found induced cultures is *Sf*Acn^{C6XHis} (Fig. 5.5.4.a lane 3).

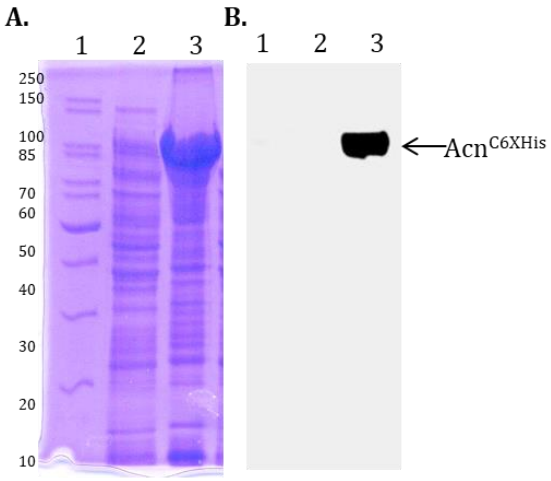

5.5.4.a. Expression of Acn^{C6xHis}. Panel A shows coomassie stained 10% SDS-PAGE to analyze the expression of Acn^{C6xHis}. Lane 1 shows the molecular marker, lane 2 shows protein uninduced whole cell lysate, lane 3 shows 1.5h induced protein. Panel B shows a corresponding western blot probed with anti-His antibodies to detect the expression of Acn^{C6xHis}.

Once the expression of *Sf*Acn^{C6xHis} was standardized, the protein purification was performed using Ni-NTA matrix as described in the methodology section. The clear lysate containing *Sf*Acn^{C6xHis} was obtained by inducing the expression of *Sf*Acn^{C6xHis} in 2000 ml of *E. coli* NiCo (DE3) (pNS10)

cells. The clear lysate was passed through a 1.5cmx14cm Ni-NTA column at a flow rate of 1ml/minute. After passing the clear lysate through column it was washed extensively and the $_{Sf}$Acn^{C6xHis} adsorbed to the column was eluted by passing elution buffer (20mMTris/HCl and 500mM NaCl) containing 200mM imidazole. Elution fraction was then analyzed on 10% SDS-PAGE and the purity of $_{Sf}$Acn^{C6xHis} was ascertained (Fig.5.5.4.b, lane 8). The fractions obtained with 200mM imidazole were pooled and the concentration of pure $_{Sf}$Acn^{C6xHis} was determined and stored at -30^{0}C until further use.

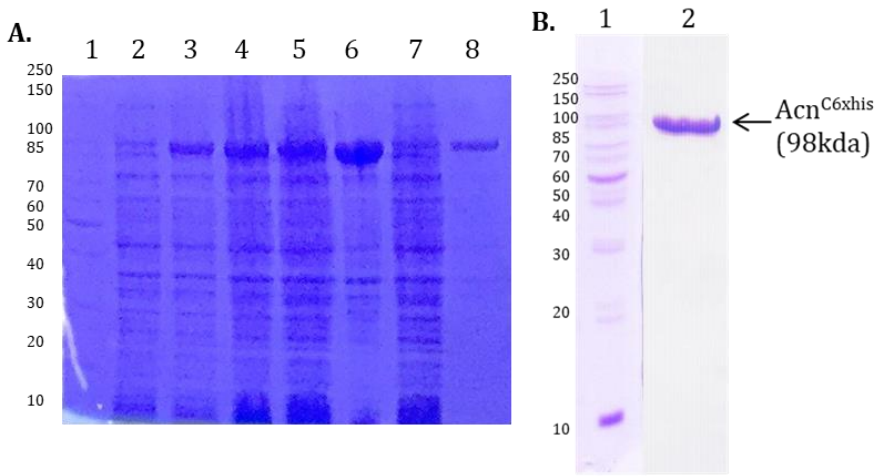

Fig.5.5.4.b. Affinity purification of $_{Sf}$Acn^{C6xHis}: Panel A shows coomassie stained 10% SDS-PAGE showing the various stages of $_{Sf}$Acn^{C6xHis} purification. Lane 1 shows the molecular marker, lane 2 shows proteins extracted from uninduced cultures, lane 3 indicates whole cell lysate fraction obtained from induced cultures, lanes 4 & 5 show pellet soluble protein fractions from induced cultures. The clear lysate used as input is shown in lane 6. The proteins found in flow-through fraction is shown in lane 7, lane 8 corresponds to elution fraction, obtained when eluted using 200mM imidazole. Panel B indicates the pure $_{Sf}$Acn^{C6xHis}.

5.5.5. Aconitase activity assay:

Aconitase or aconitate hydratase is an iron-sulfur cluster (4Fe-4S) containing protein which catalyzes the reversible isomerization of citrate to isocitrate via *cis*-aconitate (Trujillo et al., 2010). It is the second enzyme involved in krebs cycle of eukaryotic respiration (Ciccarone et al., 2018). The activity of aconitase is due to the presence of intact iron-sulfur clusters within the enzyme. The enzyme activity is reduced when these clusters are disrupted (Theil, 2015). Aconitases act as moon lighting enzymes in response to iron status in the cell (Marcos et al., 2014). Under iron

sufficient conditions, when the iron-sulfur clusters are filled in, they act in conversion of citrate to isocitrate while under iron limiting conditions, the iron-sulfur clusters are disturbed, then they act as RNA binding proteins (IRP), bind to their cognate IRE molecules and function by modulating their expression (Harrell et al., 1991; Erlitzki et al., 2002; Mande, 2011). The aconitase activity was measured before proceeding to elucidate the RNA binding activity of *Sf*Acn. This experiment was performed by using 50µg of pure protein with or without EDTA and isocitrate was used as a substrate. This metal chelator was used to chelate the iron from Fe-S clusters found in aconitase. The protein was reconstituted with ferrous ammonium sulfate to re-establish the iron-sulfur clusters. The absorption at 240nm was measured to detect the formation of cis-aconitate and the activity was indicated as µM/min/mg of protein. As shown Fig. 5.5.5, aconitase activity was significantly lowered when the protein was treated with EDTA, clearly indicating the loss of intact iron-sulfur clusters of the protein.

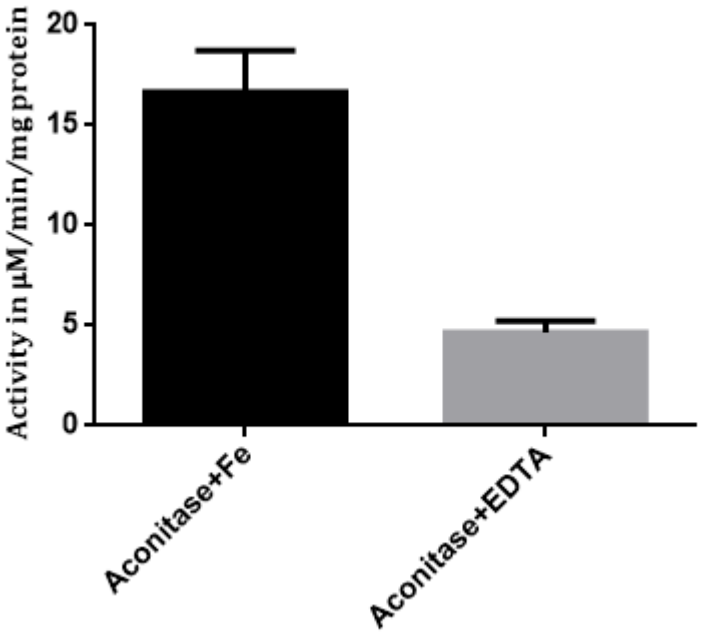

Fig.5.5.5. Aconitase activity: The aconitase activity determined for 50µg of aconitase (Fe) and apo-aconitase (EDTA).

5.5.6. Interactions between *IRE*^{opd} and *Sf*Acn^{C6xHis} IRP:

As described in the preceding chapters and sections a novel secondary structure

that shows similarity with well characterized IREs exists at the 5' coding region of *opd* mRNA. It shared structural similarity with a few well characterized IREs. This IRE-like element was structurally characterized and was proved to possess a simple stem-loop structure which is a well-defined characteristic feature of IREs. The IRE interacts with IRP under iron limiting conditions and post-transcriptionally regulates the expression of its cognate genes. Usually, aconitases serve as IRPs. Once the structure of IRE^{opd} was determined, initial attempts were made to perform *in vitro* assays to assess the interactions between IRE^{opd} and $_{Sf}Acn^{C6xHis}$. As described previously, the IRE^{opd} was generated through IVT and $_{Sf}Acn^{C6xHis}$ was overexpressed and purified. Further experiments were conducted to assess metal dependent interaction between these two components. EMSA experiments were conducted to detect mobility shifts due to formation of IRE^{opd}-$_{Sf}Acn^{C6xHis}$ complexes. During EMSA experiments the IRE^{opd} concentration was kept constant (20cps), and incubated with increasing concentrations of $_{Sf}Acn^{C6xHis}$ in the absence of metal ion. A clear shift in electrophoretic mobility was observed in the mobility of IRE^{opd} when it is incubated with $_{Sf}Acn^{C6xHis}$ indicating the formation of IRE^{opd}- $_{Sf}Acn^{C6xHis}$ complex. The concentration of IRE^{opd}-$_{Sf}Acn^{C6xHis}$ complex increased with an increase of $_{Sf}Acn^{C6xHis}$ indicating the formation of concentration dependent IRE^{opd}-$_{Sf}Acn^{C6xHis}$ complexes in the reaction mixture. Formation of such complexes got abrogated in the presence of metal ions (Fig.5.5.6, lane 9). This experiment gave a clear *in vitro* evidence on the interactions existing between IRE^{opd}/$_{Sf}Acn^{C6xHis}$. Including the metal chelators in reaction mixture enhanced association of the IRE^{opd}-$_{Sf}Acn^{C6xHis}$ complex (Lanes 2-8, Fig.5.5.6) suggesting that the interactions between IRE^{opd}-$_{Sf}Acn^{C6xHis}$ are dependent on metal ions.

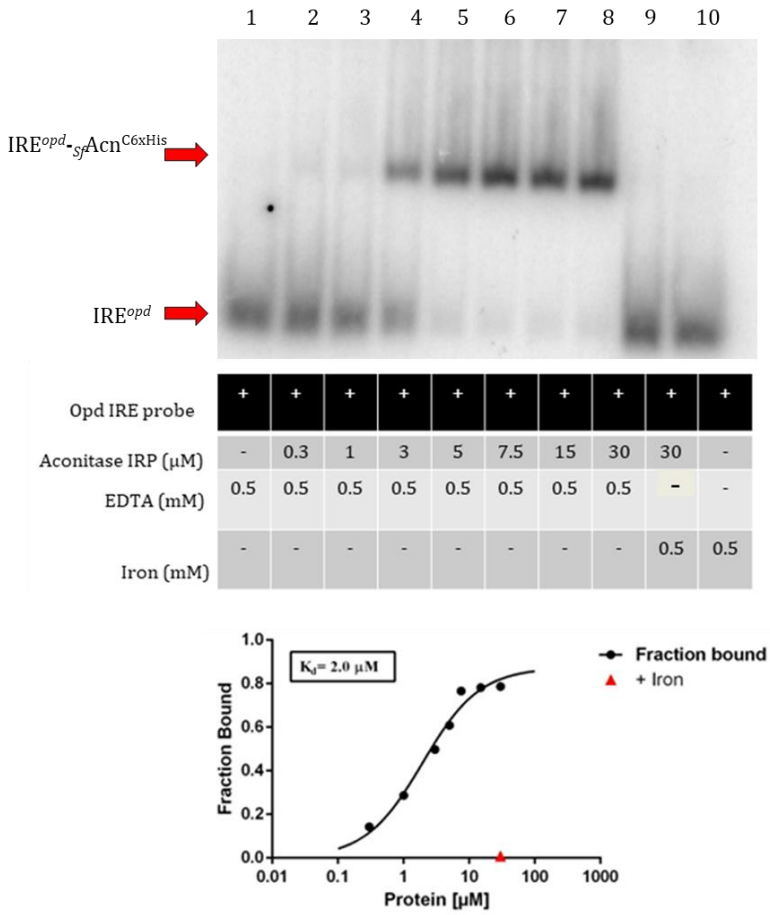

Fig.5.5.6. EMSA to show *IRE*^{opd}-$_{Sf}$Acn^{C6xHis} interactions. Panel A shows the shift in the mobility of radiolabeled *IRE*^{opd} caused due to binding of $_{Sf}$Acn to *IRE*^{opd} (indicated by dark red arrows) in the absence of metal ions. Panel B depicts binding constant determined for $_{Sf}$Acn and IRE interactions.

5.6 Discussion:

Cellular iron metabolism is stringently regulated all living organisms (Hentze & Kuhn, 1996; Crosa, 1997; Selezneva et al., 2013). Iron regulatory proteins (IRPs) play a central role in this iron mediated post-transcriptional regulation where they modulate expression of other proteins involved in maintaining iron homeostasis. They possess Fe–S clusters (Beinert, 1997; Bian & Cowan, 1999; Kiley & Beinert, 2003). IRPs control translation process by interacting with IREs often identified either at 5′ or 3′ un-translated regions of the mRNAs (Selezneva et al., 2013). The IRPs do not have an RNA binding domain but they recognize and interact with several IREs with affinities ranging upto picomolar concentrations (Volz, 2008). The secondary structure of IREs contain two separate regions that play a crucial role in recognition of IRPs: an

apical loop and a mid-stem bulge (Walden et al., 2006, 2012).

In eukaryotes, an important reaction of iron deprivation is the non-enzymatic activity of iron responsive proteins (Hentze & Kuhn, 1996; Rouault & Klausner, 1996). Aconitase (Acn) is the second enzyme of citric acid cycle and contains 4Fe-S cluster, that stereo-specifically converts citric acid to isocitric acid via *cis*-aconitate (Ciccarone et al., 2018). Under conditions of iron starvation the protein loses its Fe-S clusters. The apo-aconitase thus formed binds IREs found in mRNAs. Interactions between IRE-IRP either shield the mRNAs against degradation or repress their translation (Ma et al., 2012; Zhou & Tan, 2017). The $_{\text{rabbit}}\text{IRE}^{feritin}$ is located at the 5' un-translated of its mRNA. The translation of this ferritin mRNA is inhibited when this is bound by a apo-Acn (Aziz & Munro, 1987). Contrarily, $_{\text{rabbit}}\text{IRE}^{transferrin}$ is located at the 3' un-translated region of its mRNA. Interaction of IRP at this region, enhances the stability of the mRNA (Owen & Kühn, 1987; Casey et al., 1988). In both circumastances, interaction occurs under iron depletion (Constable et al., 1992).

This exceptional enzymatic or regulating behaviour of IRP (aconitase) is elucidated in certain bacteria (Gardner, 1997; Gardner et al., 1997; Wilson et al., 1998; Alen & Sonenshein, 1999; Tang & Guest, 1999; Serio et al., 2006; Banerjee et al., 2007). Aconitase from bacteria, are classified into two types. AcnA is identical to eukaryotic aconitases and is expressed under stress. AcnB functions majorly as a TCA enzyme (Gruer et al., 1997; Williams et al., 2002). Both AcnA and AcnB interact with unique sequences in the 3' un-translated regions of *acnA* and *acnB* mRNAs in 4Fe-4S free forms (Tang & Guest, 1999). Hence, the inactive aconitases moderate a post-transcriptional autoregulatory switch.

The $_{Bs}$Acn and $_{Mtb}$Acn interact with IRE-like elements, similarly as in eukaroytes (Alen & Sonenshein, 1999; Banerjee et al., 2007). The $_{Bs}$Acn is required in modulating genes coding for major respiratory oxidases, iron uptake system and also in sporulation (Alen & Sonenshein, 1999; Serio et al., 2006). Much information on *M. tuberculosis* Acns is not available, the available literature indicates existence of roles in iron homeostasis for the $_{Mtb}$Acn (Banerjee et al., 2007).

The five conserved nucleotides CAGUG found in the apical loop region of each IRE sequence forms the terminal pseudo-triloop, with the AGU triplet at the apex (Selezneva et al., 2013). The other main structural characteristic is the conserved C8 hinge in the middle of the stem. This hinge region is capable of forming several interactions when bound to IRP. The Cytosine at position 1 forms a base pair with Guanine at position 5 (Addess et al., 1997; McCallum & Pardi, 2003). This base pairing interaction is assumed to enhance IRP binding to IRE (Addess et al., 1997; Henderson et al., 1994). Most IREs have a conserved C residue, five bases upstream of the CAGUGN sequence, creating a bulge in the hairpin, whereas others, present in ferritin mRNAs, instead have a conserved bulge/loop UGC/C. In the UGC/C-type IRE the G and C are paired (Gdaniec et al., 1998), and the results of *in vitro* selection experiments indicated that this base pair favours high-affinity binding by IRPs (Butt et al., 1996). IRE stems forms an A-helix with a small distortion due to the conserved, unpaired C or the internal loop bulge (Gdaniec et al., 1998). The helix between the UGC/C distortion and the apical loop seems significant since it contributes to protein binding (Leibold et al., 1990).

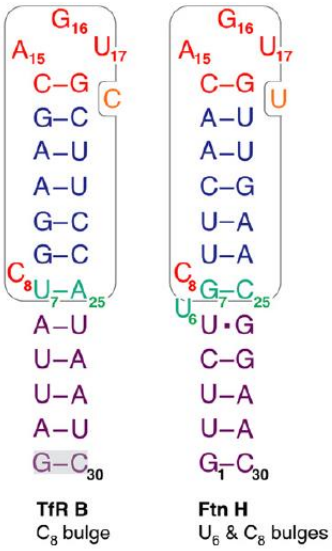

Fig.5.6.1. Comparison of ferritin and transferrin IREs. (A) Secondary structures of transferrin receptor 1 B and ferritin H IREs. The GC base pair at the bottom of the TfR B IRE (grey box) was introduced for stability. The outlined regions have the same three-dimensional structures (Walden et al., 2012).

IRP is a bi-functional protein. In one mode of operation, IRP binds to

stem–loop of iron-responsive element (IRE) in mRNAs encoding proteins of iron metabolism to control their rate of translation. In its other mode, IRP functions as cytoplasmic aconitase to correlate iron availability with the energy and oxidative stress status of the cell. The highly specific binding between IRE and IRP occurs through two separate binding interfaces that contribute to strong RNA:protein interactions. Approximately two dozen hydrogen bonds are identified in the crystal structure of the IRP:ferritin IRE complex but only five amino acids make base-specific contacts and these putative bonds are sequence specific. Though these hydrogen bonds do not constitute the strongest interactions between protein and RNA, they are responsible for binding specificity (Morozova et al., 2006). The five amino acid residues of IRP - Arg269, Ser371, Lys379, Ser681, and Asn685 have been identified to strongly interact with IRE (Selezneva et al., 2013). In a mutagenesis study, each of the five base-specific amino acids was changed to alter binding at each site. Analysis of IRE binding affinity and translational repression activity of the resulting IRP mutants showed that four of the five contact points contribute uniquely to the overall binding affinity of the IRP:IRE interaction, while one site was found to be unimportant. The stronger-than-expected effect on binding affinity of mutations at Lys379 and Ser681, residues that make contact with the conserved nucleotides G16 and C8, respectively, identified them as particularly critical for providing specificity and stability to IRP:IRE complex formation. Arg269, Ser371, Lys379, and Ser681-significantly impaired interaction of IRP with ferritin IRE, confirming the importance of these bonds for IRP:IRE recognition. The base-specific RNA-binding residues are not part of the aconitase active site but their substitutions can affect the aconitase activity of holo-IRP, positively or negatively (Selezneva et al., 2013).

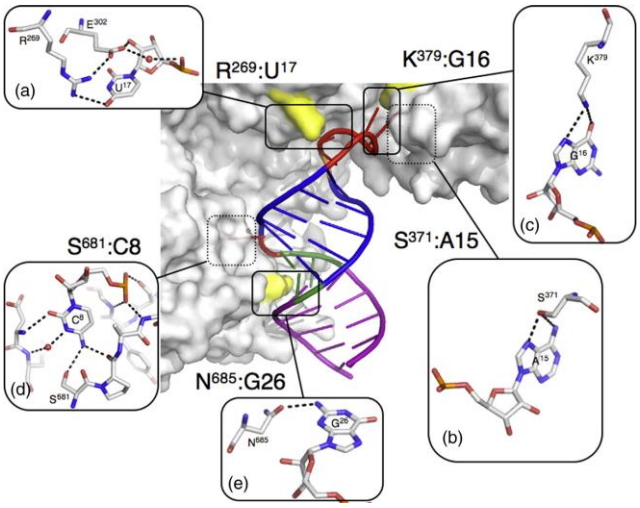

Fig.5.6.2. Structural interactions between IRE-IRP. The five IRP1 residues that form base-specific hydrogen bonds to the IRE RNA in the IRP1:IRE complexes. The IRE (cartoon) is shown as bound to the IRP protein (solvent-accessible surface). The amino acids Arg269, Lys379, and Asn685 are visible (yellow), while Ser371 and Ser681 are hidden from view. Details of the five base-specific contacts are shown by insets. Note that these residues are different from the four aconitase active-site arginines (Arg536, Arg541, Arg699, and Arg780) previously studied based on homology modeling (Hirling et al., 1994; Philpott et al., 1994; Butt et al., 1996; Selezneva et al., 2013).

Ferritin and transferrin receptor mRNA are two classical examples of eukaryotic IREs. The mechanism of interactions between these IREs and their cognate IRPs are extensively elucidated. Ferritin mRNAs, encoding the subunits of a large iron storage protein, contain a regulatory sequence in the 5' noncoding region that is conserved among all vertebrates (Theil, 1990). The conserved mRNA sequence, IRE, is a 28-nucleotide hairpin loop, which is required for self-regulation of ferritin synthesis by iron; IRE flanking sequences form a 9- to 17-base-paired stem near the cap (Wang et al., 1990; Wang et al., 1991). Increased cellular iron acts as the regulatory signal, increasing ferritin synthesis and iron storage by recruiting ferritin mRNA for polyribosomes, while decreasing transferrin receptor synthesis and iron uptake by degrading the receptor mRNA (Zahringer et al., 1976; Casey et al., 1988; Müllner & Kühn, 1988; Koeller et al., 1989). Concerted regulation of the mRNA for the two metabolically related proteins uses the same RNA-protein interactions (Owen & Kühn, 1987; Aziz & Munro, 1987; Casey et al., 1988; Caughman et al., 1988; Koeller et al., 1989; Theil, 1990). Opposite effects of iron on translation of ferritin mRNA and destabilization of the transferrin receptor mRNA coincide with the different

locations of the IRE, in either the 5' noncoding region (ferritin mRNA) or the 3' noncoding region (transferrin receptor mRNA) (Harrell et al., 1991).

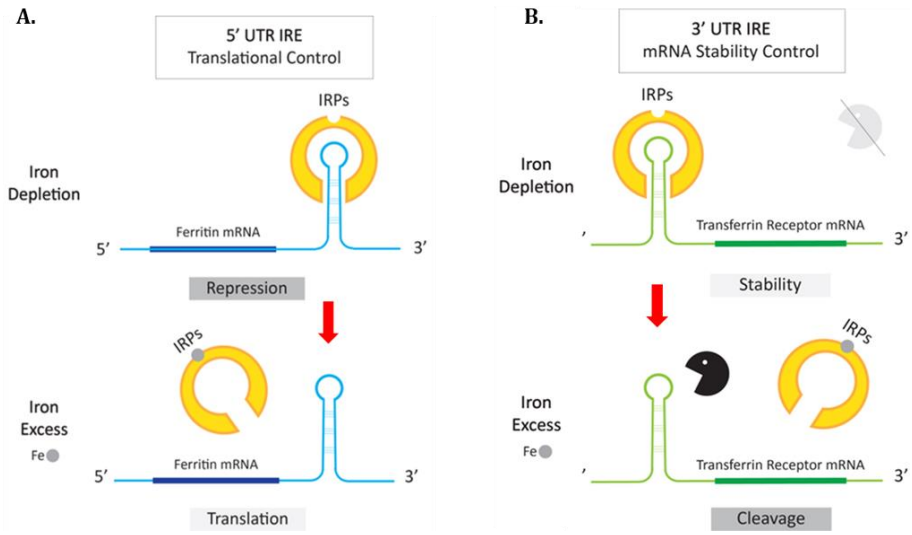

Fig.5.6.3. IRP/IRE regulatory system in ferritin and transferrin receptor genes. In the case of ferritin mRNA, when iron is depleted, IRP binds $IRE^{ferritin}$ present at its 5'UTR and represses the translation. Under iron excess condition, $IRE^{ferritin}$ cannot bind IRP hence enhances translation. On the other hand, in the case of transferrin mRNA, when iron is depleted, IRP binds $IRE^{transferrin}$ present at its 3'UTR and enhances the stability of transferrin mRNA. Under iron excess condition, $IRE^{transferrin}$ cannot bind IRP hence causes endonucleolytic cleavage of transferrin receptor mRNAs.

Based on available literature, an attempt was made to understand interactions between IRE^{opd} and $_{Sf}$Acn. As discussed previously, the location of *opd* IRE is unique. It is identified in the coding region of *opd* mRNA. The location of IRE did not influence interactions between IRE^{opd} and $_{Sf}$Acn IRE. The IRE^{opd} interacts with IRP with a similar binding affinity (at picomolar concentration) as a conventional IRE.

Before proceeding to understand the structural aspects pertaining to the binding of IRE^{opd} and IRP, attempts were made to compare the $_{Sf}$Acn sequence with four Acn paralogs Viz. *E. coli* (*acnA, acnB*); *B. subtilis*, *M. tuberculosis* and rabbit. The $_{Sf}$Acn showed 64% and 25% homology with $_{Ec}$*acnA* and $_{Ec}$*acnB* respectively; 55% similarity with $_{Bs}$Acn and $_{Mtb}$Acn and 52% with $_{\text{rabbit}}$Acn. The alignment of $_{Sf}$Acn with the structurally characterized Acns of rabbit (eukaryotic), *B. subtilis* and *E. coli* (prokaryotic) helped to gain insights on IRE^{opd} and $_{Sf}$Acn interactions. Interestingly, the amino acids that facilitate interactions between IRE and IRPs were conserved in $_{Sf}$Acn. In fact, there exists absolute

conservation at positions of R269, and S681 and at position R379 instead of arginine lysine (K379) is identified. If the charge conservation is seen both of them have basic side chains, at this position. Interestingly, the other amino acid residues showing minimum hydrogen bond distances during IRE-IRP interactions (Walden et al., 2012) are also found to be conserved in $_{Sf}$Acn. They are H207, R269, N298, E302, T438, N439, N535, R536, P682, G684, S708, G710, R728, R780 and D781.

The structural similarities between IRE^{opd} and $_{Sf}$Acn, if seem together with EMSA results generated in this study, clearly indicate a role for OPH in iron metabolism (Fig.5.5.6). However, how the IRE^{opd} and $_{Sf}$Acn interactions relieve IRE^{opd} mediated translational repression is difficult to explain with available data. The IRE^{opd} dependent translational repression of *opd* mRNA is clear as the relief of translational inhibition is clearly seen in expression constructs made using $opd^{\Delta IRE}$ and *opd'* (Fig.5.5.3 and Fig.5.5.3.a). In *opd'* the IRE structure is destabilized and the OPH^{C6XHis} encoded by *opd'* has also gone up. The enhanced OPH translation encoded by mRNA transcribed from *opd'* gene could be due to destabilization of the stem loop structure of IRE, which is rather masking the translational initiation site (Fig.5.5.3.a; Fig.6.5.7a). It is not clear from the data presented in this chapter if such destabilization of IRE is possible due to $_{Sf}$IRP-IRE^{opd} interactions. Further experiments were conducted to understand the role of IRE mediated translational inhibition of *opd* gene expression and described in fourth chapter.

Fig.5.6.4. Alignment of rabbit, *B. subtilis*, *S. fuliginis*, *E. coli* Acn sequences. The amino acid residues essential for IRE interaction with IRP are highlighted in a red box.

Chapter-IV

Background:

In the preceding chapters of the thesis, we have described the experiments performed to gather evidence on transcriptional regulation of *opd* gene. The third chapter of the thesis is devoted to describe experiments performed to prove existence of IRE element in *opd* mRNA. The current chapter describes experiments conducted to elucidate the role of IRE in post-transcriptional regulation of *opd* gene. The secondary structures of mRNA, like IRE elements or pseudoknots serve as targets either to regulatory proteins such as IRE and regulatory small RNAs. Depending on the physiological cues they interact with the mRNA secondary structures and regulate the gene expression by either inhibiting or activating the process of translation (Jagodnik et al., 2017; Leppek et al., 2018). Although, the physiological significance was unclear, in the third chapter the interactions between IRE^{opd}–$_{Sf}$Acn (IRP) interactions were demonstrated. This chapter describes identification of a small regulatory RNA in the intergenic region of *opd* and *istB* genes, and its role on expression of *opd* gene by establishing direct interactions with IRE^{opd}.

6.1. Objective specific methodology:

Table 6.1: Primers used in this study

NS16 P	TTGTCGAGGCGGTGCTTTCATCTGCTGTGCTG	Oligonucleotide complementary to sRNA, *CrpR54* used as probe while performing northern blot analysis.
NS17 FP	AATTCCTGCTGTGCTGAACGGCCTTCCGCTACGCTCTGCA	Forward (FP)/ Reverse primers (RP) used to generate the core promoter of *crpR54*-gene encoding sRNA, *CrpR54*. The *EcoR*I and *PstI* sites appended to facilitate cloning in pMP220 are underlined.
NS17 RP	GAGCGTAGCGGAAGGCCGTTCAGCACAGCAGG	

NS18 FP	AATTCCCTGATCAGAAAACCCCTCATCTGCTGTGCTGAACGGCCTTCCGCTACGCTCTGCA	Forward (FP)/ Reverse primers (RP) used to generate the promoter of *crpR54*-gene encoding sRNA, *CrpR54* along with *crp* binding motif. The *EcoR*I and *PstI* sites appended to facilitate cloning in pMP220 are underlined.
NS18 RP	GAGCGTAGCGGAAGGCCGTTCAGCACAGCAGATGAGGGGTTTTCTGATCAGGG	
NS19 FP	TCTAGAAGACCGTTCAGCACAGCAGATGAAAGCACCGCCTCGACAAGAGGCTTTTTGTTCAATCCAAAGCTT	Complementary oligos used to anneal while obtaining sRNA gene, *crpR54* of *S. fuliginis.* The *XbaI* and *HindIII* sites appended to facilitate cloning in pET23b are underlined.
NS19 RP	AAGCTTTGGATTGAACAAAAAGCCTCTTGTCGAGGCGGTGCTTTCATCTGCTGTGCTGAACGGTCTTCTAGA	
NS20 FP	AAAGAATTCCCAACTGGTACACTCTTAC	Forward primer (FP)/ Reverse primers (RP) used to amplify *IRE*^{opd} along with the core promoter of *opd* gene. The *EcoRI* and *BamHI* sites, appended to the primers facilitate cloning of *opd* gene promoter in the translational fusion vector, pRS552.
NS20 RP	AAAGGATCCCACCCAGCCAGGCCGCCGAG	
NS21 FP	GCCAGAATTCAGGGAGACCACAACGGTTTCACT	Forward (FP) / reverse (RP) primers used to amplify full length ORFs *opd* and *opd'* genes from expression plasmids pPHYS/pPHIR. The *EcoRI*/ *BamHI* sites appended to facilitate cloning of
NS21 RP	GCCAGGATCCCAAAAAACCCCTCAAGACCC	

		opd gene and its variant *opd'* in low copy expression vector pMMB206 are underlined.
NS22 FP	AAACATATGGCCGACAAAGTGAACAAC	Forward primer (FP)/ reverse primer (RP) used to amplify *hfq* from *S. fuliginis*. The *Nde*I/XhoI sites appended to facilitate cloning in pET23b are underlined.
NS22 RP	AAACTCGAGATCCTCGCCCTCACCCTC	
NS23 FP	TAGCTCACTCATTAGGCACC	Forward and reverse primers used to amplify *lacZ* region from the genomic DNA of *E.coli* NiCo21(DE3)
NS23 RP	ATATGGAAACCGTCGATATT	
NS24 FP	AGGCTGAATGTGTACAATTGAGACG	Forward (FP) and reverse primers (RP) used to amplify *hfq* region from the genomic DNA of *E.coli* NiCo21(DE3)
NS24 RP	ACAGGATCGCTGGCTCCC	
NS25 FP	AAAAGGCTTTAATACGACTCACTATAGG	Forward primer used to amplify the *Sfhfq* gene from pNS16 which carries *Sfhfq* as an *NdeI/XhoI* fragment cloned in pET23b (along with the T7 promoter) using vector specific primer. The *HindIII* site appended to facilitate cloning in pET23b- *crpR54* (pNS13) is underlined

Table 6.2: Strains used in this study

E. coli DH5α	*λsupE*44, Δ*lacU*169 (*Δ80 lacZΔM*15) *hsdR*17 *recA*1 *endA*1 *gyrA*96 *thi*1 *relA*1	(Hanahan, 1983)
Sphingobium fuliginis ATCC 27551	Wild type strain, Sm^r, PmB^r, *opd+*	(Kawahara et al., 2010; Sethunathan & Yoshida, 1973)
E.coli NiCo (DE3)	BL21(DE3) $glmS_{6Ala}$ *slyD-CBD can-CBD arnA-CBD*	(Robichon et al., 2011)
E. coli BW25113 Δ*hfq*::kan	*Δ(araD-araB)*567, ΔlacZ4787(::rrnB-3), F- *λ*-, *rph-1, Δ(rhaD-rhaB)568*, *hsdR514,* Δ*hfq*::kan	(Baba et al., 2006; Datsenko & Wanner, 2000)
E. coli BW25113 Δ*lacZ*::kan	*Δ(araD-araB)*567, ΔlacZ4787(::rrnB-3), F- *λ*-, *rph-1, Δ(rhaD-rhaB)568*, *hsdR514,* Δ*lacZ*::kan	(Baba et al., 2006; Datsenko & Wanner, 2000)
E. coli NS002	Km^r. *E. coli* NiCo (DE3) derivative. Generated by deleting *hfq* gene.	This study
E. coli NS003	Km^r. *E. coli* NiCo (DE3) derivative. Generated by deleting *lacZ* gene.	This study
E. coli K-12 MG1655 AM001	MG1655 with *lacZ* deletion	(Madikonda et al., 2020)

Table 6.3: Plasmids used in this study

pET23b	Amp^r. The T7 promoter driven expression vector. Facilitates expression of cloned genes with C-terminal 6xHis-tag.	Novagen
pMP220	Tet^r, promoter probe vector	(Spaink et al., 1987)
pRS552	Amp^r, Km^r. translational fusion vector with *lacZ* reporter gene.	(Simons et al., 1987)
pMMB206	Cm^r, low copy, broad host range, mobilizable expression vector. Facilitates expression of cloned genes from an IPTG inducible *tac* promoter.	(Morales et al., 1991)
pNS11	Tet^r, *crpR54-lacZ* transcriptional fusion. Generated by cloning promoter of *crpR54*gene as *EcoR*I-*PstI* fragment in pMP220.	This study
pNS12	Tet^r, *lacZ* transcriptional fusion. Generated by cloning promoter of *crpR54* gene along with the CRP binding motif, as *EcoR*I- *PstI* fragment in pMP220.	This study

pNS13	Amp^r, plasmid generated by cloning *crpR54* gene of *S. fuliginis* in pET23b as *XbaI* and *HindIII* fragment. Codes sRNA, *CrpR54*.	This study
pNS14	Amp^r, Km^r, *opd* -lacZ translational fusion. Generated by cloning the promoter of *opd* gene along with *IRE^{opd}* coding sequence in pRS552 as *EcoR*I and *BamHI* fragment.	This study
pSM5	Cm^r, Low copy expression plasmid. Generated by ligating full length ORF of *opd* gene in pMMB206 as *EcoRI* and *BamHI* fragment. Codes OPH^{C6xHis}.	(Siddavatta m et al., 2003)
pNS15	Cm^r, low copy expression plasmid. Generated by ligating full length ORF of *opd'* gene in pMMB206 as *EcoRI* and *BamHI* fragment. Codes OPH^{C6xHis}.	This study
pNS16	Amp^r, Expression plasmid. Generated by cloning *hfq* gene of *S. fuliginis* in pET23b as *Nde*I and *Xho*I fragment. Codes Hfq^{C6xHis}.	This study
pNS17	Amp^r, expression plasmid. Generated by cloning *$_{Sf}$hfq* gene amplified from pNS16 along with T7 promoter as a *HindIII-XhoI* fragment in pET23b-*crpR54* (pNS13). Codes Hfq^{C6xHis} and sRNA, *CrpR54*.	This study

6.4.1. Prediction of non-coding RNA:

The presence of any non-coding RNAs in the indigenous plasmid (pPDL2) of *S. fuliginis* was predicted by using sRNAscanner webserver (http://cluster.physics.iisc.ernet.in/sRNAscanner/) (Sridhar et al., 2010). The analysis of non-coding RNA was done by giving the plasmid sequence of pPDL2 to the sRNAscanner.

6.4.2. Detection of sRNA by northern blot analysis:

In order to validate the expression of predicted non-coding sRNA, northern blot analysis was performed using total RNA isolated from *S. fuliginis* cultures grown to early log, log and stationary phases in LB medium. The methodology of RNA isolation is described elsewhere in the thesis. The RNA isolated from *E. coli*, in a similar manner served as a negative control. The RNA was analyzed on a 7M urea-PAGE. Prior to electrophoresis, the wells of the gel were flushed with 1X TBE buffer and was subjected to a pre-run for 45 min at

room temperature. The RNA samples were prepared by mixing 30µg of RNA with appropriate amount of loading dye having 7M urea. Subsequently, the samples were resolved on a 15% urea-PAGE. Following electrophoresis, RNA was transferred onto a NC membrane using Transblot transfer (BioRad) unit for 1h at 18 V. After successful transfer, the RNA was immobilized onto the membrane by UV crosslinking using the Stratagene crosslinker for 2 min at 1200 KJ. The UV cross linked membrane was subjected to pre-hybridization by soaking the membrane in 40 ml of PerfectHyb Plus hybridization buffer (Sigma-Aldrich) for 3h at 65^0C. Following pre-hybridization, the radiolabelled probe complementary to sRNA was added and incubated at 40^0C for 16-20h with constant rotation. Subsequently, the blot was washed thrice with 2X SSC buffer at an interval of 5 min and was exposed to a phosphor imaging screen to visualize the sRNA specific signal.

6.4.3. Prediction of putative promoter of sRNA coding gene, *crpR54*:

The potential promoter of the gene encoding sRNA and regulatory motifs present upstream of sRNA coding region were predicted by using the online tool Bprom (Solovyev Victor and Salamov Asaf, 2010) and MEME Suite (http://meme-suite.org/tools/meme) respectively. While predicting sRNA promoter, 100 bps upstream sequence of sRNA gene, was submitted to the webserver. This tool predicts promoter elements based on the conserved promoter motifs. To identify the presence of sequence motifs that serve as binding sites to any carbon responsive regulatory proteins, the gene encoding sRNA along with its predicted promoter was given as input to MEME Suite.

6.4.4. Construction of transcriptional fusions:

The *crpR54* -*lac*Z fusions were constructed by cloning the promoter elements of sRNA coding gene, *crpR54* in pMP220 (promoter test vector). The complementary oligos NS17FP/NS17RP were annealed to generate the promoter region of *crpR54,* whereas the complementary oligos NS18FP/NS18RP were annealed to get the DNA with the promoter of *crpR54* along with CRP binding

motif. These set of self-complimentary oligos appended with *EcoR*I and *Pst*I were annealed before ligating to pMP220 digested with the similar enzymes. After ligation, the transformants obtained after transformation of the ligation mixture into DH5α were selected on LB agar plates supplemented with appropriate amounts of of tetracycline and X-gal and couple of recombinant colonies with blue colour were sent sequencing using NS5RP. The resulting *lacZ* fusions were designated as pNS11 and pNS12.

6.4.5. Construction of translational fusion:

The *opd-lac*Z translational fusion was generated by translationally fusing *opd* gene promoter along with the DNA region coding IRE^{opd} to the promoter less *lacZ* gene of pRS552. This region was amplified with NS20FP/NS20RP with *EcoRI* and *BamHI* restriction sites. Amplicon of 227bp was analyzed on a 0.8% agarose gel and then subjected to purification by gel extraction using methods mentioned earlier in the thesis. The purified amplicon was ligated to pRS552 digested with similar enzymes. After ligation, the transformants obtained after transformation of the ligation mixture were selected on LB agar plates supplemented with appropriate amounts of ampicillin and X-gal. The resulting *lacZ* translational fusion was designated as pNS14.

6.4.6. Prediction of complementary base pairing between sRNA, *CrpR54* and IRE^{opd}:

Once the sRNA expression was confirmed using northern blotting, further attempts were made to analyze interactions between sRNA and IRE^{opd} using Bielefeld Bioinformatics Server-BiBiServ (https://bibiserv.cebitec.uni-bielefeld.de/).

6.4.7. Cloning of *crpR54* in a high copy vector:

The gene coding for sRNA was generated. By annealating self-complementary NS19FP/NS19RP oligos appended with *XbaI* and *HindIII* sites. The annealed oligos were ligated to similarly digested pET23b vector. The transformants obtained after transformation of the ligation mixture into DH5α

were selected on LB plates supplemented with appropriate amounts of ampicillin. The recombinant plasmids isolated from transformants were sub-cultured and screened for the existence of insert by isolating recombinant plasmid and digestion with *XbaI* and *HindIII* enzymes. The cloned gene was verified by sequencing using vector specific primer. The resulting plasmid was designated as pNS13.

6.4.8. Generation *lacZ* null mutant of *E. coli* NiCo (DE3):

Initially the *E. coli* BW25113 Δ*lacZ*::kan was obtained (generous gift from Dr. Manjula Reddy, CCMB, Hyderabad) and used to generate *lacZ* null mutant of *E. coli* NiCo21(DE3) strain by following P1 Transduction method (Thomason et al., 2007).

Transduction

a) Phage P1 lysate preparation: In order to create *lacZ* null mutant of *E. coli* NiCo21(DE3), 2.0 ml of overnight culture of donor *E. coli* BW25113 strain having Δ*lacZ*::kan was mixed with 0.2ml of P1 phage and incubated at 37^0C without shaking to facilitate phage adsorption. About 10ml of LB broth and sterile $CaCl_2$ (5mM) was added to this infection mixture prior to its incubation with shaking at 37^0C for 4 to 6 h or till the complete lysis of cells. After observing the cell lysis, 0.2ml of chloroform was added to the phage lysate to avoid further growth of the cells. This preparation was subjected to centrifugation for 10 min at 6000 rpm to remove cellular debris. The obtained supernatant containing transducing particles was stored at 4^0C until further use.

b) Phage infection: To the 2ml of overnight culture of *E. coli* NiCo21(DE3) cells, 5mM $CaCl_2$ and 0.2ml of phage preparation was added. After addition of phage lysate, the cells were incubated at 37^0C for about 15 min to allow phage adsorption. Unadsorbed phage particles were separated by centrifugation for 10 min at 6000 rpm. Further 5ml of LB broth containing 10mM sodium citrate was added to the infected *E. coli* cells and allowed to incubate for 45min at 37^0C. Finally the harvested cells were resuspended in 0.2ml of LB broth, plated on LB agar plates containing 10mM sodium citrate and 50μg/ml of kanamycin. Finally

the mutation in *lacZ* gene was confirmed by performing PCR amplification by using primer set NS23FP/NS23RP which were designed taking DNA region 100bp upstream and downstream of the *lacZ* from *E. coli.* Thus obtained strain named as *E. coli* NS003, was resistant to kanamycin.

6.4.9. Genetic Screen to validate sRNA and *IRE^{opd}* interactions:

The genetic screen was developed by using two compatible plasmids. One of them was pNS13, which codes for sRNA, *CrpR54*. The other plasmid was *opd-lacZ* translational fusion, pNS14 (The *opd* gene promoter along with the DNA region coding *IRE^{opd}* is fused with promoter less *lacZ* gene). In order to validate the interactions of sRNA and *IRE^{opd}*, *E. coli* NS003 (pNS13) was transformed with pNS14. Then the *E. coli* NS003 (pNS13+pNS14) cells were plated on X-gal containing LB plates, in the presence and absence of IPTG. If *CrpR54* interacts with *IRE^{opd}* upon induction of its expression the *E. coli* NS003 cells containing pNS14 should show *lac* positive phenotype on an X-gal plate. The *E. coli* NS003 (pNS13) and *E. coli* NS003 (pNS14) cells served as controls and remain *lac* negative both in presence and absence of IPTG.

6.4.10. Generation of *opd* variants:

6.4.10a. Cloning of full length ORF of *opd* gene (with IRE) in a low copy, expression vector

The plasmid pPHYS400 (Pandey et al., 2009) was used as a template to amplify full length ORF of *opd* gene (with IRE) using NS21FP/NS21RP primer set appended with *EcoRI* and *BamHI*. The amplicon was gel extracted and ligated to pMMB206 digested with similar enzymes. The transformants obtained after transformation of the ligation mixture into DH5α were selected on LB agar plates supplemented with appropriate amounts of chloramphenicol, IPTG and X-gal. The recombinant plasmids isolated from transformants were sub-cultured and screened for the existence of insert by isolating recombinant plasmid followed by digesion using *EcoRI* and *BamHI*. Resulting plasmid was designated as pSM5 and codes for OPH^{C6xHis} (Siddavattam et al., 2003).

6.4.10b. Cloning of *opd* variant *opd'* in a low copy, expression vector

The plasmid pPHIR400 (Pandey et al., 2009) was used to amplify *opd'* having non-complementary mutations at the third base of IRE^{opd} coding region using NS21FP/NS21RP primer set appended with *EcoRI* and *BamHI*. The amplicon was gel extracted and ligated to pMMB206 digested with similar enzymes. The transformants obtained after transformation of the ligation mixture into DH5α were selected on LB agar plates supplemented with appropriate amounts of Chloramphenicol, IPTG and X-gal. The plasmids obtained from transformants were sub-cultured and screened for the existence of insert by isolating recombinant plasmid and digestion with *EcoRI* and *BamHI*. The plasmid thus obtained, was designated as pNS15 and codes for wild type OPH^{C6xHis} as mutations were introduced at the third base of the codon.

6.4.11. The effect of sRNA on expression of *opd*:

Following successful generation of the low copy, expression plasmids (pSM5 and pNS15) coding for OPH^{C6xHis}, they were independently transformed into *E. coli* NiCo cells. The expression of OPH^{C6XHis} was assessed by co-transforming *E. coli* NiCo (pSM5) and (pNS15) cells with pNS13 coding sRNA, *CrpR54*. The *E. coli* NiCo (pSM5+pNS13) and *E. coli* NiCo (pNS15+pNS13) cells were cultured till mid exponential phase at 37^0C and the expression of OPH and sRNA, CrpR54 were induced for 1h after adding 1.0mM IPTG. Following incubation, 1ml cells were lysed by sonication with 30% amplitude, 4^0C temperature, 30 sec on and off sonic cycles. The cellular lysate was centrifuged at 13,000 rpm for 5 min to remove the debris. Clear lysate obtained was suspended in appropriate volumes of 2X loading dye and the samples were boiled and analyzed on an SDS-PAGE (12.5%) and a corresponding western blot was carried out with the aid of anti-His antibodies.

6.4.12. Relative quantification of *opd* transcripts:

The expression levels of *opd* were quantified using RNA extracted from *E. coli* NiCo (pSM5 + pNS13) and *E. coli* NiCo (pNS15 + pNS13). The cultures were

grown in LB medium and induced with IPTG, as described above. The total RNA was isolated from these cultures and the relative quantification was performed following the procedures mentioned elsewhere in the thesis. The primer sets NS6FP/NS6RP and NS7FP/NS7RP were used to quantify the expression levels of *opd* and *16S*rRNA respectively. The relative expression of *opd* with respect to *16S*rRNA coding gene was calculated using $2^{-\Delta Ct}$ method (Livak & Schmittgen, 2001).

6.4.13. Generation of *hfq* null mutant of *E. coli* NiCo21(DE3):

Initially the *E. coli* BW25113 Δ*hfq*::kan was obtained (generous gift from Dr. Manjula Reddy, CCMB, Hyderabad) and used to generate *hfq* null mutant of *E. coli* NiCo21(DE3) strain by following P1 Transduction method (Thomason et al., 2007).

Transduction

a) Phage P1 lysate preparation: The *hfq* null mutant of *E. coli* NiCo21(DE3) was created following P1 transduction method described in earlier section except that Δ*hfq*::kan mutant of *E. coli* BW25113 strain was used as donor.

6.4.14. Analysis of Hfq dependent interactions of sRNA, *CrpR54* and *IRE^{opd}*:

The interaction between sRNA, *CrpR54* and *IRE^{opd}* was analyzed in both *hfq* positive and negative backgrounds. The expression plasmid, pSM5 (full length ORF of *opd* gene) and pNS13 (which codes for sRNA, *CrpR54*) were co-transformed into *hfq* positive *E. coli* NiCo21(DE3) cells and *hfq* negative *E. coli* NS002 cells. The expression of OPH and sRNA, *CrpR54* were induced by addition of 1.0mM IPTG. They were grown at 37^0C for 1h after induction. Cells were harvested from 1 ml of induced cultures were mixed with appropriate amounts of 2X loading dye before boiling the contents for 5 min in a boiling water bath. The contents were then briefly spun at a maximum speed in microfuge and 10µl of clear soluble fraction was analyzed on a 12.5% SDS-PAGE. The corresponding western blot was performed using antibodies aginst His epitope, to analyze the positive/negative influence of Hfq on interactions between *CrpR54* and OPH.

6.4.15. Construction of expression plasmid encoding $_{Sf}$Hfq and sRNA, *CrpR54*:

An expression plasmid is generated to co-express *crpR54* ans $_{Sf}$Hfq This strategy involves two steps. The initial step is cloning of $_{Sf}$*hfq* gene in high copy expression plasmid, pET23b. In this, *hfq* gene was amplified from *S. fuliginis* using NS22FP and NS22RP appended with *NdeI* and *XhoI* respectively. The amplified fragment was gel extracted and purified following the procedure described in methodology section. The purified DNA fragment was ligated to similarly digested pET23b vector. After ligation, the ligation mixture was transformed into *E. coli* DH5α cells and the transformants were selected on LB agar plates substituted with appropriate amounts of ampicillin. The recombinant plasmids isolated from transformants were sub-cultured and screened for the existence of insert by isolating recombinant plasmid and digestion with *NdeI* /*XhoI* enzymes. The plasmid obtained was designated pNS16 and codes for $_{Sf}$Hfq^{C6xHis}.

In the subsequent step, the sRNA, *CrpR54* coding plasmid (pNS13) was used to sub-clone $_{Sf}$*hfq* gene. The $_{Sf}$*hfq* gene, cloned as an *NdeI* and *XhoI* fragment in pNS16 was taken as a template to amplify $_{Sf}$*hfq* along with the T7 promoter using NS25FP appended with *HindIII* and NS22 RP appended with *XhoI*. The amplified fragment was gel extracted and purified following the procedure described in methodology section. The purified DNA fragment was ligated to similarly digested pNS13 vector. After ligation, the mixture was transformed into *E. coli* DH5α cells and the transformants were selected on LB agar plates substituted with appropriate amounts of ampicillin. The recombinant plasmids isolated from transformants were sub-cultured and screened for the existence of insert by isolating recombinant plasmid and digestion with *HindIII* and *XhoI*. The plasmid thus obtained was designated as pNS17 and codes for $_{Sf}$Hfq^{C6xHis} and sRNA, *CrpR54*.

6.4.16. Role of Hfq in *CrpR54–IRE^{opd}* interactions:

The Hfq role on sRNA, *CrpR54* and *IRE^{opd}* interactions were determined by

transforming the *E. coli* NS002 (pSM5+pNS13) cells with pNS17. The expression of sRNA, *CrpR54,* Hfq and OPH were induced as described in methods section. The *E. coli* NS002 (pSM5+pNS13) and *E. coli* NiCo21(pSM5+pNS13) served as control. The cell growth was allowed till mid log phase and expression of sRNA, *CrpR54*, OPH and Hfq were induced as described in materials and methods section. The expression levels of OPH were monitored by western blot against His epitope.

6.4.17. Influence of carbon source on expression of OPH:

Initially, the cells of *S. fuliginis* were grown in rich LB medium, till the OD_{600} of the culture is reached to 0.60. Then the cells were harvested and re-inoculated in Minimal salts medium (OD_{600} of 0.20) having either glucose, or protocatechuate or 3,4-dihydroxybenzoic acid and grown till 0.5 OD (in cells grown in glucose), 0.45 OD (in cells grown in protocatechuic acid or 3,4-dihydroxybenzoic acid). Subsequently, the cells (1ml) from each subset were harvested by spinning at 6000 rpm for 10min at 4^0C. The proteins extracted from cell pellet were used to analyze on SDS-PAGE and to perform western blot using anti-OPH antibodies. The cultures grown under similar conditions were used to extract total RNA and subsequently to quantify *opd* mRNA by performing qPCR as described elsewhere in the thesis. The relative expression of *opd* was calculated using $2^{-\Delta Ct}$ method. The *16S* rRNA served as internal control (Livak & Schmittgen, 2001).

6.5. Results:

Here the main objective is to identify regulatory RNA that influences the translation of *opd* gene in *S. fuliginis*. The regulatory small RNAs are two types, cis-encoded sRNAs and trans-encoded sRNAs. Since *opd* gene is found as part of plasmid pPDL2 borne integrative mobilizable element the sequence of pPDL2 was used as input to the sRNAscanner webserver (http://cluster.physics.iisc.ernet.in/sRNAscanner/). Interestingly, a 54nt non-coding RNA coding gene was found in this intergenic region found between *opd* and *istB*

gene of IS-element *IS21*. The RNA hybrid prediction webserver (bibiserve) has shown a potential base pairing with an mfe of -36.4kcal/mol. There existed potential base pairing of sRNA with *IRE*^{opd}, initiated at left arm of the stem and has gone upto the right arm of stem through the loop region of *IRE*^{opd} (Fig 6.5.1.a) Such extensive complementarity between the predicted sRNA and one of the arms of the stem region of *IRE*^{opd} suggested a regulatory role for sRNA in expression of *opd* gene.

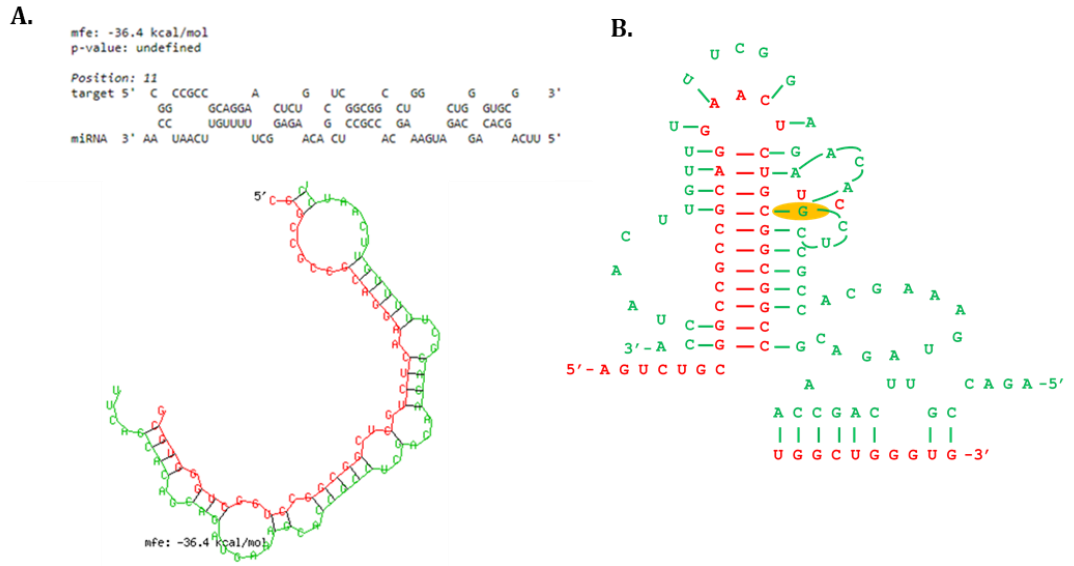

Fig.6.5.1.a. The base pairing interactions between *CrpR54* and *IRE*^{opd}. Panel A indicates the predicted interactions between sRNA and *IRE*^{opd} with a minimum free energy of -36.4kcal/mol. The complementary base pairing is clearly shown in the panel B. In both the panels red font corresponds to mRNA of *IRE*^{opd} and green font corresponds to sRNA. Pseudo loop of *IRE*^{opd} is indicated by dark yellow color in panel B.

Before going into the details of its regulatory role a detailed analysis was done on the promoter element and regulatory elements of sRNA coding gene. The putative promoter region was initially mapped using Bprom (Solovyev Victor and Salamov Asaf, 2010). As indicated in Fig. 6.5.1.b, the sRNA coding sequence starts from 'T' and ends at 'A' (Fig. 6.5.1b, panel B). The promoter region overlaps the inverted repeat sequence found at the terminus of IS element IS21. The promoter hexamers of gene encoding sRNA were identified to be 'GCTACG' as the -10 box and 'CTGCTG' as the -35 box. The predicted promoter region is identified within the right IR (inverted repeat) sequence of IS element of IS21. The left arm of inverted repeat overlapped the -35 hexameric sequence

of the promoter of sRNA coding gene (Fig. 6.5.1.a).

Once the promoter was mapped using *in silico* tool, further analysis was made to identify regulatory region, if any (overlapping promoter region). About 150 bp, found upstream of the putative TSS was given as input to RegRNA (http://regrna.mbc.nctu.edu.tw/html/prediction.html), a regulatory motif finder, which predicts regulatory motifs in the vicinity of promoter sequence. A sequence motif that shows strong similarity to the *crp* binding motif was identified overlapping the predicted promoter motif of sRNA coding gene. This observation gave a preliminary indication on its role in carbon catabolism (Fig.6.5.1.b).

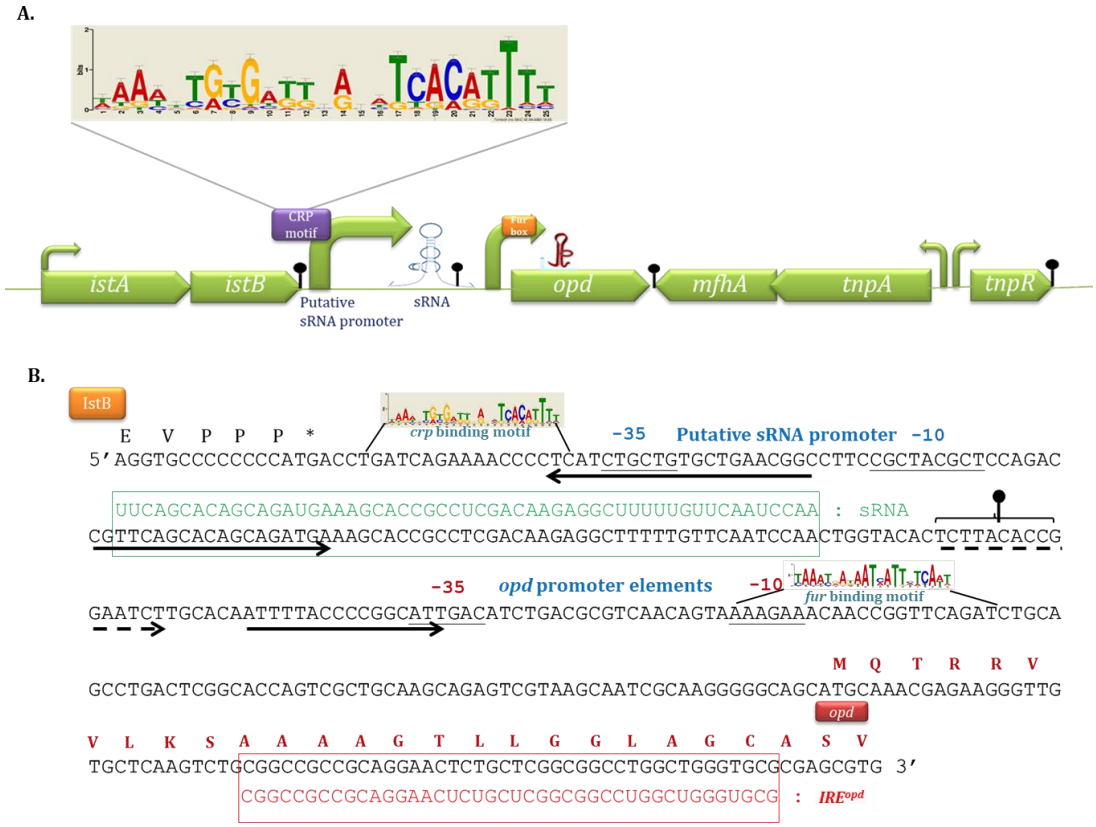

Fig.6.5.1.b. Structure of sRNA coding gene: Panel A shows genetic map of the DNA region containing *opd* and sRNA coding genes. Panel B shows the nucleotide sequence of the intergenic region found between *istB* and *opd* genes. The gene coding for sRNA is shown in green color box. The putative promoter elements are underlined and indicated as -10 and -35 in blue font. The sequence of *crp* binding motif overlapping the -35 sequence is highlighted. The inverted repeat sequence of IS-element IS21 is indicated with dark arrows. The predicted Rho-independent terminator sequence is indicated by dotted lines. The experimentally validated promoter element of *opd* gene is underlined and indicated with red color font.

6.5.2. Promoter validation:

The functional status of *in silico* predicted promoter and *crp* binding motif was elucidated by performing *in vivo* studies. Initially two transcriptional fusions were generated as described in methodology section of this chapter. One of them pNS11 contained only core promoter sequence fused to the promoter less *lacZ* gene of promoter test vector pMP220. In the second plasmid, pNS12, core promoter along with the *crp* binding motif was fused to the *lacZ* gene (Fig.6.5.2, panel A). Both the plasmids were independently transformed in *E. coli* MG1655 AM001.The *E. coli* AM001 (pNS11) cells and *E. coli* AM001 (pNS12) cells were then used to measure promoter activity by performing qualitative and quantitative β-galactosidase assay. In qualitative assays performed to determine promoter activity of sRNA coding gene the *E. coli* AM001 (pNS11) containing sRNA promoter-*lacZ* fusion was plated on LB, X-gal plate (sector I) along with *E. coli* AM001 (pNS12) containing sRNA promoter+*crp* binding motif-*lacZ* fusion (sector II); *E. coli* AM001 empty vector (pMP220) cells (sector IV) and *E. coli* AM001 (pNS2), containing *opd* promoter *lacZ* fusion was used as positive control (sector III). As seen in Fig 6.5.2, panel C, *E. coli* AM001 (pNS11) (sector I) showed intense blue color which indicated that the promoter element predicted using *in silico* tools was functional. Interestingly, LacZ activity was drastically reduced in *E. coli* AM001 (pNS12) (sector II), similar to *E. coli* AM001 empty vector (pMP220) control (sector IV).

In cells containing promoter test vector pMP220 (sector IV) there exists no promoter and hence appearance of pale colored colonies is expected. However, in sector containing *E. coli* AM001 (pNS12) appearance of pale colored colonies indicates existence of regulatory role for the predicted *crp*-binding motif overlapping sRNA gene promoter. The *E. coli* Crp protein must have bound to the *crp* motif sequence repressing the expression of *lacZ* gene. Similar trend was seen in quantitative assays (Fig.6.5.2, panel D). About 150 Miller units of β-galactosidase activity was obtained with *E. coli* AM001 (pNS11) cells, whereas the activity with *E. coli* AM001 (pNS12) cells were marginal (50 Miller units) and was close to the activity observed with control cultures of *E. coli* AM001

(pMP220). The data obtained here clearly show repressive role of *crp*-motif in expression of sRNA coding gene. While validating this observation further experiments were conducted. The Crp is known to regulate carbon catabolism. It represses the genes or operons involved in alternate carbon catabolism. Further the Crp responsive genes show growth dependent expression (Guebel & Torres, 2018). In early growth phase, where there exists no nutrient limitation the Crp responsive genes are repressed (Li et al., 2002). However, in stationary phase they are de-repressed. If the sRNA coding gene has role in carbon catabolism it should show growth phase dependent expression. As hypothesized the sRNA showed less expression in early growth phase and its expression reached to maximum during stationary phase suggesting a role for this sRNA coding gene in carbon catabolic regulation hence the gene coding sRNA is designated as *crpR54*.

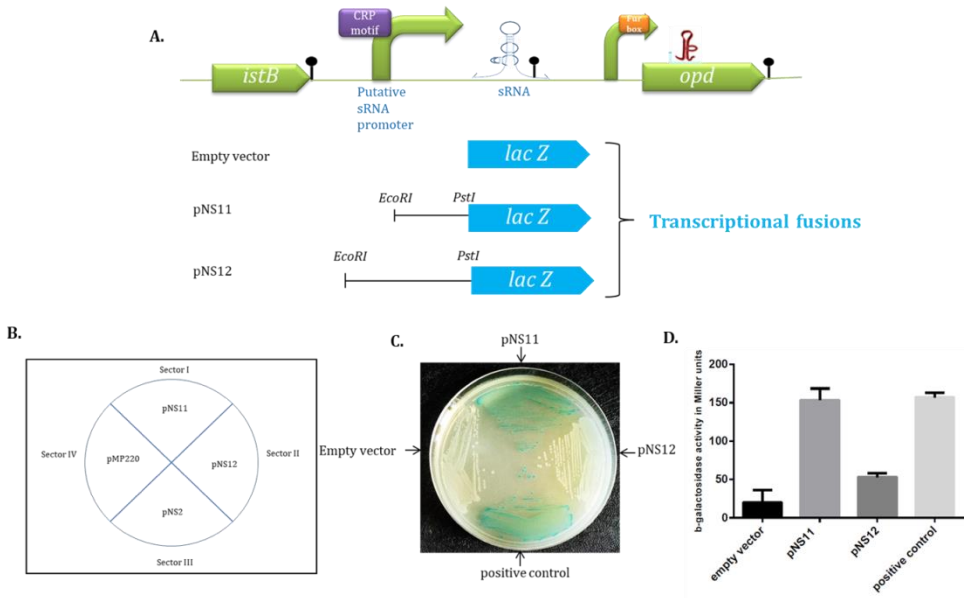

Fig.6.5.2. Role of CRP on expression of sRNA. Panel A shows extent of promoter region fused while generating *crpR54-lacZ* fusions, pNS11 and pNS12. Panel B indicates a representative LB plate showing sectors used in qualitative β-galactosidase activity assay. Panel C shows the qualitative β-galactosidase activity assay of *E. coli* AM001 obtained in *E. coli* AM001 cells transformed with pNS11 (sector I), pNS12 (sector II), pNS2 (*opd*-lacZ fusion positive control) (sector III) and empty vector, pMP220 (sector IV). Results of quantitative β -galactosidase activities obtained in these cells are shown in panel D.

6.5.3. Analysis *CrpR54* and *IRE^{opd}* interactions:

The predicted interactions between *CrpR54* and *IRE^{opd}* suggest influence of sRNA, *CrpR54* on expression of *opd* gene. In order to validate these interactions a two-plasmid assay was developed. One of the plasmid codes *CrpR54* from an IPTG

inducible promoter. The second compatible plasmid codes for a full length OPH^{C6XHis} from a *tac* promoter. Expression of full length OPH in presence and absence of sRNA *CrpR54* indicates its influence on expression of *opd* gene.

6.5.4. Cloning of *CrpR54* in a high copy vector:

The gene encoding sRNA, *crpR54* along with its putative transcriptional start site was generated by annealing self-complementary primer set NS19FP/NS19RP, appended with *XbaI* and *HindIII* restriction sites. The 60bp product was ligated to pET23b vector digested with the same enzymes. Thus obtained plasmid was named as pNS13 (Fig.6.5.4, panel C). Before proceeding to the further experiments the cloned *crpR54* gene of *S. fuliginis* was sequenced to ascertain that no mutations were inserted while cloning (Fig.6.5.4, panel D).

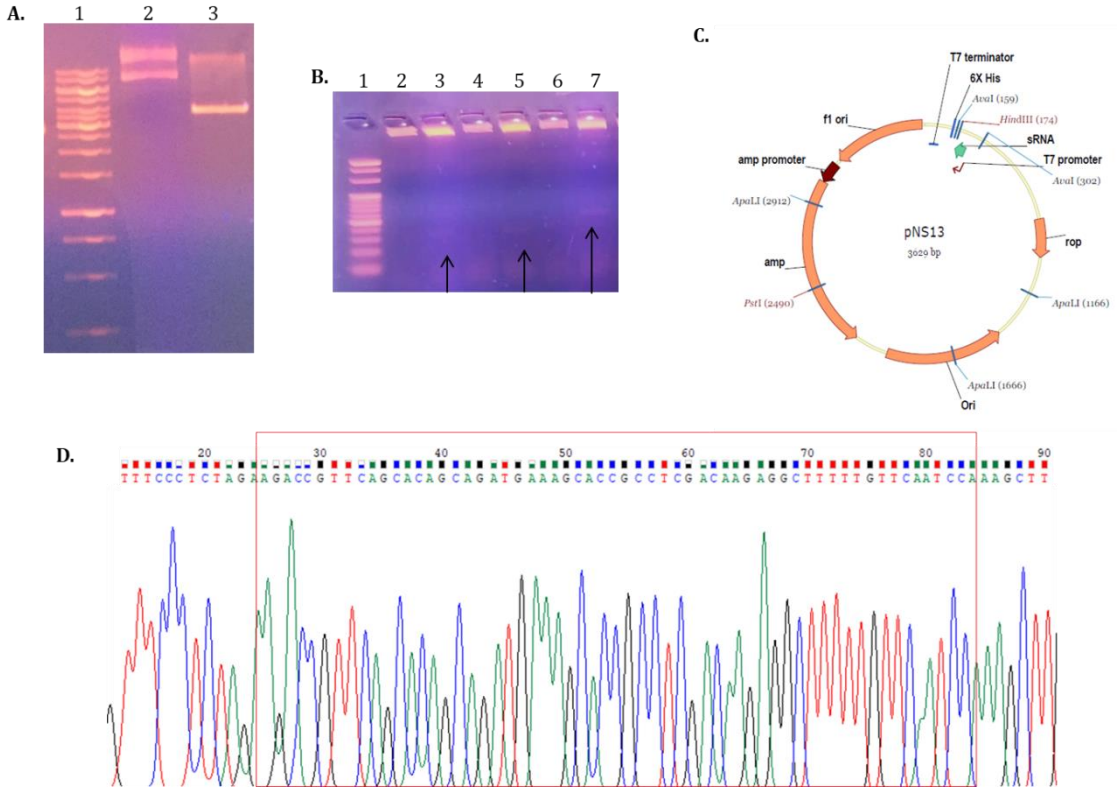

Fig.6.5.4. Construction of pNS13. The pNS13 digested with *XbaI* and *HindIII* is shown in panel 3. Molecular size markers are loaded in lane 1. The undigested pNS13 is loaded in lanes 2 and 4. The pNS13 digested with *XbaI* and *HindIII* is loaded in lanes 3 and 5. The arrow marks show the release of insert containing *crpR54*. Lanes 5 and 6 indicate undigested and digested pET23b vector, used as a positive control for digestion. Panel C shows plasmid map of pNS13. Panel D shows the sequence of pNS13 using vector specific primer. The red box indicates the sequence of *CrpR54*.

6.5.5. Construction *opd-lacZ* translational fusion:

The promoter region of *opd* gene along with IRE^{opd} was subjected to PCR using NS20FP/NS20RP attached with *EcoRI*/*BamHI* respectively. The amplicon obtained was digested with the above mentioned enzymes. Then ligated to pRS552 digested with the similar enzymes. The cloning strategy followed fuses *opd* gene along with IRE^{opd} specifying region coding the first 29 N-terminal amino acids of OPH in frame of *lacZ* gene specifying the β-galactosidase. The resulting *lacZ* fusion including IRE^{opd} was designated as pNS14.

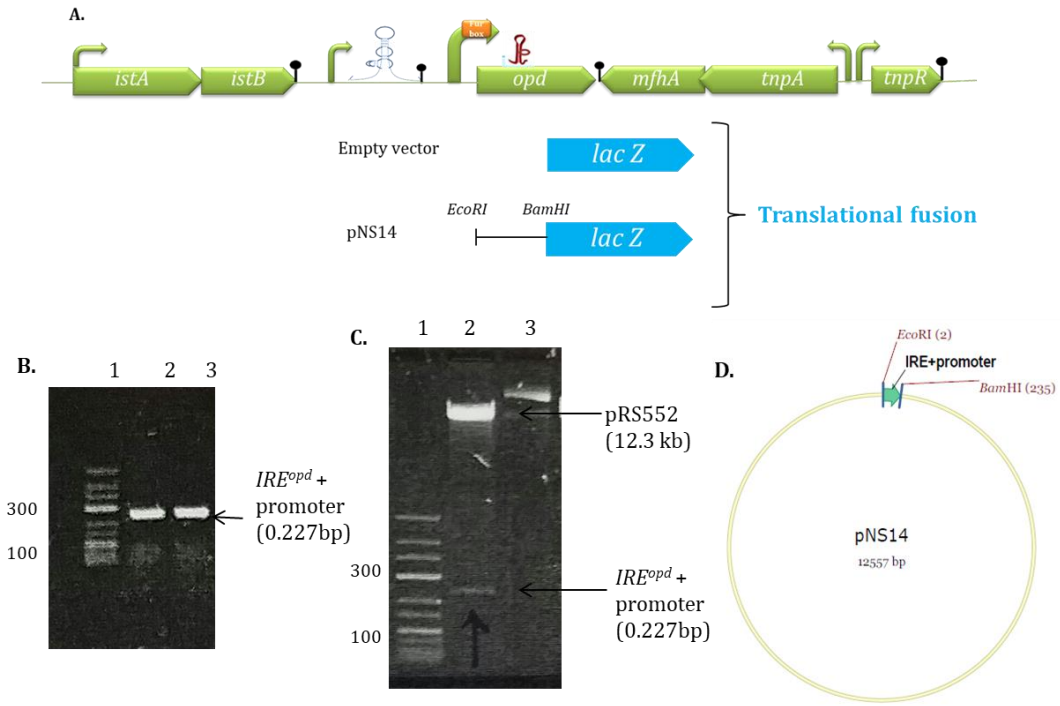

Fig.6.5.5. Construction of pNS14. Panel A shows the extent of *opd* region used to generate *opd-lacZ* fusion pNS14. Panel B shows 0.8% agarose gel used to analyze the amplicon of *opd* gene promoter along with the region specifying IRE^{opd}. Molecular size markers are loaded in lane 1. Lanes 2 and 3 show the amplicon containing desired *opd* promoter region. Panel C shows the digestion profile of pNS14. Molecular size markers are loaded in lane 1. The pNS14 digested with *EcoRI*/*BamHI* is loaded and the bands corresponding to the vector and insert containing IRE^{opd} are shown with arrows (lane 2). Undigested pNS14 is loaded in lane 3. Panel D shows plasmid map of pNS14.

6.5.6. Generation of *lacZ* negative *E. coli* NiCo21(DE3) strain:

Plasmid pNS13 codes sRNA *CrpR54* from a T7 promoter, whereas the pNS14 codes fusion protein $_{N29}$OPH-LacZ from the native *opd* gene promoter. In order to monitor *CrpR54* influence on expression of $_{N29}$OPH-LacZ, a *lacZ* null mutant of *E. coli* NiCo21(DE3) strain is required. Therefore the *lacZ* negative

derivative of *E. coli* NiCo21(DE3), *E. coli* NS003 was generated by transducing *E. coli* NiCo21(DE3) with phage P1 particle propagated using *E. coli* BW25113 Δ*lacZ*::kan strain in which *lacZ* gene is replaced with kanamycin cassette. The kanamycin resistant colonies were taken and colony PCR was performed using primer set NS23FP/NS23RP to detect replacement of *lacZ* with kanamycin cassette. As seen in Fig.6.5.6, panel B in all kanamycin resistant colonies an amplicon with a size of 1.5 Kb got amplified rather 500 bp amplicon seen in *lacZ* positive *E. coli* NiCo21(DE3) strain (Fig.6.5.6, panel B). The resulting strain was designated as *E. coli* NS003 and stored at -80^{0}C as a glycerol stock. When necessary *E. coli* NS003 was sub-cultured and used for analyzing expression of *opd* translational fusion.

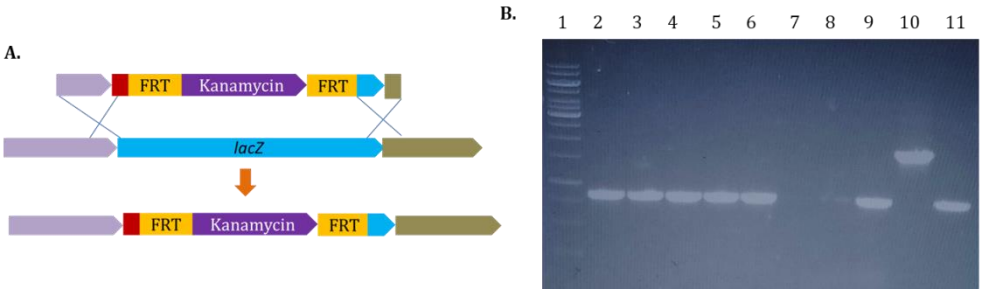

Fig.6.5.6. Generation of *E. coli* NS003. The strategy used to delete *lacZ* gene from *E. coli* NiCo21(DE3) strain is shown in panel A. Agarose gel (0.8%) indicating amplification of *lacZ* gene from NiCo21(DE3) is shown in panel B. Lane 1 represents molecular weight marker. Lane 2-6, 8, 9 and 11 represent amplicons generated from wild type *E. coli* NiCo21(DE3) cells. Lanes 10 shows amplicon size generated in a similar PCR reaction using *E. coli* NS003. No template (negative) control is shown in lane 7.

6.5.7. Generation of genetic screen:

A genetic screen was developed using *E. coli* NS003, plasmid pNS13 coding *CrpR*54 and translation fusion pNS14 coding fusion protein $_{N29}$OPH-LacZ. In the translational fusion the 5' region of *opd* gene along with *IRE^{opd}* is fused in frame of the *lacZ* gene and hence codes for $_{N29}$OPH-LacZ fusion protein. Expression levels of $_{N29}$OPH-LacZ can be monitored by measuring LacZ activity. The *E. coli* NS003 (pNS13) was co-transformed either with pNS14 or with pMP220, promoter probe vector. The LacZ activity was measured qualitatively and quantitatively after inducing the expression of sRNA, *CrpR54* with 1mM IPTG. The blue color phenotype of the colonies was observed on an X-gal plate only when $_{N29}$OPH-lacZ fusion protein was expressed from plasmid pNS14. Since

the 5' region of *opd* gene along with *IRE*^{opd} was fused to the *lacZ* gene, levels of β-galactosidase activity will be minimal as the *IRE*^{opd} masks translational initiation site (Fig.6.5.7a) of the *opd-lacZ* chimeric mRNA. However, if sRNA, *CrpR54* disrupts *IRE*^{opd} and exposes translational initiation site, the LacZ activity goes up as *IRE*^{opd} disruption leads to the enhanced production of $_{N29}$OPH-LacZ protein. As expected in plates made without IPTG the expression of sRNA, *CrpR54* is negligible and hence there will be no disruption to the *IRE*^{opd}. Therefore, expression levels of $_{N29}$OPH-LacZ will be low, yielding low levels of β-galactosidase activity. In accordance with the proposed hypothesis there was negligible amounts of blue color in *E. coli* NS003 (pNS13+pNS14) cells (Fig.6.5.7. panel C, sector IV). They appeared pale in color as seen in control cultures of *E. coli* NS003 (pNS14+pET23b) cells (sector I), *E. coli* NS003 (pNS13) cells (sector II) and *E. coli* NS003 (pNS14) cells (sector III). In a similar assay done in presence of IPTG, a clear blue color was seen in *E. coli* NS003 (pNS13+pNS14) indicating enhanced expression of $_{N29}$OPH-LacZ chimeric protein in presence of sRNA, *Crp54* (sector IV). Such activity was not seen in control cultures. The quantitative assays clearly indicated an increased β-galactosidase activity only in *E. coli* NS003 (pNS13+pNS14) cells.

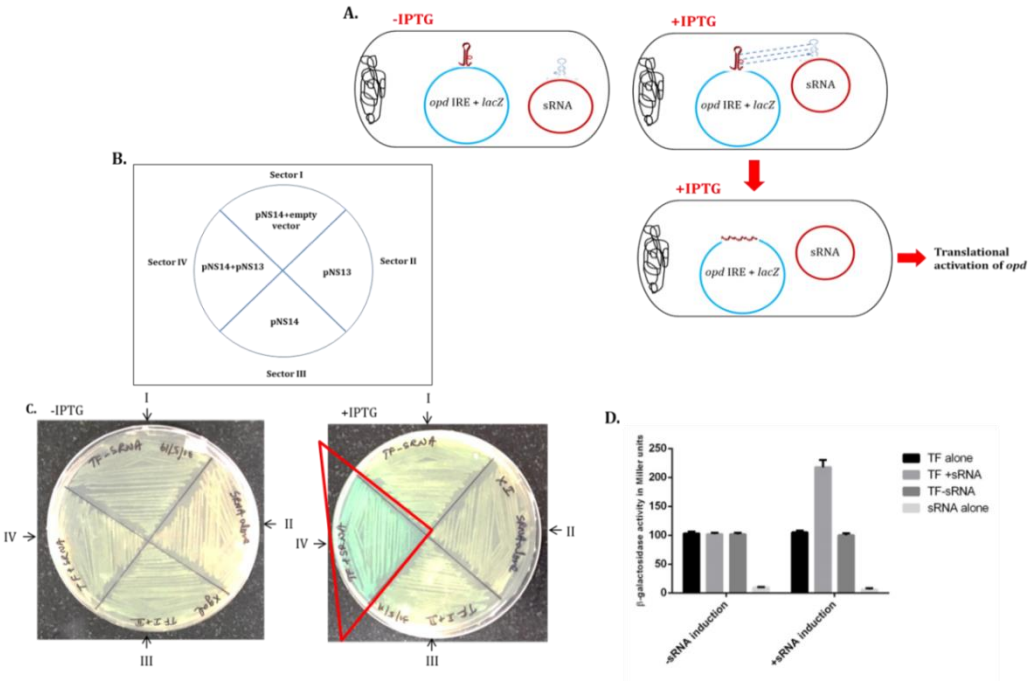

Fig.6.5.7. Two plasmid assay. Panel A shows functional details of genetic screen. Panel B indicates a representative LB+X-gal plate used for the two plasmid assay. Panel C shows either uninduced or induced *E. coli* NS003 (pNS14+pET23b) cells in sector I, *E. coli* NS003 (pNS13) cells in sector II, *E. coli* NS003 (pNS14) cells in sector III, *E. coli* NS003 (pNS14+pNS13) cells in sector IV. The red triangle is indicative of enhanced LacZ activity in *E. coli* NS003 (pNS14+pNS13) cells under IPTG induction. The values of quantitative assays from similar cultures are shown in panel D.

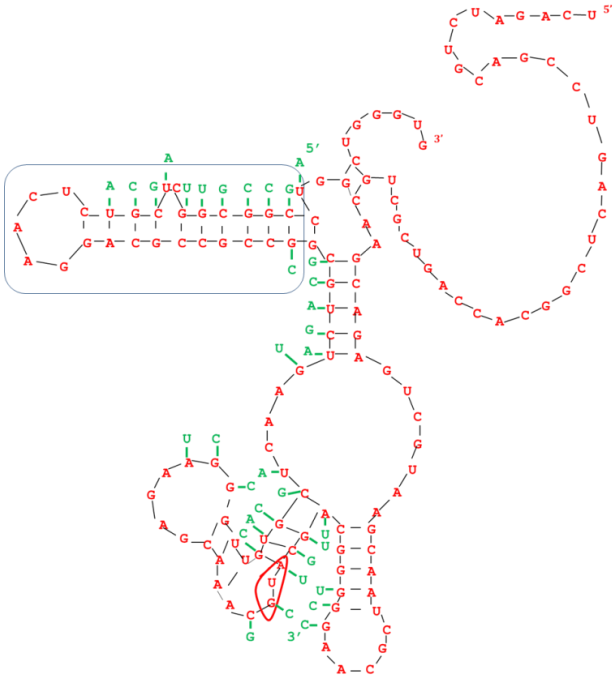

Fig.6.5.7a. Formation of sRNA-mRNA hybrid. The sRNA base pairs with the *opd* mRNA region and occludes the translation initiation site and also interacts by direct base pairing with the left arm of *IRE*^{opd}. The red font indicates transcript of *opd* mRNA (starting from TSS till IRE region) and green font indicates sRNA and its base pairing. The translation initiation site is highlighted in a red triangle. The blue box highlights *IRE*^{opd}.

6.5.8. Expression of OPH from *opd* and *opd'* genes:

The earlier work from our laboratory had explained generation of *opd'* gene (Pandey et al., 2009). In *opd'* the IRE^{opd} structure is disrupted. While validating the influence of IRE^{opd} on expression of OPH a low copy, expression plasmid pNS15 was generated by cloning the *opd'* in low copy number expression vector pMMB206. The full length ORF of *opd'* gene along with the upstream sequence including RBS was amplified from a previously constructed high copy, expression plasmid pPHIR by using NS21FP/NS21RP, appended with *EcoRI* and *BamHI* sites. The plasmid map of pNS15 is shown in (Fig.6.5.8, Panel C). The plasmid pSM5 constructed by cloning the ORF of *opd* gene was used as an expression plasmid coding OPH from a wild type *opd* gene having intact IRE^{opd} (Siddavattam et al., 2003). Both the constructs code for OPH^{C6xHis}.

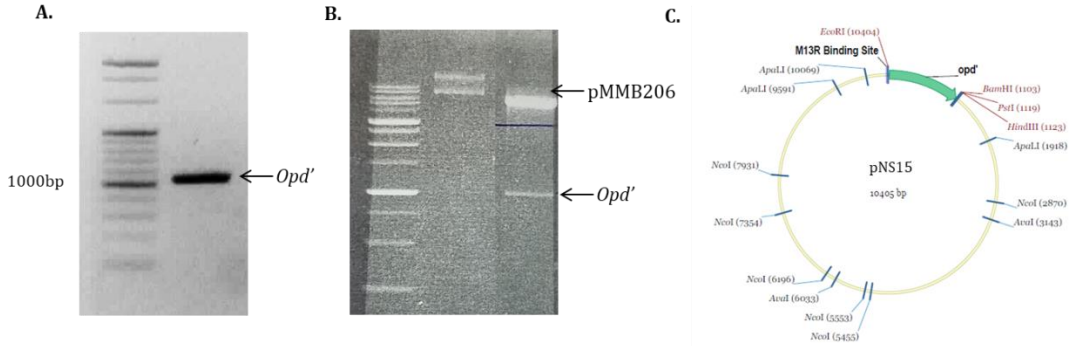

Fig.6.5.8. Construction of pNS15. Panel A shows 0.8% agarose gel used to analyse the amplicon of *opd'* (with non-complementary mutations introduced in third base of every codon in IRE^{opd} region). Molecular size markers are loaded in lane 1. Lanes 2 shows the amplicon of *opd* indicated by an arrow. Panel B shows the digestion profile of pNS16. Molecular size markers are loaded in lane 1. Undigested pNS15 is loaded in lane 2. The pNS15 digested with *EcoRI*/*BamHI* is loaded and the bands corresponding to the vector and insert are shown with arrows (lane 3). Panel C shows plasmid map of pNS15.

6.5.9. Influence of *CrpR54* on expression of OPH:

The genetic screen gave clear indication on positive influence of *CrpR54* on $_{N29}$OPH-LacZ expression. Therefore, further experiments were conducted to validate influence of *CrpR54* on the expression of OPH. Previous studies from our laboratory have generated a low copy expression vector pSM5 which codes OPH from IPTG inducible *tac* promoter. In this study, a similar expression plasmid

was generated using similar vector backbone by cloning *opd* variant *opd'* in which IRE^{opd} was disrupted. These two expression plasmids are compatible to the pNS13, which codes *CrpR54* from a T7 promoter. *E. coli* NiCo cells were then independently transformed with plasmids pSM5 and pNS15. These cells were co-transformed with *crpR54* encoding pNS13. These *E. coli* NiCo (DE3) cells with appropriate controls were induced with 1mM IPTG and incubated for 1hr. The expression levels of OPH from these cultures were analyzed by performing western blots using anti-OPH antibodies. A considerable elevation of OPH expression was observed in cells having expression plasmid pSM5 and *CrpR54* encoding pNS13 (Fig.6.5.9, panel B, lane 3) when compared to the levels of OPH coded by pSM5 in the absence of pNS13 (Fig.6.5.9, panel B, lane 2). As shown in third chapter the *opd'* (in which IRE-like structure is disrupted) encoded mRNA was shown to enhance OPH expression in cultures having expression plasmid coding OPH from *opd'* gene (Page No. 99, Fig.5.5.3.a). Interestingly the sRNA, *CrpR54* influence on expression of OPH was not seen in cultures expressing OPH from *opd'* gene, probably due to its lack of interactions with *CrpR54*. The influence of IRE^{opd} on translational repression of *opd'* mRNA was not seen as mutations introduced in *opd'* gene disrupted IRE^{opd} structure (Fig.6.5.9, panel B, lane 4 and 5). If these observations are seen along with reporter assays performed involving genetic screen, a clear inference can be drawn on a *CrpR54* dependent post-transcriptional regulation in *opd* expression. Supporting this proposition, no difference in the quantities of *opd* specific mRNA was seen in all these cultures, suggesting that the *CrpR54* dependent increase in OPH expression was due to increased translational efficiency (Fig.6.5.9, panel C).

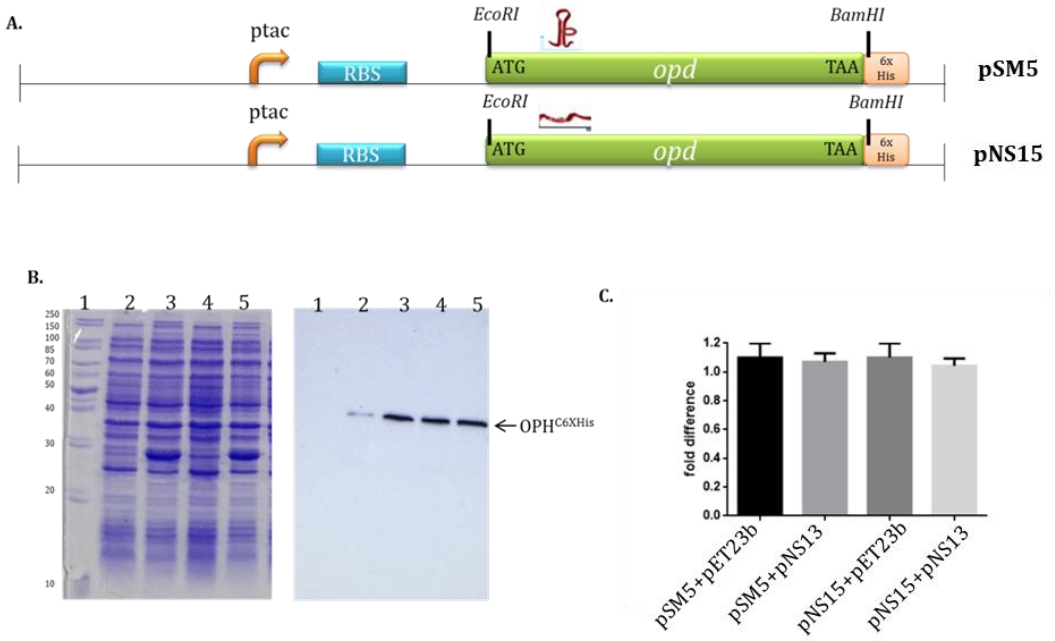

Fig.6.5.9. *CrpR54* dependent post-transcriptional regulation of *opd* gene expression. Panel A shows the extent of *opd* region used to construct pSM5 and pNS15. Panel B shows the coomassie stained, 12.5% SDS-PAGE and its corresponding western blot probed with anti-His antibodies, showing the expression of OPH^{C6XHis}. Lane 1 shows the molecular marker, lane 2 indicates expression of OPH^{C6XHis} from *E. coli* NiCo(pSM5+pET23b) cells. Lane 3 shows *E. coli* NiCo (pSM5+pNS13) cells. Lane 4 shows *E. coli* NiCo (pNS15+pET23b) cells. Lane 5 shows *E. coli* NiCo (pNS15+pNS13) cells. Panel C indicates relative quantification of *opd* transcripts in total RNA isolated from the cultures isolated from the cells grown under similar conditions.

6.5.10. Role of Hfq in *CrpR54* and IRE^{opd} interactions:

Hfq is an RNA chaperone which facilitates formation of sRNA-mRNA hybrid. The results described in earlier sections clearly show existence of interactions between IRE^{opd} and *CrpR54*. It is not known if Hfq is required for IRE^{opd}-*CrpR54* interactions. Therefore, the influence of Hfq on *CrpR54* and IRE^{opd} interactions is studied in *E. coli* as there exist significant (55%) similarities between $_{Ec}$Hfq and $_{Sf}$Hfq (Fig.6.5.10).

```
CLUSTAL O(1.2.4) multiple sequence alignment


fig|6666666.225841.peg.1539      MADKVNNLQDIFLNSLRKSKTPVTMFLVKGVKLQGIITWFDNFSVLLRRDGQSQLVYKHA   60
ENA|AAA97068|AAA97068.1          -MAKGQSLQDPFLNALRRERVPVSIYLVNGIKLQGQIESFDQFVILLK-NTVSQMVYKHA   58
                                    * :.*** ***:**:.:.**:::**:*:**** *  **:* :**: :  **:*****

fig|6666666.225841.peg.1539      ISTVMPAQSMDLTELRKASDGNGKSKLLQEIF----LSAVRKSGSPVTMFLVNGVMLQGE   116
ENA|AAA97068|AAA97068.1          ISTVVPSRPVSHHSNNA---GGGTSSNYHHGSSAQNTSAQQDSEETE-------------   102
                                 ****:*:: :.  . .    *.*.*.  :.       ** :.* .

fig|6666666.225841.peg.1539      IAAFDLFCMLLERDGMVQLVYKHAISTVQPLHALDLTGEGEGED   160
ENA|AAA97068|AAA97068.1          ---------------------------------------------   102
```

Fig.6.5.10. Alignment of $_{Sf}$Hfq with $_{Ec}$Hfq.

6.5.11. Confirmation of *hfq* null mutant *E. coli* NiCo21(DE3):

Initially *hfq* null mutant was generated in *E. coli* NiCo21(DE3) strain by transducing it with phage P1 particle propagated using *E. coli* BW25113 Δ*hfq*::kan strain in which *hfq* gene is replaced with kanamycin cassette. The kanamycin resistant colonies were taken and colony PCR was performed using primer set NS24FP/NS24RP to detect replacement of *hfq* with kanamycin cassette. As seen in Fig.6.5.11, panel B in all kanamycin resistant colonies an amplicon with a size of 1.5 Kb got amplified rather 500 bp amplicon seen in *hfq* positive *E. coli* NiCo21(DE3) strain. The resulting strain is designated as *E. coli* NS002 and stored at -80^{0}C as a glycerol stock. When necessary *E. coli* NS002 was sub-cultured and used for *opd* expression studies.

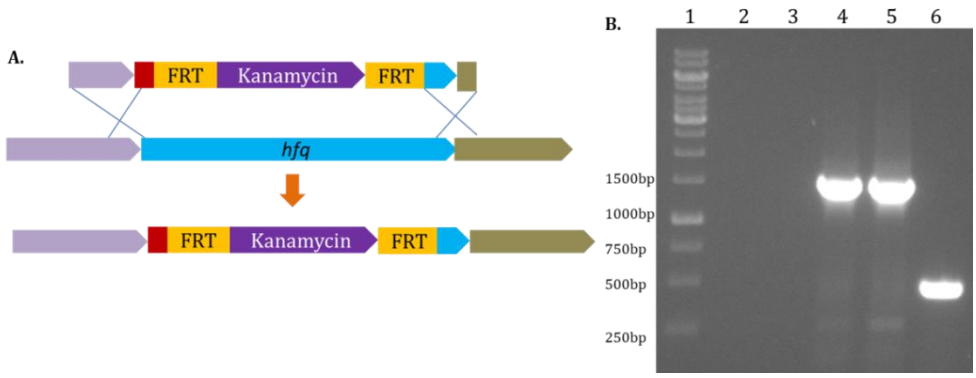

Fig.6.5.11. Generation of *E. coli* NS002. Strategy followed to delete *hfq* gene from *E. coli* NiCo21(DE3) strain is shown in panel A. Panel B shows 0.8% agarose gel to analyse the amplicon generated when PCR was performed using primer set NS24FP/NS24RP. Lane 1 shows molecular weight marker. Lane 2 represents no template control PCR reaction. Lane 3 indicates negative control. Lane 4 shows *E. coli* BW25113 Δ*lacZ*::kan. Lane 5 shows amplicon size generated in a similar PCR reaction using kanamycin resistant colonies of *E.coli* NS002. The lane 6 represents amplicon obtained in a PCR reaction having wild type *E. coli* NiCo21(DE3) having intact *hfq* gene.

6.5.12. Analysis of Hfq dependent interactions of sRNA-*opd* mRNA:

After successful deletion of *hfq* gene we have co-expressed both OPH and *CrpR54* in *E. coli* NS002 by transforming pSM5 and pNS13 in both Hfq (*E. coli* NiCo) positive and negative *E. coli* NS002 cells. The expression levels of OPH were examined by performing western blots against His epitope. Fig.6.5.12.a, panel B, lane 3, shows that the OPH expression got enhanced in Hfq positive

back ground and its expression got drastically reduced in *E. coli* NS002 (pSM5+pNS13) cells generated by deleting *hfq* gene. When *E. coli* NS002 (pSM5) cells were complemented by transforming pNS17 encoding both sRNA, *CrpR45* and Hfq from a T7 promoter the expression levels of OPH were increased and its level of expression was comparable to OPH expression obtained in *hfq* positive cells (Fig.6.5.12a, panel B, lane 6). These results clearly indicate requirement of Hfq to facilitate interactions between sRNA and IRE^{opd}.

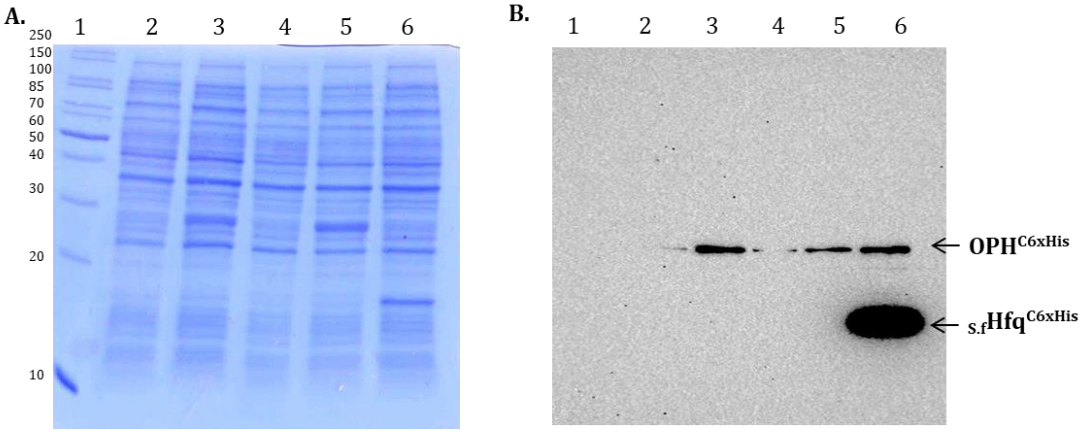

Fig.6.5.12a. The Hfq dependent interactions of sRNA-*opd* mRNA: Whole cell lysate loaded on a 12.5% SDS-PAGE after induction with 1mM IPTG is shown in panel A. Lane 1 corresponds to molecular marker. Lane 2 indicates expression of OPH in *E. coli* NiCo (pSM5+pET23b) cells. Lane 3 shows *E. coli* NiCo (pSM5+pNS13) cells. Lane 4 indicates *E. coli* NS002 (pSM5+pET23b cells. Lane 5 shows *E. coli* NS002 (pSM5+pNS13) cells. Lane 6 shows *E. coli* NS002 (pSM5+pNS17). Panel B shows its corresponding western blot probed with anti-His antibodies to detect the expression of OPH^{C6XHis}.

6.5.13. Influence of Carbon source on OPH expression:

S. fuliginis utilizes several aromatic carbon compounds as a unique source of carbon. Utilization of aromatic compounds requires unique catabolic pathways, where ring cleaving oxygenases play a critical role. These monooxygenases and dioxygenases require non-heme iron as cofactor (Fig.6.6.3). Previous studies from our lab have shown involvement of OPH in outer membrane transport, especially in transport of Ferric-enterobactin (Parapatla et al., 2020). Since growth on aromatic compounds necessitates increased iron influx, further studies were conducted to test influence of carbon source on OPH expression. The *S. fuliginis* cells were grown using 3,4-Dihydrobenzoic acid (protocatechuic acid) and 2,4-Dihydrobenzoic acid as carbon source (Fig. 6.5.13.b) and the proteins extracted were subjected to SDS-PAGE (Fig.6.5.14, panel A).

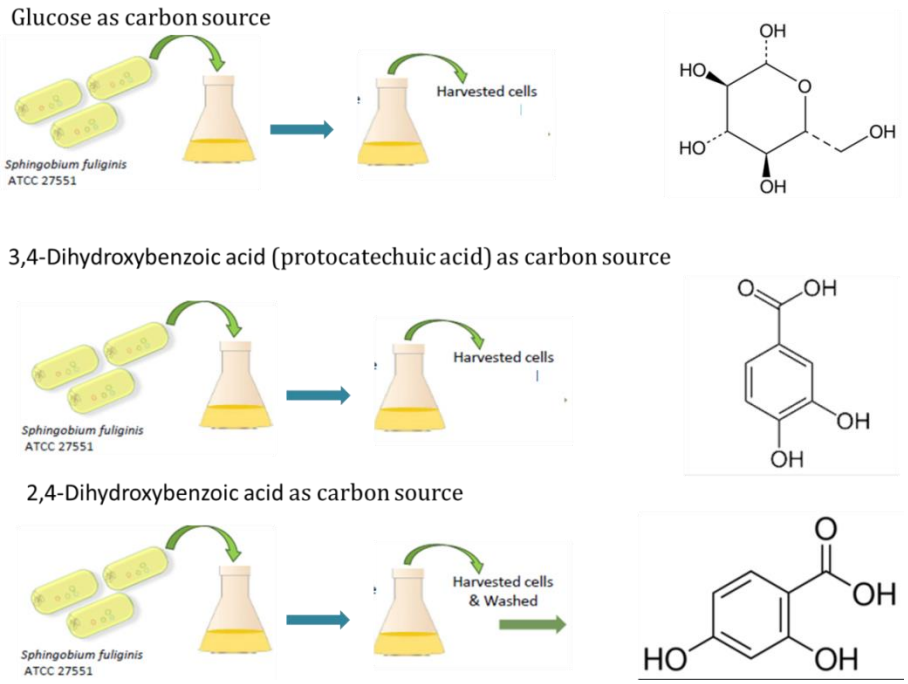

Fig.6.5.13.a. Schematic representation of *S. fuliginis* used for growth and expression studies of OPH.

. Initially growth of the bacteria was assessed for atleast 40h. The growth was optimum when glucose was used as carbon source. Cells reached to OD_{600} of 0.5 within 20 hours of incubation. However, the same cultures grown in alternative carbon sources reached an OD_{600} of 0.45 at the end of 40h (Fig. 6.5.13.b).

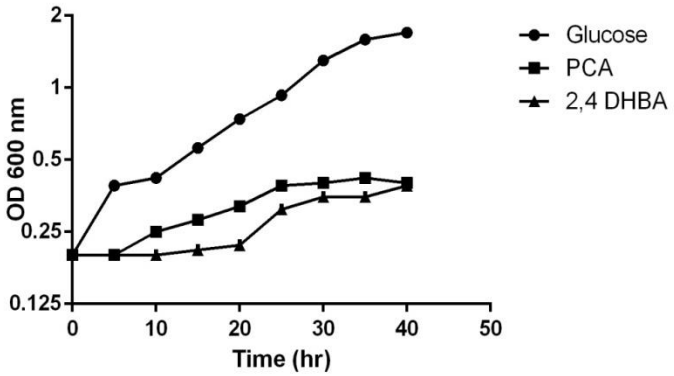

Fig.6.5.13.b. Growth curve of *S. fuliginis* grown in alternative carbon sources. *S. fuliginis* was inoculated at initial OD_{600} of 0.20 and growth was monitored for every 5h time period. The cells grown in glucose reached an OD_{600} of approximately 1.90 at the end of 40 hr. The cells grown in protocatechuic acid and 2,4 dihydroxybenzoic acid reached an OD_{600} of 0.45.

Cells were harvested from (1 ml cultures, OD_{600}) the cultures were used to isolate proteins and thus isolated proteins were analyzed on 12.5% SDS-PAGE. The OPH expression was quantified based on the intensity of the signal. Interestingly, in cells grown in less preferred carbon sources such as protocatechuic acid and 2,4 dihydroxybenzoic acid, the OPH signal intensity has significantly gone up. OPH expression in these cultures appeared to be doubled (Fig.6.5.14, panel B, lanes 3 and 4) when compared to the OPH specific signal intensity found in proteins isolated from glucose grown cultures (Fig.6.5.14, panel B, lane 2). Subsequently, relative quantification of *opd* transcripts was carried out by using the RNA isolated from the same set of cells grown using alternative carbon sources. The total RNA from each set of cells (1ml) was isolated and subjected to quantitative Real-time PCR and the data was normalized by *16S*rRNA transcripts. The data clearly showed that the *opd* specific transcripts were identical in the cells grown in either glucose or any other alternative carbon source (Fig.6.5.14, Panel C). The increase in expression of OPH despite having similar *opd* transcripts indicated the sRNA, *CrpR54* dependent activation of *opd* mRNA translation by destabilizing IRE^{opd}. Since *CrpR54* expression is induced only under carbon limiting condition, the increased expression of *CrpR54* appears to have relieved IRE^{opd} mediated translational repression of *opd* mRNA.

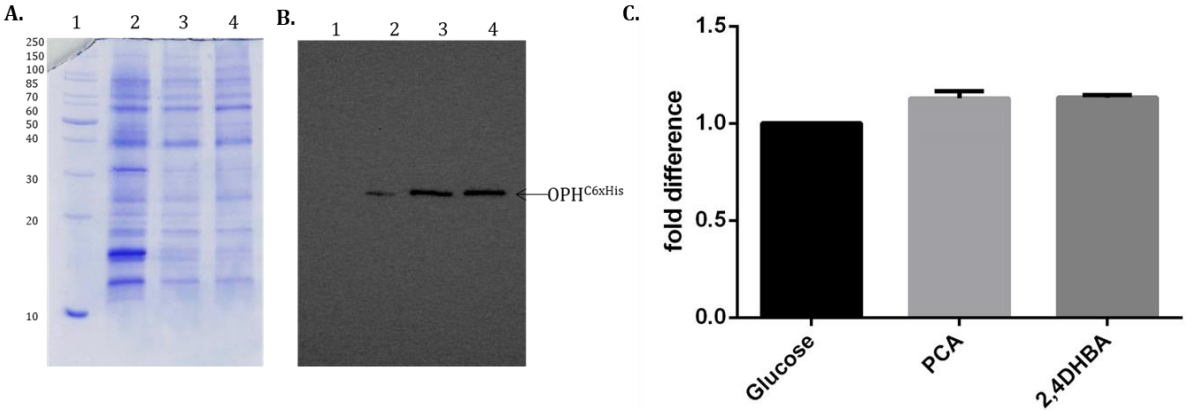

Fig.6.5.14. Influence of carbon source on OPH expression. Panel A shows a coomassie stained, 12.5% SDS-PAGE used for analysis of proteins extracted from cultures grown using glucose (lane 2), protocatechuic acid (Lane 3), 2,4 DHBA (lane 4). The corresponding western blot performed using anti-OPH antibodies is shown in panel B. Panel C shows the relative quantification of *opd* transcripts under similar conditions of growth.

6.6. Discussion:

The metabolism of iron is stringently regulated in all organisms (Hentze & Kuhn, 1996; Crosa, 1997). A huge number of RNA regulators identified as sRNAs are elucidated in a large variety of bacteria (Storz et al., 2011). The promoter elements regulating sRNA expression are sensitive for any specific cellular stress hence might serve as reporters of conditions encountered by a cell (Mutalik et al., 2009). The vital post-transcriptional regulators of bacterial gene expression are sRNAs. They usually control the gene expression by base pairing to target mRNAs, which might lead to either enhanced or inhibition of translation and/or change in mRNA stability (McQuail et al., 2019). A few classes of sRNAs utilize sequence-specific RNA–RNA interactions to regulate mRNA expression (Masse & Gottesman, 2002).

The current chapter shows existence of a similar non-coding RNA in the intergenic region of *opd* and *istB* of IS-element, *IS21*. Interestingly this sRNA showed potent complementarity with IRE^{opd}. The sRNA showed maximum base pairing on the left arm of IRE stem region and partial base pairing with the loop region as well as the right stem region. Out of 29 base forming IRE, 19 bases interact with the sRNA, *CrpR54* (Fig.6.5.1a). The influence of *CrpR54* on the expression of OPH was assessed using genetic screen (Fig.6.5.7). Further, *in vivo* experiments performed in the presence of *CrpR54* demonstrated a considerable increase of OPH expression, despite containing equal amounts of *opd* transcripts, indicating a role for *CrpR54* is in relieving the post-transcriptional regulation of *opd* expression (Fig.6.5.9). In Gram-negative bacteria, the RNA binding protein Hfq is usually required for the function and/or stability of this family of sRNAs (Storz et al., 2011). In *E. coli*, the RNA-binding protein Hfq is generally required to mediate sRNA–mRNA hybrid formation. In this role, Hfq acts as a RNA chaperone to facilitate base pair formation and stabilizes the sRNA against degradation (Desnoyers & Masse, 2012; Peer & Margalit, 2014). The experiments described in the chapter gave clear indication regarding the requirement of Hfq for formation of IRE^{opd} and *CrpR54*, duplex. In summary, the role of *CrpR54* is evident in relieving translational inhibition on *opd* mRNA in association with Hfq

protein.

Interestingly, the expression of this sRNA, *CrpR54* is critical for expressing OPH. The *crpR54* appears to be under the influence of carbon catabolite repressor protein (Crp). The Crp is known to de-repress genes/operons involved in alternate carbon catabolism to facilitate survival of cells using less preferred carbon sources. The Crp protein shows dual regulation when bound to cAMP and *crp*-binding motif by either activating or repressing the transcription of genes. Some genes are subject to both positive and negative regulation by the cAMP-Crp complex due to the presence of multiple promoters (Irani et al., 1989). The functional interactions between these regulons are believed to coordinate the activities of the different metabolons so that the supply of one type of nutrient matches the supply of other essential types of nutrients (Gutierrez-Rios, 2003). The consensus of *crp* binding motif of *E. coli* was compared with that of *S. fuliginis*. The *E. coli* Crp has a consensus of 5'-AAATGTGATCTAGATCACATTT-3'.

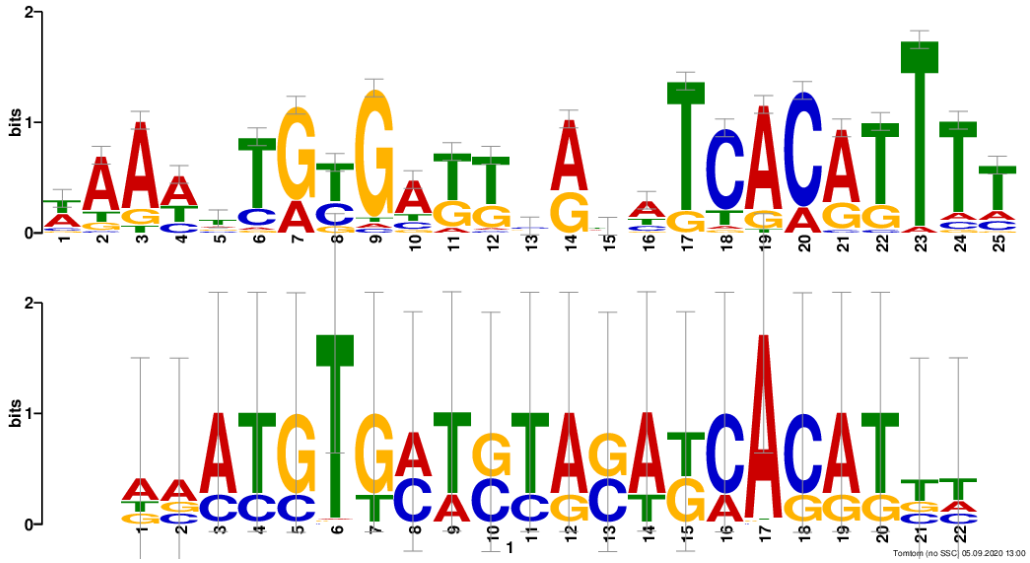

Fig.6.6.1. Comparison of CRP binding of *E. coli* with *S. fuliginis*. The consensus sequence logo, prepared by using MEME Suite in shown. The height of individual letters within a stack of letters represents the relative frequency of that letter at a given position. The overall height of the stack represents the degree of conservation at that position.

The presence of *crp* binding motif in the promoter region of *crpR54* and loss of promoter activity in *crpR54-lacZ* fusion constructed by including the *crp*-binding motif are clearly indicative of its repressive role on expression of *crpR54* gene (Fig 6.5.2).

Spingomonads play crucial role in the detoxification of polycyclic aromatic hydrocarbons (Cerniglia, 1992; St. Martin, 1997). The family of Sphingomonadaceae contains several strains competent to degrade particular compounds such as polycyclic aromatic hydrocarbons and lignin-derived aromatic compounds (Sohn et al., 2004; Copley et al., 2012; Chai et al., 2016; Kamimura et al., 2017). Metabolism of aromatic compounds requires novel oxygenases and transporters to facilitate their transport and conversion into TCA cycle intermediates. The ring-cleavage enzymes, aromatic-ring hydroxylating oxygenases etc., which are required for microbial degradation of aromatic compounds, require iron for their activity (Ladino-Orjuela et al., 2016; Mallinson et al., 2018; Peng et al., 1998; Sugimoto et al., 1999, 2014; Yoshikata et al., 2014).

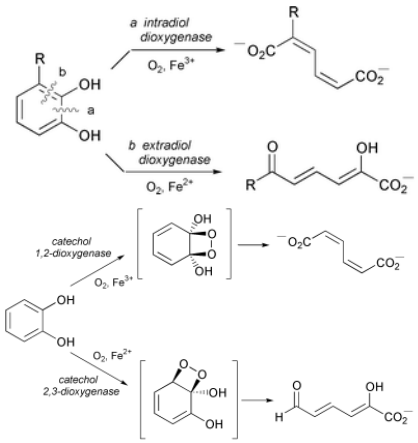

Fig.6.6.2. Reactions catalyzed by intradiol and extradiol dioxygenases (Wang et al., 2017)

Usually, the transition metal-containing oxygenases use iron as a cofactor for activation of oxygen. After this sort of activation, the O_2 atoms are transferred to the substrate. Oxygenases are divided into dioxygenases and monooxygenases based on the number of O_2 atoms incorporated into the substrate. The "pure" dioxygenation reactions are catalyzed by certain classes of iron-dependent dioxygenases such as intradiol dioxygenases, Rieske dioxygenases and extradiol dioxygenases (Wang et al., 2017).

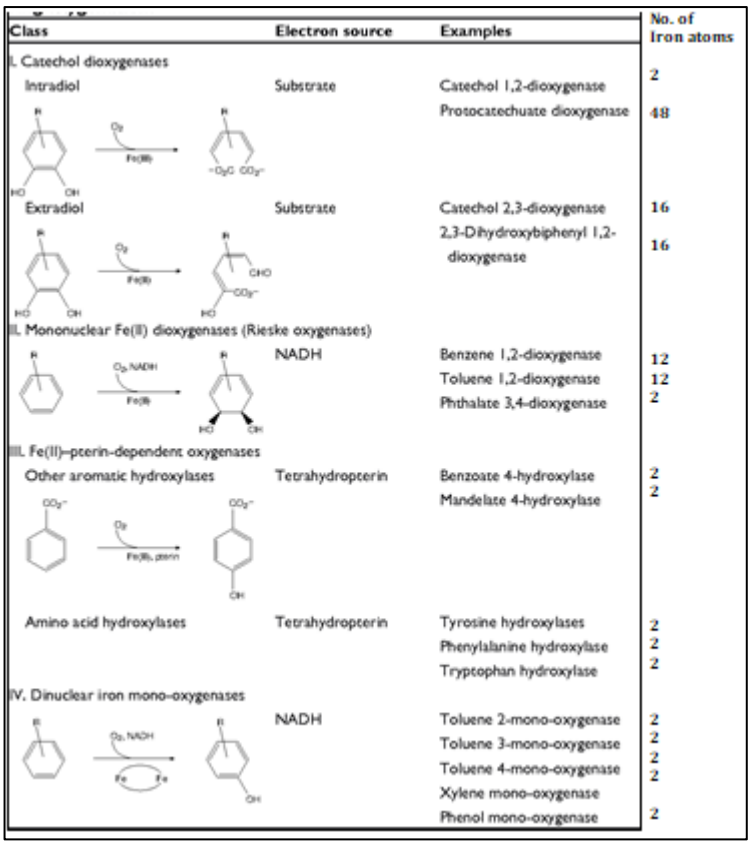

Class	Electron source	Examples	No. of Iron atoms
I. Catechol dioxygenases			
Intradiol	Substrate	Catechol 1,2-dioxygenase	2
		Protocatechuate dioxygenase	48
Extradiol	Substrate	Catechol 2,3-dioxygenase	16
		2,3-Dihydroxybiphenyl 1,2-dioxygenase	16
II. Mononuclear Fe(II) dioxygenases (Rieske oxygenases)			
	NADH	Benzene 1,2-dioxygenase	12
		Toluene 1,2-dioxygenase	12
		Phthalate 3,4-dioxygenase	2
III. Fe(II)–pterin-dependent oxygenases			
Other aromatic hydroxylases	Tetrahydropterin	Benzoate 4-hydroxylase	2
		Mandelate 4-hydroxylase	2
Amino acid hydroxylases	Tetrahydropterin	Tyrosine hydroxylases	2
		Phenylalanine hydroxylase	2
		Tryptophan hydroxylase	2
IV. Dinuclear iron mono-oxygenases			
	NADH	Toluene 2-mono-oxygenase	2
		Toluene 3-mono-oxygenase	2
		Toluene 4-mono-oxygenase	2
		Xylene mono-oxygenase	2
		Phenol mono-oxygenase	2

Fig.6.6.3. Classification of non-haem iron oxygenases that catalyze aromatic ring oxygenations (Coulter & Ballou, 1999)

The levels of OPH has gone up when cells of *S. fuliginis* were grown in aromatic compounds such as protocatechuic acid and 2,4-dihydrobenzoic acid. The increased expression of OPH appears to be due to concomitant rise in the levels of *CrpR54* due to its de-repression under carbon limiting conditions. Why is OPH expression increased when cells are grown in aromatic compounds? What role it plays in aromatic compound metabolism? The activities of OPH need to be examined to formulate a viable hypothesis. The OPH, in addition to its triesterase activity, plays a role in outer membrane transport system (Parapatla et al., 2020). This unique transport mechanism is needed for transport of aromatic compounds across energy deprived outer membrane. Further the assimilation of aromatic compounds requires more iron as both dioxygenases and monoxygenases depend on iron cofactor for activity. Enhanced expression of OPH in cells grown in aromatic compounds seems to satisfy both of these requirements. Further studies are required to prove this potential hypothesis.

Conclusion

The work described in the thesis provides conclusive evidences on iron dependent regulation of OPH expression. Previous studies from our lab have deciphered molecular mechanisms involved in membrane targeting of OPH along with components of outer membrane transport, ExbB/ExbD, TonB and TonR. Research work done by the other colleagues in the lab have successfully shown OPH involvement in transport of ferric-enterobactin (Fe-Ent). Proteins/enzymes involved in iron metabolism/transport are encoded by genes regulated by a transcription factor, Fur. Based on the intracellular concentration of iron, Fur either activates or represses iron responsive genes. Fur binds to ferrous ions to become an active repressor. This interacts with *fur* motif identified, overlapping promoter regions of genes responsive to iron and represses their expression. Under iron limiting conditions or in the absence of iron, Fur remains inactive and loses its ability to bind to *fur*-box motif, causing de-repression of iron responsive genes.

Previous work done in your lab has convincingly shown role of OPH in iron acquisition. The outer membrane transport system reconstituted in *E. coli* by including OPH showed dramatic increase in iron transport suggesting a convincing role for OPH in iron uptake. If OPH is truly involved in iron transport, the *opd* gene coding OPH should be part of iron regulon. Therefore, as a first step *in silico* studies were performed to identify typical regulatory motifs associated with well characterized iron response genes. The results described in the first chapter revealed existence of *fur*-box motif overlapping the -10 hexameric region of *opd* promoter. In support of this observation, under iron limiting conditions the *opd* gene is de-repressed. Almost double the quantity of OPH was found when *S. fuliginis* was grown under iron limiting conditions when compared to iron sufficient conditions. Enhanced expression of OPH was due to increased transcription of *opd* gene. The *opd* specific mRNA concentration was found two-fold higher in cells grown under iron limiting conditions.

The most interesting finding of this thesis is the identification of IRE in coding region of *opd* mRNA. The IRE^{opd} shared structural homology to both prokaryotic and eukaryotic IREs. In *E. coli*, the expression plasmids constructed

by deleting *IRE*^{opd} region enhanced OPH expression, suggesting a repressive role for *IRE*^{opd}. Similar increase was seen in OPH cells having expression plasmid generated by cloning *opd'* in which the structure of *IRE*^{opd} was disrupted by introducing non-complementary mutations in the stem region. These two studies have proved conclusively on the repressive role of *IRE*^{opd} on translation of *opd* mRNA. The *IRE*^{opd} successfully interacted with iron response protein (IRP), $_{Sf}$Acn as well as with a small RNA encoded by a gene located within the *opd* element. This mobile element coded sRNA, *CrpR54* appears to be under carbon catabolite repressor protein (Crp). The *CrpR54* repressed under carbon limiting condition interacted with *IRE*^{opd} and relieved the translation inhibition of *opd* mRNA. These extensive studies described in the thesis show the role of iron on expression of *opd* gene in *Sphingobium fuliginis* ATCC27551.

Sphingobium fuliginis survives on a variety of aromatic compounds. Metabolism of aromatic compounds requires more influx of iron as the oxygenases involved in conversion of aromatics to aliphatic acids require iron cofactor. Growth of aromatic compounds creates carbon limiting conditions. If sRNA, *CrpR54* expression is induced when cells are grown using aromatic compounds, the induced *CrpR54* is expected to relieve translation inhibition on *opd* mRNA causing increased OPH. As proposed the OPH expression has gone up in cells grown on aromatic compounds, suggesting that the increased OPH contributes for the increased iron influx, to generate intracellular iron pool required to produce active dioxygenases, involved in aromatic carbon catabolism.

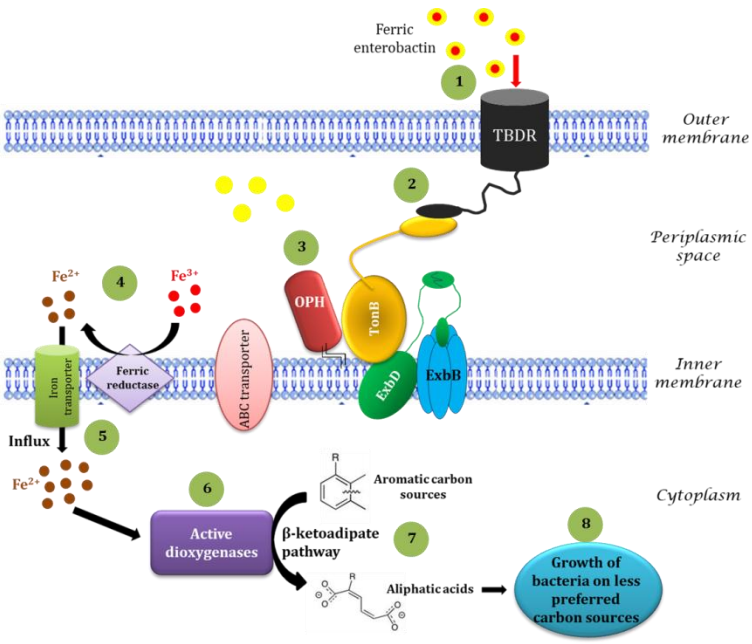

Fig. 7.1. Proposed model to understand the link between OPH dependent enhancement in iron uptake and carbon catabolism in *S. fuliginis*. Step 1 indicates the influx of ferric-enterobactin into the periplasmic space in iron limiting conditions. Step 2 shows the signal transduction between TonB dependent transporter (TBDR) and TonB. Step 3 indicates interactions between OPH and Ton-components ExbB/ExbD and TonB. Step 4 shows the reduction of ferric iron to ferrous form on the outer face of inner membrane, mediated by ferric reductase. Step 5 shows the influx of ferrous ions into the cytoplasm and activation of the dioxygenases (step 6). Step 7 shows the conversion of aromatic carbon compounds to their respective aliphatic acids via β-ketoadipate pathway (step 8).

References

Addess, K. J., Basilion, J. P., Klausner, R. D., Rouault, T. A., & Pardi, A. (1997). Structure and dynamics of the iron responsive element RNA: implications for binding of the RNA by iron regulatory binding proteins. *Journal of Molecular Biology*, *274*(1), 72–83. https://doi.org/10.1006/jmbi.1997.1377

Ahmad, R., Hjerde, E., Hansen, G. Å., Haugen, P., & Willassen, N.-P. (2009). Prediction and Experimental Testing of Ferric Uptake Regulator Regulons in Vibrios. *Journal of Molecular Microbiology and Biotechnology*, *16*(3–4), 159–168. https://doi.org/10.1159/000128322

Alen, C., & Sonenshein, A. L. (1999). Bacillus subtilis aconitase is an RNA-binding protein. *Proceedings of the National Academy of Sciences*, *96*(18), 10412–10417. https://doi.org/10.1073/pnas.96.18.10412

Andrews, S. C., Robinson, A. K., & Rodríguez-Quiñones, F. (2003). Bacterial iron homeostasis. *FEMS Microbiology Reviews*, *27*(2–3), 215–237. https://doi.org/10.1016/S0168-6445(03)00055-X

Artsimovitch, I., & Henkin, T. M. (2009). In vitro approaches to analysis of transcription termination. *Methods*, *47*(1), 37–43. https://doi.org/10.1016/j.ymeth.2008.10.006

Azam, S., Parthasarathy, S., Singh, C., Kumar, S., & Siddavattam, D. (2019). Genome Organization and Adaptive Potential of Archetypal Organophosphate Degrading Sphingobium fuliginis ATCC 27551. *Genome Biology and Evolution*, *11*(9), 2557–2562. https://doi.org/10.1093/gbe/evz189

Aziz, N., & Munro, H. N. (1987). Iron regulates ferritin mRNA translation through a segment of its 5' untranslated region. *Proceedings of the National Academy of Sciences*, *84*(23), 8478–8482. https://doi.org/10.1073/pnas.84.23.8478

Baba, T., Ara, T., Hasegawa, M., Takai, Y., Okumura, Y., Baba, M., Datsenko, K. A., Tomita, M., Wanner, B. L., & Mori, H. (2006). Construction of Escherichia coli K-12 in-frame, single-gene knockout mutants: the Keio collection. *Molecular Systems Biology*, *2*(1). https://doi.org/10.1038/msb4100050

Bagg, A, & Neilands, J. B. (1985). Mapping of a mutation affecting regulation of iron uptake systems in Escherichia coli K-12. *Journal of Bacteriology*, *161*(1), 450–453. https://doi.org/10.1128/JB.161.1.450-453.1985

Bagg, Anne, & Neilands, J. B. (1987). Ferric uptake regulation protein acts as a repressor, employing iron(II) as a cofactor to bind the operator of an iron transport operon in Escherichia coli. *Biochemistry*, *26*(17), 5471–5477. https://doi.org/10.1021/bi00391a039

Baichoo, N., & Helmann, J. D. (2002). Recognition of DNA by Fur: a Reinterpretation of the Fur Box Consensus Sequence. *Journal of Bacteriology*, *184*(21), 5826–5832. https://doi.org/10.1128/JB.184.21.5826-5832.2002

Baier, F., & Tokuriki, N. (2014). Connectivity between Catalytic Landscapes of the Metallo-β-Lactamase Superfamily. *Journal of Molecular Biology*, *426*(13), 2442–2456. https://doi.org/10.1016/j.jmb.2014.04.013

Banerjee, S., Nandyala, A. K., Raviprasad, P., Ahmed, N., & Hasnain, S. E. (2007). Iron-Dependent RNA-Binding Activity of Mycobacterium tuberculosis Aconitase. *Journal of Bacteriology*, *189*(11), 4046–4052. https://doi.org/10.1128/JB.00026-07

Beinert, H. (1997). Iron-Sulfur Clusters: Nature's Modular, Multipurpose Structures. *Science*, *277*(5326), 653–659. https://doi.org/10.1126/science.277.5326.653

Benning, M. M., Kuo, J. M., Raushel, F. M., & Holden, H. M. (1994). Three-Dimensional Structure of Phosphotriesterase: An Enzyme Capable of Detoxifying Organophosphate Nerve Agents. *Biochemistry*, *33*(50), 15001–15007. https://doi.org/10.1021/bi00254a008

Benning, M. M., Shim, H., Raushel, F. M., & Holden, H. M. (2001). High Resolution X-ray Structures of Different Metal-Substituted Forms of Phosphotriesterase from Pseudomonas diminuta † , ‡. *Biochemistry*, *40*(9), 2712–2722.

https://doi.org/10.1021/bi002661e
Berg, K., Pedersen, H. L., & Leiros, I. (2020). Biochemical characterization of ferric uptake regulator (Fur) from Aliivibrio salmonicida. Mapping the DNA sequence specificity through binding studies and structural modelling. *BioMetals*, *33*(4–5), 169–185. https://doi.org/10.1007/s10534-020-00240-6
Berks, B. C. (1996). A common export pathway for proteins binding complex redox cofactors? *Molecular Microbiology*, *22*(3), 393–404. https://doi.org/10.1046/j.1365-2958.1996.00114.x
Berks, B. C., Palmer, T., & Sargent, F. (2005). Protein targeting by the bacterial twin-arginine translocation (Tat) pathway. *Current Opinion in Microbiology*, *8*(2), 174–181. https://doi.org/10.1016/j.mib.2005.02.010
Bian, S., & Cowan, J. A. (1999). Protein-bound iron–sulfur centers. Form, function, and assembly. *Coordination Chemistry Reviews*, *190–192*, 1049–1066. https://doi.org/10.1016/S0010-8545(99)00157-5
Birnboim, H. C., & Doly, J. (1979). A rapid alkaline extraction procedure for screening recombinant plasmid DNA. *Nucleic Acids Research*, *7*(6), 1513–1523. https://doi.org/10.1093/nar/7.6.1513
Brown, K. A. (1980). Phosphotriesterases of flavobacterium sp. *Soil Biology and Biochemistry*, *12*(2), 105–112. https://doi.org/10.1016/0038-0717(80)90044-9
Bsat, N., Herbig, A., Casillas-Martinez, L., Setlow, P., & Helmann, J. D. (1998). Bacillus subtilis contains multiple Fur homologues: identification of the iron uptake (Fur) and peroxide regulon (PerR) repressors. *Molecular Microbiology*, *29*(1), 189–198. https://doi.org/10.1046/j.1365-2958.1998.00921.x
Butt, J., Kim, H. Y., Basilion, J. P., Cohen, S., Iwai, K., Philpott, C. C., Altschul, S., Klausner, R. D., & Rouault, T. A. (1996). Differences in the RNA binding sites of iron regulatory proteins and potential target diversity. *Proceedings of the National Academy of Sciences*, *93*(9), 4345–4349. https://doi.org/10.1073/pnas.93.9.4345
Cairo, G., & Recalcati, S. (2007). Iron-regulatory proteins: molecular biology and pathophysiological implications. *Expert Reviews in Molecular Medicine*, *9*(33), 1–13. https://doi.org/10.1017/S1462399407000531
Calderwood, S. B., & Mekalanos, J. J. (1988). Confirmation of the Fur operator site by insertion of a synthetic oligonucleotide into an operon fusion plasmid. *Journal of Bacteriology*, *170*(2), 1015–1017. https://doi.org/10.1128/JB.170.2.1015-1017.1988
Campillos, M., Cases, I., Hentze, M. W., & Sanchez, M. (2010). SIREs: searching for iron-responsive elements. *Nucleic Acids Research*, *38*(Web Server), W360–W367. https://doi.org/10.1093/nar/gkq371
Carey, J. (1991). *[8] Gel retardation* (pp. 103–117). https://doi.org/10.1016/0076-6879(91)08010-F
Casey, J., Hentze, M., Koeller, D., Caughman, S., Rouault, T., Klausner, R., & Harford, J. (1988). Iron-responsive elements: regulatory RNA sequences that control mRNA levels and translation. *Science*, *240*(4854), 924–928. https://doi.org/10.1126/science.2452485
Castro, L., Tórtora, V., Mansilla, S., & Radi, R. (2019). Aconitases: Non-redox Iron–Sulfur Proteins Sensitive to Reactive Species. *Accounts of Chemical Research*, *52*(9), 2609–2619. https://doi.org/10.1021/acs.accounts.9b00150
Caughman, S. W., Hentze, M. W., Rouault, T. A., Harford, J. B., & Klausner, R. D. (1988). The iron-responsive element is the single element responsible for iron-dependent translational regulation of ferritin biosynthesis. Evidence for function as the binding site for a translational repressor. *The Journal of Biological Chemistry*, *263*(35), 19048–19052. http://www.ncbi.nlm.nih.gov/pubmed/3198610
Cerniglia, C. E. (1992). Biodegradation of polycyclic aromatic hydrocarbons. *Biodegradation*, *3*(2–3), 351–368. https://doi.org/10.1007/BF00129093
Chai, B., Tsoi, T. V., Iwai, S., Liu, C., Fish, J. A., Gu, C., Johnson, T. A., Zylstra, G., Teppen,

B. J., Li, H., Hashsham, S. A., Boyd, S. A., Cole, J. R., & Tiedje, J. M. (2016). Sphingomonas wittichii Strain RW1 Genome-Wide Gene Expression Shifts in Response to Dioxins and Clay. *PLOS ONE*, *11*(6), e0157008. https://doi.org/10.1371/journal.pone.0157008

Chai, S., Welch, T. J., & Crosa, J. H. (1998). Characterization of the Interaction between Fur and the Iron Transport Promoter of the Virulence Plasmid in Vibrio anguillarum. *Journal of Biological Chemistry*, *273*(50), 33841–33847. https://doi.org/10.1074/jbc.273.50.33841

Chan, V. L., Louie, H., & Bingham, H. L. (1995). Cloning and transcription regulation of the ferric uptake regulatory gene of Campylobacter jejuni TGH9011. *Gene*, *164*(1), 25–31. https://doi.org/10.1016/0378-1119(95)00477-N

Chaudhry, G. R., Ali, A. N., & Wheeler, W. B. (1988). Isolation of a methyl parathion-degrading Pseudomonas sp. that possesses DNA homologous to the opd gene from a Flavobacterium sp. *Applied and Environmental Microbiology*, *54*(2), 288–293. https://doi.org/10.1128/AEM.54.2.288-293.1988

Cheng, T. C., Harvey, S. P., & Stroup, A. N. (1993). Purification and Properties of a Highly Active Organophosphorus Acid Anhydrolase from Alteromonas undina. *Applied and Environmental Microbiology*, *59*(9), 3138–3140. https://doi.org/10.1128/AEM.59.9.3138-3140.1993

Cheng, T., DeFrank, J. J., & Rastogi, V. K. (1999). Alteromonas prolidase for organophosphorus G-agent decontamination. *Chemico-Biological Interactions*, *119–120*, 455–462. https://doi.org/10.1016/S0009-2797(99)00058-7

Chu, X., Zhang, X., Chen, Y., Liu, H., & Song, D. (2003). [Study on the properties of methyl parathion hydrolase from Pseudomonas sp. WBC-3]. *Wei Sheng Wu Xue Bao = Acta Microbiologica Sinica*, *43*(4), 453–459. http://www.ncbi.nlm.nih.gov/pubmed/16276919

Ciccarone, F., Di Leo, L., & Ciriolo, M. R. (2018). Aberrations of the TCA Cycle in Cancer. In *Reference Module in Biomedical Sciences*. Elsevier. https://doi.org/10.1016/B978-0-12-801238-3.65066-3

Constable, A., Quick, S., Gray, N. K., & Hentze, M. W. (1992). Modulation of the RNA-binding activity of a regulatory protein by iron in vitro: switching between enzymatic and genetic function? *Proceedings of the National Academy of Sciences*, *89*(10), 4554–4558. https://doi.org/10.1073/pnas.89.10.4554

Copley, S. D., Rokicki, J., Turner, P., Daligault, H., Nolan, M., & Land, M. (2012). The Whole Genome Sequence of Sphingobium chlorophenolicum L-1: Insights into the Evolution of the Pentachlorophenol Degradation Pathway. *Genome Biology and Evolution*, *4*(2), 184–198. https://doi.org/10.1093/gbe/evr137

Cornelis, P., Matthijs, S., & Van Oeffelen, L. (2009). Iron uptake regulation in Pseudomonas aeruginosa. *BioMetals*, *22*(1), 15–22. https://doi.org/10.1007/s10534-008-9193-0

Coulter, E. D., & Ballou, D. P. (1999). Non-haem iron-containing oxygenases involved in the microbial biodegradation of aromatic hydrocarbons. *Essays in Biochemistry*, *34*, 31–49. https://doi.org/10.1042/bse0340031

Coy, M., & Neilands, J. B. (1991). Structural dynamics and functional domains of the Fur protein. *Biochemistry*, *30*(33), 8201–8210. https://doi.org/10.1021/bi00247a016

Crosa, J. H. (1997). Signal transduction and transcriptional and posttranscriptional control of iron-regulated genes in bacteria. *Microbiology and Molecular Biology Reviews : MMBR*, *61*(3), 319–336. http://www.ncbi.nlm.nih.gov/pubmed/9293185

Datsenko, K. A., & Wanner, B. L. (2000). One-step inactivation of chromosomal genes in Escherichia coli K-12 using PCR products. *Proceedings of the National Academy of Sciences*, *97*(12), 6640–6645. https://doi.org/10.1073/pnas.120163297

de Lorenzo, V., Wee, S., Herrero, M., & Neilands, J. B. (1987). Operator sequences of the aerobactin operon of plasmid ColV-K30 binding the ferric uptake regulation (fur) repressor. *Journal of Bacteriology*, *169*(6), 2624–2630.

https://doi.org/10.1128/JB.169.6.2624-2630.1987
Deng, Z., Wang, Q., Liu, Z., Zhang, M., Machado, A. C. D., Chiu, T.-P., Feng, C., Zhang, Q., Yu, L., Qi, L., Zheng, J., Wang, X., Huo, X., Qi, X., Li, X., Wu, W., Rohs, R., Li, Y., & Chen, Z. (2015). Mechanistic insights into metal ion activation and operator recognition by the ferric uptake regulator. *Nature Communications*, *6*(1), 7642. https://doi.org/10.1038/ncomms8642
Desai, P. J., Angerer, A., & Genco, C. A. (1996). Analysis of Fur binding to operator sequences within the Neisseria gonorrhoeae fbpA promoter. *Journal of Bacteriology*, *178*(16), 5020–5023. https://doi.org/10.1128/JB.178.16.5020-5023.1996
Desnoyers, G., & Masse, E. (2012). Noncanonical repression of translation initiation through small RNA recruitment of the RNA chaperone Hfq. *Genes & Development*, *26*(7), 726–739. https://doi.org/10.1101/gad.182493.111
Dinkla, I. J. T., Gabor, E. M., & Janssen, D. B. (2001). Effects of Iron Limitation on the Degradation of Toluene by Pseudomonas Strains Carrying the TOL (pWWO) Plasmid. *Applied and Environmental Microbiology*, *67*(8), 3406–3412. https://doi.org/10.1128/AEM.67.8.3406-3412.2001
Donarski, W. J., Dumas, D. P., Heitmeyer, D. P., Lewis, V. E., & Raushel, F. M. (1989). Structure-activity relationships in the hydrolysis of substrates by the phosphotriesterase from Pseudomonas diminuta. *Biochemistry*, *28*(11), 4650–4655. https://doi.org/10.1021/bi00437a021
Dong, Y.-J., Bartlam, M., Sun, L., Zhou, Y.-F., Zhang, Z.-P., Zhang, C.-G., Rao, Z., & Zhang, X.-E. (2005). Crystal Structure of Methyl Parathion Hydrolase from Pseudomonas sp. WBC-3. *Journal of Molecular Biology*, *353*(3), 655–663. https://doi.org/10.1016/j.jmb.2005.08.057
Dumas, D. P., Caldwell, S. R., Wild, J. R., & Raushel, F. M. (1989). Purification and properties of the phosphotriesterase from Pseudomonas diminuta. *The Journal of Biological Chemistry*, *264*(33), 19659–19665. http://www.ncbi.nlm.nih.gov/pubmed/2555328
Erlitzki, R., Long, J. C., & Theil, E. C. (2002). Multiple, Conserved Iron-responsive Elements in the 3′-Untranslated Region of Transferrin Receptor mRNA Enhance Binding of Iron Regulatory Protein 2. *Journal of Biological Chemistry*, *277*(45), 42579–42587. https://doi.org/10.1074/jbc.M207918200
Ernst, J. F., Bennett, R. L., & Rothfield, L. I. (1978). Constitutive expression of the iron-enterochelin and ferrichrome uptake systems in a mutant strain of Salmonella typhimurium. *Journal of Bacteriology*, *135*(3), 928–934. https://doi.org/10.1128/JB.135.3.928-934.1978
Escolar, Lucía, Lorenzo, V. de, & Pérez-Martíín, J. (1997). Metalloregulation in vitro of the aerobactin promoter of Escherichia coli by the Fur (ferric uptake regulation) protein. *Molecular Microbiology*, *26*(4), 799–808. https://doi.org/10.1046/j.1365-2958.1997.6211987.x
Escolar, Lucía, Pérez-Martín, J., & de Lorenzo, V. (1998). Coordinated Repression In Vitro of the DivergentfepA-fes Promoters of Escherichia coli by the Iron Uptake Regulation (Fur) Protein. *Journal of Bacteriology*, *180*(9), 2579–2582. https://doi.org/10.1128/JB.180.9.2579-2582.1998
Escolar, Lucía, Pérez-Martín, J., & de Lorenzo, V. (1999). Opening the Iron Box: Transcriptional Metalloregulation by the Fur Protein. *Journal of Bacteriology*, *181*(20), 6223–6229. https://doi.org/10.1128/JB.181.20.6223-6229.1999
Ferguson, A. D., & Deisenhofer, J. (2004). Metal Import through Microbial Membranes. *Cell*, *116*(1), 15–24. https://doi.org/10.1016/S0092-8674(03)01030-4
Fetherston, J. D., Bertolino, V. J., & Perry, R. D. (1999). YbtP and YbtQ: two ABC transporters required for iron uptake in Yersinia pestis. *Molecular Microbiology*, *32*(2), 289–299. https://doi.org/10.1046/j.1365-2958.1999.01348.x

Fitzgerald, K. D., & Semler, B. L. (2009). Bridging IRES elements in mRNAs to the eukaryotic translation apparatus. *Biochimica et Biophysica Acta (BBA) - Gene Regulatory Mechanisms*, *1789*(9–10), 518–528. https://doi.org/10.1016/j.bbagrm.2009.07.004

Fried, M. G. (1989). Measurement of protein-DNA interaction parameters by electrophoresis mobility shift assay. *Electrophoresis*, *10*(5–6), 366–376. https://doi.org/10.1002/elps.1150100515

Fried, M. G., & Garner, M. M. (1998). The Electrophoretic Mobility Shift Assay (EMSA) for Detection and Analysis of Protein-DNA Interactions. In *Nucleic Acid Electrophoresis* (pp. 239–271). Springer Berlin Heidelberg. https://doi.org/10.1007/978-3-642-58924-9_10

Friedman, Y. E., & O'Brian, M. R. (2003). A Novel DNA-binding Site for the Ferric Uptake Regulator (Fur) Protein from Bradyrhizobium japonicum. *Journal of Biological Chemistry*, *278*(40), 38395–38401. https://doi.org/10.1074/jbc.M306710200

Fröhlich, K. S., Förstner, K. U., & Gitai, Z. (2018). Post-transcriptional gene regulation by an Hfq-independent small RNA in Caulobacter crescentus. *Nucleic Acids Research*. https://doi.org/10.1093/nar/gky765

Fuchs, G., Boll, M., & Heider, J. (2011). Microbial degradation of aromatic compounds — from one strategy to four. *Nature Reviews Microbiology*, *9*(11), 803–816. https://doi.org/10.1038/nrmicro2652

Fujita, M., Sakumoto, T., Tanatani, K., Yu, H., Mori, K., Kamimura, N., & Masai, E. (2020). Iron acquisition system of Sphingobium sp. strain SYK-6, a degrader of lignin-derived aromatic compounds. *Scientific Reports*, *10*(1), 12177. https://doi.org/10.1038/s41598-020-68984-2

Furrer, J. L., Sanders, D. N., Hook-Barnard, I. G., & McIntosh, M. A. (2002). Export of the siderophore enterobactin in Escherichia coli: involvement of a 43 kDa membrane exporter. *Molecular Microbiology*, *44*(5), 1225–1234. https://doi.org/10.1046/j.1365-2958.2002.02885.x

Furukawa, K., Ramesh, A., Zhou, Z., Weinberg, Z., Vallery, T., Winkler, W. C., & Breaker, R. R. (2015). Bacterial Riboswitches Cooperatively Bind Ni 2+ or Co 2+ Ions and Control Expression of Heavy Metal Transporters. *Molecular Cell*, *57*(6), 1088–1098. https://doi.org/10.1016/j.molcel.2015.02.009

Gaballa, A., & Helmann, J. D. (1998). Identification of a zinc-specific metalloregulatory protein, Zur, controlling zinc transport operons in Bacillus subtilis. *Journal of Bacteriology*, *180*(22), 5815–5821. https://doi.org/10.1128/JB.180.22.5815-5821.1998

Gao, H., Zhou, D., Li, Y., Guo, Z., Han, Y., Song, Y., Zhai, J., Du, Z., Wang, X., Lu, J., & Yang, R. (2008). The Iron-Responsive Fur Regulon in Yersinia pestis. *Journal of Bacteriology*, *190*(8), 3063–3075. https://doi.org/10.1128/JB.01910-07

Gardner, P. R. (1997). Superoxide-Driven Aconitase FE-S Center Cycling. *Bioscience Reports*, *17*(1), 33–42. https://doi.org/10.1023/A:1027383100936

Gardner, P. R., Costantino, G., Szabó, C., & Salzman, A. L. (1997). Nitric Oxide Sensitivity of the Aconitases. *Journal of Biological Chemistry*, *272*(40), 25071–25076. https://doi.org/10.1074/jbc.272.40.25071

Garner, M. M., & Revzin, A. (1986). The use of gel electrophoresis to detect and study nucleic acid— protein interactions. *Trends in Biochemical Sciences*, *11*(10), 395–396. https://doi.org/10.1016/0968-0004(86)90149-0

Gdaniec, Z., Sierzputowska-Gracz, H., & Theil, E. C. (1998). Iron Regulatory Element and Internal Loop/Bulge Structure for Ferritin mRNA Studied by Cobalt(III) Hexammine Binding, Molecular Modeling, and NMR Spectroscopy †. *Biochemistry*, *37*(6), 1505–1512. https://doi.org/10.1021/bi9719814

Giedroc, D. P., & Arunkumar, A. I. (2007). Metal sensor proteins: nature's metalloregulated allosteric switches. *Dalton Transactions*, *29*, 3107. https://doi.org/10.1039/b706769k

Gorla, P., Pandey, J. P., Parthasarathy, S., Merrick, M., & Siddavattam, D. (2009). Organophosphate Hydrolase in Brevundimonas diminuta Is Targeted to the Periplasmic Face of the Inner Membrane by the Twin Arginine Translocation Pathway. *Journal of Bacteriology*, *191*(20), 6292–6299. https://doi.org/10.1128/JB.00824-09

Gruer, M. J., & Guest, J. R. (1994). Two genetically-distinct and differentially-regulated aconitases (AcnA and AcnB) in Escherichia coli. *Microbiology*, *140*(10), 2531–2541. https://doi.org/10.1099/00221287-140-10-2531

Gruer, Megan J., Artymiuk, P. J., & Guest, J. R. (1997). The aconitase family: three structural variations on a common theme. *Trends in Biochemical Sciences*, *22*(1), 3–6. https://doi.org/10.1016/S0968-0004(96)10069-4

Gudla, R., Konduru, G. V., Nagarajaram, H. A., & Siddavattam, D. (2019). Organophosphate hydrolase interacts with Ton components and is targeted to the membrane only in the presence of the ExbB/ExbD complex. *FEBS Letters*, *593*(6), 581–593. https://doi.org/10.1002/1873-3468.13345

Guebel, D. V., & Torres, N. V. (2018). Influence of Glucose Availability and CRP Acetylation on the Genome-Wide Transcriptional Response of Escherichia coli: Assessment by an Optimized Factorial Microarray Analysis. *Frontiers in Microbiology*, *9*. https://doi.org/10.3389/fmicb.2018.00941

Gutierrez-Rios, R. M. (2003). Regulatory Network of Escherichia coli: Consistency Between Literature Knowledge and Microarray Profiles. *Genome Research*, *13*(11), 2435–2443. https://doi.org/10.1101/gr.1387003

Haddock, J. D. (2010). Aerobic Degradation of Aromatic Hydrocarbons: Enzyme Structures and Catalytic Mechanisms. In *Handbook of Hydrocarbon and Lipid Microbiology* (pp. 1057–1069). Springer Berlin Heidelberg. https://doi.org/10.1007/978-3-540-77587-4_74

Hanahan, D. (1983). Studies on transformation of Escherichia coli with plasmids. *Journal of Molecular Biology*, *166*(4), 557–580. https://doi.org/10.1016/S0022-2836(83)80284-8

Hantke, K. (1981). Regulation of ferric iron transport in Escherichia coli K12: Isolation of a constitutive mutant. *Molecular and General Genetics MGG*, *182*(2), 288–292. https://doi.org/10.1007/BF00269672

Hantke, K. (1984). Cloning of the repressor protein gene of iron-regulated systems in Escherichia coli K12. *Molecular and General Genetics MGG*, *197*(2), 337–341. https://doi.org/10.1007/BF00330982

Hantke, K. (2001). Iron and metal regulation in bacteria. *Current Opinion in Microbiology*, *4*(2), 172–177. https://doi.org/10.1016/S1369-5274(00)00184-3

Hantke K, B. V. (2000). *The art of keeping low and high iron concentrations in balance. In: Storz G, Hengge-Aronis R. eds. Bacterial stress responses. Washington, D.C.: ASM Press*.

Harrell, C. M., McKenzie, A. R., Patino, M. M., Walden, W. E., & Theil, E. C. (1991). Ferritin mRNA: interactions of iron regulatory element with translational regulator protein P-90 and the effect on base-paired flanking regions. *Proceedings of the National Academy of Sciences*, *88*(10), 4166–4170. https://doi.org/10.1073/pnas.88.10.4166

Helmann, J. D. (1998). Metal Cation Regulation in Gram-Positive Bacteria. In *Metal Ions in Gene Regulation* (pp. 45–76). Springer US. https://doi.org/10.1007/978-1-4615-5993-1_3

Helmann, J. D. (2002). The extracytoplasmic function (ECF) sigma factors. *Advances in Microbial Physiology*, *46*, 47–110. https://doi.org/10.1016/s0065-2911(02)46002-x

Helmann, J. D. (2014). Specificity of Metal Sensing: Iron and Manganese Homeostasis in Bacillus subtilis. *Journal of Biological Chemistry*, *289*(41), 28112–28120. https://doi.org/10.1074/jbc.R114.587071

Henderson, B. R., Menotti, E., Bonnard, C., & Kühn, L. C. (1994). Optimal sequence and structure of iron-responsive elements. Selection of RNA stem-loops with high affinity for iron regulatory factor. *The Journal of Biological Chemistry*, *269*(26), 17481–17489.

http://www.ncbi.nlm.nih.gov/pubmed/8021254
Hentze, M. W., & Kuhn, L. C. (1996). Molecular control of vertebrate iron metabolism: mRNA-based regulatory circuits operated by iron, nitric oxide, and oxidative stress. *Proceedings of the National Academy of Sciences*, *93*(16), 8175–8182. https://doi.org/10.1073/pnas.93.16.8175
Hickey, E. K., & Cianciotto, N. P. (1994). Cloning and sequencing of the Legionella pneumophila fur gene. *Gene*, *143*(1), 117–121. https://doi.org/10.1016/0378-1119(94)90615-7
Hider, R. C., & Kong, X. (2010). Chemistry and biology of siderophores. *Natural Product Reports*, *27*(5), 637. https://doi.org/10.1039/b906679a
Hirling, H., Henderson, B. R., & Kühn, L. C. (1994). Mutational analysis of the [4Fe-4S]-cluster converting iron regulatory factor from its RNA-binding form to cytoplasmic aconitase. *The EMBO Journal*, *13*(2), 453–461. http://www.ncbi.nlm.nih.gov/pubmed/7508861
Holm, L., Sander, C., Rüterjans, H., Schnarr, M., Fogh, R., Boelens, R., & Kaptein, R. (1994). LexA repressor and iron uptake regulator from Escherichia coli : new members of the CAP-like DNA binding domain superfamily. *"Protein Engineering, Design and Selection," 7*(12), 1449–1453. https://doi.org/10.1093/protein/7.12.1449
Horne, I., Sutherland, T. D., Harcourt, R. L., Russell, R. J., & Oakeshott, J. G. (2002). Identification of an opd (Organophosphate Degradation) Gene in an Agrobacterium Isolate. *Applied and Environmental Microbiology*, *68*(7), 3371–3376. https://doi.org/10.1128/AEM.68.7.3371-3376.2002
Hubert, N., Walczak, R., Sturchler, C., Myslinski, E., Schuster, C., Westhof, E., Carbon, P., & Krol, A. (1996). RNAs mediating cotranslational insertion of selenocysteine in eukaryotic selenoproteins. *Biochimie*, *78*(7), 590–596. https://doi.org/10.1016/S0300-9084(96)80005-8
Hutchins, A. P., Diez, D., Takahashi, Y., Ahmad, S., Jauch, R., Tremblay, M. L., & Miranda-Saavedra, D. (2013). Distinct transcriptional regulatory modules underlie STAT3's cell type-independent and cell type-specific functions. *Nucleic Acids Research*, *41*(4), 2155–2170. https://doi.org/10.1093/nar/gks1300
Irani, M., Musso, R., & Adhya, S. (1989). Cyclic-AMP-dependent switch in initiation of transcription from the two promoters of the Escherichia coli gal operon: identification and assay of 5'-triphosphate ends of mRNA by GTP:RNA guanyltransferase. *Journal of Bacteriology*, *171*(3), 1623–1630. https://doi.org/10.1128/JB.171.3.1623-1630.1989
Jacob, F., & Monod, J. (1961). On the Regulation of Gene Activity. *Cold Spring Harbor Symposia on Quantitative Biology*, *26*, 193–211. https://doi.org/10.1101/SQB.1961.026.01.024
Jaffrey, S. R., Haile, D. J., Klausner, R. D., & Harford, J. B. (1993). The interaction between the iron-responsive element binding protein and its cognate RNA is highly dependent upon both RNA sequence and structure. *Nucleic Acids Research*, *21*(19), 4627–4631. https://doi.org/10.1093/nar/21.19.4627
Jagodnik, J., Chiaruttini, C., & Guillier, M. (2017). Stem-Loop Structures within mRNA Coding Sequences Activate Translation Initiation and Mediate Control by Small Regulatory RNAs. *Molecular Cell*, *68*(1), 158-170.e3. https://doi.org/10.1016/j.molcel.2017.08.015
Kamimura, N., Takahashi, K., Mori, K., Araki, T., Fujita, M., Higuchi, Y., & Masai, E. (2017). Bacterial catabolism of lignin-derived aromatics: New findings in a recent decade: Update on bacterial lignin catabolism. *Environmental Microbiology Reports*, *9*(6), 679–705. https://doi.org/10.1111/1758-2229.12597
Kawahara, K., Tanaka, A., Yoon, J., & Yokota, A. (2010). Reclassification of a parathione-degrading Flavobacterium sp. ATCC 27551 as Sphingobium fuliginis. *The Journal of General and Applied Microbiology*, *56*(3), 249–255.

https://doi.org/10.2323/jgam.56.249
Kehrer, J. P. (2000). The Haber–Weiss reaction and mechanisms of toxicity. *Toxicology*, *149*(1), 43–50. https://doi.org/10.1016/S0300-483X(00)00231-6
Khan, M. A., Walden, W. E., Theil, E. C., & Goss, D. J. (2017). Thermodynamic and Kinetic Analyses of Iron Response Element (IRE)-mRNA Binding to Iron Regulatory Protein, IRP1. *Scientific Reports*, *7*(1), 8532. https://doi.org/10.1038/s41598-017-09093-5
Kiley, P. J., & Beinert, H. (2003). The role of Fe–S proteins in sensing and regulation in bacteria. *Current Opinion in Microbiology*, *6*(2), 181–185. https://doi.org/10.1016/S1369-5274(03)00039-0
Koebnik, R. (2005). TonB-dependent trans-envelope signalling: the exception or the rule? *Trends in Microbiology*, *13*(8), 343–347. https://doi.org/10.1016/j.tim.2005.06.005
Koeller, D. M., Casey, J. L., Hentze, M. W., Gerhardt, E. M., Chan, L. N., Klausner, R. D., & Harford, J. B. (1989). A cytosolic protein binds to structural elements within the iron regulatory region of the transferrin receptor mRNA. *Proceedings of the National Academy of Sciences*, *86*(10), 3574–3578. https://doi.org/10.1073/pnas.86.10.3574
Kurth, C., Kage, H., & Nett, M. (2016). Siderophores as molecular tools in medical and environmental applications. *Organic & Biomolecular Chemistry*, *14*(35), 8212–8227. https://doi.org/10.1039/C6OB01400C
Ladino-Orjuela, G., Gomes, E., da Silva, R., Salt, C., & Parsons, J. R. (2016). *Metabolic Pathways for Degradation of Aromatic Hydrocarbons by Bacteria* (pp. 105–121). https://doi.org/10.1007/978-3-319-23573-8_5
Lawrence, J. G. (2002). Shared Strategies in Gene Organization among Prokaryotes and Eukaryotes. *Cell*, *110*(4), 407–413. https://doi.org/10.1016/S0092-8674(02)00900-5
Lee, J.-W., & Helmann, J. D. (2007). Functional specialization within the Fur family of metalloregulators. *BioMetals*, *20*(3–4), 485–499. https://doi.org/10.1007/s10534-006-9070-7
Lee, T. I., & Young, R. A. (2013). Transcriptional Regulation and Its Misregulation in Disease. *Cell*, *152*(6), 1237–1251. https://doi.org/10.1016/j.cell.2013.02.014
Leibold, E. A., Laudano, A., & Yu, Y. (1990). Structural requirements of iron-responsive elements for binding of the protein involved in both transferrin receptor and ferritin mRNA post-transcriptional regulation. *Nucleic Acids Research*, *18*(7), 1819–1824. https://doi.org/10.1093/nar/18.7.1819
Leibold, E. S. H. & E. A. (1999). Regulation of the Iron Regulatory Proteins by Reactive Nitrogen and Oxygen Species. *Gene Expr*.
Leppek, K., Das, R., & Barna, M. (2018). Functional 5′ UTR mRNA structures in eukaryotic translation regulation and how to find them. *Nature Reviews Molecular Cell Biology*, *19*(3), 158–174. https://doi.org/10.1038/nrm.2017.103
Li, C. C., Merrell, D. S., Camilli, A., & Kaper, J. B. (2002). ToxR interferes with CRP-dependent transcriptional activation of ompT in Vibrio cholerae. *Molecular Microbiology*, *43*(6), 1577–1589. https://doi.org/10.1046/j.1365-2958.2002.02845.x
Lin, J., Zhang, W., Cheng, J., Yang, X., Zhu, K., Wang, Y., Wei, G., Qian, P.-Y., Luo, Z.-Q., & Shen, X. (2017). A Pseudomonas T6SS effector recruits PQS-containing outer membrane vesicles for iron acquisition. *Nature Communications*, *8*(1), 14888. https://doi.org/10.1038/ncomms14888
Litwin, C. M., & Calderwood, S. B. (1993). Role of iron in regulation of virulence genes. *Clinical Microbiology Reviews*, *6*(2), 137–149. https://doi.org/10.1128/CMR.6.2.137
Livak, K. J., & Schmittgen, T. D. (2001). Analysis of Relative Gene Expression Data Using Real-Time Quantitative PCR and the 2−ΔΔCT Method. *Methods*, *25*(4), 402–408. https://doi.org/10.1006/meth.2001.1262
Llamas, M. A., Imperi, F., Visca, P., & Lamont, I. L. (2014). Cell-surface signaling in Pseudomonas : stress responses, iron transport, and pathogenicity. *FEMS Microbiology Reviews*, *38*(4), 569–597. https://doi.org/10.1111/1574-6976.12078

LORENZO, V., HERRERO, M., GIOVANNINI, F., & NEILANDS, J. B. (1988). Fur (ferric uptake regulation) protein and CAP (catabolite-activator protein) modulate transcription of fur gene in Escherichia coli. *European Journal of Biochemistry*, *173*(3), 537–546. https://doi.org/10.1111/j.1432-1033.1988.tb14032.x

Ma, J., Haldar, S., Khan, M. A., Sharma, S. D., Merrick, W. C., Theil, E. C., & Goss, D. J. (2012). Fe2+ binds iron responsive element-RNA, selectively changing protein-binding affinities and regulating mRNA repression and activation. *Proceedings of the National Academy of Sciences*, *109*(22), 8417–8422. https://doi.org/10.1073/pnas.1120045109

Ma, Z., Faulkner, M. J., & Helmann, J. D. (2012). Origins of specificity and cross-talk in metal ion sensing by Bacillus subtilis Fur. *Molecular Microbiology*, *86*(5), 1144–1155. https://doi.org/10.1111/mmi.12049

Madikonda, A. K., Shaikh, A., Khanra, S., Yakkala, H., Yellaboina, S., Lin-Chao, S., & Siddavattam, D. (2020). Metabolic remodeling in Escherichia coli MG 1655. A prophage e14-encoded small RNA , co293 , post-transcriptionally regulates transcription factors HcaR and FadR. *The FEBS Journal*, *287*(21), 4767–4782. https://doi.org/10.1111/febs.15247

Mallinson, S. J. B., Machovina, M. M., Silveira, R. L., Garcia-Borràs, M., Gallup, N., Johnson, C. W., Allen, M. D., Skaf, M. S., Crowley, M. F., Neidle, E. L., Houk, K. N., Beckham, G. T., DuBois, J. L., & McGeehan, J. E. (2018). A promiscuous cytochrome P450 aromatic O-demethylase for lignin bioconversion. *Nature Communications*, *9*(1), 2487. https://doi.org/10.1038/s41467-018-04878-2

Mande, C. M. S. K. and S. C. (2011). *Protein chaperones and non-protein substrates: on substrate promiscuity of GroEL*. https://www.jstor.org/stable/24077768

Martínez-Pastor, M., Llanos, R., Romero, A., & Puig, S. (2013). Post-Transcriptional Regulation of Iron Homeostasis in Saccharomyces cerevisiae. *International Journal of Molecular Sciences*, *14*(8), 15785–15809. https://doi.org/10.3390/ijms140815785

Masse, E., & Gottesman, S. (2002). A small RNA regulates the expression of genes involved in iron metabolism in Escherichia coli. *Proceedings of the National Academy of Sciences*, *99*(7), 4620–4625. https://doi.org/10.1073/pnas.032066599

Mattei, E., Ausiello, G., Ferrè, F., & Helmer-Citterich, M. (2014). A novel approach to represent and compare RNA secondary structures. *Nucleic Acids Research*, *42*(10), 6146–6157. https://doi.org/10.1093/nar/gku283

McCallum, S. A., & Pardi, A. (2003). Refined Solution Structure of the Iron-responsive Element RNA Using Residual Dipolar Couplings. *Journal of Molecular Biology*, *326*(4), 1037–1050. https://doi.org/10.1016/S0022-2836(02)01431-6

McGary, K., & Nudler, E. (2013). RNA polymerase and the ribosome: the close relationship. *Current Opinion in Microbiology*, *16*(2), 112–117. https://doi.org/10.1016/j.mib.2013.01.010

McQuail, J., Switzer, A., & Wigneshweraraj, R. (2019). Post-transcriptional regulation of gene expression in Escherichia coli experiencing sustained nitrogen starvation. *Access Microbiology*, *1*(1A). https://doi.org/10.1099/acmi.ac2019.po0500

Menscher, E. A., Caswell, C. C., Anderson, E. S., & Roop, R. M. (2012). Mur Regulates the Gene Encoding the Manganese Transporter MntH in Brucella abortus 2308. *Journal of Bacteriology*, *194*(3), 561–566. https://doi.org/10.1128/JB.05296-11

Mey, A. R., Wyckoff, E. E., Kanukurthy, V., Fisher, C. R., & Payne, S. M. (2005). Iron and Fur Regulation in Vibrio cholerae and the Role of Fur in Virulence. *Infection and Immunity*, *73*(12), 8167–8178. https://doi.org/10.1128/IAI.73.12.8167-8178.2005

Miethke, M., & Marahiel, M. A. (2007). Siderophore-Based Iron Acquisition and Pathogen Control. *Microbiology and Molecular Biology Reviews*, *71*(3), 413–451. https://doi.org/10.1128/MMBR.00012-07

Miller, J. H. (1972). *Experiments in molecular genetics*.

Mills, S. A., & Marletta, M. A. (2005). Metal Binding Characteristics and Role of Iron

Oxidation in the Ferric Uptake Regulator from Escherichia coli †. *Biochemistry*, *44*(41), 13553–13559. https://doi.org/10.1021/bi0507579
Morales, V. M., Bäckman, A., & Bagdasarian, M. (1991). A series of wide-host-range low-copy-number vectors that allow direct screening for recombinants. *Gene*, *97*(1), 39–47. https://doi.org/10.1016/0378-1119(91)90007-X
Morozova, N., Allers, J., Myers, J., & Shamoo, Y. (2006). Protein-RNA interactions: exploring binding patterns with a three-dimensional superposition analysis of high resolution structures. *Bioinformatics*, *22*(22), 2746–2752. https://doi.org/10.1093/bioinformatics/btl470
Muckenthaler, M. U., Galy, B., & Hentze, M. W. (2008). Systemic Iron Homeostasis and the Iron-Responsive Element/Iron-Regulatory Protein (IRE/IRP) Regulatory Network. *Annual Review of Nutrition*, *28*(1), 197–213. https://doi.org/10.1146/annurev.nutr.28.061807.155521
Mulbry, W. W., & Karns, J. S. (1989a). Parathion hydrolase specified by the Flavobacterium opd gene: relationship between the gene and protein. *Journal of Bacteriology*, *171*(12), 6740–6746. https://doi.org/10.1128/JB.171.12.6740-6746.1989
Mulbry, W. W., & Karns, J. S. (1989b). Purification and characterization of three parathion hydrolases from gram-negative bacterial strains. *Applied and Environmental Microbiology*, *55*(2), 289–293. https://doi.org/10.1128/AEM.55.2.289-293.1989
Müllner, E. W., & Kühn, L. C. (1988). A stem-loop in the 3′ untranslated region mediates iron-dependent regulation of transferrin receptor mRNA stability in the cytoplasm. *Cell*, *53*(5), 815–825. https://doi.org/10.1016/0092-8674(88)90098-0
Murari, A., Thiriveedi, V. R., Mohammad, F., Vengaldas, V., Gorla, M., Tammineni, P., Krishnamoorthy, T., & Sepuri, N. B. V. (2015). Human mitochondrial MIA40 (CHCHD4) is a component of the Fe–S cluster export machinery. *Biochemical Journal*, *471*(2), 231–241. https://doi.org/10.1042/BJ20150012
Mutalik, V. K., Nonaka, G., Ades, S. E., Rhodius, V. A., & Gross, C. A. (2009). Promoter Strength Properties of the Complete Sigma E Regulon of Escherichia coli and Salmonella enterica. *Journal of Bacteriology*, *191*(23), 7279–7287. https://doi.org/10.1128/JB.01047-09
Neilands, J. B. (1993). Siderophores. *Archives of Biochemistry and Biophysics*, *302*(1), 1–3. https://doi.org/10.1006/abbi.1993.1172
Noinaj, N., Guillier, M., Barnard, T. J., & Buchanan, S. K. (2010). TonB-Dependent Transporters: Regulation, Structure, and Function. *Annual Review of Microbiology*, *64*(1), 43–60. https://doi.org/10.1146/annurev.micro.112408.134247
Nudler, E. (2004). The riboswitch control of bacterial metabolism. *Trends in Biochemical Sciences*, *29*(1), 11–17. https://doi.org/10.1016/j.tibs.2003.11.004
Ochsner, U. A., Vasil, A. I., & Vasil, M. L. (1995). Role of the ferric uptake regulator of Pseudomonas aeruginosa in the regulation of siderophores and exotoxin A expression: purification and activity on iron-regulated promoters. *Journal of Bacteriology*, *177*(24), 7194–7201. https://doi.org/10.1128/JB.177.24.7194-7201.1995
Ochsner, U. A., & Vasil, M. L. (1996). Gene repression by the ferric uptake regulator in Pseudomonas aeruginosa: cycle selection of iron-regulated genes. *Proceedings of the National Academy of Sciences*, *93*(9), 4409–4414. https://doi.org/10.1073/pnas.93.9.4409
Ohlendorf, D. H., Lipscomb, J. D., & Weber, P. C. (1988). Structure and assembly of protocatechuate 3,4-dioxygenase. *Nature*, *336*(6197), 403–405. https://doi.org/10.1038/336403a0
Omburo, G. A., Kuo, J. M., Mullins, L. S., & Raushel, F. M. (1992). Characterization of the zinc binding site of bacterial phosphotriesterase. *The Journal of Biological Chemistry*, *267*(19), 13278–13283. http://www.ncbi.nlm.nih.gov/pubmed/1320014
Owen, D., & Kühn, L. C. (1987). Noncoding 3′ sequences of the transferrin receptor gene are

required for mRNA regulation by iron. *The EMBO Journal*, *6*(5), 1287–1293. https://doi.org/10.1002/j.1460-2075.1987.tb02366.x

Paget, M. S. B., & Helmann, J. D. (2003). The sigma70 family of sigma factors. *Genome Biology*, *4*(1), 203. https://doi.org/10.1186/gb-2003-4-1-203

Pandeeti, E. V. P., Chakka, D., Pandey, J. P., & Siddavattam, D. (2011). Indigenous organophosphate-degrading (opd) plasmid pCMS1 of Brevundimonas diminuta is self-transmissible and plays a key role in horizontal mobility of the opd gene. *Plasmid*, *65*(3), 226–231. https://doi.org/10.1016/j.plasmid.2011.02.003

Pandeeti, E. V. P., Longkumer, T., Chakka, D., Muthyala, V. R., Parthasarathy, S., Madugundu, A. K., Ghanta, S., Medipally, S. R., Pantula, S. C., Yekkala, H., & Siddavattam, D. (2012). Multiple Mechanisms Contribute to Lateral Transfer of an Organophosphate Degradation (opd) Island in Sphingobium fuliginis ATCC 27551. *G3: Genes|Genomes|Genetics*, *2*(12), 1541–1554. https://doi.org/10.1534/g3.112.004051

Pandey, J. P., Gorla, P., Manavathi, B., & Siddavattam, D. (2009). mRNA secondary structure modulates the translation of organophosphate hydrolase (OPH) in E. coli. *Molecular Biology Reports*, *36*(3), 449–454. https://doi.org/10.1007/s11033-007-9200-5

Parapatla, H., Gudla, R., Konduru, G. V., Devadasu, E. R., Nagarajaram, H. A., Sritharan, M., Subramanyam, R., & Siddavattam, D. (2020). Organophosphate hydrolase interacts with ferric-enterobactin and promotes iron uptake in association with TonB dependent transport system. *Biochemical Journal*. https://doi.org/10.1042/BCJ20200299

Park, S. J., & Gunsalus, R. P. (1995). Oxygen, iron, carbon, and superoxide control of the fumarase fumA and fumC genes of Escherichia coli: role of the arcA, fnr, and soxR gene products. *Journal of Bacteriology*, *177*(21), 6255–6262. https://doi.org/10.1128/JB.177.21.6255-6262.1995

Parthasarathy, S., Azam, S., Lakshman Sagar, A., Narasimha Rao, V., Gudla, R., Paraptla, H., Yakkala, H., Ghanta Vemuri, S., & Siddavattam, D. (2016). Genome-guided insights reveal organophosphate-degrading Brevundimonas diminuta as Sphingopyxis wildii and define its versatile metabolic capabilities and environmental adaptations. *Genome Biology and Evolution*, evw275. https://doi.org/10.1093/gbe/evw275

Parthasarathy, S., Parapatla, H., Nandavaram, A., Palmer, T., & Siddavattam, D. (2016). Organophosphate Hydrolase Is a Lipoprotein and Interacts with P i -specific Transport System to Facilitate Growth of Brevundimonas diminuta Using OP Insecticide as Source of Phosphate. *Journal of Biological Chemistry*, *291*(14), 7774–7785. https://doi.org/10.1074/jbc.M116.715110

Parthasarathy, S., Parapatla, H., & Siddavattam, D. (2017). Topological analysis of the lipoprotein organophosphate hydrolase from Sphingopyxis wildii reveals a periplasmic localisation. *FEMS Microbiology Letters*, *364*(19). https://doi.org/10.1093/femsle/fnx187

Parthasarathy Sunil, G. R. and S. D. (2017). Evolution of Phosphotriesterases (PTEs): How Bacteria Can Acquire New Degradative Functions? *Proc Indian Natn Sci Acad*, *83*(4), 865–875.

Pedersen, H. L., Ahmad, R., Riise, E. K., Leiros, H.-K. S., Hauglid, S., Espelid, S., Brandsdal, B. O., Leiros, I., Willassen, N.-P., & Haugen, P. (2010). Experimental and computational characterization of the ferric uptake regulator from Aliivibrio salmonicida (Vibrio salmonicida). *The Journal of Microbiology*, *48*(2), 174–183. https://doi.org/10.1007/s12275-010-9199-5

Peer, A., & Margalit, H. (2014). Evolutionary patterns of Escherichia coli small RNAs and their regulatory interactions. *RNA*, *20*(7), 994–1003. https://doi.org/10.1261/rna.043133.113

Peng, X., Egashira, T., Hanashiro, K., Masai, E., Nishikawa, S., Katayama, Y., Kimbara, K., & Fukuda, M. (1998). Cloning of a Sphingomonas paucimobilis SYK-6 Gene Encoding

a Novel Oxygenase That Cleaves Lignin-Related Biphenyl and Characterization of the Enzyme. *Applied and Environmental Microbiology*, *64*(7), 2520–2527. https://doi.org/10.1128/AEM.64.7.2520-2527.1998

Philpott, C. C., Klausner, R. D., & Rouault, T. A. (1994). The bifunctional iron-responsive element binding protein/cytosolic aconitase: the role of active-site residues in ligand binding and regulation. *Proceedings of the National Academy of Sciences*, *91*(15), 7321–7325. https://doi.org/10.1073/pnas.91.15.7321

Piccinelli, P., & Samuelsson, T. (2007). Evolution of the iron-responsive element. *RNA*, *13*(7), 952–966. https://doi.org/10.1261/rna.464807

Posey, J. E. (2000). Lack of a Role for Iron in the Lyme Disease Pathogen. *Science*, *288*(5471), 1651–1653. https://doi.org/10.1126/science.288.5471.1651

Postle, K. (2007). *TonB System, In Vivo Assays and Characterization* (pp. 245–269). https://doi.org/10.1016/S0076-6879(06)22012-3

Quail, M. A., Jordan, P., Grogan, J. M., Butt, J. N., Lutz, M., Thomson, A. J., Andrews, S. C., & Guest, J. R. (1996). Spectroscopic and Voltammetric Characterisation of the Bacterioferritin-Associated Ferredoxin ofEscherichia coli. *Biochemical and Biophysical Research Communications*, *229*(2), 635–642. https://doi.org/10.1006/bbrc.1996.1856

Quatrini, R., Lefimil, C., Holmes, D. S., & Jedlicki, E. (2005). The ferric iron uptake regulator (Fur) from the extreme acidophile Acidithiobacillus ferrooxidans. *Microbiology*, *151*(6), 2005–2015. https://doi.org/10.1099/mic.0.27581-0

Regulski, E. E., & Breaker, R. R. (2008). *In-Line Probing Analysis of Riboswitches* (pp. 53–67). https://doi.org/10.1007/978-1-59745-033-1_4

Ricky S. Joshi, E. M. and M. S. (2012). *Cellular Iron Metabolism – The IRP/IRE Regulatory Network*.

Robichon, C., Luo, J., Causey, T. B., Benner, J. S., & Samuelson, J. C. (2011). Engineering Escherichia coli BL21(DE3) Derivative Strains To Minimize E. coli Protein Contamination after Purification by Immobilized Metal Affinity Chromatography. *Applied and Environmental Microbiology*, *77*(13), 4634–4646. https://doi.org/10.1128/AEM.00119-11

Rohs, R., Jin, X., West, S. M., Joshi, R., Honig, B., & Mann, R. S. (2010). Origins of Specificity in Protein-DNA Recognition. *Annual Review of Biochemistry*, *79*(1), 233–269. https://doi.org/10.1146/annurev-biochem-060408-091030

Rouault, T A, & Klausner, R. D. (1996). Iron-sulfur clusters as biosensors of oxidants and iron. *Trends in Biochemical Sciences*, *21*(5), 174–177. http://www.ncbi.nlm.nih.gov/pubmed/8871401

Rouault, Tracey A. (2006). The role of iron regulatory proteins in mammalian iron homeostasis and disease. *Nature Chemical Biology*, *2*(8), 406–414. https://doi.org/10.1038/nchembio807

SAITO, T., WORMALD, M. R., & WILLIAMS, R. J. P. (1991). Some structural features of the iron-uptake regulation protein. *European Journal of Biochemistry*, *197*(1), 29–38. https://doi.org/10.1111/j.1432-1033.1991.tb15878.x

Samantarrai, D., Lakshman Sagar, A., Gudla, R., & Siddavattam, D. (2020). TonB-Dependent Transporters in Sphingomonads: Unraveling Their Distribution and Function in Environmental Adaptation. *Microorganisms*, *8*(3), 359. https://doi.org/10.3390/microorganisms8030359

Sargent, F. (1998). Overlapping functions of components of a bacterial Sec-independent protein export pathway. *The EMBO Journal*, *17*(13), 3640–3650. https://doi.org/10.1093/emboj/17.13.3640

Schaible, U. E., & Kaufmann, S. H. E. (2004). Iron and microbial infection. *Nature Reviews Microbiology*, *2*(12), 946–953. https://doi.org/10.1038/nrmicro1046

Schauer, K., Rodionov, D. A., & de Reuse, H. (2008). New substrates for TonB-dependent transport: do we only see the ‘tip of the iceberg’? *Trends in Biochemical Sciences*,

33(7), 330–338. https://doi.org/10.1016/j.tibs.2008.04.012
Sebastian, S., Agarwal, S., Murphy, J. R., & Genco, C. A. (2002). The Gonococcal Fur Regulon: Identification of Additional Genes Involved in Major Catabolic, Recombination, and Secretory Pathways. *Journal of Bacteriology*, *184*(14), 3965–3974. https://doi.org/10.1128/JB.184.14.3965-3974.2002
Selezneva, A. I., Walden, W. E., & Volz, K. W. (2013). Nucleotide-Specific Recognition of Iron-Responsive Elements by Iron Regulatory Protein 1. *Journal of Molecular Biology*, *425*(18), 3301–3310. https://doi.org/10.1016/j.jmb.2013.06.023
Seo, S. W., Kim, D., Latif, H., O'Brien, E. J., Szubin, R., & Palsson, B. O. (2014). Deciphering Fur transcriptional regulatory network highlights its complex role beyond iron metabolism in Escherichia coli. *Nature Communications*, *5*(1), 4910. https://doi.org/10.1038/ncomms5910
Serdar, C. M., Gibson, D. T., Munnecke, D. M., & Lancaster, J. H. (1982). Plasmid Involvement in Parathion Hydrolysis by Pseudomonas diminuta. *Applied and Environmental Microbiology*, *44*(1), 246–249. https://doi.org/10.1128/AEM.44.1.246-249.1982
Serio, A. W., Pechter, K. B., & Sonenshein, A. L. (2006). Bacillus subtilis Aconitase Is Required for Efficient Late-Sporulation Gene Expression. *Journal of Bacteriology*, *188*(17), 6396–6405. https://doi.org/10.1128/JB.00249-06
Sethunathan, N., & Yoshida, T. (1973). A Flavobacterium sp. that degrades diazinon and parathion. *Canadian Journal of Microbiology*, *19*(7), 873–875. https://doi.org/10.1139/m73-138
Siddavattam, D., Khajamohiddin, S., Manavathi, B., Pakala, S. B., & Merrick, M. (2003). Transposon-Like Organization of the Plasmid-Borne Organophosphate Degradation (opd) Gene Cluster Found in Flavobacterium sp. *Applied and Environmental Microbiology*, *69*(5), 2533–2539. https://doi.org/10.1128/AEM.69.5.2533-2539.2003
Siddavattam, D., Raju, E. R., Paul, P. V. E., & Merrick, M. (2006). Overexpression of parathion hydrolase in Escherichia coli stimulates the synthesis of outer membrane porin OmpF. *Pesticide Biochemistry and Physiology*, *86*(3), 146–150. https://doi.org/10.1016/j.pestbp.2006.02.007
Simons, R. W., Houman, F., & Kleckner, N. (1987). Improved single and multicopy lac-based cloning vectors for protein and operon fusions. *Gene*, *53*(1), 85–96. https://doi.org/10.1016/0378-1119(87)90095-3
Singh, B. K. (2009). Organophosphorus-degrading bacteria: ecology and industrial applications. *Nature Reviews Microbiology*, *7*(2), 156–164. https://doi.org/10.1038/nrmicro2050
Singh, B. K., & Walker, A. (2006). Microbial degradation of organophosphorus compounds. *FEMS Microbiology Reviews*, *30*(3), 428–471. https://doi.org/10.1111/j.1574-6976.2006.00018.x
Singh, B., Kaur, J., & Singh, K. (2014). Microbial degradation of an organophosphate pesticide, malathion. *Critical Reviews in Microbiology*, *40*(2), 146–154. https://doi.org/10.3109/1040841X.2013.763222
Slattery, M., Zhou, T., Yang, L., Dantas Machado, A. C., Gordân, R., & Rohs, R. (2014). Absence of a simple code: how transcription factors read the genome. *Trends in Biochemical Sciences*, *39*(9), 381–399. https://doi.org/10.1016/j.tibs.2014.07.002
Smith, A., Hooper, N. I., Shipulina, N., & Morgan, W. T. (1996). Heme binding by a bacterial repressor protein, the gene product of the ferric uptake regulation (fur) gene ofEscherichia coli. *Journal of Protein Chemistry*, *15*(6), 575–583. https://doi.org/10.1007/BF01908539
Sohn, J. H., Kwon, K. K., Kang, J.-H., Jung, H.-B., & Kim, S.-J. (2004). Novosphingobium pentaromativorans sp. nov., a high-molecular-mass polycyclic aromatic hydrocarbon-degrading bacterium isolated from estuarine sediment. *International Journal of*

Systematic and Evolutionary Microbiology, *54*(5), 1483–1487. https://doi.org/10.1099/ijs.0.02945-0

Solovyev Victor and Salamov Asaf. (2010). Automatic Annotation Of Microbial Genomes And Metagenomic Sequences. In *In: Metagenomics and its Applications in Agriculture*.

Somara, S., & Siddavattam, D. (1995). Plasmid mediated organophosphate pesticide degradation by Flavobacterium balustinum. *Biochemistry and Molecular Biology International*, *36*(3), 627–631. http://www.ncbi.nlm.nih.gov/pubmed/7549962

Spaink, H. P., Okker, R. J. H., Wijffelman, C. A., Pees, E., & Lugtenberg, B. J. J. (1987). Promoters in the nodulation region of the Rhizobium leguminosarum Sym plasmid pRL1JI. *Plant Molecular Biology*, *9*(1), 27–39. https://doi.org/10.1007/BF00017984

Sridhar, J., Narmada, S. R., Sabarinathan, R., Ou, H.-Y., Deng, Z., Sekar, K., Rafi, Z. A., & Rajakumar, K. (2010). sRNAscanner: A Computational Tool for Intergenic Small RNA Detection in Bacterial Genomes. *PLoS ONE*, *5*(8), e11970. https://doi.org/10.1371/journal.pone.0011970

Sruti DebRoy, Peng Gao, Danielle A. Garsin, Barret R. Harvey, Veronica Kos, Ingolf F. Nes, and M. S. (2014). *Transcriptional and Post Transcriptional Control of Enterococcal Gene Regulation*. https://www.ncbi.nlm.nih.gov/books/NBK190422/

St. Martin, E. J. (1997). Microbial transformation and degradation of toxic organic chemicals Lily Y. Young and Carl E. Cerniglia, Wiley-Liss Inc., New York, NY, (1995), 654 pages,[ISBN No.: 0–471–52109–4], U.S. List Price: $99.95. *Environmental Progress*, *16*(2), A7–A7. https://doi.org/10.1002/ep.3300160204

Stepankova, A., Dušková, J., Skálová, T., Hašek, J., Koval', T., Østergaard, L. H., & Dohnálek, J. (2013). Organophosphorus acid anhydrolase from Alteromonas macleodii : structural study and functional relationship to prolidases. *Acta Crystallographica Section F Structural Biology and Crystallization Communications*, *69*(4), 346–354. https://doi.org/10.1107/S1744309113002674

Stojiljkovic, I., Bäumler, A. J., & Hantke, K. (1994). Fur Regulon in Gram-negative Bacteria. *Journal of Molecular Biology*, *236*(2), 531–545. https://doi.org/10.1006/jmbi.1994.1163

Stojiljkovic, I., & Hantke, K. (1995). Functional domains of theEscherichia coli ferric uptake regulator protein (Fur). *Molecular and General Genetics MGG*, *247*(2), 199–205. https://doi.org/10.1007/BF00705650

Storz, G., Opdyke, J. A., & Zhang, A. (2004). Controlling mRNA stability and translation with small, noncoding RNAs. *Current Opinion in Microbiology*, *7*(2), 140–144. https://doi.org/10.1016/j.mib.2004.02.015

Storz, G., Vogel, J., & Wassarman, K. M. (2011). Regulation by Small RNAs in Bacteria: Expanding Frontiers. *Molecular Cell*, *43*(6), 880–891. https://doi.org/10.1016/j.molcel.2011.08.022

Studier, F. W., & Moffatt, B. A. (1986). Use of bacteriophage T7 RNA polymerase to direct selective high-level expression of cloned genes. *Journal of Molecular Biology*, *189*(1), 113–130. https://doi.org/10.1016/0022-2836(86)90385-2

Sugimoto, K., Senda, M., Kasai, D., Fukuda, M., Masai, E., & Senda, T. (2014). Molecular Mechanism of Strict Substrate Specificity of an Extradiol Dioxygenase, DesB, Derived from Sphingobium sp. SYK-6. *PLoS ONE*, *9*(3), e92249. https://doi.org/10.1371/journal.pone.0092249

Sugimoto, K., Senda, T., Aoshima, H., Masai, E., Fukuda, M., & Mitsui, Y. (1999). Crystal structure of an aromatic ring opening dioxygenase LigAB, a protocatechuate 4,5-dioxygenase, under aerobic conditions. *Structure*, *7*(8), 953–965. https://doi.org/10.1016/S0969-2126(99)80122-1

Tanabe, T., Naka, A., Aso, H., Nakao, H., Narimatsu, S., Inoue, Y., Ono, T., & Yamamoto, S. (2005). A Novel Aerobactin Utilization Cluster in Vibrio vulnificus with a Gene Involved in the Transcription Regulation of the iutA Homologue. *Microbiology and Immunology*, *49*(9), 823–834. https://doi.org/10.1111/j.1348-0421.2005.tb03671.x

Tang, Y., & Guest, J. R. (1999). Direct evidence for mRNA binding and post-transcriptional regulation by Escherichia coli aconitases. *Microbiology*, *145*(11), 3069–3079. https://doi.org/10.1099/00221287-145-11-3069

Tanui, C. K., Shyntum, D. Y., Priem, S. L., Theron, J., & Moleleki, L. N. (2017). Influence of the ferric uptake regulator (Fur) protein on pathogenicity in Pectobacterium carotovorum subsp. brasiliense. *PLOS ONE*, *12*(5), e0177647. https://doi.org/10.1371/journal.pone.0177647

Tawfik, D. S. (2006). BIOCHEMISTRY: Loop Grafting and the Origins of Enzyme Species. *Science*, *311*(5760), 475–476. https://doi.org/10.1126/science.1123883

Theil, E C. (1990). Regulation of ferritin and transferrin receptor mRNAs. *The Journal of Biological Chemistry*, *265*(9), 4771–4774. http://www.ncbi.nlm.nih.gov/pubmed/2156853

Theil, Elizabeth C. (2015). IRE mRNA riboregulators use metabolic iron (Fe 2+) to control mRNA activity and iron chemistry in animals. *Metallomics*, *7*(1), 15–24. https://doi.org/10.1039/C4MT00136B

Thomason, L. C., Costantino, N., & Court, D. L. (2007). E. coli Genome Manipulation by P1 Transduction. In *Current Protocols in Molecular Biology* (pp. 1.17.1-1.17.8). John Wiley & Sons, Inc. https://doi.org/10.1002/0471142727.mb0117s79

Thompson, D. K., Beliaev, A. S., Giometti, C. S., Tollaksen, S. L., Khare, T., Lies, D. P., Nealson, K. H., Lim, H., Yates, J., Brandt, C. C., Tiedje, J. M., & Zhou, J. (2002). Transcriptional and Proteomic Analysis of a Ferric Uptake Regulator (Fur) Mutant of Shewanella oneidensis: Possible Involvement of Fur in Energy Metabolism, Transcriptional Regulation, and Oxidative Stress. *Applied and Environmental Microbiology*, *68*(2), 881–892. https://doi.org/10.1128/AEM.68.2.881-892.2002

Touati, D. (1988). Transcriptional and posttranscriptional regulation of manganese superoxide dismutase biosynthesis in Escherichia coli, studied with operon and protein fusions. *Journal of Bacteriology*, *170*(6), 2511–2520. https://doi.org/10.1128/JB.170.6.2511-2520.1988

Trujillo, M., Alvarez, B., Souza, J. M., Romero, N., Castro, L., Thomson, L., & Radi, R. (2010). Mechanisms and Biological Consequences of Peroxynitrite-Dependent Protein Oxidation and Nitration. In *Nitric Oxide* (pp. 61–102). Elsevier. https://doi.org/10.1016/B978-0-12-373866-0.00003-4

Tseng, C.-P. (2006). Regulation of fumarase (fumB) gene expression in Escherichia coli in response to oxygen, iron and heme availability: role of the arcA, fur, and hemA gene products. *FEMS Microbiology Letters*, *157*(1), 67–72. https://doi.org/10.1111/j.1574-6968.1997.tb12754.x

Vanhooke, J. L., Benning, M. M., Raushel, F. M., & Holden, H. M. (1996). Three-Dimensional Structure of the Zinc-Containing Phosphotriesterase with the Bound Substrate Analog Diethyl 4-Methylbenzylphosphonate † , ‡. *Biochemistry*, *35*(19), 6020–6025. https://doi.org/10.1021/bi960325l

Vassinova, N., & Kozyrev, D. (2000). A method for direct cloning of Fur-regulated genes: identification of seven new Fur-regulated loci in Escherichia coli. *Microbiology*, *146*(12), 3171–3182. https://doi.org/10.1099/00221287-146-12-3171

Venturi, V., Weisbeek, P., & Koster, M. (1995). Gene regulation of siderophore-mediated iron acquisition in Pseudomonas: not only the Fur repressor. *Molecular Microbiology*, *17*(4), 603–610. https://doi.org/10.1111/j.1365-2958.1995.mmi_17040603.x

Visca, P., Leoni, L., Wilson, M. J., & Lamont, I. L. (2002). Iron transport and regulation, cell signalling and genomics: lessons from Escherichia coli and Pseudomonas. *Molecular Microbiology*, *45*(5), 1177–1190. https://doi.org/10.1046/j.1365-2958.2002.03088.x

Volz, K. (2008). The functional duality of iron regulatory protein 1. *Current Opinion in Structural Biology*, *18*(1), 106–111. https://doi.org/10.1016/j.sbi.2007.12.010

Walczak, R., Westhof, E., Carbon, P., & Krol, A. (1996). A novel RNA structural motif in the

selenocysteine insertion element of eukaryotic selenoprotein mRNAs. *RNA (New York, N.Y.)*, *2*(4), 367–379. http://www.ncbi.nlm.nih.gov/pubmed/8634917

Walden, W. E., Selezneva, A. I., Dupuy, J., Volbeda, A., Fontecilla-Camps, J. C., Theil, E. C., & Volz, K. (2006). Structure of Dual Function Iron Regulatory Protein 1 Complexed with Ferritin IRE-RNA. *Science*, *314*(5807), 1903–1908. https://doi.org/10.1126/science.1133116

Walden, W. E., Selezneva, A., & Volz, K. (2012). Accommodating variety in iron-responsive elements: Crystal structure of transferrin receptor 1 B IRE bound to iron regulatory protein 1. *FEBS Letters*, *586*(1), 32–35. https://doi.org/10.1016/j.febslet.2011.11.018

Wang, Y.-H., Sczekan, S. R., & Theil, E. C. (1990). Structure of the 5' untranslated regulatory region of ferritin mRNA studied in solution. *Nucleic Acids Research*, *18*(15), 4463–4468. https://doi.org/10.1093/nar/18.15.4463

Wang, Y., Li, J., & Liu, A. (2017). Oxygen activation by mononuclear nonheme iron dioxygenases involved in the degradation of aromatics. *JBIC Journal of Biological Inorganic Chemistry*, *22*(2–3), 395–405. https://doi.org/10.1007/s00775-017-1436-5

Wang, Yuh-Hwa, Lin, P.-N., Sczekan, S. R., McKenzie, R. A., & Theil, E. C. (1991). Ferritin mRNA probed, near the iron regulatory region, with protein and chemical (1,10-phenanthroline-Cu) nucleases A possible role for base-paired flanking regions. *Biology of Metals*, *4*(1), 56–61. https://doi.org/10.1007/BF01135558

Waters, L. S., & Storz, G. (2009). Regulatory RNAs in Bacteria. *Cell*, *136*(4), 615–628. https://doi.org/10.1016/j.cell.2009.01.043

Watnick, P. I., Butterton, J. R., & Calderwood, S. B. (1998). The interaction of the Vibrio cholerae transcription factors, Fur and IrgB, with the overlapping promoters of two virulence genes, irgA and irgB. *Gene*, *209*(1–2), 65–70. https://doi.org/10.1016/S0378-1119(98)00018-3

Weaver, J., Watts, T., Li, P., & Rye, H. S. (2014). Structural Basis of Substrate Selectivity of E. coli Prolidase. *PLoS ONE*, *9*(10), e111531. https://doi.org/10.1371/journal.pone.0111531

Weiner, J. H., Bilous, P. T., Shaw, G. M., Lubitz, S. P., Frost, L., Thomas, G. H., Cole, J. A., & Turner, R. J. (1998). A Novel and Ubiquitous System for Membrane Targeting and Secretion of Cofactor-Containing Proteins. *Cell*, *93*(1), 93–101. https://doi.org/10.1016/S0092-8674(00)81149-6

Wexler, M., Todd, J. D., Kolade, O., Bellini, D., Hemmings, A. M., Sawers, G., & Johnston, A. W. B. (2003). Fur is not the global regulator of iron uptake genes in Rhizobium leguminosarum. *Microbiology*, *149*(5), 1357–1365. https://doi.org/10.1099/mic.0.26130-0

WIENER, M. (2005). TonB-dependent outer membrane transport: going for Baroque? *Current Opinion in Structural Biology*, *15*(4), 394–400. https://doi.org/10.1016/j.sbi.2005.07.001

Williams, C. H., Stillman, T. J., Barynin, V. V., Sedelnikova, S. E., Tang, Y., Green, J., Guest, J. R., & Artymiuk, P. J. (2002). E. coli aconitase B structure reveals a HEAT-like domain with implications for protein–protein recognition. *Nature Structural Biology*, *9*(6), 447–452. https://doi.org/10.1038/nsb801

Wilson, T. J. G., Bertrand, N., Tang, J.-L., Feng, J.-X., Pan, M.-Q., Barber, C. E., Dow, J. M., & Daniels, M. J. (1998). The rpfA gene of Xanthomonas campestris pathovar campestris, which is involved in the regulation of pathogenicity factor production, encodes an aconitase. *Molecular Microbiology*, *28*(5), 961–970. https://doi.org/10.1046/j.1365-2958.1998.00852.x

Winkler, W. C. (2005). Riboswitches and the role of noncoding RNAs in bacterial metabolic control. *Current Opinion in Chemical Biology*, *9*(6), 594–602. https://doi.org/10.1016/j.cbpa.2005.09.016

Winterbourn, C. C. (1995). Toxicity of iron and hydrogen peroxide: the Fenton reaction.

Toxicology Letters, *82–83*, 969–974. https://doi.org/10.1016/0378-4274(95)03532-X
Yang, W., Zhou, Y.-F., Dai, H.-P., Bi, L.-J., Zhang, Z.-P., Zhang, X.-H., Leng, Y., & Zhang, X.-E. (2008). Application of methyl parathion hydrolase (MPH) as a labeling enzyme. *Analytical and Bioanalytical Chemistry*, *390*(8), 2133–2140. https://doi.org/10.1007/s00216-008-1987-y
Yang, X., & Ma, C. (2016). In Vitro Transcription Assays and Their Application in Drug Discovery. *Journal of Visualized Experiments*, *115*. https://doi.org/10.3791/54256
Yoshikata, T., Suzuki, K., Kamimura, N., Namiki, M., Hishiyama, S., Araki, T., Kasai, D., Otsuka, Y., Nakamura, M., Fukuda, M., Katayama, Y., & Masai, E. (2014). Three-Component O -Demethylase System Essential for Catabolism of a Lignin-Derived Biphenyl Compound in Sphingobium sp. Strain SYK-6. *Applied and Environmental Microbiology*, *80*(23), 7142–7153. https://doi.org/10.1128/AEM.02236-14
Zahringer, J., Baliga, B. S., & Munro, H. N. (1976). Novel mechanism for translational control in regulation of ferritin synthesis by iron. *Proceedings of the National Academy of Sciences*, *73*(3), 857–861. https://doi.org/10.1073/pnas.73.3.857
Zhang, L., Wang, H., Liu, X., Zhou, W., & Rao, Z. (2019). The crystal structure of the phosphotriesterase from M. tuberculosis, another member of phosphotriesterase-like lactonase family. *Biochemical and Biophysical Research Communications*, *510*(2), 224–229. https://doi.org/10.1016/j.bbrc.2019.01.069
Zhongli, C., Shunpeng, L., & Guoping, F. (2001). Isolation of Methyl Parathion-Degrading Strain M6 and Cloning of the Methyl Parathion Hydrolase Gene. *Applied and Environmental Microbiology*, *67*(10), 4922–4925. https://doi.org/10.1128/AEM.67.10.4922-4925.2001
Zhou, Z. D., & Tan, E.-K. (2017). Iron regulatory protein (IRP)-iron responsive element (IRE) signaling pathway in human neurodegenerative diseases. *Molecular Neurodegeneration*, *12*(1), 75. https://doi.org/10.1186/s13024-017-0218-4
Zuker, M. (2003). Mfold web server for nucleic acid folding and hybridization prediction. *Nucleic Acids Research*, *31*(13), 3406–3415. https://doi.org/10.1093/nar/gkg595

THE JOURNAL OF BIOLOGICAL CHEMISTRY VOL. 290, NO. 50, pp. 29920–29930, December 11, 2015

The Organophosphate Degradation (*opd*) Island-borne Esterase-induced Metabolic Diversion in *Escherichia coli* and Its Influence on *p*-Nitrophenol Degradation*

Received for publication, May 2, 2015, and in revised form, September 24, 2015 Published, JBC Papers in Press, October 9, 2015, DOI 10.1074/jbc.M115.661249

Deviprasanna Chakka[1], **Ramurthy Gudla**[1], **Ashok Kumar Madikonda**[1], **Emmanuel Vijay Paul Pandeeti, Sunil Parthasarathy, Aparna Nandavaram, and Dayananda Siddavattam**[2]

From the Department of Animal Biology, School of Life Sciences, University of Hyderabad, Hyderabad 500 046, India

Background: Because of the mobile nature of the *opd* island, identical *opd* and *orf306* sequences are found among soil bacteria.

Results: In *E. coli*, Orf306 suppresses glycolysis and the TCA cycle and promotes up-regulation of alternate carbon catabolic operons.

Conclusion: The up-regulated *hca* and *mhp* operons contribute to PNP-dependent growth of *E. coli*.

Significance: Together with *opd*, *orf306* contributes to the complete mineralization of OP residues.

In previous studies of the organophosphate degradation gene cluster, we showed that expression of an open reading frame (*orf306*) present within the cluster in *Escherichia coli* allowed growth on *p*-nitrophenol (PNP) as sole carbon source. We have now shown that expression of *orf306* in *E. coli* causes a dramatic up-regulation in genes coding for alternative carbon catabolism. The propionate, glyoxylate, and methylcitrate cycle pathway-specific enzymes are up-regulated along with *hca* (phenylpropionate) and *mhp* (hydroxyphenylpropionate) degradation operons. These *hca* and *mhp* operons play a key role in degradation of PNP, enabling *E. coli* to grow using it as sole carbon source. Supporting growth experiments, PNP degradation products entered central metabolic pathways and were incorporated into the carbon backbone. The protein and RNA samples isolated from *E. coli* (pSDP10) cells grown in ^{14}C-labeled PNP indicated incorporation of ^{14}C carbon, suggesting Orf306-dependent assimilation of PNP in *E. coli* cells.

Bacterial phosphotriesterases (PTEs)[3] are a group of structurally unrelated enzymes that cleave the triester linkage found in both organophosphate (OP) insecticides and OP nerve agents (1). Because of their broad substrate range and high catalytic efficiency, they have been exploited for detection and decontamination of OP compounds (2). The PTEs have been classified into three main groups: (i) the organophosphate hydrolases (OPHs), (ii) methyl parathion hydrolases (MPHs), and (iii) organophosphate acid anhydrases. Among the PTEs, only the organophosphate acid anhydrases have known physiological substrates: they have been shown to be dipeptidases that cleave dipeptides with a prolyl residue at the carboxyl terminus and hence are described as prolidases (3). The OP hydrolyzing activity of prolidases is considered to be an ancillary activity due to the structural similarity of OP compounds to their usual substrates (3).

The physiological substrates for OPH and MPH enzymes are unknown. These enzymes are believed to have evolved in soil bacteria to counter the toxic effects of OP insecticide residues released into agricultural soils (4, 5). Bacterial OPH enzymes, besides showing high structural similarities with the quorum-quenching lactonases, possess weak lactonase activity (6, 7). Consequently the quorum-quenching lactonases are considered to be the possible progenitors of the bacterial OPH enzymes (7). Unlike the OPH enzymes, the MPHs have no structural similarity with quorum-quenching lactonases but instead are highly similar to β-lactamases (8). The structurally diverse PTEs are therefore assumed to have evolved independently in response to OP residues accumulated in agricultural soils (9, 10).

The genetics of organophosphate degradation has attracted considerable attention among soil microbiologists. Both the OPH-encoding organophosphate degradation (*opd*) genes and the MPH-encoding methyl parathion degradation (*mpd*) genes have been shown to be part of mobile genetic elements (11–13). The lateral transfer of *opd* and *mpd* genes is evidenced by the existence of identical *opd* and *mpd* genes among taxonomically unrelated soil bacteria (14, 15). Even dissimilar indigenous plasmids found in bacteria collected from diverse geographical regions contained identical *opd* gene clusters (14). There are four indigenous plasmids in OP-degrading *Sphingobium fuliginis* ATCC 27551. Of these four plasmids, the *opd* containing pPDL2 has been shown to be a mobilizable plasmid within which the *opd* region has unique organizational features (11).

* This work was supported by Indian Council of Medical Research and Council for Scientific and Industrial Research (CSIR) research fellowships (to D. C., R. G., and A. K. M.). The authors declare that they have no conflicts of interest with the contents of this article.

[1] These authors contributed equally to this work.

[2] To whom correspondence should be addressed: Dept. of Animal Biology, School of Life Sciences, University of Hyderabad, Prof. C. R. Rao Rd., Gachibowli, Hyderabad 500 046, India. Tel.: 91-40-23134578; Fax: 91-40-23010120/145; E-mail: sdsl@uohyd.ernet.in.

[3] The abbreviations used are: PTE, phosphotriesterase; PNP, *p*-nitrophenol; OP, organophosphate; *orf306*, open reading frame 306; OPH, organophosphate hydrolase; MPH, methyl parathion hydrolase; *opd*, organophosphate degradation gene; *mpd*, methyl parathion degradation gene; TCA, tricarboxylic acid; IPTG, isopropyl 1-thio-β-D-galactopyranoside; qPCR, quantitative PCR; PP, phenylpropionate; HPP, hydroxyphenylpropionate; Tn, transposon; IS, insertion element.

THE JOURNAL OF BIOLOGICAL CHEMISTRY VOL. 291, NO. 14, pp. 7774–7785, April 1, 2016

Organophosphate Hydrolase Is a Lipoprotein and Interacts with P_i-specific Transport System to Facilitate Growth of *Brevundimonas diminuta* Using OP Insecticide as Source of Phosphate*

Received for publication, January 11, 2016, and in revised form, February 7, 2016 Published, JBC Papers in Press, February 9, 2016, DOI 10.1074/jbc.M116.715110

Sunil Parthasarathy[‡1], **Hari Parapatla**[‡], **Aparna Nandavaram**[‡], **Tracy Palmer**[§], **and Dayananda Siddavattam**[‡2]
From the [‡]*Department of Animal Biology, School of Life Sciences, University of Hyderabad, Hyderabad, 500 046, India and the* [§]*Division of Molecular Microbiology, College of Life Sciences, University of Dundee, Dundee, United Kingdom*

Organophosphate hydrolase (OPH), encoded by the organophosphate degradation (*opd*) island, hydrolyzes the triester bond found in a variety of organophosphate insecticides and nerve agents. OPH is targeted to the inner membrane of *Brevundimonas diminuta* in a pre-folded conformation by the twin arginine transport (Tat) pathway. The OPH signal peptide contains an invariant cysteine residue at the junction of the signal peptidase (Spase) cleavage site along with a well conserved lipobox motif. Treatment of cells producing native OPH with the signal peptidase II inhibitor globomycin resulted in accumulation of most of the pre-OPH in the cytoplasm with negligible processed OPH detected in the membrane. Substitution of the conserved lipobox cysteine to serine resulted in release of OPH into the periplasm, confirming that OPH is a lipoprotein. Analysis of purified OPH revealed that it was modified with the fatty acids palmitate and stearate. Membrane-bound OPH was shown to interact with the outer membrane efflux protein TolC and with PstS, the periplasmic component of the ABC transporter complex (PstSACB) involved in phosphate transport. Interaction of OPH with PstS appears to facilitate transport of P_i generated from organophosphates due to the combined action of OPH and periplasmically located phosphatases. Consistent with this model, *opd* null mutants of *B. diminuta* failed to grow using the organophosphate insecticide methyl parathion as sole source of phosphate.

Membrane-associated organophosphate hydrolase (OPH)[3] hydrolyzes the triester bond found in a variety of organophosphate insecticides and nerve agents (1, 2). The 39-kDa monomer requires Zn^+ ions as cofactor (3). OPH is encoded by the *opd* (organophosphate degrading) gene found on dissimilar plasmids and the *opd* gene has recently been shown to be a part of an integrative mobilizable element (IME) (4). Due to the mobile nature of the *opd* island, identical *opd* genes are found among bacterial strains isolated from different geographical regions (4, 5). Although its physiological substrate is unknown, OPH hydrolyzes paraoxon at a rate approaching the diffusion limit (k_{cat}/K_m 10^8 M^{-1} s^{-1}) (6). Considering its catalytic efficiency and broad substrate range, it has been assumed that OPH has evolved to degrade organophosphate (OP) insecticides accumulated in agricultural soils (7). Structural analysis shows that OPH contains a TIM barrel-fold as seen in most of the members of amidohydrolase superfamily proteins (8).

OPH associates with cell membranes and membrane-associated OPH has been purified from a number of sources (3, 9–13). Analysis of the amino acid sequences of OPH proteins indicates that all of them contain a predicted signal peptide harboring a well defined twin-arginine (Tat) motif. Twin-arginine signal peptides serve to target proteins to the twin-arginine protein transport (Tat) pathway, which translocates folded proteins across the bacterial cytoplasmic membrane (14). Proteinase K treatment confirmed that OPH is exported to the periplasmic side of the inner membrane in *Brevundimonas diminuta* and dependence on the Tat pathway was demonstrated because substitution of the invariant arginine residues of the Tat signal peptide affected both processing and localization of OPH (15). However, the mechanism by which OPH is anchored to the inner membrane and the physiological role of OPH are currently unclear. In this report we demonstrate that OPH is a lipoprotein and that it plays an essential role in the acquisition of phosphate from OP insecticides.

Experimental Procedures

Media, Strains, and Plasmids—Strains and plasmids used in the present work are shown in Table 1. Primers used for PCR amplification and site-directed mutagenesis are listed in Table 2. *B. diminuta* cultures were grown either in LB medium or in HEPES minimal medium. HEPES minimal medium was pre-

* This work was supported in part by the Department of Biotechnology, Govt. of India (to D. S. Laboratory). Department of Animal Biology was supported by the DST-FIST (Department of Science and Technology–Fund for Improvement of S&T Infrastructure), and the School of Life Sciences, University of Hyderabad is supported by DBT-CREBB/BUILDER (Department of Biotechnology–Centre for Research and Education in Biology and Biotechnology/Boost to University Interdisciplinary Life Science Departments for Education and Research). The authors declare that they have no conflicts of interest with the contents of this article.

[1] Supported by a Shantha Biotechnics Junior Research Fellowship (JRF) and Commonwealth Split-Site Fellowships, British Council, UK.

[2] To whom correspondence should be addressed: Dept. of Animal Biology, School of Life Sciences, University of Hyderabad, Prof. C. R. Rao Rd., Gachibowli, Hyderabad 500 046, India. Tel.: 91-40-23134578; Fax: 91-40-23010120/145; E-mail: sdsl@uohyd.ernet.in.

[3] The abbreviations used are: OPH, organophosphate hydrolase; OP, organophosphate insecticides; Tat, Twin arginine transport; SPase, signal peptidase; DDM, *n*-dodecyl β-D-maltoside; Tricine, *N*-[2-hydroxy-1,1-bis(hydroxymethyl)ethyl]glycine; IMAC, immobilized-metal affinity chromatography; BN-PAGE, blue native-PAGE.

Aparna Nandavaram, Annapoorni Lakshman Sagar, Ashok Kumar Madikonda and Dayananda Siddavattam*

Proteomics of *Sphingobium indicum* B90A for a deeper understanding of hexachlorocyclohexane (HCH) bioremediation

DOI 10.1515/reveh-2015-0042
Received October 13, 2015; accepted October 13, 2015; previously published online March 8, 2016

Abstract: Genome wide expression profiling of *Sphingobium indicum* B90A revealed induction of *lin* genes, *linA* and *linB*, involved in dechlorination of hexachlorocyclohexane (HCH), in the presence of all four isomers of HCH. Supporting proteomics data, the qPCR and promoter assay showed upregulation of *linA* transcription in the presence of HCH isomers. Analysis of the upstream region of the *linA* gene revealed the existence of the GntR binding site overlapping the -10 hexamer of the putative promoter motif. As GntR is a known transcription repressor its dissociation from the *linA* promoter is expected to induce *lin* genes in the presence of HCH isomers. Comparison of *in situ* and in-culture proteomics indicated expression *lin* genes at the dumpsite, an indication for the *in situ* HCH degradation.

Keywords: biodegradation; bioremediation; hexachlorocyclohexane (HCH); *lin* genes; proteomics.

Introduction

Hexachlorocyclohexane (HCH), an organochlorine compound, has extensively been used as an insecticide to control important agricultural pests. The commercial formulation of HCH primarily consists of α, β, γ, δ isomers of which the γ isomer (lindane) has potent insecticidal activity. One ton purification of lindane from technical HCH produces 10 tons of HCH muck consisting of α, β, γ and δ HCH. During the past 60 years around 60,000 tons of lindane has been used worldwide, leading to the formation of 4–7 million tons of HCH muck that is scattered in different places around the globe. Regardless of the stereochemistry, stability and persistence of HCH isomers they have been shown to cause adverse effects to the environment and human health (1). Considering its influence on environment and human health it has been declared as one of the key global pollutants.

The persistence of HCH isomers in the environment is chiefly due to the absence of microbes that can degrade/use them as sole source of carbon. A number of attempts have been made to evaluate microbial degradation of HCH. However, very few reports are available on microbial degradation of HCH both under aerobic and anaerobic conditions. Detailed investigations revealed the existence of upper and lower degradation pathway enzymes in HCH degrading *Sphingobium japonicum* UT26S (2) and *Sphingobium indicum* B90A (3). The upper pathway enzymes, primarily the dehalogenases, contribute to the dehalogenation of HCH. The lower pathway enzymes, the dioxygenases, convert the dehalogenated HCH into the tricarboxylic acid cycle intermediates. HCH dehydrochlorinase (LinA), haloalkane dehalogenase (LinB) and dehydrogenase (LinC/LinX) are upper pathway enzymes. The reductive dechlorinase (LinD), ring cleavage oxygenase (LinE), maleylacetate reductase (LinF), an acyl-CoA transferase (LinG, H), a thiolase (LinJ) contribute to the lower degradation pathway. The HCH degrading (*lin*) genes are organized as clusters. Along with *linI* and *linR*, the genes that code for regulatory proteins, the *linK*, *linL*, *linM* and *linN* coding for a putative ABC-type transporter form a cluster that resembles a genomic island (3). The existence of transposase and recombinase coding genes flanking the *lin* cluster suggests extensive recombination and horizontal transfer of *lin* genes among soil bacteria.

The meta-genome sequence extracted from the soil samples collected from the dumpsite revealed the coexistence of several HCH degraders and non-degraders (4). Interestingly, most of the *Sphingomonads* found enriched at the HCH dumpsites, have shown existence

*Corresponding author: **Dayananda Siddavattam**, Department of Animal Biology, School of Life Sciences, Room No- S40, University of Hyderabad, Hyderabad, Telangana 500046, India, E-mail: siddavattam@gmail.com
Aparna Nandavaram, Annapoorni Lakshman Sagar and Ashok Kumar Madikonda: Department of Animal Sciences, School of Life Sciences, University of Hyderabad, Hyderabad, India

Transcriptional and Post-transcriptional Regulation of Organophosphate Degradation (opd) Gene in Sphingobium fuliginis ATCC 27551

by N. Aparna

Transcriptional and Post-transcriptional Regulation of Organophosphate Degradation (opd) Gene in Sphingobium fuliginis ATCC 27551

ORIGINALITY REPORT

14%	6%	5%	9%
SIMILARITY INDEX	INTERNET SOURCES	PUBLICATIONS	STUDENT PAPERS

PRIMARY SOURCES

1	Submitted to University of Hyderabad, Hyderabad Student Paper	8%
2	baadalsg.inflibnet.ac.in Internet Source	1%
3	jb.asm.org Internet Source	<1%
4	Zengqin Deng, Qing Wang, Zhao Liu, Manfeng Zhang et al. "Mechanistic insights into metal ion activation and operator recognition by the ferric uptake regulator", Nature Communications, 2015 Publication	<1%
5	hypothes.is Internet Source	<1%
6	krishikosh.egranth.ac.in Internet Source	<1%

भारतीय जीवाणुतत्ववेत्त संगठन
Association of Microbiologists of India

59th Annual Conference of Association of Microbiologists of India (AMI-2018)

&

International Symposium on Host-Pathogen Interactions

Certificate

This is to certify that

Aparna Nandavaram

has presented oral/poster/participated in the AMI 2018 conference organized from 9th - 12th December 2018 by School of Life Sciences, University of Hyderabad, Hyderabad, Telangana - 500046, India.

Prof. Appa Rao Podile	Prof. Pratyoosh Shukla	Prof. Ch. Venkata Ramana
President	General Secretary	Organizing Secretary